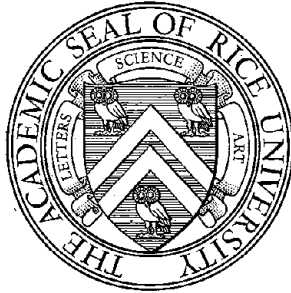# STRUCTURAL RESEARCH AT RICE

Report No. 41

SEISMIC RESPONSE OF CONNECTIONS IN INDETERMINATE FLAT-SLAB SUBASSEMBLIES
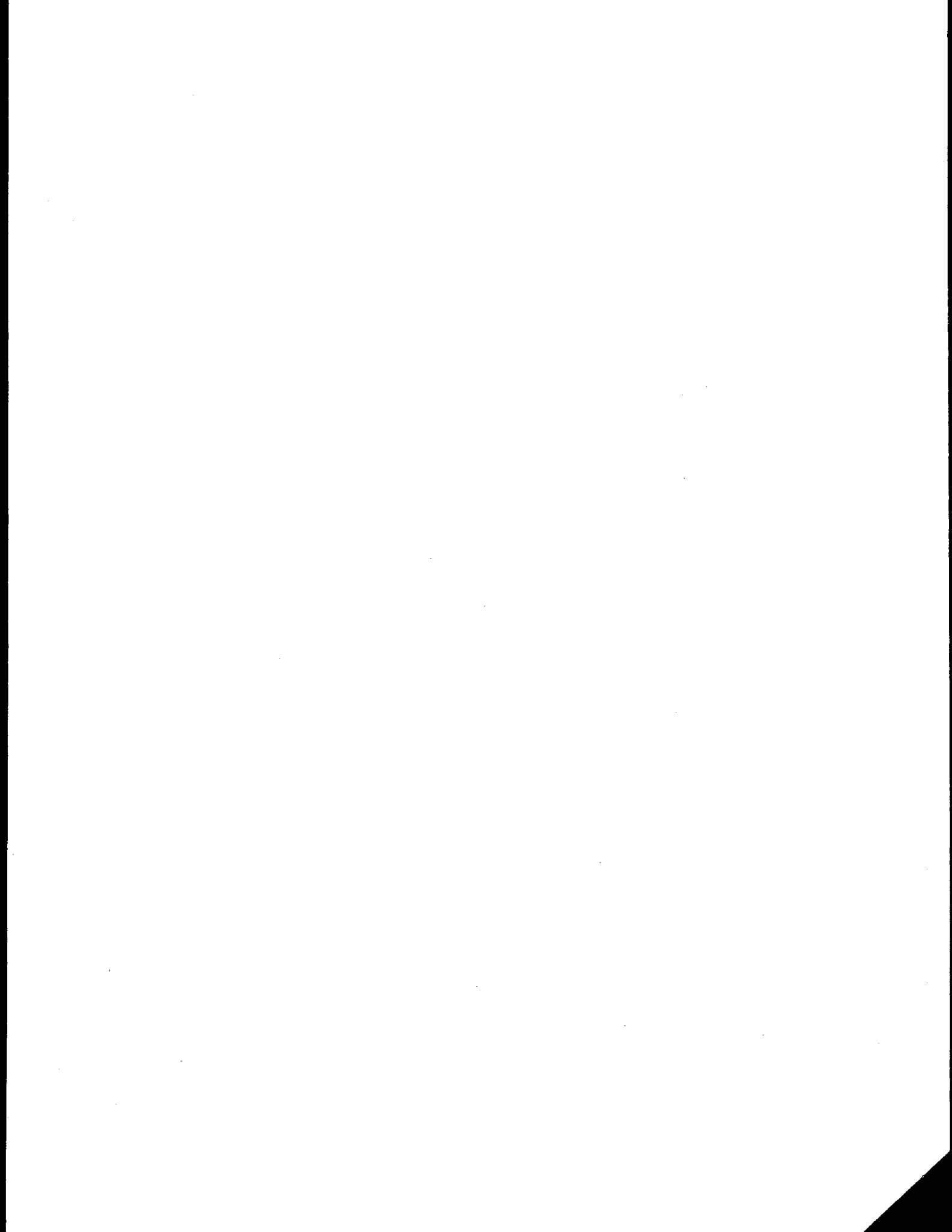
by

I. N. Robertson and A. J. Durrani

Department of Civil Engineering
Rice University
Houston, Texas

July, 1990

SEISMIC RESPONSE OF CONNECTIONS IN INDETERMINATE FLAT-SLAB SUBASSEMBLIES

by

Ian Nicol Robertson

Ahmad Jan Durrani

Department of Civil Engineering
Rice University
Houston, Texas

July, 1990
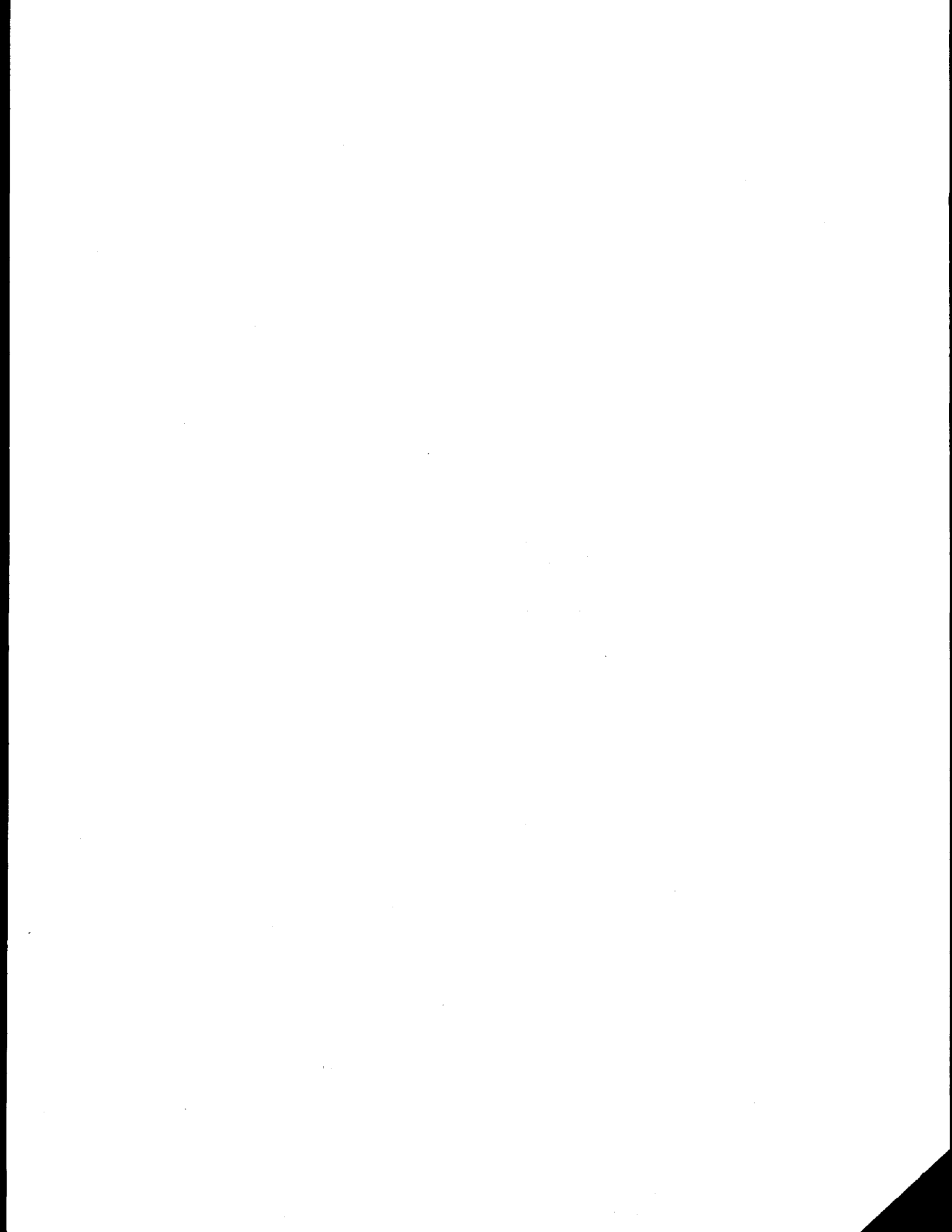
ABSTRACT

Recent earthquakes have shown the vulnerability of flat-slab structures to severe ground motion. The failure in such structures typically initiates at the slab-column connections in the form of a punching failure. This investigation was carried out to evaluate the adequacy of current procedures for the design of slab-column connections. The variables studied included the intensity of gravity loading, slab shear reinforcement at the column line, slab overhang and stiff edge beam at exterior connections, and the indeterminacy of the connection subassembly.

Nine half scale slab-column subassemblies were tested under simulated earthquake loading. Seven of the subassemblies simulated a single floor of a two-bay flat-plate structure. Each subassembly consisted of one interior and two exterior slab-column connections. The remaining two specimens were individual interior and exterior connections. All specimens were subjected to the same predefined displacement routine which consisted of twenty cycles of incremental displacements increasing to a maximum of eight percent drift.

Increased slab gravity load significantly reduced the drift capacity of both interior and exterior connections. To achieve a minimum of 1.5 percent lateral drift prior to failure, the ultimate shear from gravity loads on flat-plate connections must be limited to $V_u \leq C_d \sqrt{f_c'} b_o d$, where $C_d = 2.0$ for exterior connections and $C_d = 1.4$ for interior connections. For the range of shear stress levels studied in these tests, the ACI Committee 352 recommendation that moment and shear be treated independently for design of exterior connections appears reasonable.
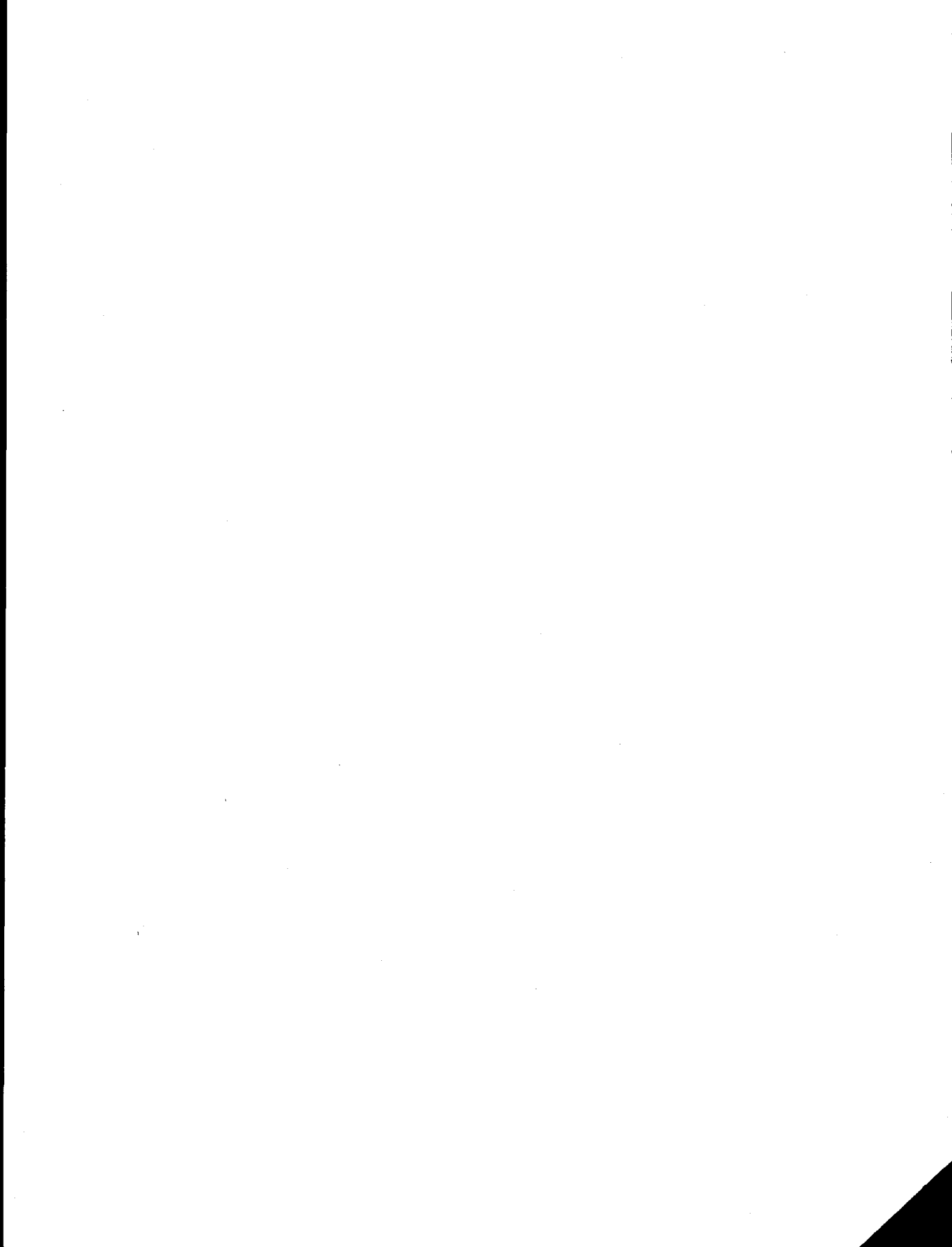
Closed hoop stirrups enclosing the slab flexural reinforcement passing through the interior connections were effective in preventing punching shear failure and increased the ductility of the connection. A stiff edge beam or slab overhang at the exterior connections increased both the strength and ductility of these connections. The behavior of connections in indeterminate subassemblies was observed to be similar to the behavior of the individual connections especially at drift levels less than 1.5 percent.

ACKNOWLEDGEMENTS

LIST OF CONTENTS

Preceding page blank

LIST OF TABLES

LIST OF FIGURES

Chapter 4 - Effect of Gravity Shear on Exterior Connection Behavior

Chapter 6 - Interior Connection Model

LIST OF PHOTOGRAPHS

CHAPTER 1

INTRODUCTION

1.1 General

The performance of flat-slab structures subjected to seismic loading has attracted increasing attention recently. Considerable research has focused on the slab-column connections, culminating in the recently published recommendations by the ACI Committee 352 (Ref. 1.1). The research reported in this thesis investigated the effect of a number of variables on the response of slab-column connections subjected to earthquake-type loading.

The bulk of existing research on flat-slab connections has been performed on individual interior or exterior connections subjected to some combination of moment and shear. While there is considerable data on monotonic loading, the data on the response of connections to cyclic loading is somewhat limited. This research program incorporated the indeterminacy present in actual structures by modeling a single storey of a two bay frame. Each specimen consisted of one interior connection and two exterior connections. The specimens were each subjected to the same lateral displacement history to simulate the effect of earthquake-type loading on the connections.

A total of nine specimens were tested. Of these, seven were multiple connection subassemblies, while the remaining two were individual interior and exterior connections. The variables considered during this project included the slab edge condition at the exterior connection, the use of slab shear stirrups, and the level of gravity load applied to the slab during the test.

1.2 Literature Review

A considerable amount of research has been performed in the past on slab-column connections. The majority of this research focused initially on the performance of connections subjected to direct punching shear failure (Ref. 1.3, 1.4). This research was performed on individual connections, predominantly interior connections. Later research included the effect of an unbalanced moment at the connection (Ref. 1.5 to 1.7) and the effect of continuity on both interior and exterior connection behavior (Ref. 1.8, 1.9).

Grossman (Ref. 6.1) chronicles the development of the present ACI 318-83 code provisions (Ref. 1.2) for transfer of shear and unbalanced moment at slab-column connections. From the fairly simple empirical design method of the 1956 ACI code, the code provisions have steadily evolved to the present model based on transfer of portion of the unbalanced moment by means of linear variation of the shear stress around a slab critical

section. The ACI model was also extended to exterior connections. This empirical model has come under increased criticism recently, especially when applied to exterior and corner columns (Ref. 4.1).

Apart from research on the connection behavior, many researchers have attempted to arrive at a realistic method of analyzing flat-plate frames subjected to lateral load. Practical experience with buildings has shown lateral drift levels far in excess of the design values. To date only thumb rules are used to estimate the lateral stiffness of flat-slab structures.

The Mexico City earthquake of 19 Sept, 1985 brought renewed attention to the issue of flat slabs subjected to earthquake loading. Many of the structures destroyed or severely damaged by that earthquake were flat-slab structures (Ref. 1.10 to 1.15). This lead to major changes in the Mexican design code requirements for design of slab-column connections and flat slab buildings. It also lead to increased scrutiny of the existing ACI code requirements.

A number of recent research publications have attempted to assimilate past research in the area of slab-column connection behavior (Ref. 1.7, 4.1, 4.2, 4.3, 7.1). Further review of relevant literature is presented in each of the subsequent chapters of this thesis.

CHAPTER 2

EXPERIMENTAL PROGRAM

2.1 General Testing Program

Nine large scale specimens were tested as part of this research program. Seven of these specimens were multiple-connection subassemblies representing a half scale model of a single story of a two-bay prototype frame, as shown in Fig. 2.1. The specimen configuration is based on the assumption that under lateral loading, the points of contraflexure in a multistory frame remain stationary at mid-height of the columns. Each of the seven multiple-connection subassemblies, therefore, consisted of one interior and two exterior slab-column connections, as shown in Fig. 2.2 and Photo 2.1. In addition, two specimens representing individual interior and exterior connections were also tested to determine the effect of load redistribution on the behavior of connections in indeterminate systems (Fig. 2.3 and Photos 2.2 and 2.3).

Two of the multiple-connection subassemblies were identical in all respects and represented the control specimens. The remaining five subassemblies were used to study the effect of a number of variables. The four variables considered were,

5

i)   the effect of a torsionally stiff edge beam at the exterior connections,

ii)   the effect of slab shear stirrups,

iii) the effect of a slab overhang beyond the exterior connections, and

iv)   the effect of varying levels of slab gravity load.

These variables were incorporated in the five specimens as set out in Table 2.1.

The test specimens were sized as half scale models of a prototype structure. The prototype structure (Fig. 2.1) was chosen as representative of a typical flat slab residential or office building. It consisted of a 9 inch thick flat plate supported on 20 inch square columns at 20 ft. and 18 ft. centers in orthogonal directions. The story height was set at 10 ft.

For a true half-scale modeling of the chosen prototype, the specimens would have a span of 10 ft. and slab width of 9 ft. Due to constraints of the testing frame, these dimensions were reduced to 9.5 ft. and 6.5 ft. respectively, as shown in Fig. 2.2. Observations from previous research studies have shown that discontinuity in the lateral direction may not have a significant effect on the behavior of the slab-column connections (Ref. 2.1). The columns in the test subassemblies were pinned at the assumed inflection points at mid-height of the story above and below the slab.

The two single-connection specimens represent the interior and exterior connections of the control specimen. The slabs of these specimens were pinned at mid-span as shown in Fig. 2.3. As with previous individual connection tests, the point of contraflexure is assumed to be at midspan, so no lateral or rotational restraint was provided at the slab edge. Steel channels were attached above and below the slab edge to distribute the single vertical reaction along the slab edge (See Photos 2.2 and 2.3).

2.2 Prototype Design

For the prototype building shown in Fig. 2.1, the design gravity loading on each floor consisted of the slab self weight plus 20 psf superimposed dead load and 50 psf superimposed live load, which is typical of an office or apartment building. The lateral earthquake loading was based on the NEHRP design recommendations (Ref. 2.3) for a Category 2 or moderate earthquake. The frame was analyzed for this lateral loading to find the moments and shears at the connections at the second floor level. These moments and shears were then added to those obtained from a gravity load analysis to get the design slab moments and shears. The slab was then designed using the ACI 318 Building Code. The final slab thickness of 9 in. was selected such that the maximum ultimate shear on the slab critical perimeter was $v_c = 4\sqrt{f_c'}$ (psi units).

8

2.3 Subassembly Design

The subassemblies were designed following the procedure used in the design of the prototype building to obtain slab moments for the column and middle strips, and unbalanced moments at each connection. The ultimate shear stresses at all connections were again close to $4\sqrt{f_c'}$ as for the prototype. The flexure reinforcement in the model slab consisted of No. 3 deformed bars positioned in accordance with present code procedures. Additional reinforcement was placed in a slab strip $c_2 + 3h$ wide and centered on the column, to resist portion of the unbalanced moment $\gamma_f M_{ub}$, as prescribed by the code, where c_2 is the column dimension parallel to the slab edge, h is the slab thickness and $\gamma_f M_{ub}$ is the portion of unbalanced moment carried in flexure.

Additional bottom reinforcement was added through the columns in accordance with Committee 352 recommendations to prevent progressive collapse (Ref. 1.1, 2.4, 2.5). All longitudinal slab reinforcement was continuous through the length of the model. Steel ratios, ρ_c for flexural reinforcement perpendicular to the slab edge in a slab width $c_2 + 3h$, ρ_t outside this width, and ρ_t parallel to the slab edge, are given in Table 4.1.

At the exterior connections, the slab edge was reinforced for torsion as required by the code. This was achieved by

adding No.2 smooth bar closed hoop stirrups at 2.5 in. on center along the slab edge. These stirrups enclosed six transverse No.3 slab bars to form a "beam" within the slab depth. All longitudinal slab reinforcement was anchored by means of a 90 degree bend into this "beam". The specimen reinforcement layout is shown in Fig. 2.5 and Photo 2.4 for the control specimen, 2C. The columns in the model were designed to remain elastic during the test.

2.4 Specimen Variables

A number of variables were considered in this test program. These included the effect of the edge beam condition, the effect of slab shear reinforcement in the form of closed hoop stirrups, and the level of gravity load applied to the slab during testing. Details of the individual specimens and the variables studied in each specimen are given in Table 2.1.

2.4.1 Control Specimen.

Specimen 1 was to be the control specimen. During the testing of this specimen however, after reaching the 3 percent drift cycle, an electronic failure resulted in the sudden application of 5 inch stroke, or 8 percent drift. This caused failure of both the interior and west exterior connections. Because of the sudden nature of this loading, no data could be recovered during failure. The early cycles of this test are, however, still valid and are utilized in this report. Since this specimen

could no longer be considered a control specimen, an identical specimen 2C was fabricated and tested. Specimen 2C is therefore referred to as the control specimen in the remainder of this report.

2.4.2 Stiff Edge Beams

Specimen 3SE was identical to the control specimen except that it included a stiff edge beam at both exterior connections so as to study the change of behavior of the specimen when rigid edge beams or walls are present. These 12 inch deep by 8 inch wide edge beams were designed to remain uncracked throughout the test. In case cracking did occur, the edge beams were reinforced so as to prevent substantial twisting of the section after cracking. Photo 2.5 shows the edge beam reinforcement in specimen 3SE prior to pouring concrete.

2.4.3 Slab Shear Reinforcement

Specimen 4S contained slab shear reinforcement in the form of closed hoop stirrups consisting of smooth No. 2 mild steel bars. These stirrups were placed in the slab at all connections, in both directions, along the column lines (See Photo 2.6 and 2.7). They enclosed the three top and three bottom slab bars passing through the columns. The stirrups were continued the entire length of the column strip to ensure full effectiveness of the shear reinforcement.

2.4.4 Slab Overhang at Exterior Connection

Specimen 5SO included an edge overhang beyond the exterior columns. Often such an overhang is included to provide support for the window wall system. The slab overhang extended 10 inches beyond the column at both exterior connections. The longitudinal slab reinforcement was continued to the edge of the overhang, however, the slab edge torsional reinforcement was still located on the column line as shown in Photo 2.8.

2.4.5 Increased Slab Gravity Load

Specimens 6LL and 7L were identical to the control specimen in all respects except that they were subjected to increased gravity loading. The slab loading and shear stresses at the connections under gravity loading for these specimens are given in Tables 4.1 and 5.1. After testing specimen 6LL, it was decided that a specimen with even greater slab load would not be as beneficial as one with an intermediate gravity load. Hence specimen 7L was subjected to less gravity load than specimen 6LL. This additional slab load was applied by adding lead weights to the slab surface as shown in Photo 2.9. Additional bottom reinforcement was provided through the columns to ensure punching failure did not result in total collapse of the slab.

2.4.6 Individual connections

Specimen 8I was an individual interior connection while specimen 9E was an exterior connection. These specimens had exactly the same reinforcing as the control specimen and were cast in the same formwork with a divider placed at midspan (See Photo 2.10). They are similar to the many individual specimens tested in previous slab-column investigations. These two individual specimens were used to study the redistribution of load between connections in an indeterminate structure.

These specimens were tested in the same test frame as the combined specimens as shown in Photos 2.2 and 2.3. The free slab edge was supported by a rigid vertical arm so as to allow rotation and movement horizontally but no vertical movement. This rigid arm was fitted with a load cell to measure the vertical reaction. The gravity loading on the slabs around the individual connections was relocated to ensure that both shear at the critical perimeter and bending moment at the face of the column were as close as possible to those in the combined specimens.

2.5 Fabrication

2.5.1 General

The specimens were all fabricated in the laboratory using Ready-mixed concrete. They were cured under polyethelene sheets

in the forms for an average of 4 days before stripping. They were then cured under wet burlap and polyethelene sheets for another 10 days. Concrete test cylinders were also made at time of casting. Some of these cylinders were kept in a curing room at 100% humidity and 75 degrees farenheit, while other cylinders were kept with the specimen under the same curing conditions as the specimen.

Steel plates were cast into the ends of the columns to provide for connection of the support clevices. The specimens were lifted by means of a wide flange steel beam attached to the column tops and lifted at two points to prevent excessive stresses in the specimen, especially while the concrete was still gaining strength.

2.5.2 Concrete Properties.

The concrete used in the test specimens was supplied by a local Ready-mixed concrete supplier. The concrete mix design is given in Table 2.2. The concrete was generally delivered to the laboratory with a low slump and the final water content adjusted prior to pouring to obtain the desired 3 inch slump.

Twelve 6in. diameter concrete cylinders and two standard test beams (for rupture modulus tests) were made while casting each test specimen. Three of the cylinders were kept in a curing room at 100% humidity and 75 degrees farenheit. These cylinders were tested at 28 days. The other nine cylinders and

test beams were kept with the test specimen and cured in the same manner as the test specimen. Three of these cylinders were tested for compressive strength at 28 days. The remaining six cylinders were kept with the specimen. Three were tested for compressive strength at the time of testing the specimen while the others were tested for split cylinder tensile strength. The test beams were also tested for modulus of rupture at the time of testing the specimen.

The results of all the concrete strength tests are summarized in Table 2.3.

2.5.3 Reinforcement Properties

The steel used as main reinforcement in both slab and column was all grade 60 Type 2 deformed bars with a specified minimum yield strength of 60 ksi. The reinforcement was all obtained from the same supplier, but delivered in two different loads. Coupons of each bar size were taken for each bar size from each delivery and tested for tensile strength. The results are summarized in Table 2.4. Sample stress strain curves for the various bar sizes are shown in Fig. 2.6. The observed test yield strengths were used in the analysis of the test results.

2.6 Test Setup

The specimens were all tested in a large steel reaction frame as shown in Photo 2.1 and Fig. 2.4. The specimen was

lifted by means of a 20 ton overhead crane attached to the lifting beam connected to the top plates of the specimen columns. This reduced the handling stresses in the test specimen during installation. The test setup was designed so that all column reactions, both shear and axial, could be monitored during the test. The tops of the columns were connected by load cells to a load distribution beam (Fig. 2.4). This beam was supported independently of the specimen and prevented any lateral out-of-plane motion. The lateral loading was applied to the distribution beam by a servo-controlled actuator. No axial load was applied to the columns as column axial load does not have a significant effect on the connection behavior since connection failure invariably occurs in the slab around the column and not in the joint itself.

The bottom of the center column rested on a load cell measuring the vertical reaction while the column base was restrained against lateral movement. The exterior columns were supported on rollers at the base with lateral restraint provided by a load cell. This arrangement allowed for shear measurement at the base of the exterior columns. The shear at the base of the interior column is then obtained from horizontal equilibrium. Equilibrium of vertical loads and reactions, and overturning moment equilibrium were used to obtain the vertical reactions under the exterior columns.

This test setup maintained the tops and bases of the columns equidistant. This arrangement closely modeled a first floor situation or the situation where one floor experiences greater inelastic action compared to the adjacent floors. This may be the result of local weaknesses or increased gravity load at the floor in question (Ref. 2.2).

Once installed, the specimen was instrumented fully as described later. All of the specimens in this research program were subjected to slab loading simulating the full dead load and 30 percent of the live load of the prototype structure. This load was applied to the slab surface by hanging forty 450 pound weights from cables anchored on the top surface of the slab. In the specimens with increased gravity load, additional lead weights were added to the top of the slab. The equivalent uniformly distributed slab loads for these specimens are listed in Tables 4.1 and 5.1. Also listed are the gravity shear stress, $v_g = V_g / A_{cs}$, and the shear stress based on the eccentric shear stress model of the ACI code including the unbalanced moment at exterior connections.

All instrumentation was monitored during application of the slab gravity loading to determine the initial condition prior to application of lateral load. The slab weights were applied individually in a symmetric sequence so as to avoid concentrated

stresses in the test specimen. Once all the loads were in place, the instrumentation was monitored to obtain the initial loads and stresses for the lateral loading test.

2.7 Loading History.

Each test specimen was subjected to the same lateral loading history shown in Fig. 2.7. This history included a number of initial small amplitude cycles to study the initial elastic response of the specimen. The history also included a number of repeated cycles and intermediate small cycles to study the strength degeneration and the loss of stiffness with the increasing drift imposed on the specimens. Not all specimens were subjected to the full loading history since the test was generally stopped after failure of the specimen connections.

2.8 Instrumentation

Considerable instrumentation in the form of load cells, displacement transducers, and strain gages was used to aid in understanding the specimen behavior. As described earlier, load cells at top and bottom of the columns enabled measurement of all reactions, and hence all moments and shears in the specimen. Linear variable differential transducers were used to measure the rotation of the slab relative to the column at interior and exterior connections and to monitor rotation of the slab edge at one exterior connection. Numerous strain gages were attached to the reinforcement around the connections to

18

monitor the extent of yielding in the slab reinforcement. Slab vertical deflections and column lateral deflections were also monitored throughout each specimen test.

Table 2.1 - Test Specimen Configuration and Variables
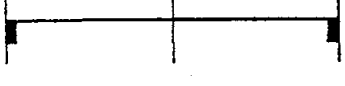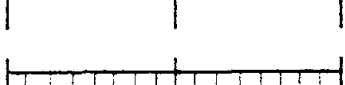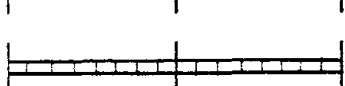
Spec No.	Specimen Configuration	Specimen Variable and Description
1		Control Specimen
2C		Control Specimen
3SE		Stiff Edge Beam at Exterior Slab-Column Connection
4S		Closed Hoop Stirrups as Slab Shear Reinforcement
5SO		Slab Overhang beyond Exterior Connection
6LL		Increased Slab Gravity Load (Heaviest load)
7L		Increased Slab Gravity Load (Intermediate load)
8I		Individual Interior Connection
9E		Individual Exterior Connection

Table 2.2 - Concrete Mix Design

Concrete Mix Proportions per cuyd of Concrete

1 inch Limestone	1800 lb
ASTM Graded Sand	1475 lb
Portland Cement	470 lb
Water	32 gal
PSI Retarder	10 oz

Table 2.3 - Mean Concrete Test Results

Spec. No.	f_c' at 28 days (psi)	Age at test (days)	f_c' at time of test (psi)	Split Cylinder		Modulus of Rupture	
				f_s (psi)	$f_s/\sqrt{f_c'}$	f_r (psi)	$f_r/\sqrt{f_c'}$
1	5275	249	5510	--	--	689	9.28
2C	4460	184	4790	382	5.52	663	9.58
3SE	5890	233	6380	435	5.45	650	8.14
4S	5730	248	6360	514	6.45	641	8.04
5SO	5308	53	5506	493	6.64	544	7.33
6LL	4440	40	4670	467	6.83	542	7.93
7L	4050	41	4460	451	6.75	567	8.49
8I	5320	55	5700	529	7.01	541	7.17
9E	5320	70	5700	529	7.01	541	7.17

Table 2.4 - Reinforcement Properties

Batch	Spec. Nos.	Bar Size	No. Tested	Area A_s (in^2)	Mean f_y (Ksi)	Mean f_u (Ksi)	Elastic Modulus E_s (Ksi)
1	1 → 5	#3 Type 2	5	0.1124	72.55	116.1	27 400
2	6 → 9	#3 Type 2	5	0.1168	76.13	116.9	29 460
1 & 2	All	#2 smooth	6	0.0475	46.67	59.1	29 500

CHAPTER 3

TEST RESULTS AND OBSERVATIONS

3.1 Introduction

A large amount of information was gained from observation and instrumentation during each of the nine specimen tests. It was not possible to report all of the results in this document. Instead, a number of important study areas, which are currently under investigation by various researchers and designers, were selected for in-depth investigation. These study areas are discussed in the remaining chapters of this document. The test results pertinent to each study area are therefore presented and discussed in detail in those chapters.

In addition, there are a number of important topics that deserve investigation. Where it was not possible to study these topics in detail, the observations and results are presented in the latter sections of this chapter. These areas warrant further study and the results and observations presented in these sections are intended as the beginning of such in depth study.

21

As an introduction to the specific study areas mentioned above, a general description of the behavior of each test specimen is necessary. The first part of this chapter covers the basic test observations and results for each of the specimens without attempting to analyse them in depth. Many of the results presented here will appear again in one or more of the subsequent study areas.

3.2 Crack Patterns

The crack patterns for all nine specimens are shown diagrammatically in Figs. 3.1 to 3.8. For each specimen (except 6LL and 7L), crack patterns are shown at 1.5 percent drift and 3.5 percent drift. For specimen 2C, crack patterns are given at various drift levels to illustrate the general progression of cracking in the typical specimen.

Generally the specimens were uncracked at the start of the test. On application of the slab gravity load, cracks occured in some of the specimens at the face of the interior connection. As lateral load was applied, the crack patterns developed into those shown in the figures. At the 1.5 percent drift level, a number of major flexural and diagonal cracks had formed at both interior and exterior connections. These cracks extended and opened while new cracks formed at increased drift levels.

By the 3.5 percent drift level, the crack patterns were generally fully developed. At higher drift levels, the existing cracks widened but few new cracks formed.

3.2.1 Interior connection cracking

The crack patterns at all the interior connections were very similar. The top surface cracks consisted of a combination of flexural cracks transverse to the direction of loading and diagonal cracks radiating from the column. In addition, a longitudinal crack formed along the centerline of the specimen extending from the column face. This crack was the result of the transverse moment caused by the slab gravity loads and the transverse tension discussed later in chapter 6 on modelling the interior connection load transfer.

The bottom surface of the slab remained uncracked for the initial small drift cycles. Once the lateral load was sufficient to cause a net sagging moment at the connection, flexural cracks formed across the full width of the slab. These cracks formed at the position of maximum moment. As the drift level increased, more and more of these cracks formed until the bottom surface of the specimen was cracked almost to midspan as shown in the figures.

3.2.2 Exterior connection cracking

The first cracks to form at the typical flat plate exterior connections during the initial small drift cycles were a flexural crack across the face of the column and diagonal torsion cracks from the side of the column to the slab edge. These cracks controlled the behavior of the connection throughout the loading history. Other flexural and torsional cracks formed as shown in the above figures, but the dominant cracks were those immediately around the column.

The torsional crack across the slab top surface spread down the back of the slab edge at about 45 degrees to the vertical. At higher drift levels this crack continued to the bottom face of the slab.

A similar crack pattern developed on the bottom of the slab but at a higher drift level, once the initial hogging moment due to slab gravity load had been overcome.

At higher drift levels, the cover over the slab edge began to spall between the torsion cracks resulting in exposure of the edge stirrups and the transverse reinforcement. The slab longitudinal reinforcement had been detailed to hook inside the slab edge reinforcement so protecting the anchorage against pull-out. Anchorage pull-out would have occured had the longitudinal reinforcement been hooked beyond the edge reinforcement.

Exceptions to the above description of edge connection cracking were observed in specimens 3SE and 5SO. In specimen 3SE with the stiff edge beam, the slab cracked in flexure across the entire width of the slab at the face of the edge beam (Fig. 3.3). No torsional cracks formed in the edge beam until large drift levels were reached. Subsequent slab flexural cracks formed along the lines of transverse slab reinforcement.

In Specimen 5SO, the crack pattern at the exterior connections was similar to the specimens without slab overhang except that the torsional cracks in specimen 5SO extended from the column to the slab edge, 10 inches beyond the outer face of the column (Fig. 3.5). In addition, a more pronounced series of torsional cracks formed on the bottom of the slab due to reverse bending than was observed in the specimens without edge overhang.

3.3 Cyclic plots of test results

3.3.1 General

Plotting the applied lateral load against the lateral drift for each of the test specimens resulted in Figs. 3.9 to 3.17. The results for all specimens are plotted on the same scale for ease of comparison. Any sudden changes in the specimen behavior due to connection failure are highlighted. Some of

26

these figures will be discussed more fully in subsequent chapters. A general introduction to the differences between the various specimen plots is presented below.

3.3.2 Load-drift Plots

The general form of the load-drift relationships for the various specimens was fairly similar. Slab cracking occured very early in the test and extended during each displacement cycle as discussed above. There was therefore no distinct cracking point as might be expected with a beam section. In addition, flexural yielding of the slab longitudinal reinforcement progressed gradually from the center bars outward across the slab. No distinct yielding point could be identified on the load-drift plots. Instead, the slope of the loading envelope gradually decreased until the peak load was reached.

If punching shear failure occured at one of the connections at peak load, the lateral load dropped dramatically and was never recovered during subsequent larger drift cycles. This was the case in specimens 5O, 6LL and 7L.

In the other specimens, the post peak-load response was characterised by a gradual decrease in load carrying capacity until failure of one of the connections, or termination of the test due to excessive drift.

3.4 Comparison of Specimens

For easier comparison of the various specimens, the above load-drift relationships were plotted in envelope form in Fig. 3.18. The allocation of loading direction as positive and negative is purely arbitrary but indicates load applied in opposite directions. Each of the combined specimens is compared below with the control specimen, 2C.

Specimen 3SE sustained the highest lateral load of all specimens with peak load 24 percent greater than specimen 2C. This was attributed to the stiff edge beams at the exterior connections which forced flexural failure across the full slab width at the face of the exterior column in contrast to the torsional failure of the slab edge adjacent to the exterior column observed in the control specimen. This also resulted in a higher shear at the interior connection and caused the punching failure which had not occured in the control specimen. After punching failure of the interior connection of specimen 3SE at 4 percent drift, the lateral load dropped to 70 percent of the peak load.

Specimen 4S displayed behavior very similar to the control specimen up until peak load at about 3.5 percent drift. In the positive loading direction the specimen carried slightly more load than specimen 2C, but exactly the same load in the negative direction. After peak load, the load capacity of specimen 4S

did not decrease as quickly as the control specimen or any of the other specimens. This was the result of the slab stirrups at both interior and exterior connections providing confinement for the concrete in the slab around the columns. This confinement prevented sudden collapse due to punching shear failure and delayed the deterioration of the concrete in the flexural compression zone, thus maintaining the flexural capacity of the column strips.

Specimen 5SO displayed initial behavior similar to specimen 3SE with the stiff edge beam. The peak load at 3.5 percent drift is on average 16 percent greater than that for specimen 2C. At peak load, the interior connection suffered punching shear failure resulting in a substantial drop in the lateral load. During subsequent cycles to larger drift levels, the lateral load never exceeded 70 percent of the peak load. Again the stiffer edge condition increased the overall lateral load carrying capacity of the specimen. As with specimen 3SE, the stiff exterior connection also resulted in higher shear transfer to the interior connection resulting in punching shear failure of this connection.

Specimen 6LL was subjected to the highest level of slab gravity loading used in this project. In all other respects it was identical to the control specimen, 2C. The interior connection of specimen 6LL failed in punching shear at 1 percent drift with a lateral load of only 48 percent of specimen 2C.

The exterior connections failed in punching shear at 2 percent drift. The effect of the increased gravity load on the behavior of this specimen and specimen 7L is discussed in greater detail in subsequent chapters.

Specimen 7L was subjected to a slab gravity load midway between that of the control specimen and specimen 6LL. The behavior was similar to that of specimen 6LL as discussed in greater detail later. The interior connection failed in punching shear at 1.5 percent drift with a lateral load 65 percent of the peak lateral load for specimen 2C.

3.5 Exterior connection edge condition

3.5.1 General

Because of exterior wall loads or deflection criteria along the slab edge, an edge beam with depth greater than the slab thickness is often provided around the exterior of a flat slab. Depending on its torsional stiffness, this edge beam may significantly alter the performance of the exterior slab-column connection (Ref. 3.1). In some instances when the exterior wall system is light and supported on the slab edge beyond the columns, an edge beam may not be neccesary. The slab edge would project beyond the exterior column to provide support for the exterior wall. Both of these conditions were considered in this research.

3.5.2 Stiff edge beam behavior

In specimen 3SE, a torsionally stiff edge beam was included at both exterior connections. The edge beam was designed with a cracking torsion equal to the moment capacity of half the slab width. It was intended to simulate a stiff edge beam or wall integral with the slab. The edge beam was 8 inches wide by 12 inches deep. The edge beam was also reinforced so that any cracks would not open significantly. The edge beam reinforcement is shown in Photo. 2.5.

At very low drift levels, a flexural crack formed across the full slab width at the face of the edge beam. As the test progressed, other flexural cracks formed parallel to the slab edge, generally positioned over transverse top reinforcement. The crack at the edge beam continued to widen until the full flexural capacity of the slab was reached (Photo 3.1). The overall lateral load resisted by this specimen was higher than any other specimen in the test program. This was due to the increased strength and stiffness of the exterior connections.

The large slab moment at the exterior connections resulted in increased shear at the face of the interior column. This increased shear resulted in the punching shear failure of the interior connection at 3.5 percent drift (Photo 3.2). In

contrast, the control specimen, 2C, with weaker edge condition, did not experience punching shear failure at the interior connection (Photo 3.3).

During the test of specimen 3SE, the edge beam remained uncracked until large drift levels at which point hairline torsional cracks formed on the exterior face of the beam.

3.5.3 Slab overhang behavior

The slab overhang beyond the exterior column was reinforced as shown in Photo. 2.8. The "beam" in the slab edge was still located at the column, however the slab longitudinal reinforcement was hooked at the end of the overhang. The slab overhang in this specimen was 10 inches which equals the column dimension or approximately two times the slab thickness.

During the test of this specimen, similarities were observed with both the control specimen, 2C, and specimen 3SE with stiff edge beam. The cracking pattern shown in Fig. 3.5 included both flexural cracks across the entire slab width at the face of the column and torsional cracks from the column to the slab edge. As with specimen 3SE, the interior connection of this specimen failed in punching shear at 3.5 percent drift (Photo 3.4). The edge connections did not display any punching failure even at a drift level of 7 percent (Photo 3.5).

3.5.4 Edge rotation

In order to measure the rotation of the edge beam at different distances from the connection, six linear variable displacement transducers (LVDTs) were suspended from the rigid test frame above the specimen and attached to the slab top surface at locations shown in Fig. 3.19. These LVDTs were placed at 8 inches on center beginning 8 inches form the side face of the column. By comparing the readings from two gages on either side of the edge beam, the rotation of the edge beam relative to its initial position was obtained. From the six LVDTs therefore, three rotation measurements were obtained at 8, 16 and 24 inches from the column. In addition, based on the assumption that the columns are considerably more rigid than the slab, the rotation of the column and connection could be estimated from the drift of the specimen. In other words, the connection rotation is $\theta_t = arctan(Drift/Height) = arctan(Dr/60)$. The peak drift rotation measurements were plotted against the drift level as shown in Figs. 3.20 to 3.27. The straight line through the origin represents the rotation of the connection.

Fig. 3.21 shows the behavior of the slab edge in specimen 2C. The slab edge 8 inches from the column had less than half the rotation of the column. More distant sections had even lower rotations. Substantial rotational deformation had therefore occured between the column and a section 8 inches away. This was the result of the torsional cracking that formed

at very low drift levels and continued to increase throughout the test. By the peak drift of 3.5 percent, the rotation of the section 8 inches from the column was 35 percent of the column rotation. At higher drift levels, the torsional stiffness of the edge deteriorated rapidly until at 5 percent drift, the section 8 inches from the connection had only 17 percent of the column rotation. Considerable torsional cracking in the slab edge within the first 8 inches from the face of the column had torsionally released the slab beyond this distance. A similar behaviour was observed in the negative loading direction, though the deterioration of the slab edge subsequent to peak load was not as pronounced.

The edge rotations for the stiff edge beam in specimen 3SE are shown in Fig. 3.22. In contrast to specimen 2C, the edge rotations were very similar to the column rotation at all drift levels and for all sections along the edge beam. Clearly the edge beam behaved as a rigid member integral with the column. The slight offset in the rotations at low drift were the result of "slack" in the test setup supports.

Fig. 3.24 shows the results for specimen 5SO with slab overhang. The edge rotations were between those measured for the previous two specimens. The edge was not as stiff as the edge beams of specimen 3SE but also not as flexible as those of specimen 2C. However, at high drift levels, the slab overhang tended to display similar characteristics to the stiff edge

beams. They were not subject to the apparent loss of torsional integrity as seen in specimen 2C. By peak lateral load at 3.5 percent drift, the slab section 8 inches from the column had 60 percent of the column rotation. At 5 percent drift, this ratio had only decreased to 50 percent. By adding additional slab width to resist torsion, the specimen with the overhang did not suffer the same torsional failure of the slab edge seen in specimen 2C.

3.5.5 Edge beam stirrup strains

In each of the test specimens, two strain gages were placed on the vertical legs of stirrups adjacent to the exterior column. The postioning of these strain gages is shown as gages 1 and 2 in Fig. 3.26. For specimens 2C, 3SE and 5SO, the strains measured by gages 1 and 2 are plotted in Fig. 3.27 for each drift level. Gage 2 in specimen 3SE was damaged during fabrication of the specimen and so no readings were obtained for the strain in that stirrup.

The slab edge stirrups in the control specimen, 2(1) and 2(2), experienced a gradual increase in strain after the first torsional cracks appeared at the exterior connection. By peak lateral load at 3.5 percent drift, gage 2(1) had reached the yield strain and continued to experience increased strains at higher drift levels. The torsional capacity of the slab edge adjacent to the column had therefore developed fully.

Specimen 3SE with the stiff edge beam experienced almost no strain in the beam strirrup. This was to be expected since the beam was sized to avoid torsional cracking under peak load. Only hairline cracks were observed on the edge beam at high drift levels.

The stirrups in specimen 5SO experienced strains between those of the previous two specimens. Gage 5(1) measured only very small strains while gage 5(2) measured strains of up to 75 percent of the yield strain. The torsional cracking of this exterior connection was less extensive than that of specimen 2C though still sufficient to require contribution from the stirrup reinforcement.

3.5.6 Conclusions

From the above discussion of edge conditions, the following observations can be made.

1. The subassemblies with stiff edge beam and slab overhang at the exterior connections carried higher lateral loads than the control specimen.

2. The increased stiffness of the exterior connections with edge beam or slab overhang resulted in higher slab moments at these connections. This in turn increased the slab shear at the interior connection and so contibuted to the punching shear failure of the interior connection.

3. The inconvenience of forming the stiff edge beam is likely to make it an unattractive option for many applications even though it clearly provides excellent protection of the exterior connection against deterioration during cyclic loading. However, the slab overhang beyond the exterior connection was able to provide similar advantages to the stiff edge beam without the drawback of complex fabrication. Clearly this presents a realistic economical alternative which should be studied further.

3.6 Slab Shear Reinforcement

3.6.1 General

According to the ACI code, if the shear stress on the slab critical section defined in Figs. 3.28 and 3.29 exceeds the nominal capacity of the concrete section, $v_c = \phi(2 + 4/\beta_c)\sqrt{f_c'}$, then the connection is inadequate. A number of options are available to the designer to modify the connection so as to satisfy the code requirements.

The geometry of the connection can be altered to increase the area of the slab critical section. This can be achieved by increasing the column size, increasing the slab thickness, or adding a drop panel or column capitol. Increasing column size may be prohibited by architectural considerations. Increasing slab thickness results in increased concrete quantities which in turn result in both higher costs and higher

gravity load on the connection. The addition of a drop panel or column capitol requires less material than thickening the slab, but increases the labor costs and removes one of the main advantages of flat plates, their ease of construction. Architectural clearances and mechanical ducting may also preclude this option.

Shear reinforcement may be added to the slab around the connection. The code allows for shear reinforcement to increase the shear on the connection to $V_n = V_c + V_s$ where $V_c = 2\sqrt{f_c'}\,A_{cs}$ and $V_s = A_v f_y d / s$. The total shear is limited to $V_n \leq 6\sqrt{f_c'}\,A_{cs}\,d$.

Numerous types of shear reinforcement have been used to increase the slab shear capacity in practice. Shear stirrups in the slab adjacent to the connection provide one option. These stirrups may be in the form of closed hoop stirrups as used in conventional beams, open beam stirrups, or galloping stirrups (Fig. 3.30) which provide vertical reinforcement but do not enclose the longitudinal slab reinforcement. Various other arrangements of vertical or inclined slab shear stirrups have also been used in construction (Ref. 3.2).

Bent up bars have also been employed as shear reinforcement (Ref. 3.2). Here the slab bottom reinforcement is bent up to the top of the slab at 45 degrees to the horizontal at some distance from the connection so as to intersect the shear rupture surface.

Disadvantages of the above types of shear reinforcement are the labor cost and time involved in positioning them in the slab. For thinner slabs, the accuracy of placement is critical if the shear reinforcement is to be fully effective. On the whole, designers are advised by the construction industry to avoid slab shear reinforcement if possible. However, it is sometimes necessary to use this solution.

Shear-head reinforcement consists of installing steel sections, usually channels or wide flange sections, at right angles to each other across the connection as shown in Fig. 3.31 (Ref. 3.2). This form of shear reinforcement has the added disadvantage that it involves the introduction of structural steel fabrication and placement into the construction of an otherwise concrete structure.

3.6.2 Test Specimen shear reinforcement

Based on previous laboratory tests (Ref. 3.2, 3.3, 3.4), it was decided to consider only closed hoop stirrups as slab shear reinforcement in this investigation. Islam and Park (Ref. 3.2) found that although all the above types of shear reinforcement increased the shear capacity of the connections under static loads, only closed hoop stirrups provided adequate confinement to the slab concrete to increase the ductility of a connection subjected to cyclic lateral loading.

3.6.3 Observed behavior

The behavior of the exterior connection in specimen 4S with shear stirrups in both slab edge and column strip was not significantly different from that of the control specimen with stirrups only in the slab edge (Photo 3.5). Strain gages were attached to the vertical legs of the slab stirrups at the locations shown in Fig. 3.26. The stirrups in the slab edge (1 and 2) experienced large strains as torsional cracking of the slab edge increased. The stirrups in the column strip (3 and 4) experienced gradually increasing strains as the slab concrete deteriorated due to flexural cracking (Fig. 3.32). It did not appear that the shear capacity of the concrete at the face of the column had been exceeded since there was no rapid transfer of load to the shear reinforcement.

At the interior connection, the slab shear stirrups along the column strip (7 and 8) registered small strains up to 4.0 percent drift (Fig. 3.33). Beyond this point, the strain in these stirrups increased rapidly. This is the point at which the interior connections of specimens 3SE and 5SO failed due to punching shear.

The load-drift envelope for specimen 4S shown in Fig. 3.18 indicates significant inprovement in the specimen behavior after the peak lateral load was reached. The test was continued to 8 percent drift at which point the slab shear stirrups were

still able to provide confinement for the concrete adjacent to the column face (Photo. 3.6). Despite the fact that the unbalanced moment capacity of the section was not significantly affected by the use of stirrups, the ductility of the connection was greatly increased.

Although the closed hoop slab stirrups are inconvenient and costly to place in the slab, they appeared to offer an effective solution to the punching shear problem without requiring adjustment of the geometry of the connection. These observations are made based on the closed hoop stirrups used in this specimen. It is the opinion of the author that "galloping stirrups" or other shear reinforcement which does not confine the main flexural reinforcement will be considerably less effective at preventing deterioration of the connection under cyclic lateral loading conditions. Although some work has been done on alternative shear reinforcement such as headed studs, further research is required to determine the effectiveness of the various forms of shear reinforcement currently in use under earthquake-type loading.

3.6.4 Conclusions

Closed hoop stirrups enclosing the slab flexural reinforcement passing through the interior connection prevented punching shear failure and increased the ductility of the connection. Although the peak lateral load carried by this

specimen was similar to that of the control specimen, the rate of strength deterioration after the peak was greatly reduced by the presence of the closed hoop stirrups.

Although inconvenient to install, closed hoop stirrups offer a viable alternative for increasing connection ductility without altering the connection geometry.
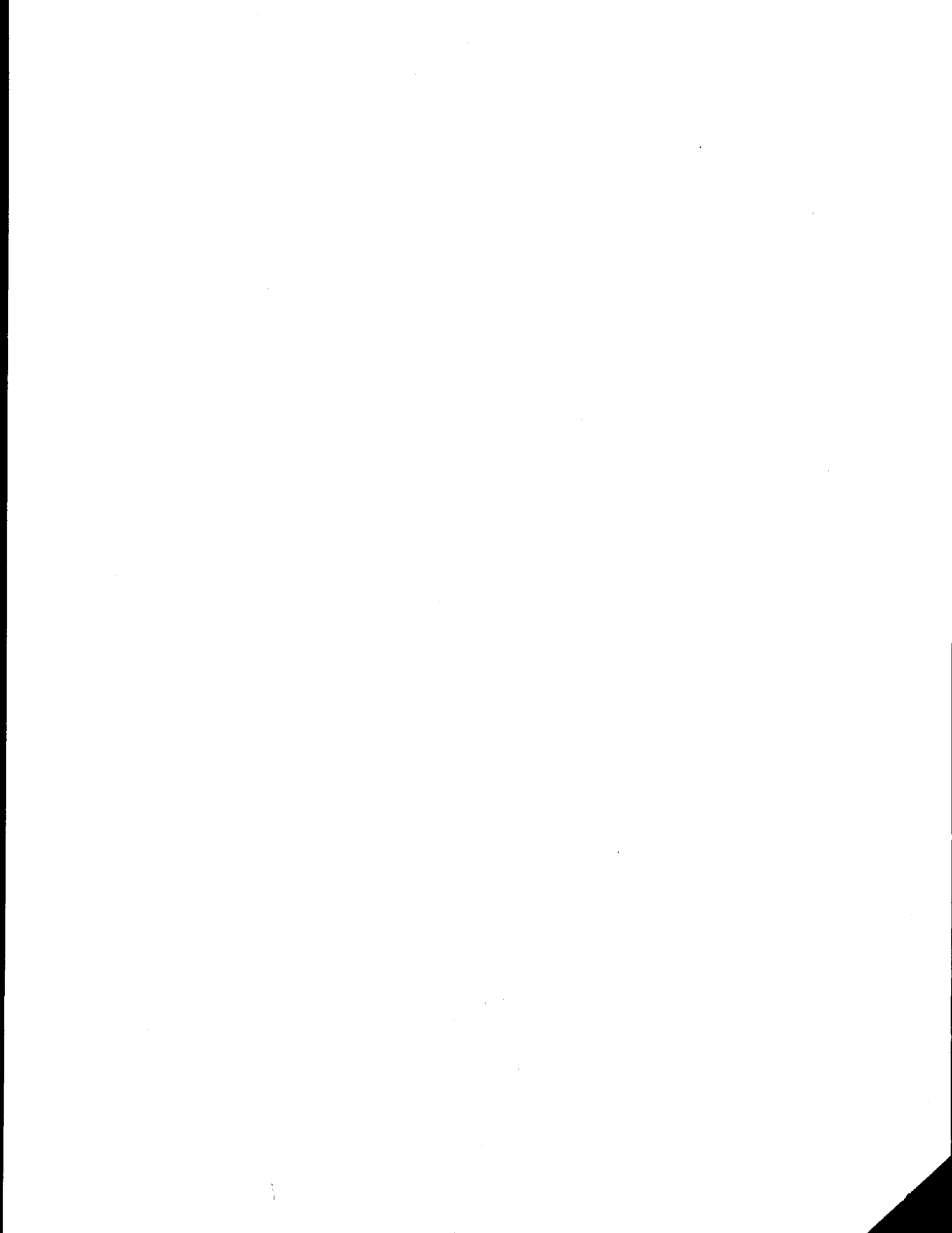
CHAPTER 4

EFFECT OF GRAVITY LOAD ON EXTERIOR CONNECTION BEHAVIOR

4.1 Introduction

The topic investigated in this chapter is the effect of superimposed slab loading on the response of exterior slab-column connections subjected to earthquake-type loading. Present design of exterior slab-column connections is based on the ACI code eccentric shear stress model (Fig. 3.29). This model was developed almost exclusively from results of tests on interior connections (Fig. 3.28). The extension of this approach to exterior connections has come under increased scrutiny (Ref. 4.1).

The recently published recommendations of the ACI Committee 352 (Ref. 1.1) recognize a significant difference between the behavior of exterior and interior connections. Based on recent research (Ref. 4.1) and the analysis of previous data, the 352 Recommendations propose that for exterior connections, the interaction between moment and shear can be ignored. The connection need only be designed for shear and flexure independently with none of the unbalanced moment being transferred by eccentric shear stresses on the critical section.

43

The test results from specimens 2C, the control specimen, 7L, with increased slab gravity load, and 6LL, with heaviest slab gravity load were compared with both the ACI code approach and the Committee 352 Recommendations. The comparisons are presented in this chapter. The effect of increased gravity load on the exterior connection ductility is also considered and drawbacks with present measures of ductility are discussed.

4.2 Exterior Connection Behavior

4.2.1 Gravity Loading

All of the specimens in this research program were subjected to slab loading simulating the full dead load and 30% of the live load of the prototype structure. In the specimens with increased gravity load, additional lead weights were added to the top of the slab. The equivalent uniformly distributed slab loads for each specimen are listed in Table 4.1. Also listed are the direct gravity shear stress, $v_g = V_g / A_{cs}$, and the shear stress based on the eccentric shear stress model of the ACI code including the unbalanced moment.

4.2.2 General Specimen Response

The overall load vs. drift relationships for each of the three specimens, 2C, 7L and 6LL are shown in Fig. 4.1. Significant differences are apparent between the responses of

the three specimens. Specimen 2C with the lightest gravity load, reached a peak lateral load of 19.8 Kips at 3.5% drift. At 4.5% drift, the lateral load had reduced to 18.4 Kips. At 5% drift, the lateral load reduced to 70% of the peak load and the East exterior connection failed in punching shear. Specimen 7L reached peak lateral load of 13.1 Kips at 1.5% drift before sudden punching shear failure of the interior connection. In specimen 6LL, the center connection suffered punching shear failure at 1% drift with a peak lateral load of 9.6 Kips. At 1.5% drift, first East and then West exterior connections failed due to punching shear. The peak loads and corresponding drifts for each specimen are listed in Table 4.2.

Continuous bottom reinforcement through the column acted as hanger bars preventing complete collapse of the slab. After failure of the interior connection, the response of the specimen changed considerably. The specimen was effectively reduced to two exterior connections with a virtual pin support at midspan, resulting in a substantial drop in overall specimen stiffness and strength.

4.2.3 Cracking Pattern

The gravity load was applied to the slab before imposing lateral load to the specimen. Application of the larger slab loads to specimens 7L and 6LL resulted in the formation of a

flexural crack across the slab at the face of the exterior column and torsional cracks from the front corners of the column to the slab edge at about 45 degrees. During the initial displacement cycles, additional flexural and torsional cracks appeared in all three specimens. These cracks spread and opened as each test progressed until the final typical crack pattern developed. In specimen 6LL, punching shear failure occurred along the rupture surface shown in Fig. 4.2. The failure plane extended from the bottom of the slab at the column face to the top of the slab at an angle of about 30 degrees to the horizontal. Considerable spalling of concrete cover was observed beyond the punched surface.

4.2.4 Moment-Drift Relationships

For the exterior connections, the slab moment at the face of the column, is plotted against the drift in Fig. 4.3. These plots are for the West exterior connections. The East exterior connections displayed virtually identical moment-drift relationships and are thus not presented here. The points at which connection failures occurred are highlighted on these plots.

The lateral load in specimens 7L and 6LL, which had higher gravity loads, reached the maximum value immediately prior to failure of the interior connection. The peak unbalanced moments

and associated peak drifts and shears at the exterior connections prior to failure of the interior connections are listed in Table 4.2 for both West and East connections and also highlighted on the plots. After failure of the interior connection, the exterior connections experienced slightly higher moments, though lower associated shears, at increased drift levels before failure of the exterior connections. These moments and the associated shears and drift levels are shown in parenthesis in Table 4.2. Because of the significant change in the specimen response after failure of the interior connection, the discussion that follows is based on the observed moments and shears at peak lateral load and not these subsequent maximum values.

4.2.5 Reinforcement Strains

Strain gages were attached to the slab flexural reinforcement across the slab width at the face of the exterior column. The distribution of strain in this reinforcement at drift levels of 1 percent and 2 percent is shown in Fig. 4.4. At 1% drift, only the center bar in specimen 6LL had yielded as a result of the high static moment due to gravity load. At 2% drift, well before failure of the connection, the exterior connection in specimen 2C had experienced yielding in all the slab top reinforcement in a strip $c_2 + 3h$ wide centered on the column. At 2% drift, specimen 7L experienced yield strains in all the

reinforcing bars passing through the column and very close to yield strains in the bars immediately adjacent to the column. In specimen 6LL, yielding had not spread beyond the center slab reinforcing bar prior to failure of the connection in punching at 1.5% drift.

Strain gages attached to the edge beam stirrups adjacent to the column recorded strains in excess of the yield strain in all three specimens well before failure of the connections. This indicated that the full torsional capacity of the slab edge adjacent to the column had been mobilized.

Specimens 7L and 6LL experienced large connection rotations at low drift levels as a result of the high gravity load. The torsional capacity of the edge beams was therefore fully developed prior to connection failure while limited flexural yielding had occurred. In specimen 2C, the torsional strength of the slab edge developed at higher drift levels. Initially, the connection moment was carried predominantly by the flexural capacity of the slab at the face of the column resulting in widespread yielding of the slab flexural reinforcement. By the peak drift of 3.5%, the torsional capacity of the slab edge adjacent to the column had also developed fully.

4.3 Connection Strength

4.3.1 Flexural strength

The exterior connections in all three specimens reached the full torsional capacity of the slab edges prior to any punching shear failure. Yielding of slab flexural reinforcement passing through the column had also occurred prior to connection failure though the extent of yielding was more limited in the specimens with higher gravity load. The full flexural capacity of the slab-column connection can therefore be considered to consist of two parts. Firstly, the torsional capacity of the slab edges, T_n, which has contributions from concrete, T_c, and torsional reinforcement, T_s. Using the ACI code approach (Eqn. 11-21, Ref. 1.2) produces values for T_n listed in Table 4.2. The second component is the flexural capacity of the slab at the column face, M_{fl}. Slab reinforcement passing within $h/2$ of the side face of the column is anchored in slab concrete integral with the column and is therefore unaffected by the torsional yielding of the slab edge. Therefore, the values for M_{fl} given in Table 4.2 are based on a slab width of $c_2 + h$ centered on the column. The theoretical moment capacity of the connection is then $M_{th} = M_{fl} + 2T_n$ listed in Table 4.2. The ratio between the moment measured at the column face, M_{cf},

and the theoretical moment capacity, M_{th}, are listed in Table 4.2. The ratios range from 1.00 to 1.38 and are compared with the connection shear ratios below.

4.3.2 Shear Strength

The observed peak direct shear stresses acting on an assumed critical section through the slab at $d/2$ from the column face are given in Table 4.2. The direct shear stress is computed as $v_u = V_u / A_{cs}$ where V_u = slab shear measured at the connection at peak lateral load, and A_{cs} = area of slab critical section. These stresses vary from 85 psi or $1.2\sqrt{f_c'}$ for specimen 2C, to 136 psi or $2\sqrt{f_c'}$ for specimen 6LL. The ACI code suggests a theoretical value for concrete shear strength in slabs of $V_o = 4\sqrt{f_c'} b_o d_{ave}$ for square columns as in this study, where b_o = perimeter of the critical section and d_{ave} = average effective depth of tension reinforcement. However, the limit for shear stress of $v_c = 4\sqrt{f_c'}$ in slabs as opposed to $v_c = 2\sqrt{f_c'}$ for beams is based predominantly on research performed on interior connections where the surrounding slab provides in-plane confinement of the failure surface.

As indicated by these tests, when torsional yielding occurred in the slab edge resulting in large torsional cracks, the in-plane confinement is greatly reduced and a shear stress of $v_c = 4\sqrt{f_c'}$ can no longer be sustained. Similar observations have

been made with regard to interior connections subjected to high gravity shear stresses and high levels of drift (Ref. 4.2). The observed peak direct shear stress in specimen 6LL, which failed due to punching shear, is $v_c = 2\sqrt{f_c'}$. This value is then compared in Table 4.2 with the measured peak direct shear stress acting at the connections, v_u.

4.3.3 Moment - Shear Interaction

The moment ratio, M_{cf}/M_{th}, is plotted against the shear ratio, v_u/v_c, in Fig. 4.5. For points falling above a 45 degree line through the origin, flexural strength governs the connection behavior, whereas below this line, punching shear stresses control. The peak values for all specimens fall above this line and so flexural failure is predicted for all connections. The plotted points for East exterior connection of specimen 6LL lie closest to the line dividing flexural and punching failure. This connection experienced a punching shear failure followed by a similar failure at the West connection. The exterior connections of specimens 2C and 7L all experienced flexural failures as predicted by the plotted theoretical values.

The procedure outlined above for calculation of flexural strength and shear strength of an exterior connection therefore provides a useful guide to the probable failure mechanism. It

will be necessary to apply this procedure to other test data to establish its applicability to different connection arrangements and parameters.

4.3.4 Comparison with ACI Code

In Table 4.3, the observed peak strengths of all six exterior connections are compared with the ACI calculated strengths. The peak shear stresses around the critical perimeter, v_{AB} and v_{CD}, are computed from the measured direct shear, V_u, plus portion of the unbalanced moment, $\gamma_f M_{ub}$, using the code prescribed eccentric shear stress model (Fig. 3.31). These shear stresses are compared with the code value of $v_c = 4\sqrt{f_c'}$. The remaining portion of the unbalanced moment is compared with the ultimate flexural strength, M_{f2}, of a strip of slab $c_2 + 3h$ wide centered on the column. According to the ACI code approach, the maximum of these three strength ratios controls the connection capacity with failure of the connection anticipated when this value reaches unity. These ratios are plotted against V_u/V_o in Fig. 4.6, along with a number of other researchers results as compiled by Pan and Moehle (Ref. 4.2).

In all three specimens, the measured capacity is equal to or greater than the ACI calculated strengths by ratios from 1.00 to 1.27. However, in all cases, the controlling strength

ratio is the shear on the critical perimeter. This is contrary to the observed behavior of specimen 2C which did not experience punching failure.

4.3.5 Comparison with ACI Committee 352 Recommendations

The recently published ACI Committee 352 Recommendations (Ref. 1.1) suggested a simplified design approach for exterior connections subjected to combined shear and unbalanced moment perpendicular to the free edge. Following these proposals, Section 5.1.1(b) states that " for resistance to moment transfer perpendicular to the edge,.., sufficient reinforcement should be placed within a width $2c_t + c_2$, centered on the column, to resist the total moment to be transferred to the column at the centroid of the slab critical section,..". Here c_t is the distance from the column front face to the slab edge ($\leq c_1$) and c_1 and c_2 are the column dimensions. For the test specimens, the observed peak moment at the centroid of the slab critical section, M_s, is given Table 4.2 and the flexural capacity of the slab width $2c_t + c_2$, M_{f3}, is given in Table 4.4. The ratio M_s / M_{f3} varies from 1.12 to 1.53 suggesting that the 352 Recommendations underestimate the flexural capacity at the connection.

The limit on shear at exterior connections, V_{352}, is given in Section 4.2.1.2(b), which states, "... edge connections

54

transferring moment only perpendicular to the slab edge may be assumed to have adequate shear strength if the factored direct shear transferred to the column does not exceed $0.75V_o"$, with $V_o = C_v 4\sqrt{f_c'} b_o d$, where $C_v = 0.75$ for connections subjected to load reversals (Section 2.2.2, Type 2). Hence the allowable shear stress for the exterior connections in the test specimens is $v_{352} = 0.75 \times 0.75 \times 4\sqrt{f_c'} = 2.25\sqrt{f_c'}$ This value is similar to that of $v_c = 2\sqrt{f_c'}$ derived earlier from the test results. The 0.75 factors applied to exterior connections subjected to flexural yielding appear to compensate for the loss of in-plane confinement at exterior connections.

The theoretical v_{352} values and the slab shear $V_{352} = v_{352} \times A_{cs}$ are listed in Table 4.4 along with the shear ratio, V_u / V_{352}. Plotting M_s / M_{f3} against V_u / V_{352} results in Fig. 4.7. The flexural strength is always in excess of the theoretical strength by ratios from 1.12 to 1.53 and appears relatively unaffected by the change in shear ratio from 0.55 to 0.88, thus substantiating the Committee 352 assumption that for this range of shear ratios, shear and moment can be considered separately for design purposes.

According to this approach, it is the flexural strength ratio which controls in each specimen. This however contradicts the behavior of specimen 6LL which failed due to punching shear

failure at a direct shear stress of $v_c = 2\sqrt{f_c'}$ prior to significant yielding of the slab flexural reinforcement. The nominal shear stress proposed by Committee 352 for these connections is $v_{352} = 2.25\sqrt{f_c'}$. In order to adjust this value based on the test results reported here, Section 4.2.1.2(b) of the Recommendations may be altered to read "...if the factored direct shear transferred to the column does not exceed $2/3V_o$" in place of $0.75V_o$.

The ACI code eccentric shear stress model considers the centroid of the slab critical section as the critical section for moment calculation (Fig. 3.31). However, if the transfer of moment and shear are separated as suggested by Committee 352, it seems appropriate to define the face of the column as the critical section for flexural strength, M_{cf}. The resulting ratios of M_{cf}/M_{f3} listed in Table 4.4, vary from 0.99 to 1.42 and provide a better approximation to the observed moments than the ratio M_s/M_{f3}.

4.4 Connection Ductility

4.4.1 Drift Capacity

The moment vs drift relationships for exterior connections of each specimen, shown in Fig. 4.3, display dramatically differing drift capacities. The increased slab gravity load reduced the drift capacity of the connection. The drift levels

at which the connections sustained peak moments are listed in Table 4.2. These values are plotted against the shear level, V_u/V_o , along with other researchers' results (Ref. 4.2), in Fig. 4.8.

It is generally accepted that a slab-column connection should have a drift capacity of at least 1.5 percent to ensure adequate performance of the connection even when stiffer lateral load carrying elements are present (Ref. 4.3). Based on the test results shown in Fig. 4.8, the value of V_u/V_o must be less than 0.50 for an exterior connection to provide this drift capacity. The Committee 352 Recommendations suggest a limit of $V_u/V_o = 0.4$ which is based on tests performed on interior connections (Ref. 4.2). Based on the test results reported here, this limit appears conservative.

4.4.2 Displacement Ductility

Traditionally the ductility of slab-column connections has been specified as the ratio between the drift at connection failure and the drift at first yielding of slab reinforcement. The concept of displacement ductility for slab-column connections has been carried over from tests on beam-column connections in which beam flexural reinforcement yields prior

to failure of the connection or shear failure. As demonstrated by these tests, the slab may well fail in punching shear prior to yielding of the steel in the column strip.

Since the yield point in slabs is not well defined, some arbitrary procedure is generally required to define the yield drift, D_y. One such definition (Ref. 4.2) is shown in Fig. 4.9. The yield drifts for each specimen based on this approach are listed in Table 4.5. The definition of the ultimate drift is also very subjective. The ultimate drift can be taken either as the drift corresponding to the peak lateral load, D_p, or as the drift at which the lateral load has dropped below some percentage of the peak load, such as 80% , D_u (Ref. 4.4). The yield and ultimate drifts calculated based on this approach and the displacement ductility obtained either from D_p/D_y or D_u/D_y are given in Table 4.5. Specimens 7L and 6LL with higher gravity load displayed less ductile behavior than specimen 2C. The exterior connections of specimen 6LL failed as a result of punching shear prior to significant flexural yielding and should therefore have a ductility of 1.0 or less. Based on this approach, the calculated displacement ductility of 2.0 for specimen 6LL could be misleading.

4.4.3 Rotational Capacity

Although the inter-story drift capacity is a convenient design driterion, it does not relate directly to the rotational capacity of the slab-column connection. A significant portion of the measured drift can result from column flexural deformation. With relatively stiff columns as used in these tests and commonly found in practice, such contribution to drift is relatively small.

Perhaps a more rational approach to the determination of connection ductility is to use the rotational capacity of the connection. During each test, the relative rotation between the West column face and a vertical plane through the slab 6 in. from the column face was measured by means of LVDTs above and below the slab. Figure 4.10 shows the slab moment at the face of the column plotted against the rotation for all three West exterior connections. The rotation at peak load for each specimen, θ_p, is listed in Table 4.5. All three specimens achieved maximum moment at about the same joint rotation with an average of 0.03 radians suggesting that exterior connections therefore achieved the same peak rotation regardless of whether failure occurred as a result of high drift, as in specimen 2C, or from a combination of high gravity load and low drift, as in specimen 6LL. To avoid failure of an exterior connection in the test specimens, the maximum relative rotation between

slab and column would therefore need to be limited to 0.03 radians under gravity and lateral loads. The prediction of this rotation by analytical procedures is however dependant on assumptions made regarding the extent of slab cracking around the connection. Further development of analytical representation of the connection region is therefore required before this observation can be used in design procedures.

4.5 Conclusions

Three identical two-bay flat-plate subassemblies were subjected to the same lateral displacement history while each supported a different superimposed gravity load. From observed behavior of the test subassemblies, the following conclusions were drawn regarding the exterior slab-column connections.

1. For exterior connections designed for seismic resistance using present ACI Code provisions, ductile flexural failure and adequate drift capacity of 1.5 percent can be achieved only if the ultimate direct shear on the critical perimeter is limited to $V_u = 2\sqrt{f'_c}b_o d$. The direct shear is the column axial force below the slab minus the column axial force above the slab. A higher direct shear resulted in slab punching shear failure prior to significant yielding of slab flexural reinforcement and at a drift level less than 1.5 percent.

2. Measurement of relative rotation between the column and slab showed that the exterior connections reached their peak moment capacity at the same rotation level (0.03 radians for the specimens in these tests), despite the variation in gravity loading. With light gravity load, as in specimen 2C, the rotation due to gravity load is small and hence a higher lateral drift can be achieved before reaching the ultimate rotation capacity of the connection. When the gravity load is high, as in specimen 6LL, the slab rotation due to the gravity load alone can be a substantial portion of the peak rotation resulting in connection failure at a much smaller lateral drift level.

3. The strength of exterior connections in all specimens was observed to be 1.0 to 1.27 times the strength calculated using the linear shear stress variation model prescribed by the ACI code. According to this model, the controlling factor in all cases was the shear stress at the critical perimeter. However, the exterior connections of specimens 2C and 7L experienced flexural failures indicating that less of the moment is transfered by eccentric shear than assumed be the ACI model.

4. For the range of shear stress levels studied in these tests, the Committee 352 recommendation that moment and shear could be treated independently for design of exterior connections appears reasonable, though slightly conservative

with respect to flexural capacity and unconservative with respect to shear capacity. The measured flexural strength of the slab exceeded the theoretical capacity by a factor of 1.12 to 1.53. Using this procedure, flexural failure of the slab would be predicted for all three specimens. In reality, however, specimen 6LL failed in punching shear before the significant flexural yielding of slab reinforcement.

5. A better estimate of the ultimate moment transfer capacity of the exterior connections was obtained by combining the torsional capacity of the slab edge with the flexural capacity of a slab strip $c_2 + h$ wide centered on the column. In conjunction with a limiting direct shear of $V_u = 2\sqrt{f_c'}b_o d$, this approach gave an indication of the mode of failure for the exterior connections of each specimen.

Table 4.1 - Test Specimen Properties

Spec No.	Material Properties			Reinforcement Ratios (%)			Superimposed Slab Load (psf)		Gravity Shear at Ext. Conn.				
	f'_c (psi)	f_y (psi)	d_{ave} (in)	ρ_l	ρ_c	ρ_t	Proto-type	Model	V_g (Kips)	v_g (psi)	v_g ($\sqrt{f'_c}$)	incl. M_{ub} (psi)	incl. M_{ub} ($\sqrt{f'_c}$)
2C	4790	72.6	3.6	0.31	0.83	0.83	40	140	7.0	49.8	0.72	70.0	1.01
7L	4460	76.1	3.6	0.31	0.83	0.83	120	285	11.8	83.9	1.26	148.9	2.23
6LL	4670	76.1	3.6	0.31	0.83	0.83	220	420	17.1	121.6	1.78	218.7	3.20

62

Table 4.2 - Exterior Connection Test Results

| Ext Conn | f_c' (psi) | Peak Drift (%) | Peak Load (Kips) | Observed Values | | | | | Theoretical Values | | | | Ratios | |
| | | | | Peak Shear | | Peak Moment (K-in) | | | Shear | Moment (K-in) | | | Shear | Moment |
				V_u (Kips)	$v_u = \dfrac{V_u}{A_{cs}}$ (psi)	M_u	M_s	M_{cf}	$v_c = 2\sqrt{f_c'}$ (psi)	T_n	M_{fl}	M_{th}	$\dfrac{v_u}{v_c}$	$\dfrac{M_{cf}}{M_{th}}$
2-w	4790	3.5	19.8	12.3	88	352	314	291	138	35	148	218	0.63	1.33
2-e	4790	3.5	18.9	12.0	85	361	324	301	138	35	148	218	0.62	1.38
7-w	4460	1.5 (2.0)	12.5	15.0 (12.8)	107 (91)	310 (336)	263 (296)	235 (272)	134	34	158	227	0.80 (0.68)	1.04 (1.20)
7-e	4460	1.5 (1.8)	13.1	15.2 (12.4)	108 (88)	303 (298)	256 (259)	227 (236)	134	34	158	227	0.81 (0.66)	1.00 (1.04)
6-w	4670	1.0 (1.5)	8.2	17.8 (17.2)	127 (122)	344 (362)	289 (308)	255 (276)	137	35	159	229	0.92 (0.89)	1.11 (1.21)
6-e	4670	1.0 (1.5)	9.6	19.1 (17.7)	136 (126)	336 (366)	277 (311)	241 (278)	137	35	159	229	0.99 (0.92)	1.05 (1.21)

Table 4.3 - Comparison with the ACI Code Procedure for Exterior Connection Design

Ext. Conn.	ACI Shear level		ACI Moment	Strength Ratios,			
	$v_c = 4\sqrt{f_c'}$ (psi)	$\dfrac{v_u}{v_o}$	M_{f2} (c_2+3h) (K-in)	$\dfrac{v_{AB}}{v_c}$	$\dfrac{v_{CD}}{v_c}$	$\dfrac{\gamma_f M_s}{M_{f2}}$	Max Ratio
2-w	277	0.32	209	1.03	1.21	0.92	1.21
2-e	277	0.31	209	1.04	1.27	0.94	1.27
7-w	267	0.40	224	1.03	1.15	0.80	1.15
7-e	267	0.40	224	1.00	0.98	0.70	1.00
6-w	273	0.46	225	1.15	1.07	0.83	1.15
6-e	273	0.50	225	1.17	1.07	0.83	1.17

Table 4.4 - Comparison with ACI Committee 352 Recommendations for Exterior Connection Design

Ext. Conn.	352 Shear level			352 Moment Ratios		
	$v_{352} =$ $2.25\sqrt{f_c'}$ (psi)	$V_{352} =$ $v_{352} A_{cs}$ (Kips)	$\dfrac{V_u}{V_{352}}$	M_{f3} (c_2+2c_1) (K-in)	$\dfrac{M_s}{M_{f3}}$	$\dfrac{M_{cf}}{M_{f3}}$
2-w	156	21.9	0.56	212	1.48	1.37
2-e	156	21.9	0.54	212	1.53	1.42
7-w	150	21.1	0.71	229	1.15	1.03
7-e	150	21.1	0.72	229	1.12	0.99
6-w	154	21.7	0.82	230	1.26	1.11
6-e	154	21.7	0.88	230	1.20	1.05

Table 4.5 - Exterior Connection Ductility

Ext Conn	Drift Levels (%)			Displacement Ductility		Rotations (Radians)
	Yield D_y	Peak D_p	Ult. D_u	$\mu_p = \dfrac{D_p}{D_y}$	$\mu_u = \dfrac{D_u}{D_y}$	Peak θ_p
2-w	1.24	3.50	5.00	2.82	4.03	0.0319
2-e	1.43	3.50	4.50	2.45	3.15	-
7-w	1.05	2.00	3.00	1.90	2.86	0.0285
7-e	0.89	1.80	2.00	2.02	2.25	-
6-w	0.64	1.50	1.88	2.34	2.94	0.0304
6-e	0.70	1.50	1.81	2.14	2.59	-
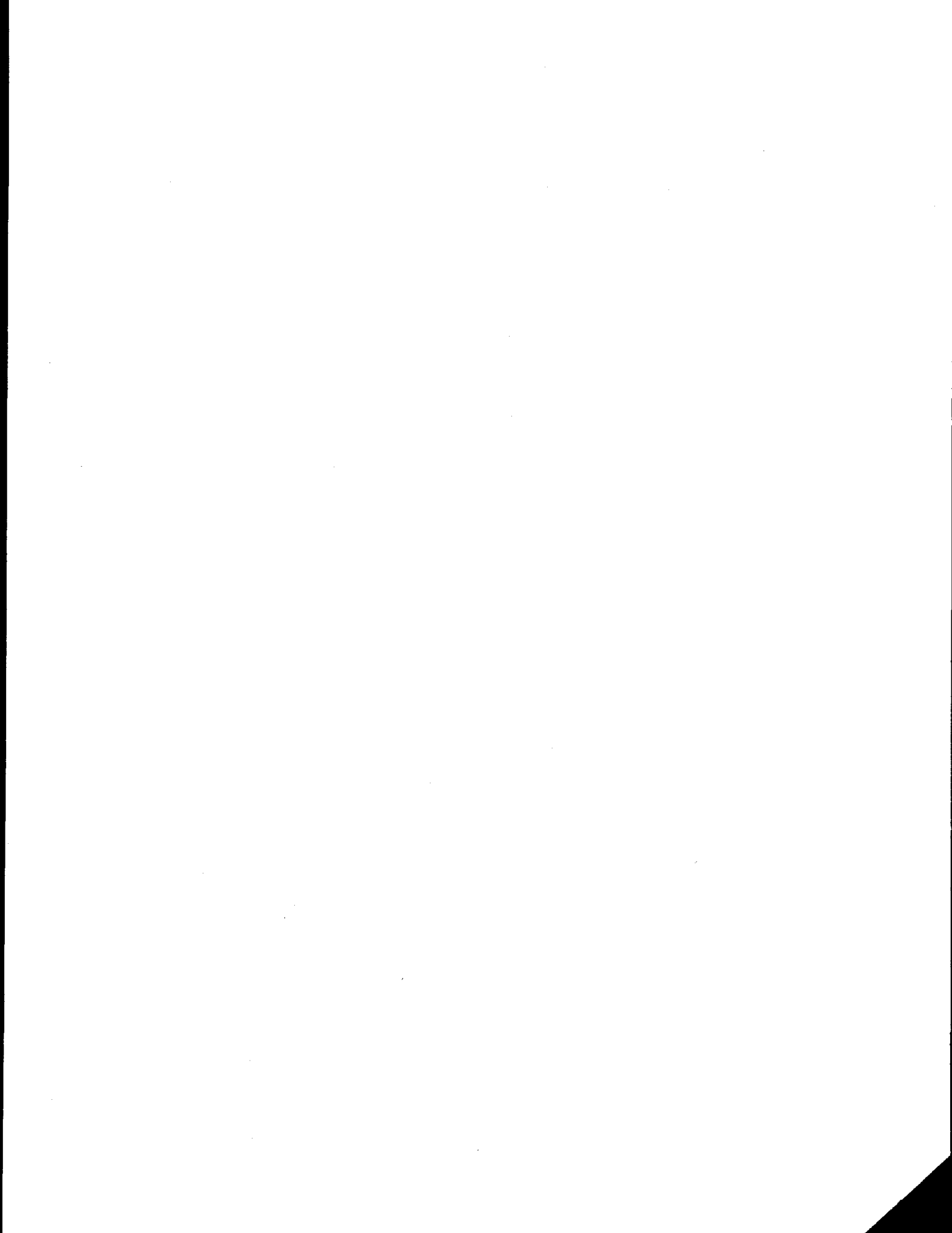
CHAPTER 5

EFFECT OF GRAVITY LOAD ON INTERIOR CONNECTION BEHAVIOR

5.1 Introduction

This chapter presents the effect of gravity load on the behavior of interior slab-column connections subjected to earthquake-type loading. As with the previous chapter on exterior connections, the discussion here is based on the results of tests on specimens 2C, 7L and 6LL, each subjected to a different slab gravity load. The slab loading is listed in Table 5.1 along with other specimen properties pertinent to this topic.

The test results are compared with the ACI code model of eccentric shear stress distribution around a critical perimeter (Fig. 3.30). The effect of gravity load on the connection drift capacity and stiffness are also discussed. A limit on the slab gravity loading is proposed which will ensure adequate drift capacity for interior slab-column connections.

5.2 General Specimen Response

The overall load vs drift relationships for each of the specimens, 2C, 7L and 6LL, are shown in Fig. 4.1. The general specimen response for these specimens was described in the previous chapter. Specimen 2C with the lightest gravity load, experienced flexural failure of the interior connection with no punching shear failure evident at drift levels up to 5 percent. Specimen 7L, with increased gravity load, experienced punching shear failure of the interior connection at 1.5 percent drift. In specimen 6LL, with highest gravity load, the center connection suffered punching shear failure at 1 percent drift. The peak loads and corresponding drifts for each specimen are listed in Table 5.2.

Continuous bottom reinforcement through the column acted as hanger bars preventing complete collapse of the slab. After failure of the interior connection, the response of the specimen changed considerably. The specimen was effectively reduced to two exterior connections with a virtual pin support at midspan, resulting in a substantial drop in overall specimen stiffness and strength.

5.3 Interior Connection Behavior

5.3.1 Crack Pattern Development

Care was taken during handling of the continuous specimens to minimize the bending moment in the slab at the interior connection so as to prevent premature concrete cracking at this section. No cracks were observed in any of the specimens once installed in the test frame. After application of the gravity load, a transverse flexural crack formed at the interior column in each of the three specimens. As lateral load was applied to the columns, both transverse and radial cracks formed in the top surface of the slab of all three specimens. These cracks extended and opened throughout each test. The cracks developed more quickly in the specimens with higher slab gravity load.

The final crack patterns and rupture surfaces for the interior connections of all three specimens are shown in Fig. 5.1. The failure planes in specimens 7L and 6LL extended from the bottom of the slab at the column face to the slab top reinforcement at an angle of between 30 and 35 degrees to the horizontal. Considerable spalling of concrete cover beyond the failure surface was observed. The top steel passing through the column buckled upwards during subsequent load cycles to

increased lateral drift levels. Were it not for the presence of continuous bottom reinforcement through the column, the slab would have separated completely from the column.

5.3.2 Moment-Drift Relationships

For the interior connection of each specimen, the unbalanced moment is plotted against the drift in Fig. 5.2. Specimen 2C achieved peak unbalanced moments of 623 K-in and 548 K-in at 3.5 percent drift in each direction of loading (Table 5.2). After reaching peak moment, the strength dropped gradually to 80 percent of the peak value at the 5 percent drift level. No punching failure was observed at this connection so this was classed as a flexural failure.

The peak unbalanced moments observed in Specimen 7L were 339 K-in at +1.5 percent drift and 366 K-in at -1.4 percent drift (Table 5.2). These values are only 60 percent of those observed in Specimen 2C. In addition, punching failure of the interior connection occurred immediately after the -1.4 percent drift level readings were taken. This punching failure occurred at the side of the column subjected to negative or hogging slab moments. On loading in the opposite direction, complete punching of the slab around the column occurred at the point high-lighted in Fig. 5.2b. The maximum unbalanced moment carried by the interior connection after punching failure was

only 50 percent of the peak strength. In addition, the stiffness of the connection dropped drastically to 19 percent of that prior to failure as discussed later.

Specimen 6LL reached peak unbalanced moments of 240 K-in at +1.0 percent drift and 214 K-in at -0.7 percent drift (Table 5.2). These values are on average 39 percent of the peak moments observed in specimen 2C. Punching failure occurred immediately after the -0.7 percent drift readings were taken. This punching occurred around the entire column perimeter but predominately on the side where a negative or hogging moment existed in the slab. The observed moment dropped suddenly to 17 percent of the peak moment. During subsequent larger displacement cycles, the maximum moment carried by the connection was 59 percent of the peak moment. The stiffness of the connection also reduced drastically to 20 percent of the stiffness prior to failure.

5.3.3 Moment-Shear Relationship

The peak unbalanced moment, M_{ub}, and corresponding shear, V_u, at the interior connections are listed in Table 5.3. In column 6, the shear force is normalized with respect to the nominal direct punching shear capacity, $V_o = v_c A_{cs}$, suggested by the ACI code, where $v_c = 4\sqrt{f_c'}$ and A_{cs} is the area of the critical section a distance $d/2$ from the column face.

Clearly as the shear level increased, the moment capacity of the section decreased as shown in Fig. 5.3. As expected, increasing the gravity load on the slab significantly reduced the ability of an interior connection to resist the unbalanced moments caused by applied lateral loads.

5.4 Comparison with ACI code procedure

The ACI code requirements for interior slab-column connections are based on the eccentric shear stress model (Fig. 3.30). Portion of the unbalanced moment, $\gamma_v M_{ub}$, is assumed to be transferred by a linear variation of the concrete shear stresses around a critical perimeter located $d/2$ from the column face. The remaining moment, $(1 - \gamma_v) M_{ub} = \gamma_f M_{ub}$, must be transferred by slab flexural reinforcement within a slab strip of width $c_2 + 3h$ centered on the column, where c_2 is the column dimension transverse to the direction of loading, and h is the slab thickness. The shear stress on the slab critical section may not exceed $v_c = (2 + 4/\beta_c)\sqrt{f_c'}$ but not greater than $v_c = 4\sqrt{f_c'}$. The value of v_c for each specimen is listed in Table 5.3.

Based on the observed unbalanced moment and corresponding shear on the test connections, the maximum shear stresses on either side of the slab critical section, v_{AB} and v_{CD}, were

obtained and are listed in Table 5.3. The ratio between the observed shear stresses and the code nominal strength are then listed under strength ratios in Table 5.3.

The nominal flexural capacity, M_f, of a strip of slab $c_2 + 3h$ wide based on the measured material properties is given in Table 5.3. The ratio $\gamma_f M_{ub}/M_f$ is listed under strength ratios.

According to the ACI model, the connection reaches its nominal capacity when any of the three strength ratios reach a value of unity. The maximum strength ratios are listed in Table 5.3 and plotted against the direct shear ratio, V_u/V_o, in Fig. 5.4.

As the gravity load increased, the connection strength decreased. For a direct shear ratio of $V_u/V_o > 0.30$, the observed maximum strength ratio dropped below the code value of 1.0 indicating that these connections failed at lower loads than anticipated by the eccentric shear stress model.

5.5 Slab Moment Distribution

Numerous strain gages were used to measure the slab reinforcement strains in top and bottom longitudinal reinforcement on both sides of the column. Using these strain measurements and the stress-strain relationships for both concrete and reinforcement, the flexural moment resisted by a certain width of slab could be calculated.

Considering the full slab width, the total moment, M_t, was obtained from the difference between the moments on either side of the column. This moment should equal the unbalanced moment, M_{ub}, obtained from the load cell readings at the top and bottom of the columns. The ratio M_{ub}/M_t is plotted in Fig. 5.5 for drift levels from 0.25 to 3.5 percent. Although strain gage readings are often unreliable because of damage during casting or water seepage, the total moment obtained from the strain gage readings, M_t, was generally within 10 percent of the applied unbalanced moment for all three specimens.

Considering a slab width of $b = c_2 + 3h$ used by the code in calculation of M_f, the slab moment M_{fo} was obtained. Fifty percent of the slab flexural reinforcement was in this width. The ratio between this moment and the total moment, M_{fo}/M_t is also plotted in Fig. 5.5. For specimen 2C with lowest gravity load, this width of slab contributed between 57 and 64 percent of the total unbalanced moment. For specimen 7L, with greater slab loading, this ratio varied from 65 to 71 percent and for specimen 6LL, with heaviest slab loading, the ratio varied from 70 to 74 percent.

The values for specimen 2C compared well with the code value of $\gamma_f = 0.60$ for the specimen dimensions. This would be expected

since the codes empirical approach has been based on tests such as these. In addition, the reinforcement was distributed in accordance with code guidelines based on $\gamma_f = 0.60$.

The higher ratios for the heavier loaded specimens indicate that the contribution of reinforcement within the column strips was more significant for a specimen with increased gravity load.

These observations appear to confirm the ACI code value of $\gamma_f = 0.60$. However, it must be remembered that the code approach is empirical and derived from tests such as these. Of greater importance is the development of a simple model accounting for the transfer of tension in the bars outside the $c_2 + 3h$ width, to the column. This issue is discussed in greater detail in Chapter 6.

5.6 Connection Drift Capacity

The moment vs drift relationships shown in Fig. 5.2 for the specimen interior connections indicate a significant reduction in connection drift capacity with increased slab gravity load. The drift levels corresponding to the peak moments are listed in Table 5.2 and are plotted against the shear level, V_t/V_o, in Fig 5.6, along with other researchers' results (Ref. 4.2).

It is generally accepted that a slab-column connection should reach a drift level of 1.5 percent without failing even

when stiffer lateral load carrying elements are present (Ref. 4.3). As shown in Fig. 5.6, the interior connection drift at failure varied from 3.5 percent for control specimen 2C to 1.0 percent for specimen 6LL with highest shear ratio. For specimen 7L, with a shear ratio of 0.37, the connection failed at around 1.5 percent drift. Based on these observations, the shear ratio V_u/V_o must not exceed 0.35 to ensure a connection drift capacity of 1.5 percent. In other words, the direct shear stress on the critical perimeter must not exceed $1.4\sqrt{f_c'}$. The recent Committee 352 Recommendations (Ref. 1.1) suggest a limit of $V_u/V_o = 0.4$ based on the other research results shown in Fig. 5.6. Consideration should be given to reducing this limit to ensure adequate performance of interior connections subjected to high shear levels.

5.7 Connection Stiffness

There are numerous approaches to quantifying the stiffness of a connection based on the experimental observations. In this report, the only stiffness considered is the peak-to-peak stiffness as shown in Fig. 5.7. This approach has the advantage of easy comparison with other research and avoids subjective assumptions.

The peak-to-peak stiffness for each specimen is plotted against the drift level in Fig. 5.8. For all three specimens,

the interior connection stiffness decreased rapidly as the specimen was subjected to successive cycles at increased drift levels. Once the connection failed, as occurred in specimens 7L and 6LL at 1.5 and 1.0 percent drift respectively, the interior connection stiffness dropped dramatically to approximately 20 percent of the value prior to failure.

It was also evident that the increased gravity load reduced the connection stiffness. At 0.5 percent drift, specimen 7L stiffness was 82 percent of that of specimen 2C, while specimen 6LL stiffness was 73 percent of specimen 2C. The increased early cracking in the specimens with greater gravity load reduced their lateral load stiffness. However, these observations highlight the effect that slab cracking has on the lateral stiffness of a flat slab connection.

5.8 Conclusions

Based on the test results described in this chapter, the following conclusions were drawn.

1. Increasing the slab gravity load and subsequent shear level at the interior connection significantly reduced the capacity of the connection to transfer unbalanced moment.

2. For a direct shear stress on the slab critical section of $v_c > 1.2\sqrt{f_c'}$, the ACI code design approach for transferring shear and unbalanced moment at an interior connection was unconservative.

3. Increasing the slab gravity load and subsequent shear level at the interior connection also significantly reduced the lateral drift that the specimen could attain prior to failure. It is generally accepted that a well-designed slab-column connection should reach a drift level of 1.5 percent prior to failure. The recent ACI Committee 352 Recommendations propose limiting the direct shear ratio, V_t/V_o, on interior connection to 0.4 to ensure adequate drift capacity. The test results discussed here suggest that this limit be reduced to $V_u/V_o \leq 0.35$, which is equivalent to $v_c \leq 1.4\sqrt{f_c'}$.

4. The stiffness of an interior connection reduced as the slab gravity load increased. This was attributed to the accelerated slab cracking around the connection as a result of the increased gravity load moments.

Table 5.1 – Test Specimen Properties – Interior Connection

Spec No.	Material Properties			Reinft. Ratios (%)		Superimposed Slab Load (psf)		Measured Gravity Shear at Specimen 2C Interior Connection		
	f_c' (psi)	f_y (psi)	d_{ave} (in)	ρ_c	ρ_l	Proto-type	Model	V_g (Kips)	v_g (psi)	v_g ($\sqrt{f_c'}$)
2C	4790	72.6	3.6	0.83	0.31	40	140	11.9	60.9	0.88
7L	4460	76.1	3.6	0.83	0.31	120	285	20.4	104.2	1.56
6LL	4670	76.1	3.6	0.83	0.31	220	420	27.2	138.7	2.03

Table 5.2 - Interior Connection Test Results

Int Conn	f'_c (psi)	Peak Drift (%)	Peak Load (Kips)	Observed Values		Peak Moment (K-in) M_u	Shear Ratio	Shear Ratio
				Peak Shear			Nominal Shear	
				V_u (Kips)	$\frac{v_u}{\sqrt{f'_c}}$		$V_o = v_c A_{cs}$ (Kips)	$\frac{V_u}{V_o}$
2C+	4790	3.5	12.8	10.0	0.74	548	54.2	0.18
2C-	4790	-3.5	11.5	10.0	0.74	623	54.2	0.18
7L+	4460	1.5	5.4	19.1	1.46	339	52.3	0.37
7L-	4460	-1.4	8.9	19.3	1.48	366	52.3	0.37
6LL+	4670	1.0	1.5	27.1	2.03	240	53.5	0.51
6LL-	4670	-0.7	6.0	28.8	2.15	214	53.5	0.54

Table 5.3 – Interior Connection Unbalanced Moment-Shear Relationship

Spec No.	f_c' (psi)	Peak Drift (%)	Observed Peak Values			ACI Nominal Strength		Shear Stress		Strength Ratios			Max. Ratio
			M_{ub}	V_u (Kips)	$\dfrac{V_u}{V_o}$	M_f (K-in)	v_c (Ksi)	v_{AB} (Ksi)	v_{CD} (Ksi)	$\dfrac{v_{AB}}{v_c}$	$\dfrac{v_{CD}}{v_c}$	$\gamma_f \dfrac{M_{ub}}{M_f}$	
2C+	4790	3.5	548	10.0	0.18	346	0.277	0.294	-0.192	1.06	-0.69	0.95	1.06
2C-	4790	-3.5	623	10.0	0.18	346	0.277	0.327	-0.225	1.18	-0.81	1.08	1.18
7L+	4460	1.5	339	19.1	0.37	379	0.267	0.248	-0.053	0.93	-0.20	0.54	0.93
7L-	4460	-1.4	366	19.3	0.37	379	0.267	0.261	-0.064	0.98	-0.24	0.58	0.98
6LL+	4670	1.0	240	27.1	0.51	362	0.273	0.245	0.032	0.90	0.12	0.40	0.90
6LL-	4670	-0.7	214	28.8	0.54	362	0.273	0.242	0.052	0.89	0.19	0.35	0.89
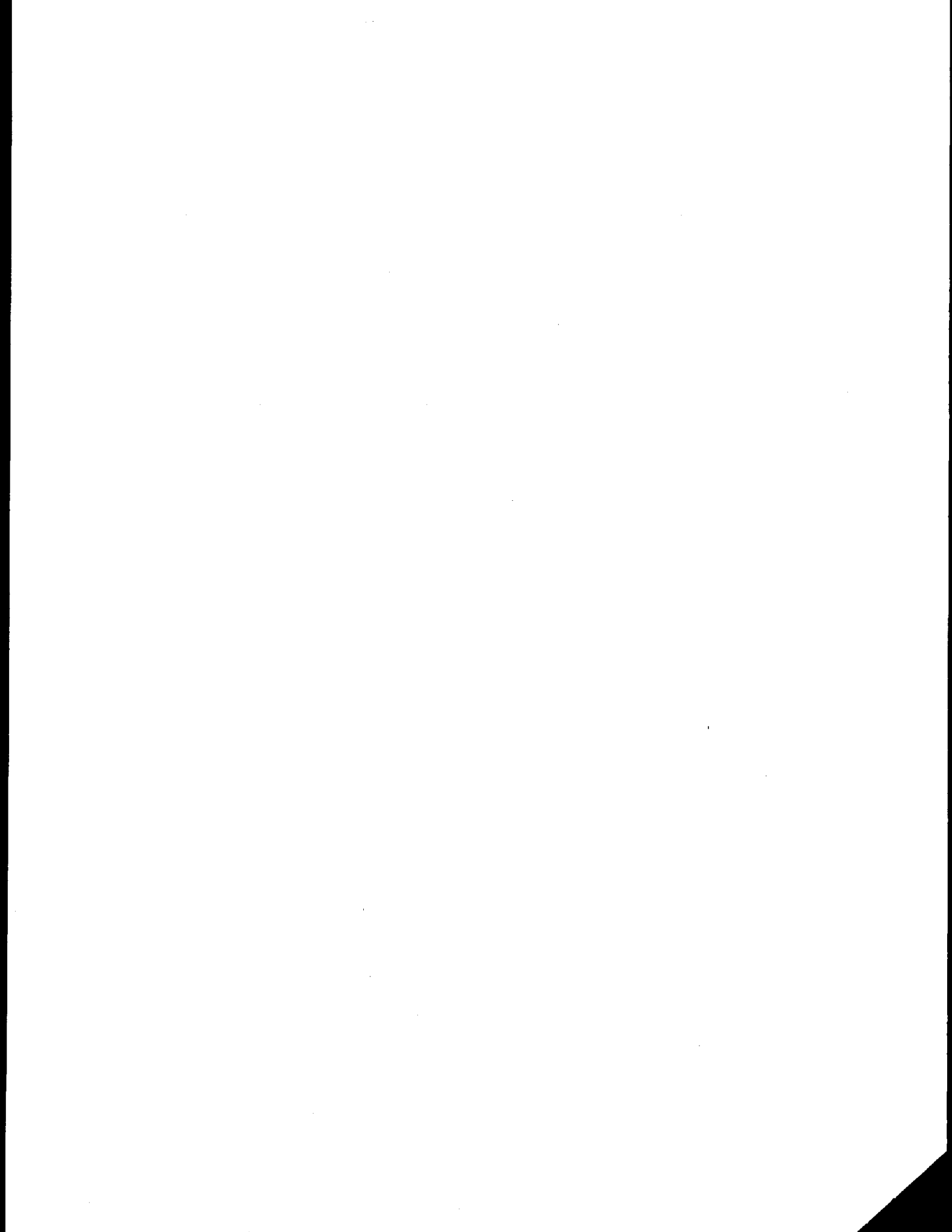
CHAPTER 6

INTERIOR CONNECTION MODEL

6.1 Introduction

Considerable discussion has recently been focused on the model used by the present ACI code to design for moment transfer between slab and interior column. The code model of linear shear variation around a critical perimeter, as shown in Fig. 3.30, is based on numerous research projects performed on interior slab column connections. It is empirical in nature and bears little resemblance to the actual failure mode observed in test specimens.

As the code model has developed over the years, the provisions have increasingly restricted the designer's options for providing adequate shear and flexural strength. Grossman (Ref. 6.1) recently highlighted the progression of revisions made to the original code model of 1956 and how each successive revision has reduced the designer's flexibility and compounded an already unrealistic model.

Considerable research has focused on this issue attempting to improve on or replace the code model. This chapter presents and discusses the current ACI code approach and compares it

84

with the test observations. A rational approach to modelling
the transfer of forces from slab to column is also developed
and compared with the test results.

6.2 Recent Research

Attempts have been made to understand and model the force
transfer occuring at an interior connection. Most notable is
the work by Alexander and Simmonds (Ref. 6.2) in presenting
a detailed rational understanding of how the load transfer
occurs for any combination of unbalanced moment and shear. By
means of compression struts fanning out from the column, they
explain how slab tension reinforcement not passing directly
through the column can be developed in flexure thus assisting
in the transfer of moment to the column (Fig. 6.1). The
compressive struts in the slab concrete are inclined from the
bottom of the slab at the column face to the top tension
reinforcement at some distance from the column. It is the
vertical component of these struts which provides the shear
transfer from slab to column.

Although this approach explains the physical behavior of
connections, it is unfortunately too elaborate and cumbersome
for frequent use and particularily for design purposes. However,
this model is valuable for an understanding of how the
slab-column connection behaves even if another approach is
used in the design of slab-column connections.

6.3 Current Code Requirements

The ACI code approach of linear variation of shear stresses around a critical perimeter is shown diagrammatically in Fig. 3.28. In this model, a critical section is defined at $d/2$ from the face of the column, where d is the average effective depth to the slab tension reinforcement shown in Fig. 3.28(a). Portion of the unbalanced moment at the connection, $\gamma_v M_u$, is assumed to be transfered by eccentric shear on this critical section. The shear stresses are assumed to vary linearly about the centroid of the critical section as shown in Fig. 3.28(b). The nominal shear stress at any point on the critical section is limited by the code to $(2+4/\beta_c)\sqrt{f_c'}$ but not to exceed $4\sqrt{f_c'}$, where β_c = the ratio of long side to short side of the reaction area.

For a connection subjected to ultimate shear force V_u, the maximum stress on the critical perimeter is given by,

$$v_u = \frac{V_u}{A_c} + \frac{\gamma_v M_u}{J_c}\frac{(c_1+d)}{2}$$

which must not exceed the code limit of

$$\phi v_c = (2+4/\beta_c)\sqrt{f_c'}$$

where,

$$A_c = \text{ area of critical section}$$

86

so $A_c = 2d(c_1 + c_2 + 2d)$

and $J_c =$ polar moment of inertia of critical section

$$= \tfrac{1}{6}d(c_1 + d)^3 + \tfrac{1}{6}(c_1 + d)d^3 + \tfrac{1}{2}d(c_2 + d)(c_1 + d)^2$$

for an interior connection

and $\gamma_v = 1 - \dfrac{1}{\left(1 + \tfrac{2}{3}\sqrt{\tfrac{c_1 + d}{c_2 + d}}\right)}$

in which $c_1 =$ column dimension in the direction of bending,

and $c_2 =$ column dimension perpendicular to direction of bending

The remainder of the unbalanced moment, $\gamma_f M_u = (1 - \gamma_v)M_u$ is assumed to be transferred by flexure. Adequate slab flexural reinforcement must be provided in a slab strip of width $c_2 + 3h$ centered on the column to resist this portion of the unbalanced moment.

6.4 Present Code Criticism

One of the major frustrations with the present ACI code approach is the lack of flexibility allowed the designer (Ref. 6.1). The code specifies a fixed γ_v portion of the unbalanced moment which must be carried in shear around the slab critical

perimeter without exceeding the code limit of $4\sqrt{f_c'}$ for a square column, at any point on that perimeter. If a particular connection is overstressed in shear as a result of this check, the designer must either include shear reinforcement, an unpopular choice because of its labor cost, or change the geometry of the column or slab to increase the area of the critical section. There is no allowance for decreasing γ_v and increasing the γ_f factor to carry more of the unbalanced moment by flexural transfer. Such flexibility was included in earlier versions of the code but was removed in the 1971 code revision (Ref. 6.1). This change was based on the 1968 recommendation by Hanson and Hanson (Ref. 6.3) that a Di Stasio and van Buren type analysis be used, in which 40 percent of the unbalanced moment is transferred by eccentricity of shear stresses on the critical perimeter (Ref. 6.4).

Because of the arbitrary nature of both the γ_v factor and the critical shear perimeter, it is unreasonable to expect that the present approach is so precise that any flexibility in the approach would lead to overstressing the connection.

6.5 Test Results Compared with ACI Code Approach

Of the test specimens in this project, most had slab and column reinforcement at the interior connections identical to the control specimen, 2C. The only exceptions were specimen 4S with slab shear reinforcement and specimens 6LL and 7L which

supported increased slab loads. In the other specimens, 3SE
and 5SO, the edge condition at the exterior connections was
changed while the interior connection remained the same as the
control specimen.

The above described ACI code approach was applied to each
of the interior connections in the test specimens. Table 6.1
lists the relevant information for all interior connections.
From the peak connection shear, V_u, and peak unbalanced moment,
M_u, the shear stresses around the critical perimeter, v_{AB} and
v_{CD} can be determined using the ACI procedure. In columns 10
and 11 of Table 6.1, these values are compared with the code
limit of $v_c = (2 + 4/\beta_c)\sqrt{f_c'}$ which reduces to $v_c = 4\sqrt{f_c'}$ for square
columns (col. 7). In addition, in column 12, the portion of
unbalanced moment assumed to be carried in flexure, $\gamma_f M_u$, is
compared with M_f, the flexural capacity of a slab strip of
width $c_2 + 3h$ centered on the column (col. 9).

These three ratios are listed in columns 10, 11 and 12 of
Table 6.1. According to the ACI code approach, the connection
loading is acceptable until one of these ratios reaches unity.
The maximum ratio for each specimen is listed in the column
13 of Table 6.1. These ratios are plotted against the shear
ratio V_u/V_o (col. 8) in Fig. 6.2, where $V_o = v_c A_{cs}$ and A_{cs} is the
area of the critical section.

As discussed in a previous chapter, the specimens with increased slab gravity loading, specimens 6LL and 7L, experienced punching shear failure at the interior connections before achieving unity in any of the strength ratios. It can therefore be concluded that the ACI code approach may be unconservative for a connection subjected to a gravity shear ratio in excess of $V_u/V_o = 0.30$, which is equivalent to a shear stress of $v_c \geq 1.2\sqrt{f_c'}$.

All the other specimens exceeded the code strengths prior to failure. The controlling strength ratios varied from 1.01 to 1.18. Apart from connections subjected to increased gravity shear as mentioned above, the ACI code empirical approach has adequately predicted the loads under which the connections will fail.

6.6 Slab Reinforcement Strain Distribution

Extensive use of strain gages on the slab reinforcement around the interior connections enabled a close study of how the unbalanced moment is transfered from the slab to the column.

To ensure that the strain gages were providing a reliable measure of the steel stress in the slab reinforcement, the total slab moments on each side of the column, M_L and M_R, were obtained from the strain gage readings as described in Fig. 6.3. The difference between these moments, $M_T = M_L + M_R$ is the unbalanced moment at the connection which can be compared with

the unbalanced moment, M_{ub} computed from the load cell readings at top and bottom of the columns. The ratios M_{ub}/M_T are plotted in Figs. 6.4 to 6.11 for each of the test specimen interior connections.

In the same way, that portion of the unbalanced moment (M_{ACI}) carried by a slab width of $c_2 + 3h$ was obtained from the strain gage readings on the reinforcement within this width. In addition, the moment (M_c) carried by a width of slab equal to the column width (b=10 inches) was also determined from the strain gage readings on the slab reinforcement passing through the column.

Comparing these values with the total unbalanced moment at the interior connections (M_t) gave the ratios M_c/M_t and M_{ACI}/M_t. For each specimen, these ratios are also plotted against drift level in Figs 6.4 to 6.11. Curves are shown for both positive and negative loading directions.

Although sometimes considered unreliable, the strain gage readings appear to provide at least a qualitative comparison of the specimens. Generally the total moment (M_t) obtained from the strain gage readings is within 20 percent of the measured unbalanced moment (M_{ub}) at the connection as seen from the plots of M_{ub}/M_t. This indicates the measure of confidence that can be placed in the strain gage readings.

From the plots of M_{ACI}/M_t, it can be seen that between 55 percent and 85 percent of the unbalanced moment was carried by the flexural reinforcement in a width $c_2 + 3h$ centered on the column.

For the column and slab dimensions of the specimen, the ACI code specifies that flexural reinforcement in this width be proportioned for 60 percent of the unbalanced moment. No flexibility is allowed for, and all remaining unbalanced moment must be resisted by eccentric shear around the slab critical section.

In most of the specimens, this ratio was higher initially and decreased gradually as the drift level increased. This occured as yielding extended to all of the interior slab reinforcing bars and spread to exterior slab bars.

Similar observations can be made for the ratio M_c/M_t though the values are lower, ranging from 30 to 45 percent, ie. approximately half of the M_{ACI}/M_t values.

The $c_2 + 3h$ slab width contained 7 of the 13 top bars in the slab and 5 of the 11 bottom bars (Fig. 2.5), that is, about 50 percent of the slab flexural reinforcement. The column width of 10 inches contained 3 top and 3 bottom flexural bars for approximately 25 percent of the total slab reinforcement.

At lower drift levels, which are more representative of the bahavior of a real structure, the ratio M_{ACI}/M_t generally exceeded 60 percent with a maximum of 85 percent. Had more reinforcement been concentrated in the $c_2 + 3h$ slab width, it is conceivable that this ratio would have increased further. It would appear therefore that the code specification of a fixed 60 percent of unbalanced moment transferred by flexural reinforcement could be relaxed to allow flexibility from 60 to 80 percent at the discretion of the engineer. This would correspondingly permit variation in the portion of unbalanced moment carried by eccentric shear from 40 to 20 percent.

Clearly more research is required to study the effect of further concentration of flexural reinforcement in the column strip especially in a case where the slab reinforcement ratio is higher than that used in these specimens. The danger of compression failure due to over reinforcement of the column strip must not be overlooked. However, as will be seen later in this Chapter, regardless of the positioning of the slab flexural reinforcement, the compression struts in the slab all impinge on the front and side faces of the column and so variations in the reinforcement distribution may not have a significant effect on the size and stress in the concrete compression zone. The overall amount of flexural reinforcement must nevertheless be maintained below the balanced condition

to prevent compression failure of the slab. This issue is introduced again under the discussion of a proposed load transfer mechanism that follows.

6.7 Unbalanced Moment Transfer Mechanism

Tom Paulay, in recent research into the moment transfer mechanism of beam to column connections including a floor slab, has introduced a possible transfer mechanism for reinforcement in the slab (Fig. 6.12), (Ref. 6.5, 6.6). Judging from the cracking pattern observed in the test specimens, it would appear that a similar mechanism may help to explain the moment transfer in interior flat slab to column connections.

Studying the typical interior connection crack pattern shown in Fig. 6.13, it is seen that radial tension cracks extended from the column to the edge of the slab on the hogging side of the connection. The slab tension reinforcement provided the tensile force at these cracks while the compressive force is transferred through diagonal compression struts. The compression struts extend from the top of the slab at the reinforcement to the bottom of the slab at the face or side of the column. Because these struts are radial, they result in a transverse tension in the slab. This tension resulted in the longitudinal cracks observed in Fig. 6.13 which extended from the face of the column along the centerline of the slab

for a distance approximately equal to half the slab width. Once the concrete cracked, this transverse tension was resisted by the transverse slab reinforcement.

The inverse mechanism will develop below the slab on the positive moment side of the column once the lateral load moment exceeds the gravity load moment.

The slab longitudinal reinforcement must be fully developed on either side of the outermost radial tension cracks before it can be effective. In addition, the tension in the top bars on one side of the connection must be transferred to the bottom bars on the other side of the connection. This transfer occurs through torsion in the slab concrete adjacent to the columns. The result is numerous diagonal torsion cracks in these regions. It is important therefore that top and bottom reinforcement lap sufficiently to allow this transfer to occur.

The compression struts introduced above are also inclined relative to the horizontal. This resulted in an out-of-plane force on the tension reinforcement. Alexander and Simmonds (Ref. 6.2) propose that this out of plane force is resisted by the tensile capacity of the concrete cover over the tension reinforcement. They make no attempt to define this tensile capacity. An alternative model for failure of the interior connection is presented below.

6.8 Proposed Interior Connection Model

In the punching shear failure of an interior connection, a rupture surface developed which extended from the bottom of the slab at the face of the column radiating outwards at 30 degrees to the horizontal and towards the hogging side of the support (Fig. 6.14). The failure of the concrete in tension along this surface resulted in a vertical shift at the line where this plane meets the tension reinforcement. It was this vertical movement that resulted in spalling of the concrete cover beyond this rupture line as seen in Photos 3.4 and 5.1.

The area of the rupture surface can be estimated as the sum of the three areas, A_{F1}, A_{F2} and A_{F3} shown in Fig. 6.15. These areas are,

$$A_{F1} = c_2 d / \sin 30$$

$$A_{F2} = A_{F3} = \text{1/4 of the surface of a cone}$$

of radius r and height d,

$$= \tfrac{1}{4} \times \tfrac{2}{3} \times (2\pi r)d$$

where $r = d / \tan 30$

For the test specimens,

$$A_{F1} = 10 \times 3.9 / \sin 30 = 78.0 in^2$$

$$A_{F2} = A_{F3} = \tfrac{1}{4} \times \tfrac{2}{3} \times 2\pi(3.9/\tan 30) \times 3.9 = 27.6 in^2$$

Therefore, $A_F = A_{F1} + A_{F2} + A_{F3} = 133.2 in^2$

The tensile stress on this surface is the result of both the vertical shear force in the slab on this side of the connection, V, and the out of plane component of the compression struts resisting the flexural moment, M_s. The compressive force in the compression struts is obtained as shown in Fig. 6.14. A reasonable estimate of the reinforcement tensile force, T, is obtained from,

$$T = M_s/d$$

The compression in the struts is then

$$C = T/\cos 30.$$

The out of plane component of this compressive force is

$$C_V = C \sin 30.$$

Combining the above expressions gives

$$C_V = (M_s/d)\tan 30.$$

The tensile stress perpendicular to the failure surface is then given by

$$\sigma_T = \frac{1}{A_f}\left(\frac{M_s}{d}tan30 + V\right)cos30 \times 1000.$$

Where M_s and V are in Kips and inches, and σ_T is in psi.

Substituting the values for A_F and d for the test specimens,

$$\sigma_T = 6.502(0.148M_s + V)$$

For all eight interior connections the relevant measured values are listed in Table 6.2. The rupture surface tensile stresses are computed using the above expression and listed in terms of stress (col. 6) and multiples of $\sqrt{f_c'}$ (col. 7). These stresses are then compared with the values of the modulus of rupture, f_r, measured at the time of testing of each specimen (col. 8). The resultant ratios (col. 9) vary from 0.49 for specimen 1 to 0.80 for specimen 5SO. These values are also shown graphically in Fig. 6.16.

Specimen 1 with a tensile stress ratio of 0.49 had not failed in punching shear by 3.0 percent drift, at which point an equipment malfunction ended the test. Specimen 2C, the control specimen, with a ratio of 0.55, did not experience punching shear failure though subjected to drift levels up to 5.0 percent. Specimen 4S, with a shear stress ratio of 0.67 was the only specimen with slab shear stirrups at the interior

connection. As described earlier, the presence of shear stirrups increased the confinement of the concrete adjacent to the column and so prevented punching shear failure.

All other specimens experienced punching shear failure at the interior connections at, or shortly after, the peak loads were reached. From Fig. 6.16 it would appear that a failure plane subjected to a tensile stress in excess of 50 percent of the modulus of rupture will fail due to punching shear.

More study is required to determine the accuracy or applicability of this model to other interior connections. This would involve application of this model to other available test results to verify the area of the rupture surface and the tensile stress level above which failure can be expected to occur. It is hoped however, that this approach may lead to a simple rational model describing the punching shear failure of slab-column connections.

An alternative failure mode is the crushing of the slab concrete at the ends of the compression struts bearing on the face of the column. In the relatively lightly reinforced specimens used in these tests, this failure was never observed. However, in a more heavily reinforced slab, it would be important to recognize that the compression zone is limited to the face and sides of the column and not to the entire slab width when

considering the maximum reinforcement ratio allowed. Hence, a width of $c_2 + 2c_1$ would seem appropriate for computation of ρ_{bal} for the full slab reinforcement.

6.9 Conclusions

Based on the above discussion of the unbalanced moment transfer at slab-column connections, the following conclusions were drawn.

1. Apart from connections subjected to increased shear loads, the interior connections failed with maximum critical section stress ratios of between 1.01 and 1.18 times the values given by the ACI code.

2. From strain gage measurements of the strain in the slab flexural reinforcement, it was found that between 55 and 85 percent of the unbalanced moment at the interior connection is transferred through flexure in a slab width $c_2 + 3h$. For the square columns in these test specimens, the ACI code requires that a fixed 60 percent of the unbalanced moment be transferred through flexure ($\gamma_f = 0.6$) while the remaining 40 percent be transferred through shear on the slab critical section ($\gamma_v = 0.4$).

Based on the results reported here, the ACI code requirements could be relaxed to permit variation of γ_f from 0.6 to 0.8 with a corresponding variation in γ_v from 0.4 to 0.2, provided

100

$\gamma_f + \gamma_v \geq 1$ at all times. This variation could be at the discretion of the designer, thereby allowing some flexibility without jeopordizing the connection strength.

3. Slab longitudinal reinforcement not passing through the column was still effective in transferring slab moment to the column. This transfer was made possible by radiating compression struts which extended from the bottom of the slab at the column face to the top reinforcing bars. The component of this compression strut perpendicular to the direction of loading was resisted by the transverse slab reinforcement.

4. All interior connections which failed in punching shear developed a rupture surface on the hogging side of the connection. When the diagonal tension on this rupture surface exceeded 50 percent of the modulus of rupture of the concrete, punching shear failure was imminent. Development of this model through comparison with other researchers' results will help to more precisely define the area of the rupture surface and the tensile stress level at which punching shear failure can be expected to occur.

Table 6.1 - Comparison of Interior Connection Results with ACI Code Approach

Spec No.	f_c' (psi)	Peak Load (Kips)	Peak Drift (%)	Moment M_u (K-in)	Shear V_u (Kips)	Stress v_c (psi)	$\frac{v_u}{v_o}$	Moment M_f (K-in)	$\frac{v_{AB}}{v_c}$	$\frac{v_{CD}}{v_c}$	$\frac{\gamma_f M_u}{M_f}$	Max. Ratio
(1)	(2)	(3)	(4)	(5)	(6)	(7)	(8)	(9)	(10)	(11)	(12)	(13)
1	4400 4400	18.7 -19.3	3.00 -2.50	581 564	10.2 10.1	0.27 0.27	0.20 0.19	343.9 343.9	-0.77 -0.75	1.17 1.14	1.01 0.98	1.17 1.14
2C	4790 4790	19.8	3.50 -3.50	548 623	10.0 10.0	0.28 0.28	0.18 0.18	346.2 346.2	-0.69 -0.81	1.06 1.18	0.95 1.08	1.06 1.18
3SE	6380 6380	24.6	3.50 -3.50	640 639	9.5 9.5	0.32 0.32	0.15 0.15	352.6 352.6	-0.74 -0.73	1.04 1.04	1.09 1.09	1.09 1.09
4S	6360 6360	21.5	3.50 -3.50	696 613	9.8 9.9	0.32 0.32	0.16 0.16	352.5 352.5	-0.81 -0.69	1.12 1.01	1.18 1.04	1.18 1.04
5SO	5500 5500	22.9	3.50 -3.50	597 585	10.0 10.1	0.30 0.30	0.17 0.17	349.5 349.5	-0.72 -0.70	1.06 1.05	1.02 1.00	1.06 1.05
6LL	4670 4670	9.6	1.00 -0.70	240 214	27.1 28.8	0.27 0.27	0.51 0.54	374.4 374.4	0.12 0.19	0.90 0.88	0.38 0.34	0.90 0.88
7L	4460 4460	13.1	1.50 -1.40	339 366	19.1 19.3	0.27 0.27	0.37 0.37	372.9 372.9	-0.20 -0.24	0.93 0.98	0.55 0.59	0.93 0.98
8I	5700 5700	8.8	3.50 -3.50	586 593	10.0 11.1	0.30 0.30	0.17 0.19	380.1 380.1	-0.69 -0.68	1.03 1.06	0.93 0.94	1.03 1.06

Table 6.2 - Calculations for the Proposed Interior Connection Model

Spec No.	f'_c	Peak Drift	Peak Slab M_s	Peak Slab V	σ_T	σ_T	f_r	$\dfrac{\sigma_T}{f_r}$
	(psi)	(%)	(K-in)	(Kips)	(psi)	$\sqrt{f_c'}$	(psi)	
(1)	(2)	(3)	(4)	(5)	(6)	(7)	(8)	(9)
1	5506	2.5	282	10.1	338	4.55	690	0.49
2	4786	3.5	306	10.3	362	5.2	663	0.55
3	6384	3.5	360	10.8	417	5.2	650	0.64
4	6357	3.5	377	10.0	429	5.4	642	0.67
5	5506	3.5	383	10.4	437	5.9	544	0.80
6	4670	1.0	191	16.3	290	4.3	542	0.54
7	4460	1.5	250	13.1	326	4.9	567	0.58
8	5700	3.5	237	10.2	295	3.9	542	0.54

CHAPTER 7

STRUCTURAL ANALYSIS METHODS

7.1 Introduction

A realistic estimate of lateral displacement and drift levels is of major importance in the design of flat slab structures for earthquake loading. Considerable research has been reported addressing this issue (Ref. 7.1 → 7.7). From all practical observations of test specimen behaviour and response of actual flat-slab structures, it is generally agreed that a flat-slab structure is considerably more flexible or less stiff than generally anticipated during the design process. Clearly the designer is in need of some simple procedure whereby a realistic drift estimate can be made.

A recent publication by Cano and Klingner (Ref. 7.1) discusses a number of the more commonly used computer modelling techniques. These include the effective width method, the equivalent frame method of the ACI Building Code, and similar methods developed by Vanderbilt and Corley (Ref. 7.2) termed extended equivalent column method and extended equivalent slab method. All of these methods involve representing the building by means of individual plane frame models for both gravity and

lateral loading. The effective width method does not incorporate any torsional members to transfer slab moment to the column side faces. The other methods incorporate these torsional members in either the column or slab stiffness resulting in an equivalent stiffness for these members. Cano and Klingner also propose the explicit transverse torsional member method discussed later in this chapter.

A major concern with the application of all of these models is the assumed member section properties when the concrete is cracked. Generally flat plates will be cracked prior to earthquake loading due to self-weight (generally a large portion of the total load), shrinkage, construction loads and superimposed dead and live loads or previous lateral loads from wind or earthquake loading. In addition, during a severe earthquake, the member stiffness will deteriorate as the structure is subjected to successive inelastic deformations.

Whichever of the analysis methods is to be used, the engineer is in need of a rational approach to estimating the actual member stiffnesses during severe lateral loading. Over-estimating the member stiffness will result in underestimated drift levels at the design stage. The subsequent unexpectedly large drifts may result in excessive interior damage, possible "pounding" with adjacent structures, increased P-Delta effects, and possible structural failure of connections subjected to drift demands beyond their designed capacity.

7.2 Literature Review

7.2.1 General

A large amount of research has focused on the lateral stiffness of flat-slab structures. The majority of this research has utilized elastic plate analysis techniques to analyse a slab-column assembly (Ref. 7.3, 7.4). Little of this research has been related to large scale experimental test results. Unfortunately, the complex behavior of reinforced concrete, especially when cracked, makes the use of elastic plate theory unreliable.

Three of the most recent experimentally based research reports are discussed below.

7.2.2 Cotran and Hall

Cotran and Hall (Ref. 7.5) developed effective width coefficients for floor systems for use in the analysis of frames subjected to lateral seismic loads. They proposed two non-dimensional constants for a given slab aspect ratio and relative column size which model the stiffness of the slab to that of an equivalent beam.

These effective width coefficients were derived from an elastic finite element study of typical interior panels supported on steel beams. The authors propose that the results are equally applicable to flat slabs.

For bending, the effective width coefficient, λ_f, was found to depend on the aspect ratio, l_1/l_2, and both the longitudinal and transverse relative column sizes, c_1/l_1 and c_2/l_2 respectively.

For the interior connections in the test specimens, $\lambda_f =$ 0.61. Hence $b_e = 0.61 \times 9\text{ft} \times 12\text{in/ft} = 66\text{in} = C_2 + 12h$. The effective moment of inertia of the slab as an equivalent beam would then be based on this effective width and the full slab thickness, $h = 4.5\text{in}$.

From the observed strain gage readings in the control specimen, the flexural reinforcement reached yield strains over the full specimen width of 78in at a drift level of 3.5 percent. However, in a typical building structure, the drift is not expected to exceed 1.5 percent drift. At this level, only reinforcement within the column width, $C_2 = 10\text{in}$, had reached yield strains. By 2 percent drift, yielding had spread to a width $C_2 + 3h = 23.5\text{in}$.

The flexural effective width coefficient suggested by Cotran and Hall correctly estimates the slab width over which flexural reinforcement was effective at ultimate flexural capacity of the slab. However, it grossly overestimates the effective stiffness of the slab since it assumes gross slab thickness for this width without consideration for extensive cracking

that had occured prior to reaching ultimate load.

The same value of b_e is considered to act at exterior connections within 10 percent of the true value.

7.2.3 Vanderbilt and Corley

Vanderbilt and Corley (Ref. 7.2) discuss three types of lateral load analysis models. Firstly, the effective width method or equivalent beam width concept. An equivalent width factor, α, is obtained from the requirement that the stiffness of a prismatic beam of width αl_2, must equal the stiffness of a plate of width l_2. This is equivalent to equating the areas under the two rotational diagrams (Ref. 7.2).

A number of researchers have used mathematical elastic models of individual connections to arrive at values of α for various values of the many variables involved. The results were plotted which, for the test specimens in this research, give an α value of 0.68.

Another approach to analysis of structures subjected to lateral load is that of the equivalent frame methods. These methods incorporate a torsional member into either the column or slab stiffness. They develop the torsional stiffness of the torsional beam as $K_t = \frac{9E_s}{l_2(1-c_2/l_2)^3}$ for slabs without beams. Then, $\frac{1}{K_{ec}} = \frac{1}{K_c} + \frac{1}{K_t}$ gives the equivalent column stiffness to be used in the equivalent frame analysis.

Another method discussed in this paper is that of the stub beam model. The slab is treated as a beam of width l_2 and span l_1 connected to the columns through stub beams attached to all four column faces. Part of the moment in the l_1 direction transfers through the flexural stub members and the remainder throught the torsional members (Ref. 7.6). Torsional rotations reduce to zero at $1.5h$ from the side faces of the column. This is a fairly complex model that is not conducive to simple analysis procedures.

In comparing these models, Vanderbilt and Corley comment that the equivalent beam width method should be used as a lower bound value as this indirectly accounts for cracking and bond slip. The various equivalent frame methods were applied to a 1/8 scale model tested in Canada (Ref. 7.7). Unfortunately, the small scale of this model made it very difficult to correctly model the behaviour of a full-scale structure (Ref. 7.8). In addition, this model was uncracked throughout testing, which is considered unlikely in a real structure.

Vanderbilt and Corley then introduce a Beta factor to account for cracking of the slab concrete, where, β=effective I/gross I. They suggest values of β=1 for uncracked and β=0.33 for cracked slabs. " A beta value of one-third is judged to represent a realistic lower bound for slab stiffness and is recommended

as the default value." " Note that Beta is intended to account for loss in stiffness from all causes including cracking of beams, columns, and torsional members".

7.2.4 Cano and Klingner

Cano and Klingner (Ref. 7.1) extended the study initiated by Vanderbilt and Corley. They introduce the previous models and discuss their advantages and disadvantages. In addition, they propose an explicit transverse torsional member method. In this non-planar model, the conventional columns are connected indirectly by two conventional slab elements, each with half the stiffness of the actual slab. The indirect connection between slab elements and column is made using explicit transverse torsional members (Fig. 7.2). Both slab and torsional member properties can be readily adjusted to accomodate cracked section properties. In this report, the authors use the factor of $\beta = 0.33$ suggested by Vanderbilt and Corley to reduce the gross member stiffness for cracked section properties. The authors then apply a number of these analysis models to a typical prototype structure. A comparison of the results shows that the explicit transverse torsional member model provides slab moments which agree well with those of the equivalent column method. The question of an equivalent stiffness for cracked section properties is not discussed further.

110

7.3 Present Analysis Methods

7.3.1 Finite Element Analysis

With the advent of affordable personal computers with advanced capability and speed, increased use is being made of finite element methods for analysis of flat slab structures. There is unfortunately an aura of exactness among many designers about finite element analysis. Its use is widespread and the output as regards moment distribution and deflections is often not questioned. However, the use of linear elastic analysis based on gross concrete properties is no longer applicable when calculated slab stresses exceed the cracking strength of the concrete. In addition, any existing cracking due to shrinkage, self weight applied at an early age, construction loads and so forth, is often completely ignored when using this approach.

From experience with one particular flat slab structure designed by finite element analysis, the observed self weight deflections were five times the values anticipated using gross section properties. In this instance, a more realistic estimation of the deflected shape was obtained, after the fact, by reducing the stiffness of slab elements around the slab-column connections to that of a fully cracked section.

This analysis method is not discussed further in this report. However, it is felt that extensive comparisons between observed deflections, both real life and experimental, and finite element analysis results could shed valuable light on the appropriate section properties to assume when using a finite element analysis.

7.3.2 Effective Width Method

In the effective width method, an effective width factor, α, is obtained such that a slab of width αl_2 correctly models the stiffness of the full slab width.

A number of methods have been used to arrive at a value for α, but generally they rely on an elastic finite element analysis of the slab-column region (Ref. 7.2). The effect of cracking in the slab is generally incorporated by means of another factor, β, which relates the cracked stiffness to the gross stiffness. Vanderbilt and Corley maintain that "a beta value of one-third is judged to represent a realistic lower bound for slab stiffness and is recommended as the default value". Cano and Klingner (Ref. 7.1) subsequently make extensive use of this unsubstantiated β value.

A significant drawback of the effective width method is that "leakage" of slab gravity moments between adjacent spans

cannot occur. All slab moment passes through the slab-column connection whereas in reality some moment will transfer directly through the slab from one span to the next.

Generally single α and β values are used for a full span regardless of the variation in level or direction of slab bending moment. In fact, portions of a span may be completely uncracked while areas close to the connections experience substantial cracking.

7.3.3 Equivalent Frame Method

A number of approaches fall under this category. The most widely used is that proposed by the ACI Building Code. Generally, these methods incorporate a transverse torsional member at the connections which models the torsional stiffness of the slab adjacent to the connection. This torsional member stiffness is then combined with either the column stiffness to give an equivalent column method (Ref. 7.2) as used by the ACI Code, or with the slab stiffness to give an equivalent slab stiffness.

The application, advantages and disadvantages of these methods are well presented by Vanderbilt and Corley (Ref. 7.2) and Cano and Klingner (Ref. 7.1). The ACI equivalent frame method is widely used for both lateral and gravity load analysis as it allows for the slab moment "leakage" mentioned earlier.

Although these methods require considerable hand calculation of torsional stiffnesses and subsequent equivalent column stiffnesses, many computer programs are currently available which simplify the designer's task. Because of the predominant use of this method at present, it is likely to remain the most popular method in the immediate future.

7.3.4 Explicit Transverse Torsional Member Method

This method is proposed by Cano and Klingner as a modification of the equivalent frame method. It is a three dimensional model in which the transverse torsional members are retained as explicit members in the model and not combined with the column or slab stiffness. The model then consists of a column with gross section properties, beam elements which each represent half of the slab width, again with gross properties, and transverse torsional members which connect the beam elements at right angles to the columns (Fig 7.2).

An obvious disadvantage is that the model is no longer a convenient two-dimensional frame. However, with the advances in computer power and speed, this is no longer a significant drawback. A major advantage of this model is that it allows for the use of cracked section properties for both the slab elements and the torsional elements. In their paper (Ref. 7.1), the authors use the beta value of 0.33 proposed by Vanderbilt and Corley. Again there is no attempt to verify this assumption.

114

They also use a single beta value for both slabs and torsional members, regardless of the degree or direction of bending of the member.

Cano and Klingner proceed to apply the above models to a prototype two story three-bay structure. They compare the results with respect to moment distribution under gravity loading and lateral loading. No information is given on the comparison of slab deflections under gravity loading or story drift under lateral loading. When considering the performance of flat-slab structures subjected to gravity and lateral loads, it is important to study not only the moment distribution between connections, but also the deflections and lateral drift.

7.4 Application to Test Specimen

7.4.1 General

The above discussion introduced a number of possible methods for analysing a slab-column sub-assembly subjected to both gravity and lateral load. Three of these methods were studied further by relating them to test specimen 2C, the control specimen, and comparing the analytical results with those observed during the test. The three methods considered here are the effective width method, the equivalent frame method,

and the explicit transverse torsional member method. These stiffness analysis methods were applied to an analytical model of the test specimen.

This analysis was performed using the 'Extended Three-dimensional Analysis of Building Structures' (ETABS) computer program (Ref. 7.9). The specimen was modelled with pinned connections at midheight of the columns above and below the slab as in the test setup, with a rigid diaphragm at the slab level to model the in-plane rigidity of the slab. Rigid beam elements were included to model the connection zone. The flexural section properties of each element of the model were derived as suggested by the respective analysis method being studied. This constituted the first trial of each method.

7.4.2 Modified Models

On examining the results of this first trial, it was apparent, as is discussed fully below, that the basic methods did not produce the same slab moment distribution or lateral drift as observed in test specimen 2C.

After consideration of the actual specimen behavior, the analytical models were modified to better reflect the cracked nature of the test specimen. These modified models resulted in substantially improved representation of the observed behavior. After a series of trial-and-error adjustments, the

modified analytical models were adjusted so as to very closely reproduce both the slab moment distribution and lateral drift observed in the test specimen.

7.5 Comparison with Test Results

7.5.1 General

At any particular drift level, the test specimen slab moments at the face of the column are known. Using the models described above, it was possible to apply the same lateral load applied to the test specimen and compare the resulting moment distribution and lateral drift with the experimentally observed values. For the purposes of this report, the theoretical models and experimental results were compared at both 0.5 percent drift and 1.5 percent drift levels. The 0.5 percent drift level represents a likely occurence during the structures life, while the 1.5 percent drift level represents the maximum drift that a structure can be expected to sustain during a design level earthquake.

7.5.2 Comparison at 0.5 percent drift

7.5.2.1 Effective Width Method

Table 7.1 lists the slab moments and column lateral drift for various effective width model assumptions. The specimen test results are given in row 1 of this table. Using the α value suggested by Vanderbilt and Corley (Ref. 7.2) of 0.4,

resulted in the values in row 2. The moment distribution was quite different from that observed during the test while the lateral drift was only 39 percent of the measured drift.

Assuming cracked slab conditions with $\beta=0.33$, as suggested by Vanderbilt and Corley, results in the values in row 3. The slab moment distribution remained unchanged while the drift increased to just over the observed drift.

The assumption of a single α and β value for the entire span irrespective of the slab moment or extent of cracking appears unrealistic. Since the slab was virtually uncracked in positive bending, a value of $\beta=1$ should be used in these areas. Where negative moments occured, significant flexural cracking had already occured in the test specimen by the 0.5 percent drift level. Hence a reduced β value should be used in these areas. The point of contraflexure was approximately 18 inches from the face of the column based on the test slab moments. This resulted in the modified analytical model shown in Fig. 7.3. Initially assuming an α value of 1, the β values were adjusted until the correct moment distribution was achieved as shown in row 4. However, the lateral drift was only 42 percent of the observed drift. Now adjusting α to a value of 0.34 resulted in the values in row 5 which correctly reproduce those in the test specimen.

7.5.2.2 Equivalent Frame Method

A procedure similar to that described above was followed for the Equivalent Frame Method with results listed in Table 7.2.

The uncracked slab assumption of full gross section properties resulted in moment distribution far removed from the test results (Row 1) and a drift of only 29 percent of the test drift as shown in row 2. Using $\beta=0.33$ for cracked properties of the slab only increased the drift to 55 percent of the measured value (Row 3). This model would require a β value of 0.15 to arrive at the correct drift though the moment distribution would remain very different from the observed values (Row 4).

A modified analytical model similar to that proposed for the effective width method above (Fig. 7.3) can also be used for the equivalent frame method. By using different β values for slab areas with different cracked properties, the moment distribution neared that observed as seen in row 5. An α value of 1 resulted in a drift of 48 percent of the observed drift. Reducing α to 0.40 produced the correct lateral drift while maintaining the observed moment distribution as shown in row 6.

7.5.2.3 Explicit Transverse Torsional Member Method.

Applying the uncracked section properties suggested by Cano and Klingner (Ref. 7.1) resulted in the moment distribution and drift shown in row 2 of Table 7.3. Again, the moment distribution does not agree with the observed values (Row 1). The drift was only 23 percent of the observed drift.

Introducing β=0.33 for slab sections only, resulted in the values listed in row 3. Only slight improvement in drift to 39 percent of the observed value was achieved.

Applying β=0.33 to both slab and torsional members resulted in the values in row 4. Moment distribution is basically unchanged while the drift improved to 58 percent of the observed value. To arrive at the observed drift, a β value of 0.20 was required (Row 5). Moment distribution was still far from the observed values.

Clearly this method has similar drawbacks to that of the previous models. As previously, the beam elements were divided into two elements with different cracked properties and hence different β values (Fig. 7.4). It was also possible to adjust the β values applied to both the slab flexural and torsional members independently. By utilizing the β values in row 6, a more accurate moment distribution was obtained. With α=1 for

slabs, this condition gave 58 percent of the observed drift. Reducing α to 0.50 resulted in accurate moment distribution and drift comparisons with the observed results.

7.5.2.4 Suggested α and β values

Values of α and β which will result in correct prediction of both moment and drift at 0.5 percent drift level are given in Table 7.4. The results of applying these values to each model are also shown here for comparison with the observed test results. Accepting a slight discrepancy in moment distribution and an underestimation of drift, these suggested values can be used for any of the three analytical models.

7.5.3 Comparison at 1.5 percent drift.

Following the same procedure outlined above for the 1.5 percent drift level resulted in the values tabulated in Tables 7.5, 7.6 and 7.7 for the three analytical models being considered. Similar observations as those discussed above can be made at this drift level as follows.

7.5.3.1 Effective Width Method.

From Table 7.5, several general observations can be made. Again, application of the unmodified model resulted in incorrect moment distribution (Row 2). In addition, a β value of 0.33

no longer resulted in the correct drift (Row 3) but had to be reduced to 0.20 for a more accurate modelling of the specimen drift (Row 4).

By adjusting the β values to more accurately represent the cracked nature of the slab, the correct moment distribution resulted (Row 5). Reducing the α value to 0.20 resulted in both moment and drift results being modelled correctly (Row 6).

7.5.3.2 Equivalent Frame Method.

The values listed in Table 7.6 for the equivalent frame method produce similar observations as before. The unmodified model resulted in incorrect moment distribution (Row 2) and even with $\alpha = 0.33$, the drift was only 38 percent of the observed drift (Row 3). An α value of 0.10 was required to obtain the correct drift (Row 4).

Again, more rational distribution of the β values (Fig. 7.3) resulted in correctly modelled moment distribution (Row 5), and combined with an α value of 0.20, the drift was also correctly modeled (Row 6).

7.5.3.3 Explicit Transverse Torsional Member Method.

Table 7.6 lists the results of applying this method at the 1.5 percent drift level. The unmodified model resulted in

incorrect moment distribution at the interior connection (Row 2). Applying $\alpha=0.33$ to both the slab flexural and torsional members gave a drift of only 53 percent of the observed drift (Row 4). An α value of 0.18 was required to arrive at the correct drift (Row 5).

By adjusting the β values for both flexural and torsional members, and reducing α to 0.20, the observed values were very closely modeled (Row 7).

7.5.3.4 Suggested α and β values.

As at the 0.5 percent drift level, it was possible to arrive at a single set of α and β coefficients which, when applied to each of these analytical models, produced reasonably accurate results. These coefficients and the resulting moment and drift values for each model are shown in Table 7.8. These suggested values did not result in exact modelling in all cases, but certainly provided a better prediction of the observed behavior than the original coefficients suggested for each model.

7.6 Conclusions

Present structural analysis methods commonly used in practice include the effective width method and the equivalent frame method. The explicit transverse torsional method is a similar method proposed more recently by Cano and Klingner (Ref. 7.1). All of these models assume a uniform slab effective

width coefficient, α, and effective cracked section factor, β, for an entire span and often entire structure without regard for any variation in the extent of cracking.

None of these models was able to reproduce the slab flexural moment distribution observed in the control specimen, 2C at either 0.5 or 1.5 percent drift levels. In addition, using the α and β coefficients suggested for each method generally resulted in underestimation of the lateral drift, especially at the 1.5 percent drift level.

Observation of the extent of cracking at various sections in the test specimen, lead to a modified model for each of the above analysis methods. By replacing the single beam element with two beam elements connected at the point of contraflexure, the difference between cracking in the positive and negative moment regions was incorporated into the model (Figs. 7.1 and 7.2). The point of contraflexure was found from the observed slab moment distribution.

The β values could now be selected for each individual beam element to correctly represent the cracking in that region of the slab. This approach resulted in correct prediction of the slab moment distribution. Adjustment of the α coefficient resulted in correct modelling of the observed lateral drift for each analysis method.

Common α and β coefficients were selected which produced reasonable results when applied to any of the three analysis methods. These coefficients are listed in Table 7.4 for the 0.5 percent drift level and Table 7.8 for the 1.5 percent drift level.

As at the 0.5 percent drift level, an α value of 0.4 was used. The β values were then half of the values found for the 0.5 percent drift level due to the increased slab cracking. For beam elements with positive moment, $\beta = 0.5$, while for negative moment, $\beta = 0.2$ at exterior connections and $\beta = 0.1$ at interior connections.

Table 7.1 - Analysis Results Using the Effective Width Method at 0.5 percent drift

ROW NO.	MODEL COEFFICIENTS $(\alpha \times \beta)$		α	β	Slab Moment (K-in) West Ext.	West Int.	East Int.	East Ext.	Drift (%)
1	TEST	SPEC	–	–	73	-82	88	-143	0.50
2	.4 .4	.4 .4	.4	1.0	26	-172	17	-168	0.19
3	.13 .13	.13 .13	.4	.33	21	-174	18	-172	0.53
4	1.0 .09	1.0 .24	1.0	–	71	-87	85	-142	0.21
5	.34 .03	.34 .08	.34	–	65	-88	88	-144	0.53

Table 7.2 - Analysis Results Using the Equivalent Frame Method at 0.5 percent drift

ROW NO.	MODEL COEFFICIENTS $(\alpha \times \beta)$		α	β	Slab Moment (K-in)				Drift (%)
					West Ext.	West Int.	East Int.	East Ext.	
1	TEST	SPEC	–	–	73	-82	88	-143	0.50
2	1.0 1.0	1.0 1.0	1.0	1.0	58	-181	-6	-152	0.15
3	.33 .33	.33 .33	1.0	.33	35	-177	8	-164	0.27
4	.15 .15	.15 .15	1.0	.15	26	-176	13	-169	0.52
5	1.0 .08	1.0 .25	1.0	–	83	-83	76	-142	0.24
6	.45 .036	.45 .113	.45	–	71	-82	85	-147	0.45

Table 7.3 – Analysis Results Using the Explicit Transverse Torsional Member Method at 0.5 percent drift

ROW NO.	MODEL COEFFICIENTS ($\alpha \times \beta$)	α	β	Slab Moment (K-in)				Drift (%)
				West Ext.	West Int.	East Int.	East Ext.	
1	TEST | SPEC	–	– –	73	-82	88	-143	0.50
2	1.0 1.0 | 1.0 1.0 / 1.0 1.0 | 1.0	1.0	1.0 1.0	79 Tors	-172	-8	-141	0.11
3	.33 .33 | .33 .33 / 1.0 1.0 | 1.0	1.0	.33 1.0	49 Tors	-177	3	-156	0.12
4	.33 .33 | .33 .33 / .33 .33 | .33	1.0	.33 .33	73 Tors	-180	-12	-144	0.29
5	.20 .20 | .20 .20 / .20 .20 | .20	1.0	.20 .20	74 Tors	-178	-10	-142	0.51
6	.5 .06 | 1.0 .25 / .5 .25 | .50	1.0	– –	89 Tors	-83	53	-159	0.29
7	.25 .03 | .5 .125 / .25 .125 | .25	.50	– –	88 Tors	-81	54	-158	0.51

Table 7.4 – Analysis Results Using the Suggested Model Coefficients at 0.5 percent drift

METHOD	SUGGESTED MODEL COEFFICIENTS $(\alpha \times \beta)$		α	β	Slab Moment (K-in)				Drift (%)
					West Ext.	West Int.	East Int.	East Ext.	
TEST SPEC.	TEST	SPEC	–	–	73	–82	88	–143	0.50
EFF. WIDTH	.4 .08	.4 .16	.4	–	48	–112	64	–161	0.35
EQUIV. FRAME	.4 .08	.4 .16	.4	–	57	–113	57	–158	0.40
TRANS. TORS.	.4 .08 .4	.4 .16 .4	.4	–	86	–118	43	–137	0.34

Table 7.5 - Analysis Results Using the Effective Width Method at 1.5 percent drift

ROW NO.	MODEL COEFFICIENTS ($\alpha \times \beta$)		α	β	Slab Moment (K-in)				Drift (%)
					West Ext.	West Int.	East Int.	East Ext.	
1	TEST	SPEC	–	–	168	-153	214	-260	1.50
2	.4 .4	.4 .4	.40	1.0	128	-276	114	-273	0.35
3	.13 .13	.13 .13	.40	.33	122	-275	118	-275	0.97
4	.08 .08	.08 .08	.40	.20	121	-275	118	-274	1.54
5	1.0 .15	1.0 .40	1.0	–	177	-150	203	-262	0.32
6	.20 .03	.20 .08	.20	–	163	-148	212	-269	1.34

Table 7.6 - Analysis Results Using the Equivalent Frame Method at 1.5 percent drift

ROW NO.	MODEL COEFFICIENTS ($\alpha \times \beta$)				α	β	Slab Moment (K-in)				Drift (%)
							West Ext.	West Int.	East Int.	East Ext.	
1	TEST		SPEC		–	–	168	-153	214	-260	1.50
2	1.0	1.0	1.0	1.0	1.0	1.0	170	-274	86	-263	0.29
3	.33	.33	.33	.33	1.0	.33	140	-275	106	-270	0.56
4	.10	.10	.10	.10	1.0	.10	126	-275	114	-273	1.50
5	.75	.15	1.0	.35	1.0	–	168	-156	205	-262	0.44
6	.18	.03	.20	.07	.20	–	162	-153	217	-260	1.50

Table 7.7 - Analysis Results Using the Explicit Transverse Torsional Member Method at 1.5 percent drift

ROW NO.	MODEL COEFFICIENTS ($\alpha \times \beta$)		α	β	Slab Moment (K-in)				Drift (%)
					West Ext.	West Int.	East Int.	East Ext.	
1	TEST	SPEC	-	-	168	-153	214	-260	1.50
				-	Tors				
2	1.0 1.0 | 1.0 1.0	1.0 1.0 | 1.0	1.0	1.0	170	-273	84	-262	0.31
				1.0	Tors				
3	.33 .33 | .33 .33	1.0 1.0 | 1.0	1.0	.33	140	-275	105	-269	0.58
				1.0	Tors				
4	.33 .33 | .33 .33	.33 .33 | .33	1.0	.33	162	-274	89	-263	0.79
				.33	Tors				
5	.18 .18 | .18 .18	.18 .18 | .18	1.0	.18	160	-274	90	-263	1.42
				.18	Tors				
6	.6 .12 | 1.0 .35	.7 .10 | .7	1.0	-	171	-152	213	-256	0.35
				-	Tors				
7	.12 .024 | .20 .07	.14 .2 | .14	.20	-	157	-150	225	-260	1.50
				-	Tors				

Table 7.8 - Analysis Results Using the Suggested Model Coefficients at 1.5 percent drift

METHOD	SUGGESTED MODEL COEFFICIENTS ($\alpha \times \beta$)		α	β	Slab Moment (K-in) West Ext.	West Int.	East Int.	East Ext.	Drift (%)
TEST SPEC.	TEST	SPEC	-	-	168	-153	214	-260	1.50
EFF. WIDTH	.2 .04	.2 .08	.4	-	164	-170	199	-259	1.27
EQUIV. FRAME	.2 .04	.2 .08	.4	-	170	-170	193	-258	1.35
TRANS. TORS.	.2 .04 / .15 .2	.2 .08 / .15	.4	-	206 Tors	-174	170	-242	1.29

CHAPTER 8

EFFECT OF CONTINUITY ON SPECIMEN BEHAVIOR

8.1 Introduction

The majority of past research on slab-column connections has consisted of tests of individual interior or exterior connections. Assumptions were necessary at the specimen boundaries in order to simulate the lack of continuity. More recently, some researchers have studied multiple connection specimens and even entire floors (Ref. 1.8). These tests have provided valuable information for the evaluation of present design criteria which are based predominantly on single connection tests.

In the test program reported here, two individual connections, one interior (specimen 8I) and one exterior (specimen 9E) were tested under the same conditions as the combined control specimen (specimen 2C). This chapter focuses on the comparison between the behavior of the individual and combined specimens.

134

8.2 Test Setup

The test setup for combined specimen 2C is described in Chapter 2. The test arrangements for each of the single specimens, 8I and 9E, are shown in Fig. 2.3. The single specimens were identical to the combined specimen but seperated at midspan. The free slab edge was stiffened by means of steel channels bolted to the slab. This edge was allowed to rotate freely (no moment restraint) and translate horizontally (no axial force in the slab). The vertical displacement was restrained and the resultant vertical shear measured by a load cell. This edge condition approximates continuity of the slab provided the point of contraflexure occurs at midspan and no axial force develops in the slab.

In order to accurately model the shear and moment at the connection resulting from the slab gravity load, it was necessary to reposition the load points on the individual specimens. The slab gravity load applied to combined specimen 2C was described earlier (Chapter 2). For simplicity, the midspan moment caused by the gravity load in the combined specimen was not imposed on the individual specimens as its effect on the connections was considered minimal.

The slab loading was applied to the single connections before connecting the slab edge support. The midspan support

therefore registered zero shear at the start of the test. The individual specimens were subjected to exactly the same lateral displacement history as the combined specimen (Fig. 2.7).

8.3 Specimen Behavior and Cracking Pattern

8.3.1 Interior Connection

After applying the slab loading, both specimens 2C and 8I had single transverse flexural cracks at the face of the interior column. As the tests progressed, very similar cracking patterns developed at the interior connections (Figs. 3.2 and 3.8). Both combined and individual interior connections achieved peak lateral load at 3.5 percent drift. At 4 percent drift, however, the individual specimen failed in punching shear around the column as seen in Photo 8.1. The interior connection in the combined specimen showed no signs of punching shear failure though the test was continued to 5 percent drift (Photo 3.3).

8.3.2 Exterior connections

No cracking had occured at any of the exterior connections prior to application of lateral load. Again, as the drift level increased, the crack development was very similar between individual and combined specimens resulting in the crack patterns shown in Figs. 3.2 and 3.8. The predominant cracking

was in the form of diagonal torsion cracks through the slab edge and flexural cracks across the full slab width at the face of the column.

All exterior connections reached peak load at 3.5 percent drift. The load decreased at higher drift levels as the connections failed under a combination of torsional failure of the slab edge and flexural failure at the face of the column (Photos. 8.2 and 8.3).

8.4 Lateral Load Comparison

The total lateral load sustained by the combined specimen at each cycle peak was compared with the summation of lateral loads sustained by the individual connections at the same drift levels. These results are listed in Table 8.1 and shown in Fig. 8.1.

Up to a drift level of 1.5 percent, the individual and combined specimens supported almost exactly the same total lateral load. Beyond this point, the individual specimens dropped below the combined to a minimum of 80 percent of the combined by 5 percent drift.

Two major factors contributed to the increased strength of the combined specimen. Firstly, the axial force developed in the slab of the combined specimen, though of little effect at

low drift levels while the slab is still elastic, does increase the ultimate flexural capacity of the slab and so has an effect at larger drift levels and closer to the peak load.

Secondly, the failure or weakening of a particular connection is slowed by the ability of the combined specimen to redistribute the load to the other connections. In the individual specimens, there is no such mechanism for relieving an overload situation and the connection deteriorates more rapidly.

8.5 Interior Connection Unbalanced Moment.

The unbalanced moment at the interior connections of specimens 2C and 8I are listed in Table 8.2 and plotted in Fig. 8.2. The unbalanced moment was almost identical up until the individual connection failed at 4 percent drift.

The individual connection has been able to simulate the overall flexural behavior of the combined specimen interior connection very closely.

8.6 Exterior Connection Unbalanced Moment.

The results from both exterior connections of specimen 2C were compared with those from specimen 9E. Depending on the loading direction, the exterior connections may be subjected to either a positive or negative unbalanced moment. These moments are tabulated for each specimen in Table 8.3. By taking the average of the unbalanced moments in each direction, the

results can be plotted as shown in Fig. 8.3. The two specimens displayed similar unbalanced moments through the 2 percent drift level. Beyond this point, the individual specimens unbalanced moment dropped below that of the combined specimen to a minimum of 86 percent at 5 percent drift.

However, this average value obscures what is occuring in the two individual directions. Comparing the positive unbalanced moments only, results in Fig. 8.4. Clearly the individual specimen supported a greater positive unbalanced moment than the combined counterpart at the same drift level, with a maximum of 47 percent greater at 1 percent drift.

At the same time, the negative unbalanced moment of the individual connection was well below that of the combined specimen at the same drift level as shown in Fig. 8.5, with a minimum of 70 percent of the combined value at 4 percent drift.

The reason for these differences lies in the assumption that the point of contraflexure is stationary at midspan of the slab. In fact, the point of contraflexure in the combined specimen moved around within the middle third of the span depending on the direction of loading as shown in the slab moment distribution diagrams for ± 3.5 percent drift shown in Fig. 8.6.

For the same lateral drift applied to the column, the shorter distance to the point of contraflexure in the combined specimen resulted in a larger negative moment at the face of the column. Hence, at the same drift level, the individual connection sustained a smaller negative moment than the combined. The inverse is true for the positive moment, where the individual specimen sustained a higher unbalanced moment at the same drift level.

A similar phenomenon occured at the interior connection. However, since the unbalanced moment is the difference between the moments on either side of the column, this phenomenon was obscured.

It is extremely important therefore that the location of the point of contraflexure be kept in mind when considering results from individual specimens. The assumption that the point of contraflexure is stationary at midspan is incorrect for a slab supporting a gravity load or for a slab with unequal top and bottom reinforcement. In other words, for almost every practical situation the point of contraflexure will not remain fixed at midspan.

8.7 Lateral Load Stiffness

The peak-to-peak lateral load stiffness is defined as the slope of a line from the peak positive load to peak negative load for a particular cycle (Fig. 5.7). This is only one of

many possible stiffness measures, but it is the most convenient for non-subjective comparisons of various tests. The peak-to-peak lateral load stiffness of the three specimens, 2C, 8I and 9E are listed in Table 8.4. Also listed is the summation of one individual interior connection and two exterior connections. This value is then compared with that for the combined specimen. All of these values are plotted in Fig. 8.7.

As expected, the individual interior connection is considerably stiffer than the individual exterior connection. When added together to simulate the combined specimen, the results are very similar to those for specimen 2C. The summation of individual connection stiffnesses is only slightly less than the stiffness of the combined specimen.

Since the peak-to-peak stiffness effectively averages the stiffnesses in the positive and negative loading directions, the effect of movement of the point of contraflexure in the combined specimen is not evident. Considering the individual tangent or secant stiffnesses for positive and negative loading curves seperately may produce a different comparison.

8.8 Axial Force in the Slab

Another significant difference between the combined and individual connections was the effect of slab elongation. Flexural cracks formed at the tension surface of the slab at

low drift levels. Subsequent compression is initially resisted by the slab reinforcement hence the crack did not close completely under load reversal. As the test progressed and more cracking occured, this resulted in elongation of the slab between the columns.

In the single connection specimens, the slab edge at midspan was free to move horizontally relative to the column and so this elongation did not induce any loads in the specimen. However, in the combined specimens, this slab elongation was resisted by the columns which were maintained equidistant at top and bottom supports. As in a typical flat slab structure, the columns were relatively stiff flexurally and so an axial compressive force developed in the slab.

In a typical flat slab structure, the columns are not restrained at midheight, but at the floor levels above and below the floor under consideration. Hence, the induced axial forces would be lower than those observed in the test specimens. However, if inelastic action is limited to the floor under consideration, the axial force in the slab could be substantial. At the first level above the foundation, the restraint at the base of the columns would also result in axial forces in the slab. The maximum slab axial stress observed in the control specimen was $0.01 f_c'$ over the gross slab cross-sectional area.

142

8.9 Conclusions

1. For low drift levels, the summation of individual connection lateral loads is identical to that of the combined specimen. Beyond 1.5 percent drift, the combined specimen supports up to 20 percent more lateral load than the individual connection specimens. This is the result of the slab axial force caused by slab elongation, and the ability of the combined specimen to redistribute load away from a weak connection.

2. The assumption that the point of contraflexure in the slab is stationary at midspan is invalid for almost all practical situations. An appreciation of the movement of the point of contraflexure is essential for the correct interpretation of results obtained from individual connection tests which make this assumption.

3. Slab moments at the face of the supports, both interior and exterior, were affected by the movement of the point of contraflexure. Negative slab moments were greater in the combined specimens while positive moments were lower at the same drift levels.

4. The summation of the stiffness of the individual connections is almost identical to the stiffness of the combined specimen.

Table 8.1 - Total Lateral Load Comparison

Drift	Specimen Lateral Load (Kip)								Sum	Ratio
(%) (1)	+2 (2)	-2 (3)	2ave (4)	+8 (5)	-8 (6)	8ave (7)	+9 (8)	-9 (9)	T* (10)	T/2ave (11)
0.25	3.5	-4.0	3.75	1.51	-1.17	1.34	0.32	-2.41	4.07	1.09
0.50	6.8	-8.5	7.65	3.21	-2.76	3.00	1.30	-2.88	7.17	0.94
0.75	9.6	-10.8	10.20	4.64	-4.34	4.49	2.22	-3.25	9.96	0.98
1.00	11.4	-12.5	11.95	5.48	-5.10	5.29	3.04	-3.56	11.89	1.00
1.50	14.0	-15.6	14.80	6.81	-6.33	6.57	3.79	-4.05	14.41	0.97
2.00	15.7	-17.6	16.65	7.38	-7.24	7.31	4.23	-4.35	15.89	0.95
2.50	17.5	-18.8	18.15	8.08	-7.72	7.90	4.49	-4.45	16.84	0.93
3.00	18.4	-19.4	18.90	8.45	-8.25	8.35	4.66	-4.49	17.50	0.93
3.50	18.9	-19.8	19.35	8.75	-8.41	8.58	4.74	-4.35	17.67	0.91
4.00	18.4	-19.1	18.75	8.54	-8.35	8.45	4.58	-3.84	16.87	0.90
4.50	17.8	-18.4	18.10	7.90	-7.45	7.68	4.50	-3.54	15.72	0.87
5.00	14.7	-16.3	15.50	4.76	-4.76	4.76	4.38	-3.16	12.30	0.79

* Note: T = 8ave + 9 - (-9)

Table 8.2 - Interior Connection Unbalanced Moment Comparison

Drift	Specimen Lateral Load						Ratios		
(%) (1)	+2 (2)	-2 (3)	2ave (4)	+8 (5)	-8 (6)	8ave (7)	+8/+2 8=5/2	-8/-2 9=6/3	(8/2)ave 11=7/4
0.25	93	-122	107	99	-84	92	1.06	0.69	0.85
0.50	188	-257	323	214	-193	204	1.14	0.75	0.92
0.75	269	-332	301	3087	-302	305	1.14	0.91	1.02
1.00	325	-384	355	365	-354	360	1.12	0.92	1.01
1.50	405	-479	442	454	-440	447	1.12	0.92	1.01
2.00	438	-543	491	491	-505	498	1.12	0.93	1.02
2.50	497	-586	542	539	-540	540	1.08	0.92	1.00
3.00	531	-607	569	565	-579	572	1.06	0.95	1.01
3.50	548	-623	586	586	-593	590	1.07	0.95	1.01
4.00	538	-607	573	575	-589	582	1.07	0.97	1.02
4.50	529	-590	560	393	-519	456	0.74	0.88	0.81
5.00	482	-559	521	314	-342	328	0.65	0.61	0.63

Table 8.3 – Exterior Connection Unbalanced Moment Comparison

Drift	Specimen Lateral Load (Kip)						Ratios		
(%) (1)	+2 (2)	-2 (3)	T_2 4=2-3	+9 (5)	-9 (6)	T_9 7=5-6	+9/+2 (8)	-9/-2 (9)	T_9/T_2 11=7/4
0.25	15	-140	155	20	-149	169	1.33	1.06	1.09
0.50	60	-180	240	81	-179	260	1.35	1.00	1.08
0.75	105	-229	334	138	-202	340	1.29	0.88	1.02
1.00	128	-259	387	188	-221	409	1.47	0.85	1.06
1.50	163	-311	474	235	-251	486	1.44	0.81	1.03
2.00	210	-328	538	262	-270	532	1.25	0.82	0.99
2.50	243	-342	585	278	-276	554	1.14	0.81	0.95
3.00	257	-345	602	289	-278	567	1.13	0.81	0.94
3.50	267	-347	614	294	-270	564	1.10	0.78	0.92
4.00	266	-326	592	284	-238	522	1.07	0.73	0.88
4.50	267	-311	578	279	-219	498	1.04	0.70	0.86
5.00	264	-279	543	272	-196	468	1.03	0.70	0.86

Table 8.4 - Peak-to-Peak Stiffness Comparison

| Drift (%) (1) | Specimen Lateral Load Stiffness (K/in) | | | | Ratio |
	2 (2)	8 (3)	9 (4)	T=9+8+9 (5)	T/2 (6)
0.25	23.6	8.65	8.81	26.3	1.12
0.50	24.7	9.63	6.74	23.1	0.94
0.75	21.9	9.66	5.88	21.4	0.98
1.00	19.3	8.53	5.32	19.2	0.99
1.50	15.9	7.06	4.22	15.5	0.97
2.00	13.4	5.90	3.46	12.8	0.95
2.50	11.7	5.10	2.88	10.9	0.93
3.00	10.2	4.49	2.46	9.4	0.93
3.50	8.9	3.95	2.09	8.1	0.91
4.00	7.5	3.41	1.70	6.8	0.90
4.50	6.5	2.75	1.44	5.6	0.87
5.00	5.0	1.71	1.22	4.2	0.83

CHAPTER 9

SUMMARY AND CONCLUSIONS

9.1 Summary

Nine large scale slab-column subassemblies were tested under simulated earthquake loading. Seven of the subassemblies represented a half scale model of a single floor of a two-bay flat plate structure. Each subassembly consisted of one interior and two exterior slab-column connections. In addition, two individual connection specimens were subjected to the same lateral loading as the combined subassemblies. They represented an interior and exterior connection disconnected at midspan. All of the specimens were subjected to the same lateral displacement history.

A number of variables were considered in this test program. The effect of a stiff edge beam or a slab overhang at the exterior connections was investigated by means of two specimens. The effect of slab shear reinforcement in the form of closed hoop stirrups in the slab along the column lines was studied using a single specimen. Two specimens were subjected to increased slab gravity load to investigate the effect of gravity load on the connection behavior.

147

148

Other areas investigated included the effect of continuity on the performance of a combined indeterminate subassembly compared with the individual interior and exterior connections. Various structural analysis methods were applied to the test subassembly and the results compared with the specimen performance to evaluate the accuracy of present analytical methods. An attempt was made to better understand the behavior of the interior slab-column connection at failure so as to develop a more rational design approach than used by current design codes.

9.2 Conclusions

Based on the test results reported in this program, the following conclusions were made regarding the behavior of slab-column connections as part of a frame subjected to earthquake-type loading.

9.2.1 Interior connections

1. Increasing the slab gravity load and subsequent shear level at the interior connection significantly reduced the capacity of the connection to transfer unbalanced moment.

2. For a direct gravity shear in excess of $1.2\sqrt{f_c'}\,b_o d$, the ACI code design approach for transferring shear and unbalanced moment at an interior connection was unconservative.

3. Increasing the slab gravity load and subsequent shear level at the interior connection also significantly reduced the lateral drift that the specimen could attain prior to failure. To achieve a drift level of 1.5 percent prior to failure, the ultimate direct shear must be limited to $V_u \leq 1.4\sqrt{f_c'}\, b_o d$.

4. The stiffness of an interior connection reduced as the slab gravity load increased. This was attributed to the accelerated slab cracking around the connection as a result of the increased gravity load moments.

5. All interior connections which failed in punching shear developed a rupture surface on the hogging side of the connection. When the diagonal tension on this rupture surface exceeded 50 percent of the modulus of rupture of the concrete, punching shear failure was imminent. Comparison with other researchers' results will help to more precisely define the area of the rupture surface and the tensile stress level at which punching shear failure can be expected to occur.

6. Closed hoop stirrups enclosing the slab flexural reinforcement passing through the interior connection prevented punching shear failure and increased the ductility of the connection. Despite the fact that the peak lateral load carried by this specimen was similar to that of the control specimen, the rate of strength deterioration after the peak was greatly

reduced by the presence of the closed hoop stirrups. Although inconvenient to install, closed hoop stirrups offer a viable alternative for increasing connection ductility.

9.2.2 Exterior connections

The following conclusions were reached regarding the behavior of exterior slab-column connections subjected to earthquake-type loading.

1. The strength of exterior connections in all specimens was observed to be 1.0 to 1.27 times the strength calculated using the linear shear stress variation model prescribed by the ACI code.

2. For the range of shear stress levels studied in these tests, the Committee 352 recommendation that moment and shear could be treated independently for design of exterior connections appears reasonable, though slightly conservative with respect to flexural capacity and unconservative with respect to shear capacity.

3. For exterior connections designed for seismic resistance using present ACI Code provisions, ductile flexural failure and a drift capacity of 1.5 percent can be achieved only if the ultimate direct shear on the critical perimeter is limited to $V_u \leq 2\sqrt{f_c'}\,b_o d$. The direct shear is the column axial force below the slab minus the column axial force above the slab.

4. A better estimate of the ultimate moment transfer capacity of the exterior connections was obtained by combining the torsional capacity of the slab edge with the flexural capacity of a slab strip $c_2 + h$ wide centered on the column. In conjunction with a limiting direct shear of $V_u = 2\sqrt{f_c'}b_o d$, this approach correctly predicted the mode of failure for the exterior connections of each specimen.

5. The subassemblies with stiff edge beam and slab overhang at the exterior connections carried higher lateral loads and sustained these loads to higher drift levels than the control specimen. The inconvenience of forming the stiff edge beam is likely to make it an unattractive option for many applications even though it clearly provided excellent protection of the exterior connection against deterioration during cyclic loading. The slab overhang beyond the exterior connection was able to provide similar advantages without the drawback of complex fabrication. Clearly this presents a realistic economical alternative which should be studied further.

9.2.3 Structural drift response

Based on analytical studies performed on the test specimens using various structural analysis methods, the following observations were made.

152

1. Present structural analysis methods commonly used in practice include the effective width method and the equivalent frame method. The explicit transverse torsional method is a similar method proposed more recently by Cano and Klinger (Ref. 7.1). All of these models assume a uniform slab effective width coefficient, α, and effective cracked section factor, β, for an entire span and often entire structure without regard for any variation in the extent of cracking. None of these models was able to reproduce the slab flexural moment distribution or drift observed in the control specimen, 2C at either 0.5 or 1.5 percent drift levels.

2. A modified double beam model which incorporates the difference between cracking in the positive and negative moment regions is proposed for each of the above analysis methods (Figs. 7.3 and 7.4). The specimen moment distribution and lateral drift were correctly predicted by this model using the following α and β factors. An effective width factor of $\alpha =0.4$ was used at both 0.5 and 1.5 percent drift levels. At 0.5 percent drift, the slab elements subjected to positive (sagging) moment were uncracked and so $\beta =1.0$ in these regions. For negative (hogging) moment, considerable cracking had occured at both exterior and interior connections, resulting in Beta values of $\beta =0.4$ at the exterior connection and $\beta =0.2$ at the interior connection. At 1.5 percent drift, the above Beta values are halved to account for the increased cracking.

9.2.4 Effect of continuity

From study of the effect of continuity on the connection behavior, the following observations were made.

1. For low drift levels, the summation of individual connection lateral loads is identical to that of the combined specimen. Beyond 1.5 percent drift, the combined specimen supports up to 20 percent more lateral load than the individual connection specimens. This is the result of the slab axial force caused by slab elongation, and the ability of the combined specimen to redistribute load away from a weak connection.

2. The assumption that the point of contraflexure in the slab is stationary at midspan is invalid for almost all practical situations. An appreciation of the movement of the point of contraflexure is essential for the correct interpretation of results obtained from individual connection tests which make this assumption.

3. Slab moments at the face of the supports, both interior and exterior, were affected by the movement of the point of contraflexure. Negative slab moments were greater in the combined specimens while positive moments were lower at the same drift levels.

154

18. When subjected to lateral load, the total stiffness of three individual connections is almost identical to the stiffness of the combined specimen which they represent.

REFERENCES

1.1 ACI-ASCE Committee 352, "Recommendations for Design of Slab-Column Connections in Monolithic Reinforced Concrete Structures," ACI Structural Journal, Vol. 85, No. 6, Nov.-Dec. 1988, pp. 675-696.

1.2 ACI Committee 318, "Building Code Requirements for Reinforced Concrete (ACI 318-83)," American Concrete Institute, Detroit, 1983, 111 pp.

1.3 Rankin, G. I. B., and Long, A. E., "Predicting the punching strength of conventional slab-column specimens," Proceedings of the Institute for Civil Engineers, Part 1, Vol 82, Apr. 1987, pp. 327-346.

1.4 Rankin, G. I. B., and Long, A. E., "Predicting the enhanced punching strength of interior slab-column connections," Proceedings of the Institute for Civil Engineers, Part 1, Vol 82, Dec. 1987, pp. 1165-1186.

1.5 Hawkins, N. M., Bao, A., and Yamazaki, J., "Moment Transfer from Concrete Slabs to Columns," ACI Structural Journal, Vol. 86, No. 6, Nov-Dec. 1989, PP. 705-716.

156

1.6 Rangan, B. V., and Hall, A. S., "Moment and Shear Transfer Between Slab and Edge Column," ACI Journal, Vol. 80, No. 3, May-June 1983, pp. 183-191.

1.7 Joint ASCE-ACI Task Committee 426 on Shear and Diagonal Tension, "The Shear Strength of Reinforced Concrete Members - Slabs," ASCE Journal of the Structural Division, Vol. 100, No. ST8, Aug. 1974, pp. 1543-1591.

1.8 Moehle, J. P., and Diebold, J. W., "Lateral Load Response of Flat-Plate Frame," ASCE Journal of the Structural Division, Vol. 111, No. 10, Oct. 1985, pp. 2149-2164.

1.9 Morrison, D. G., Hirasawa, I., and Sozen, M. A., "Lateral-Load Tests of R/C Slab-Column Connections," ASCE Journal of Structural Engineering, Vol. 109, No. 11, Nov. 1983, pp. 2698-2714.

1.10 Meli, R., and Avila, J. A., "The Mexico Earthquake of September 19, 1985 - Analysis of Building Response," Earthquake Spectra, Vol. 5, No. 1, 1989, pp. 1-17.

1.11 Sordo, E., Teran, A., Guerrero, J. J., Juarez, H., and Iglesias, J., "The Mexico Earthquake of September 19, 1985 - Ductility and Resistance Requirements Imposed on a Concrete Building," Earthquake Spectra, Vol. 5, No. 1, 1989, pp.41-50.

1.12 Rodriguez, M., and Diaz, C., "The Mexico Earthquake of September 19, 1985 - Analysis of the Seismic Performance of a Medium Rise, Waffle Flat Plate Building," Earthquake Spectra, Vol. 5, No. 1, 1989, pp. 25-40.

1.13 Meli, R., and Rodriguez, M., "Seismic Behavior of Waffle-Flat Plate Buildings," Concrete International - Design and Construction, Vol. 10, No. 7, July 1988, pp. 33-41.

1.14 Rosenblueth, E., "The Mexican Earthquake: A Firsthand Report," Civil Engineering/ASCE, Vol. 56, No. 1, Jan. 1986, pp. 38-40.

1.15 Report by the Subcommittee on Norms and Construction Procedures of the Committee for Mexico City's Metropolitan Area, National Reconstruction Commission, "The 1985 Earthquake: Causes and Effects in Mexico City," Concrete International - Design and Construction, Vol. 8, No. 5, May 1986, pp. 23-34.

2.1 Aalami, B., "Moment-Rotation Between Column and Slab," ACI Journal, Vol. 69, No. 5, May 1972, pp. 263-269.

2.2 Vecchio, F. J., and Collins, M. P., "Investigating the Collapse of a Warehouse," Concrete International - Design and Construction, Vol. 12, No. 3, March 1990, pp. 72-78.

158

2.3 Building Seismic Safety Council, "NEHRP Recommended Provisions for the Development of Seismic Regulations for New Buildings," 1985 Edition, Part 1, Washington, D.C., 1985, pp. 1-129.

2.4 Hawkins, N. M., and Mitchell, D., "Progressive Collapse of Flat Plate Structures," ACI Journal, Vol. 76, No. 7, July 1979, pp. 775-808.

2.5 Mitchell, D., and Cook, W. D., "Preventing Progressive Collapse of Slab Structures," ASCE Journal of the Structural Division, Vol. 110, No. 7, July 1984, pp. 1513-1532.

3.1 Jirsa, J. O., Baumgartner, J. L., and Mogbo, N. C., "Torsional Strength and Behavior of Spandrel Beams," ACI Journal, Vol. 66, Nov. 1969, pp. 926-932.

3.2 Islam, S., and Park, R., "Tests on Slab-Column Connections with Shear and Unbalanced Flexure," ASCE Journal of the Structural Division, Vol. 102, No. ST3, March 1976, pp. 549-568.

3.3 Park, R., and Islam, S., "Strength of Slab-Column Connections with Shear and Unbalanced Flexure," ASCE Journal of the Structural Division, Vol. 102, No. ST9, Sept. 1976, pp. 1879-1910.

3.4 Hawkins, N. M., "Siesmic Response of Reinforced Concrete Flat Plate Structures," Proceedings of the Seventh World Conference on Earthquake Engineering, Istanbul, Turkey, Sept. 9-13, 1980, pp. 33-40.

4.1 Moehle, J. P., "Strength of Slab-Column Edge Connections," ACI Structural Journal, Vol. 85, No. 1, Jan.- Feb. 1988, pp. 89-98.

4.2 Pan, A., and Moehle, J. P., "Lateral Displacement Ductility of Reinforced Concrete Flat Plates," ACI Structural Journal, Vol. 86, No. 3, May-June 1989, pp. 250-258.

4.3 Sozen, M. A., "Review of Earthquake Response of Reinforced Concrete Buildings with a View to Drift Control," State-of-the-Art in Earthquake Engineering, 7th World Conference on Earthquake Engineering, 1980, pp. 119-174.

4.4 Park, R., "Ductile Design Approach for Reinforced Concrete Frames," Earthquake Spectra, Vol. 2, No. 3, 1986, pp. 565-619.

6.1 Grossman, J. S., "Column-Slab Connection," Concrete International - Design and Construction, Vol. 11, No. 9, Sept. 1989, pp. 73-77.

160

6.2 Alexander, S. D. B., and Simmonds, S. H., "Ultimate Strength of Slab-Column Connections," ACI Structural Journal, Vol. 84, No. 3, May-June 1987, pp. 255-261.

6.3 Hanson, N. W., and Hanson, J. M., "Shear and Moment Transfer Between Concrete Slabs and Columns," Journal, PCA Research and Development Laboratories, Vol. 10, No. 1, Jan. 1968, pp. 2-16.

6.4 Di Stasio, J. Sr., and Van Buren, M. P., "Transfer of Bending Moment Between Flat Plate Floor and Column," ACI Journal, Proceedings, Vol. 57, No. 3, Sept. 1960, pp. 299-314.

6.5 Paulay, T., "Mechanisms and Magnitudes of Slab Participation in Two-Way Frames," Seminar Notes on Beam-Column Joints, Hawaii, May 1989, pp. 1-5.

6.6 Cheung, P. C., Paulay, T., and Park, R., " interior and Exterior Reinforced Concrete Beam-Column Joints of a Prototype Two_Way Frame with Floor Slab Designed for Earthquake Resistance," Research Report, University of Canterbury, New Zealand, March 1989, Appendix A, pp. 45-51.

7.1 Cano, M. T., and Klingner, R. E., "Comparison of Analysis Procedures for Two-Way Slabs," ACI Structural Journal, Vol. 85, No. 6, Nov-Dec. 1988, pp. 597-608.

7.2 Vanderbilt, M. D., and Corley, W. G., "Frame Analysis of Concrete Buildings," Concrete International - Design and Construction, Vol. 5, No. 12, Dec. 1983, pp. 33-43.

7.3 Fraser, D. J., " Simplified Frame Analysis for Flat Plate Construction," Concrete International - Design and Construction, Vol. 6, No. 9, Sept. 1984, pp. 32-41.

7.4 Gonzalez-Vidosa, F., Kotsovos, M. D., and Pavlovic, M. N., "Symmetrical Punching of Reinforced Concrete Slabs: An Analytical Investigation Based on Nonlinear Finite Element Modeling," ACI Structural Journal, Vol. 85, No. 3, May-June 1988, pp. 241-250.

7.5 Cotran, F. S., and Hall, W. J., "Effective Width of Floor Systems for Application in Seismic Analysis," Structural Research Series No. 486, Civil Engineering Department, University of Illinois, Nov. 1980, pp. 89.

7.6 Hawkins, N. M., and Corley, W. G., "Transfer of Unbalanced Moment and Shear from Flat Plates to Columns," Cracking, Deflection, and Ultimate Load of Concrete Slab Systems, SP-30, American Concrete Institute, Detroit, 1971, pp. 147-176.

7.7 Hartley, G., Rainer, J. H., and Ward, H. S., "Static and Dynamic Properties of a Reinforced Concrete Building Model,"

Building Research No. 140, Division of Building Research, National Research Council of Canada, Ottawa, Apr. 1979, pp. 1-24.

7.8 Neth, V. W., de Paiva, H. A., and Long, A. E., "Behavior of Models of Reinforced Concrete Flat Plate Edge-Column Connection," ACI Journal, Vol. 78, No. 4, July-Aug 1981, pp. 269-275.

7.9 Habibullah, A., "ETABS84 - Three Dimensional Analysis of Building Systems," Computers and Structures, Inc., Berkeley, California, Computer Program, 1984.

NOTATION

A_{cs} = area of slab critical section

A_F = area of rupture surface

A_{F1} = partial area of rupture surface

A_{F2} = partial area of rupture surface

A_{F3} = partial area of rupture surface

A_s = cross-sectional area of reinforcing bar

A_v = area of shear reinforcement within a distance s

b = slab width under consideration

b_e = slab effective width for structural analysis

b_o = perimeter of slab critical section

C = compression in inclined concrete struts

c_t = distance from column face to slab edge

c_1 = column dimension perpendicular to slab edge

c_2 = column dimension parallel to slab edge

C_v = modification factor from ACI Committee 352 Recommendations, Table 1

C_V = vertical component of concrete strut compression

d = d_{ave} = average effective depth of slab

d_l = slab effective depth for steel perpendicular to slab edge

D_P = drift at peak load

D_U = ultimate drift

D_Y = yield drift

E_c = elastic modulus of concrete

E_s = elastic modulus of slab reinforcement

f_c' = compressive strength of concrete

163

164

f_r = concrete modulus of rupture

f_s = concrete split cylinder strength

f_u = ultimate strength of slab reinforcement

f_y = yield strength of slab reinforcement

h = slab thickness

I = moment of inertia of section

J_c = polar moment of inertia of critical section

K_c = flexural stiffness of column

K_{ec} = effective stiffness of equivalent column

K_t = ACI suggested torsional stiffness of slab torsional member

l_1 = span in direction of loading

l_2 = span perpendicular to direction of loading

M_{cf} = observed slab moment at column face

M_f = theoretical flexural capacity of slab strip of width $c_2 + 3h$

M_{fc} = M_c = unbalanced moment based on measured reinforcement strains in slab width c_2 centered on column

M_{fo} = M_{ACI} = unbalanced moment based on measured reinforcement strains in slab width $c_2 + 3h$ centered on column

M_{f1} = moment capacity of slab width $c_2 + h$ at exterior connection

M_{f2} = moment capacity of slab width $c_2 + 3h$ at exterior connection

M_{f3} = moment capacity of slab width $c_2 + 2c_1$ at exterior connection

M_L = moment at left side of interior connection based on measured reinforcement strains

M_R = moment at right side of interior connection based on measured reinforcement strains

M_s = observed moment at centroid of critical section

M_t = M_T = unbalanced moment at connection based on measured reinforcement strains over full slab width

M_{th} = $M_{fl} + 2T_n$ = proposed theoretical moment capacity of an exterior connection

M_u = observed moment at centerline of column

M_{ub} = unbalanced moment at connection

r = $d/\tan 30$ = radius of rupture surface

R_{ACI} = M_{ACI}/M_t = ratio of slab moments

R_{col} = M_c/M_t = ratio of slab moments

R_{Mub} = M_{ub}/M_t = ratio of unbalanced moment from measured column moments over unbalanced moment from measured slab reinforcement strains

s = spacing of shear reinforcement in direction parallel to longitudinal reinforcement

T = tensile force in slab reinforcement

T_c = concrete torsional strength (ACI eqn. 11-22)

T_n = $T_c + T_s$ = nominal torsional capacity of slab edge

T_s = Torsional strength of steel (ACI eqn. 11-23)

V = slab shear force

v_c = nominal shear stress capacity of slab

V_c = nominal shear strength provided by concrete

v_g = direct shear stress due to gravity load only

V_g = direct shear force due to gravity load only

V_o = V_n = nominal shear capacity of slab in absence of moment transfer

V_s = nominal shear strength provided by shear reinforcement

v_u = direct shear stress at peak lateral load

V_u = direct shear force at peak lateral load

v_{AB} = shear stress computed at the front face of the slab critical section according to the eccentric shear stress model

v_{CD} = shear stress computed on exterior face of the slab critical section according to the eccentric shear stress model

v_{352} = direct shear stress on the slab critical section according to ACI Committee 352 Recommendations

V_{352} = direct shear on the slab critical section according to ACI Committee 352 Recommendations

α = effective slab width coefficient

β = coefficient representing cracked properties of slab section

β_c = ratio of long side to short side of reaction area

γ_f = $1 - \gamma_v$ = portion of unbalanced moment resisted by flexure

γ_v = portion of unbalanced moment resisted by eccentric slab shear stress

μ_p = displacement ductility based on peak drift

μ_u = displacement ductility based on ultimate drift

ϕ = strength reduction factor

ρ_{bal} = balanced reinforcement ratio

ρ_c = steel ratio of slab reinforcement at the column and perpendicular to the slab edge

ρ_l = steel ratio of slab reinforcement beyond the column and perpendicular to the slab edge

ρ_t = steel ratio of slab reinforcement parallel to the slab edge

σ_T = tensile stress perpendicular to concrete failure surface

θ_c = connection rotation

θ_p = joint rotation at peak lateral load

FIGURES
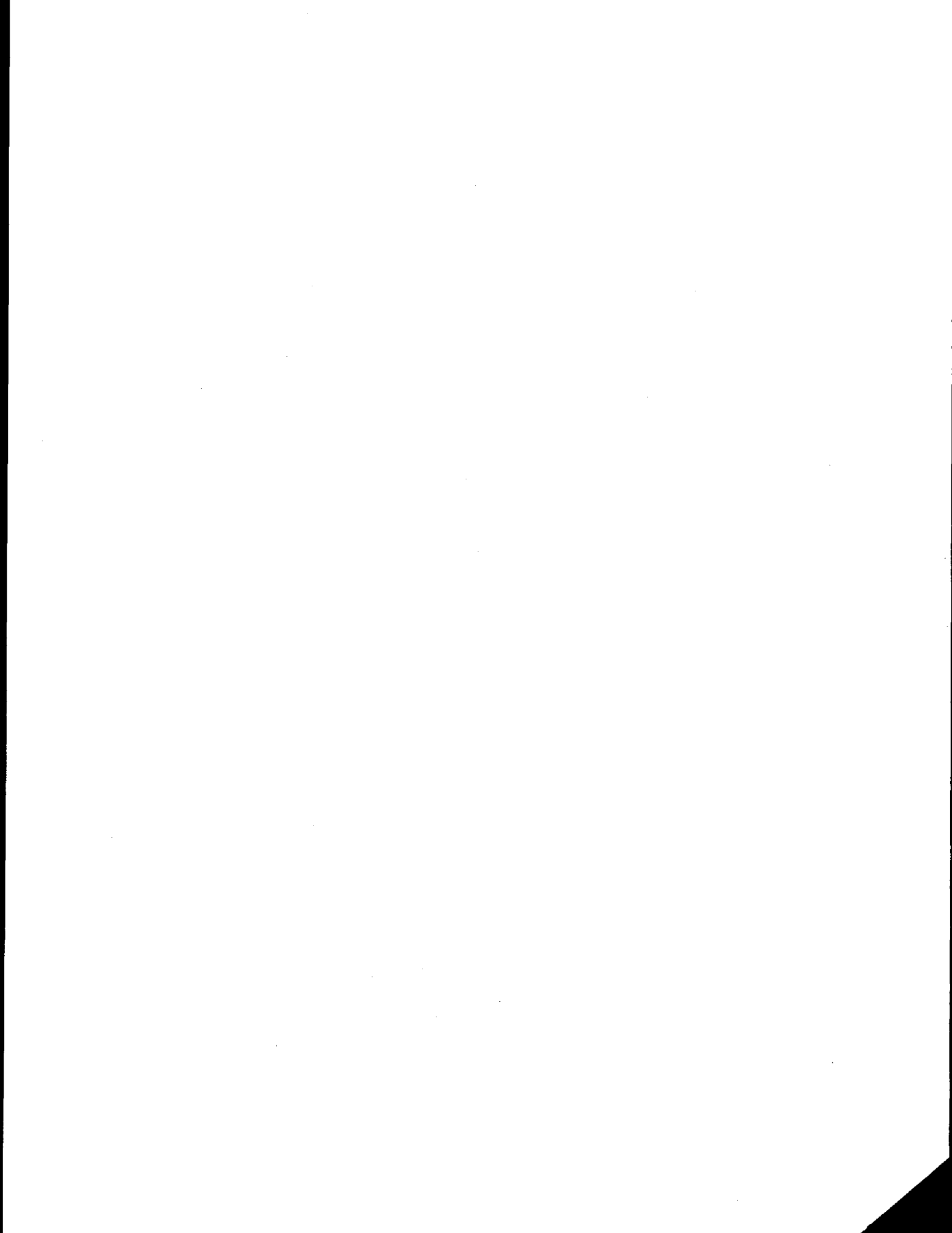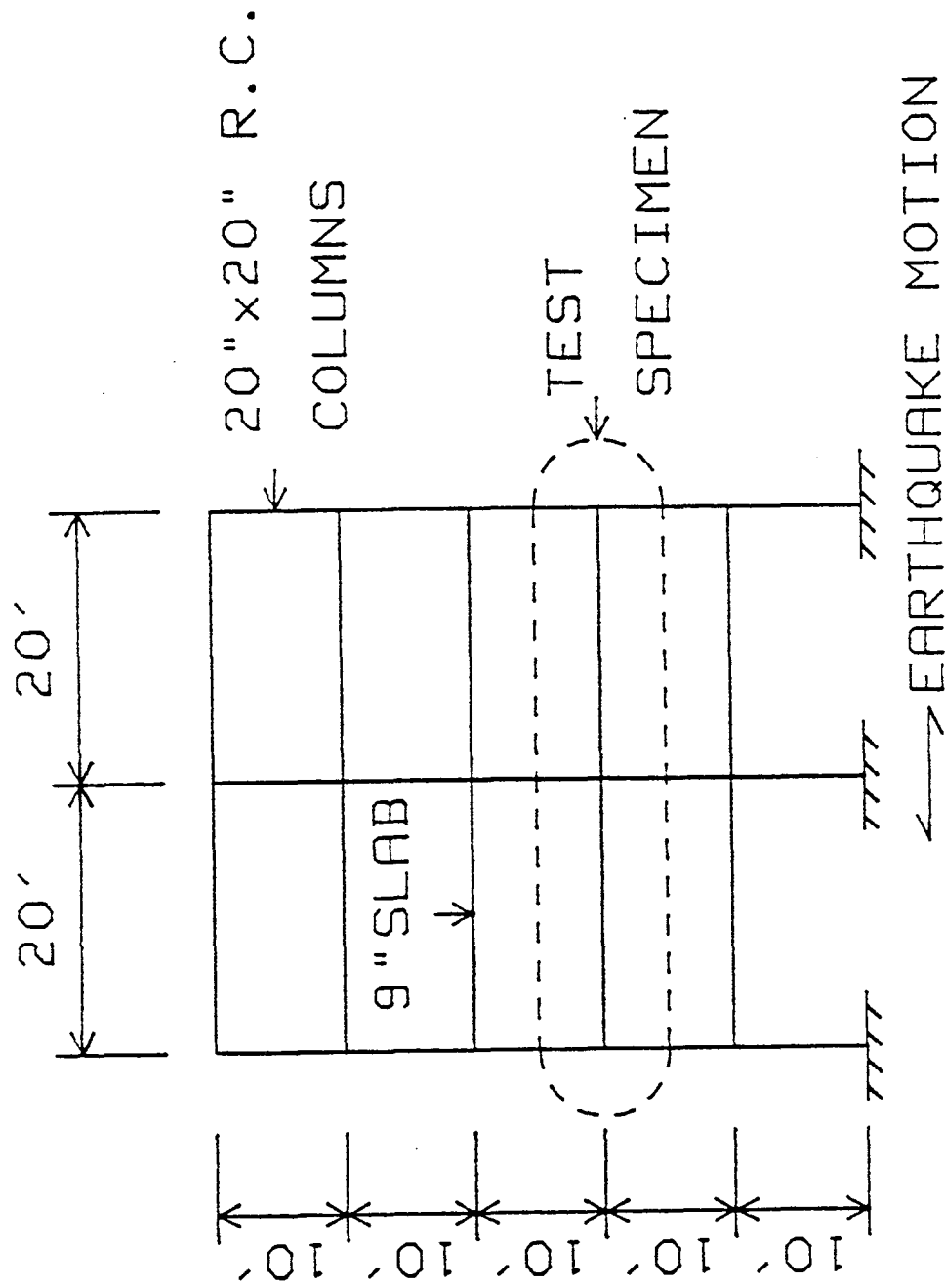
Fig. 2.1   Prototype structure

170
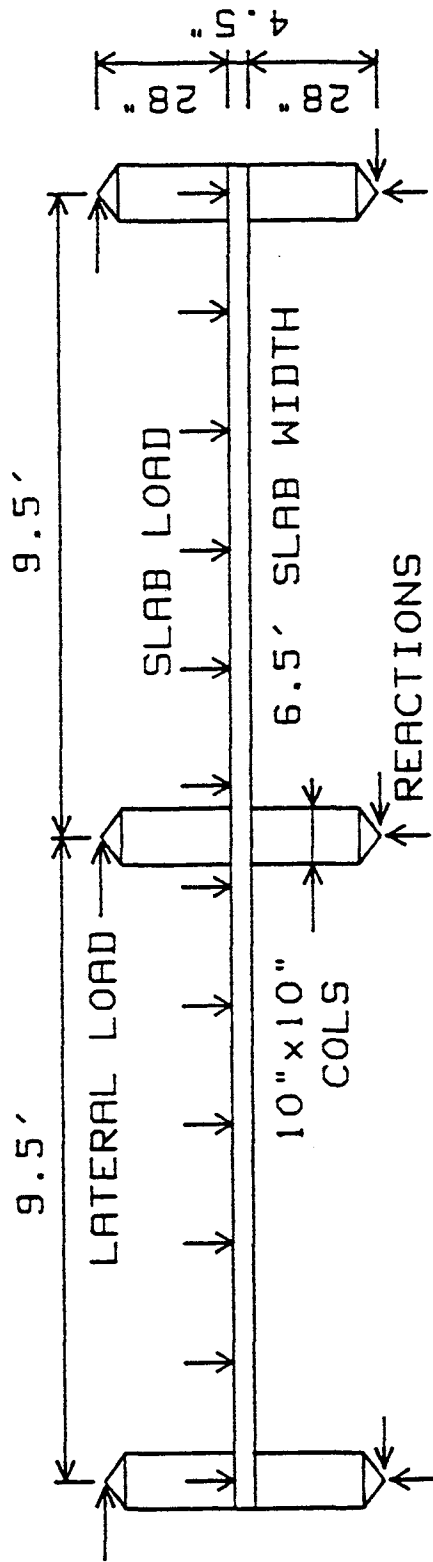
Fig. 2.2   Multiple connection test subassembly
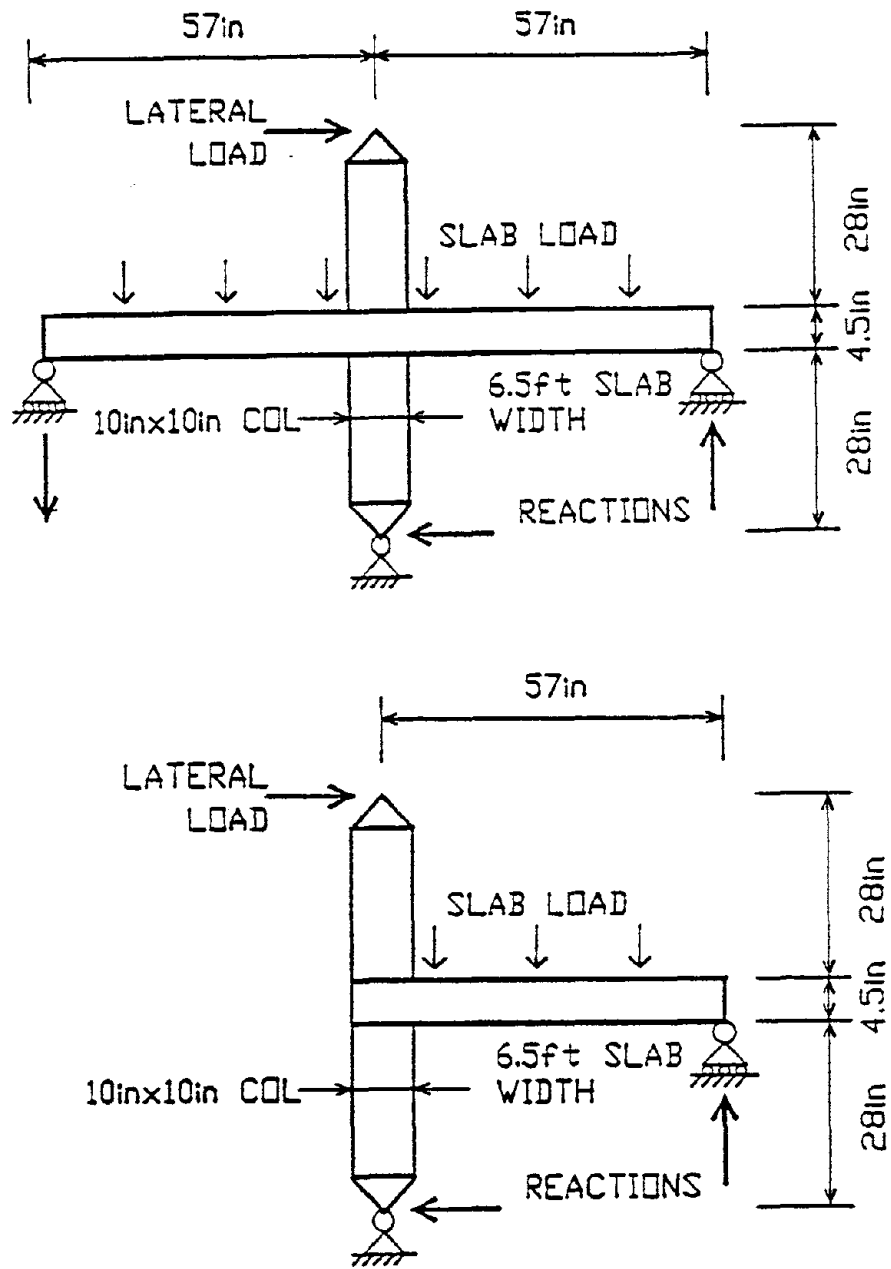
Fig. 2.3   Individual connection test specimens

172

Fig. 2.4 Test setup

LC = LOAD CELL

ACTUATOR

173
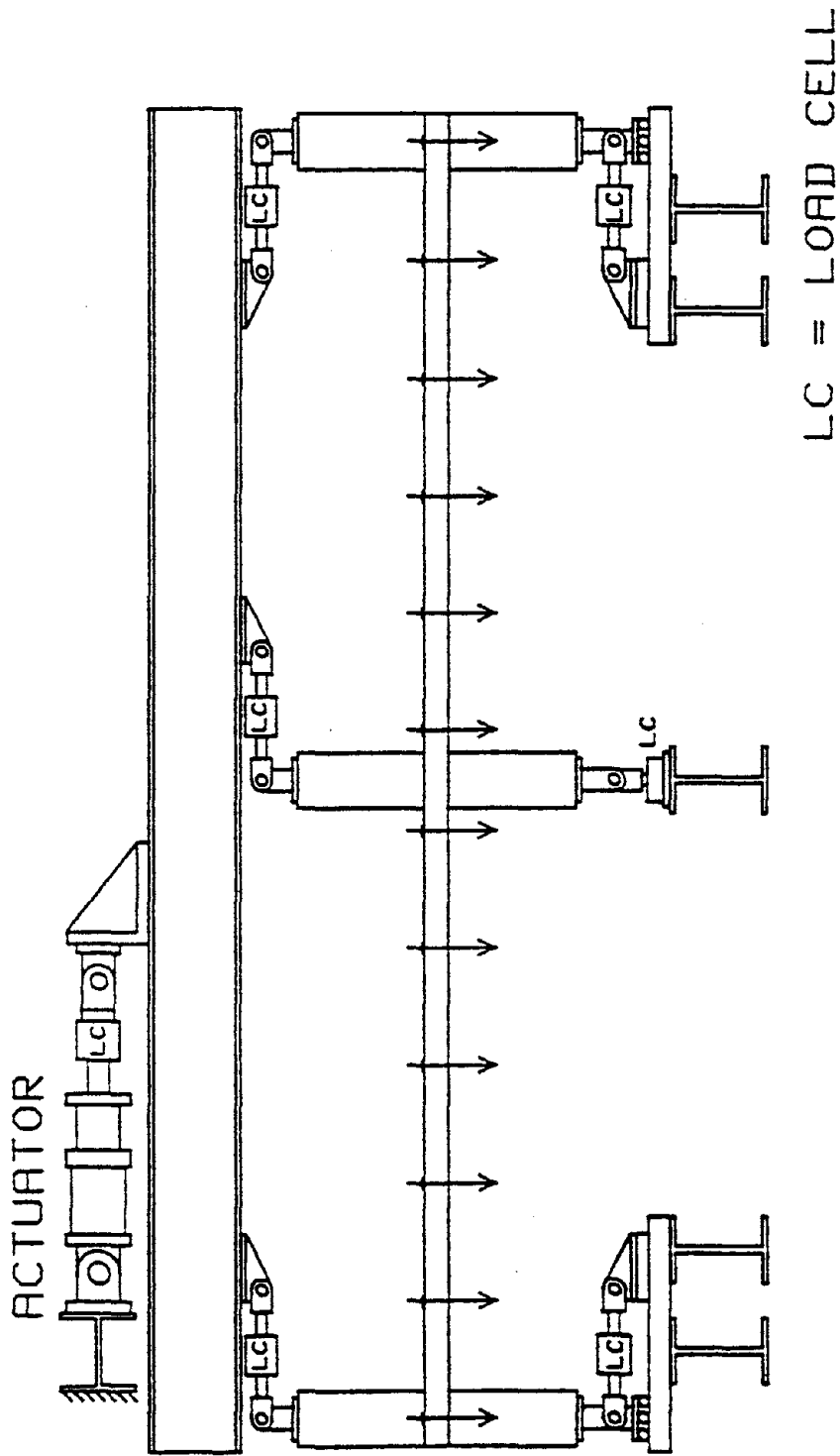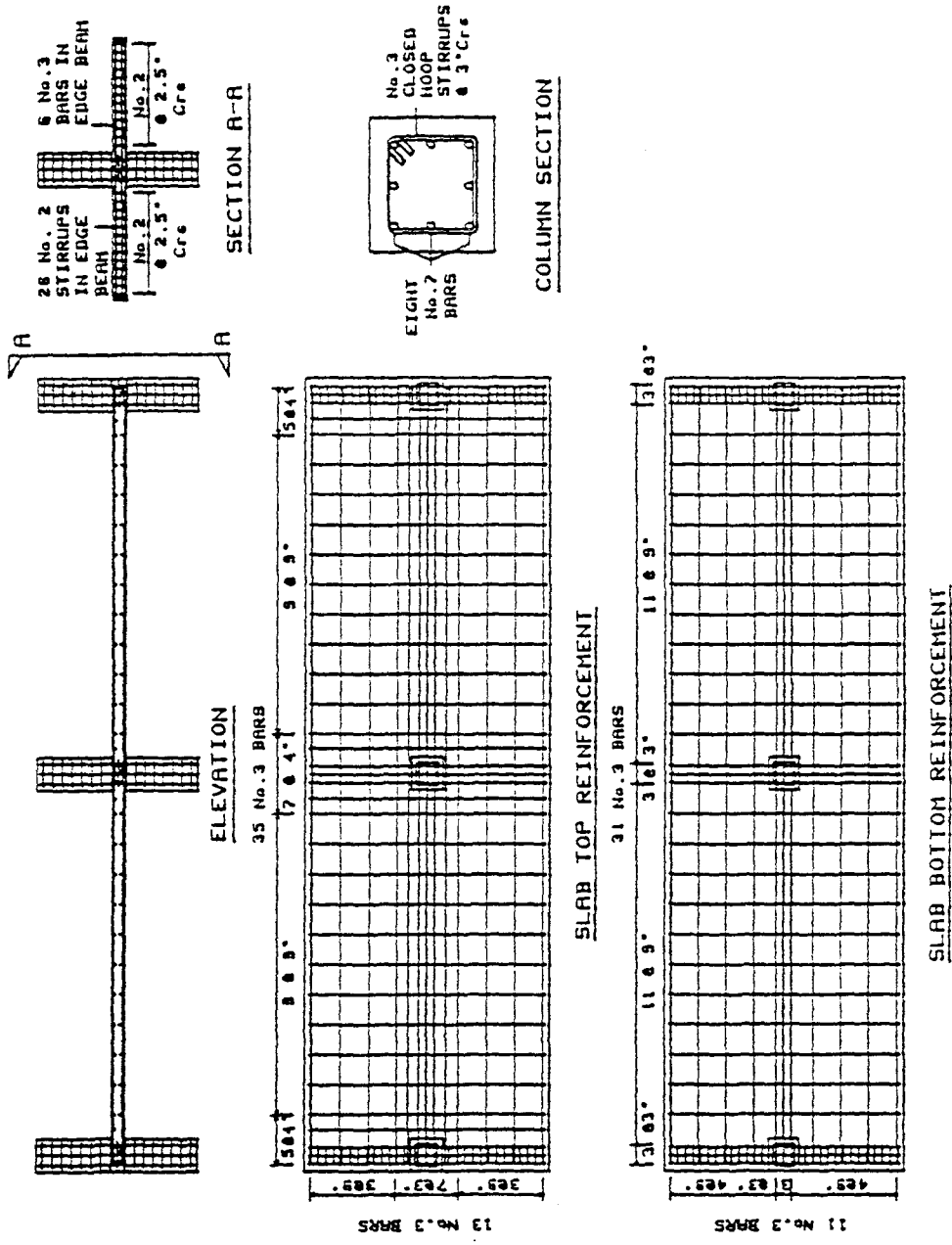
Fig. 2.5   Specimen reinforcement

174
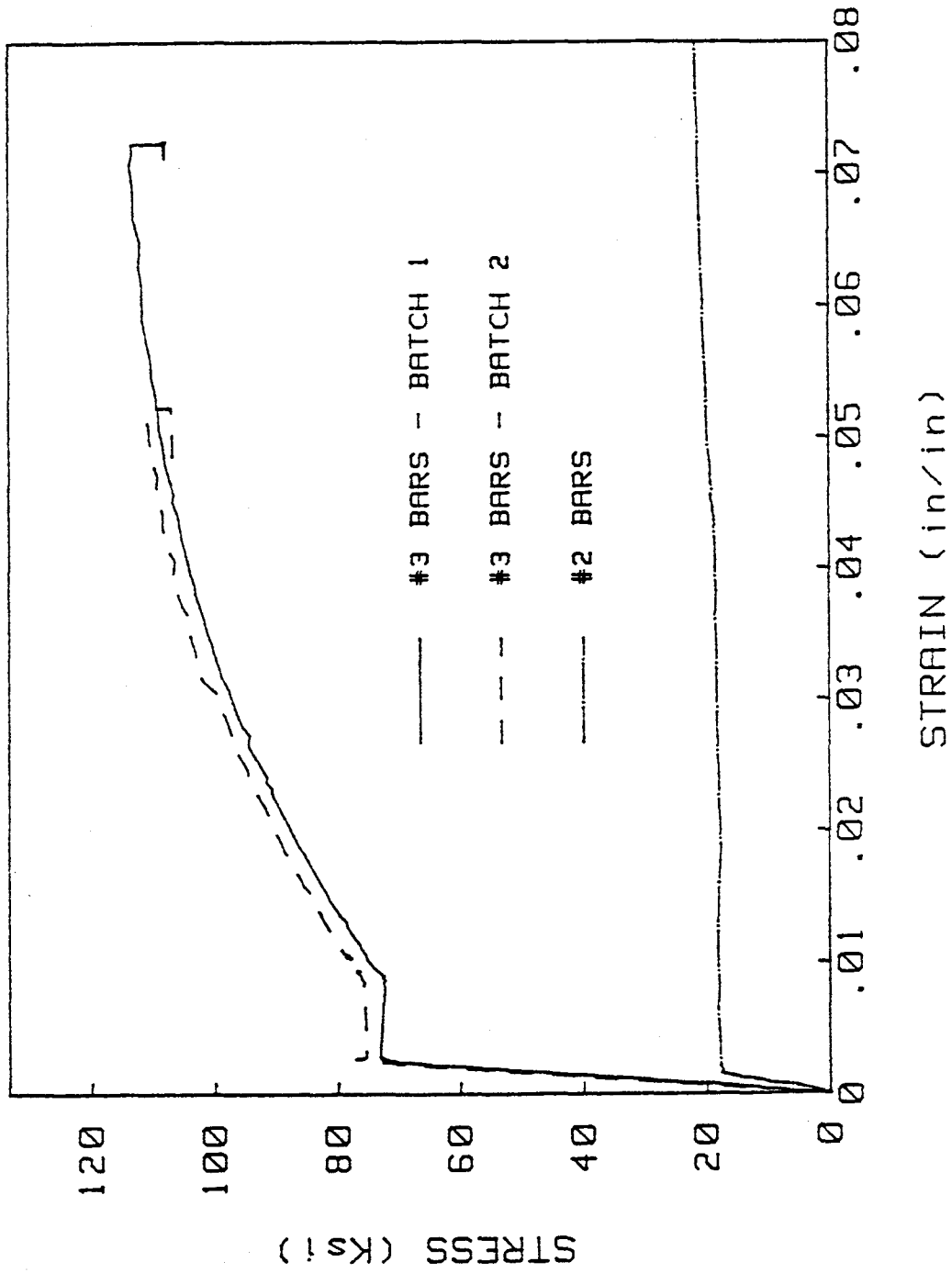
Fig. 2.6   Reinforcement stress-strain relationships

Fig. 2.7   Lateral displacement history

176

SPECIMEN 1

1.5% DRIFT

3.5% DRIFT

TOP OF SLAB

BOTTOM OF SLAB

TOP OF SLAB

BOTTOM OF SLAB
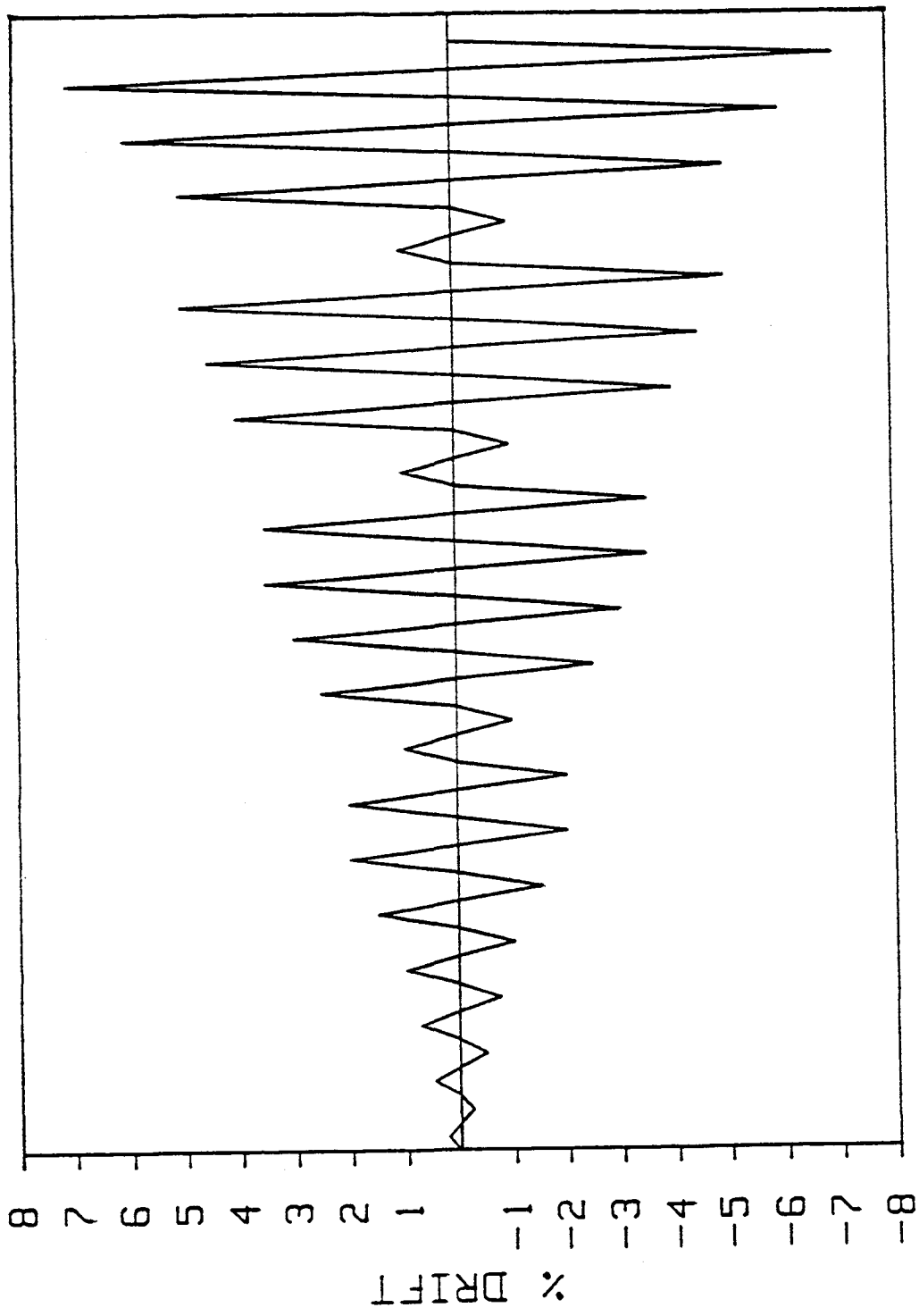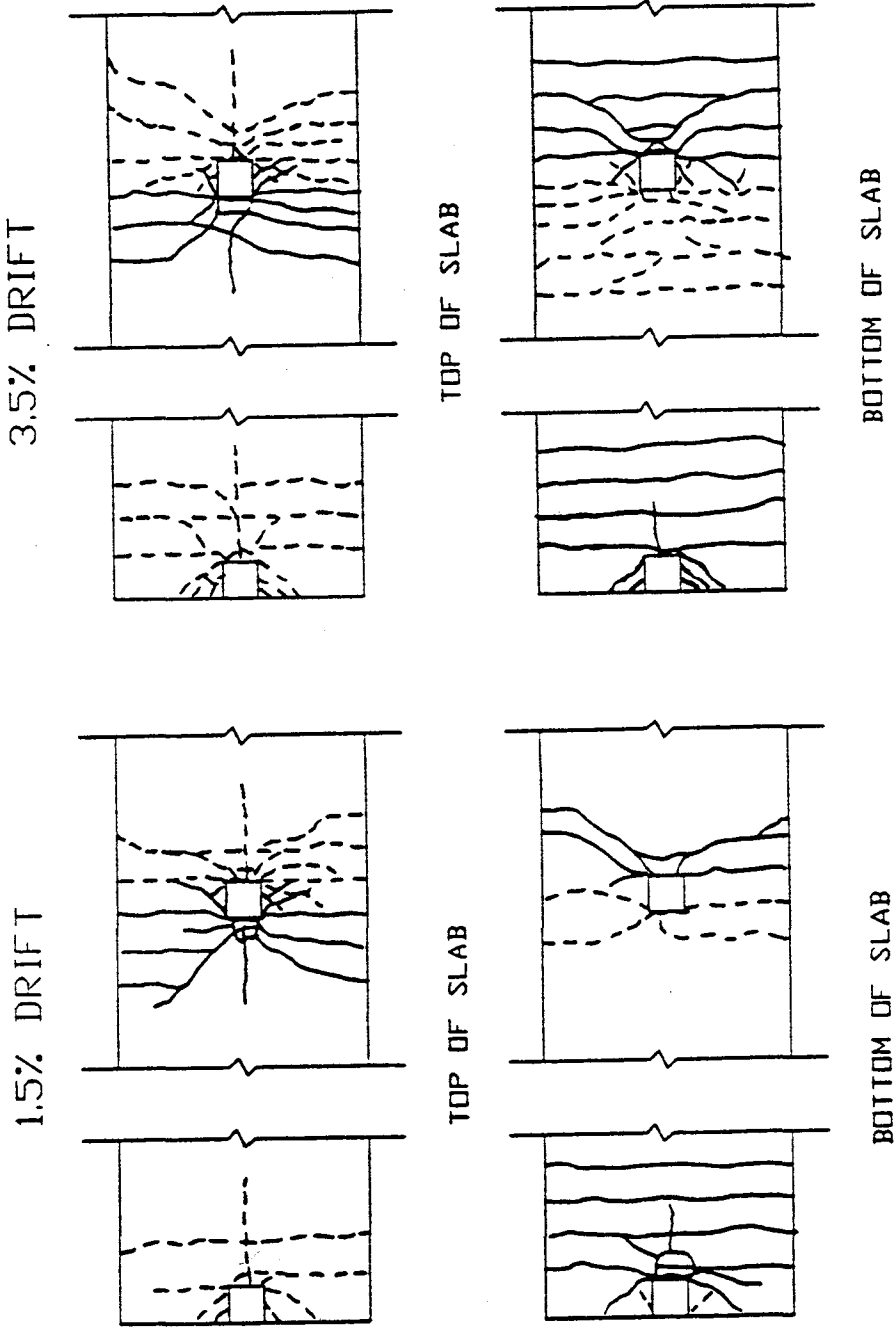
Fig. 3.1   Crack Patterns - Specimen 1

SPECIMEN 2C
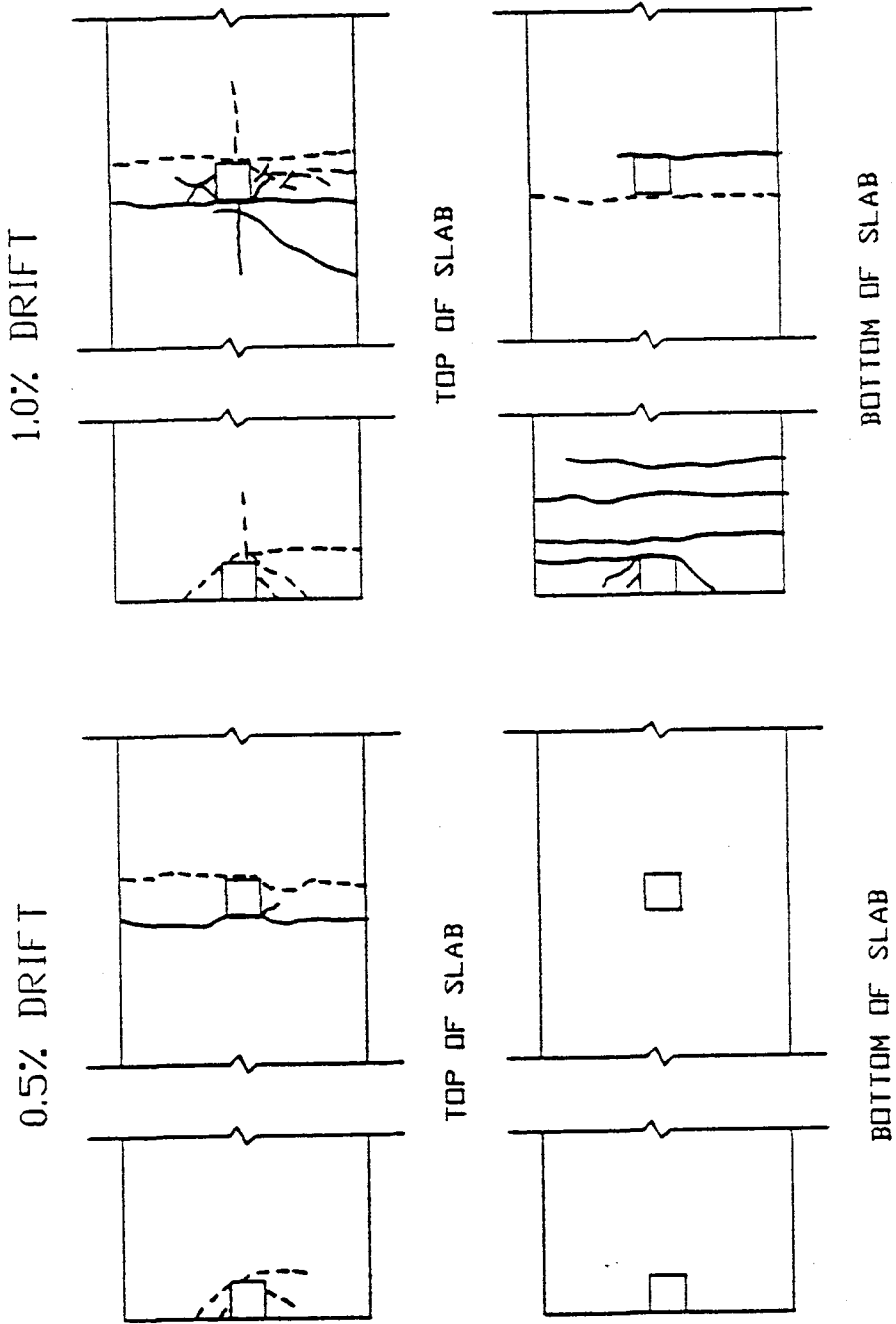
Fig. 3.2 a) Crack Patterns - Specimen 2C

178

SPECIMEN 2C

2.0% DRIFT

TOP OF SLAB

BOTTOM OF SLAB

1.5% DRIFT

TOP OF SLAB

BOTTOM OF SLAB
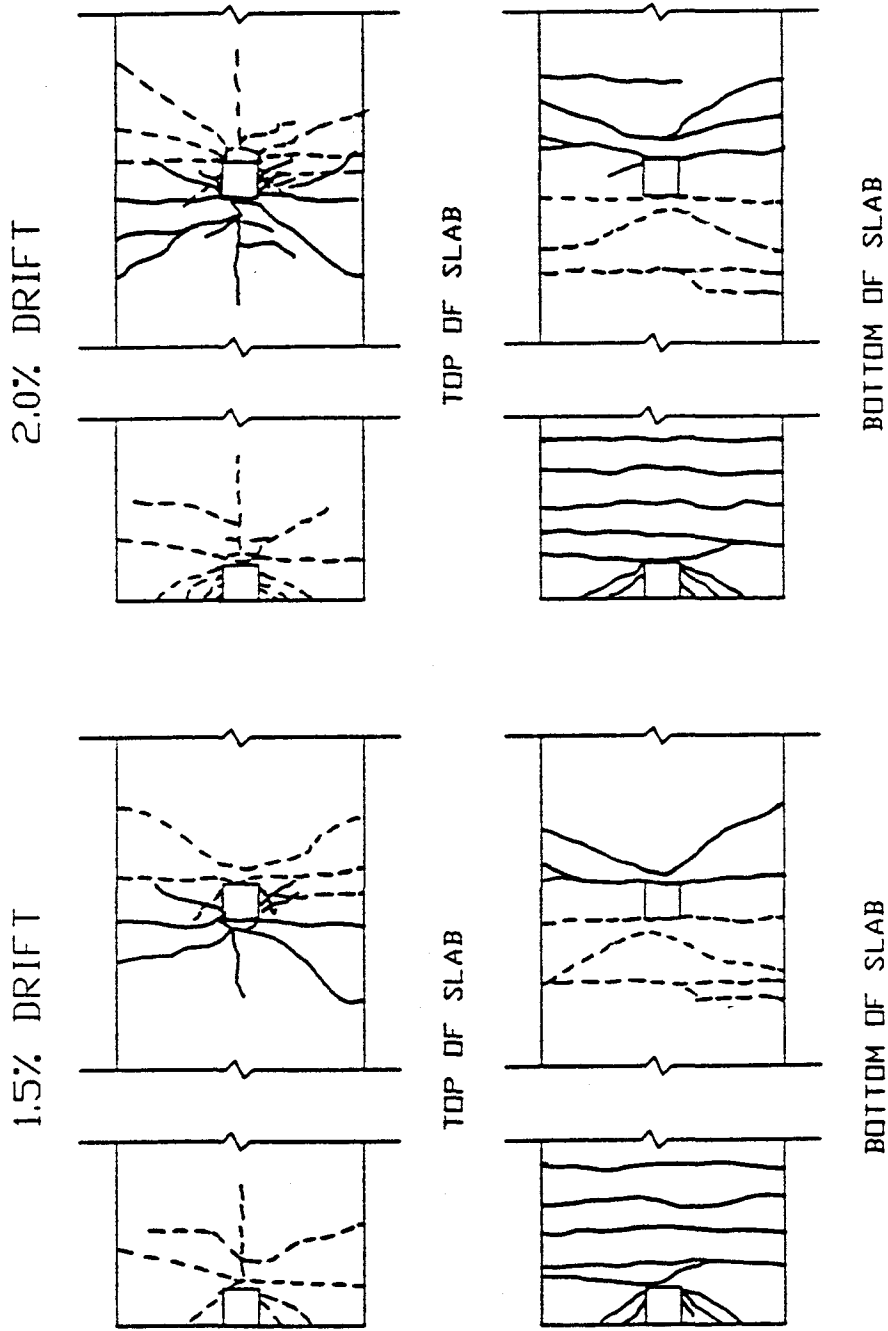
Fig. 3.2 b) Crack Patterns - Specimen 2C

179

SPECIMEN 2C

2.5% DRIFT

3.5% DRIFT

TOP OF SLAB

BOTTOM OF SLAB
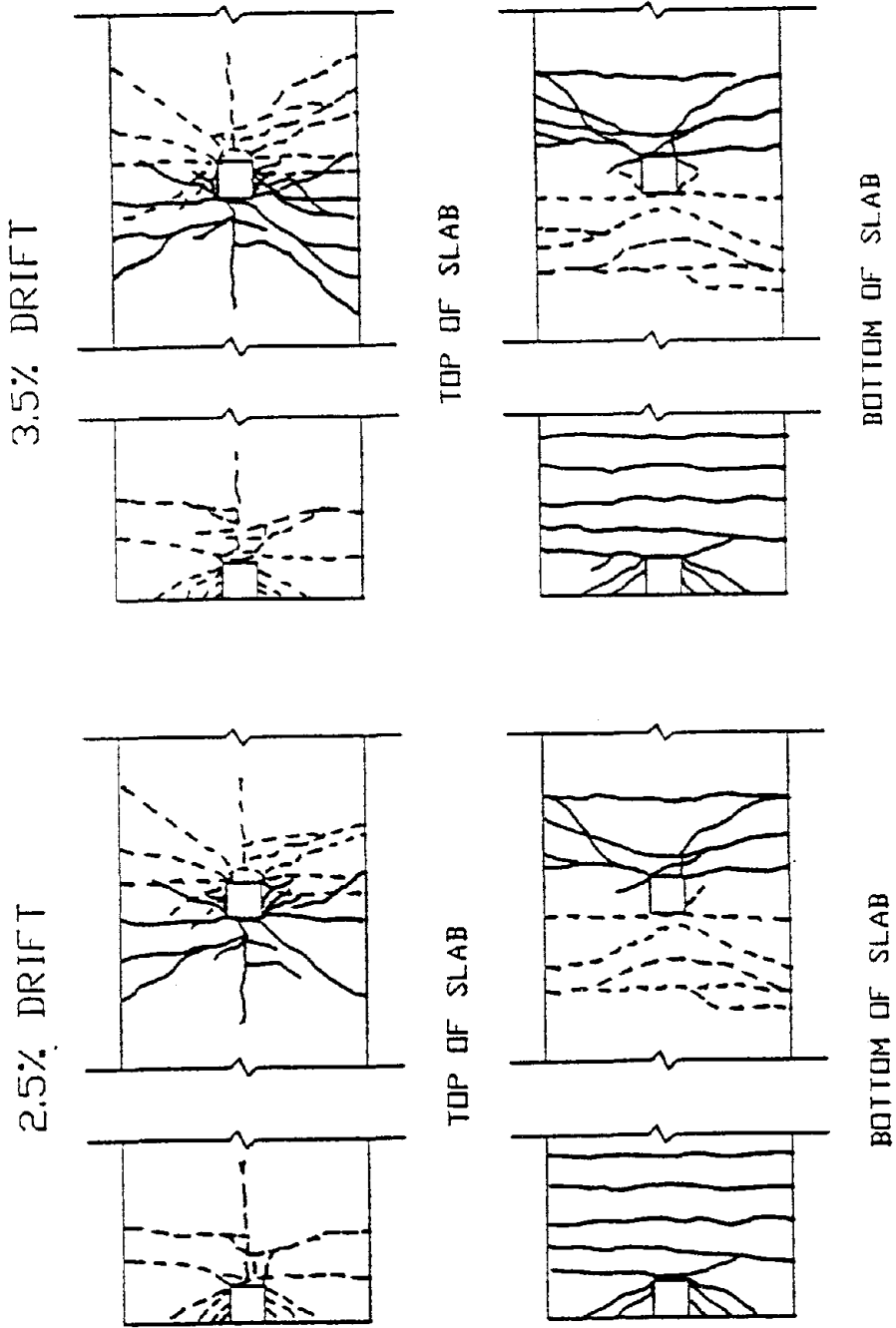
Fig. 3.2 c) Crack Patterns - Specimen 2C

180

SPECIMEN 3SE

1.5% DRIFT

3.5% DRIFT

TOP OF SLAB

BOTTOM OF SLAB
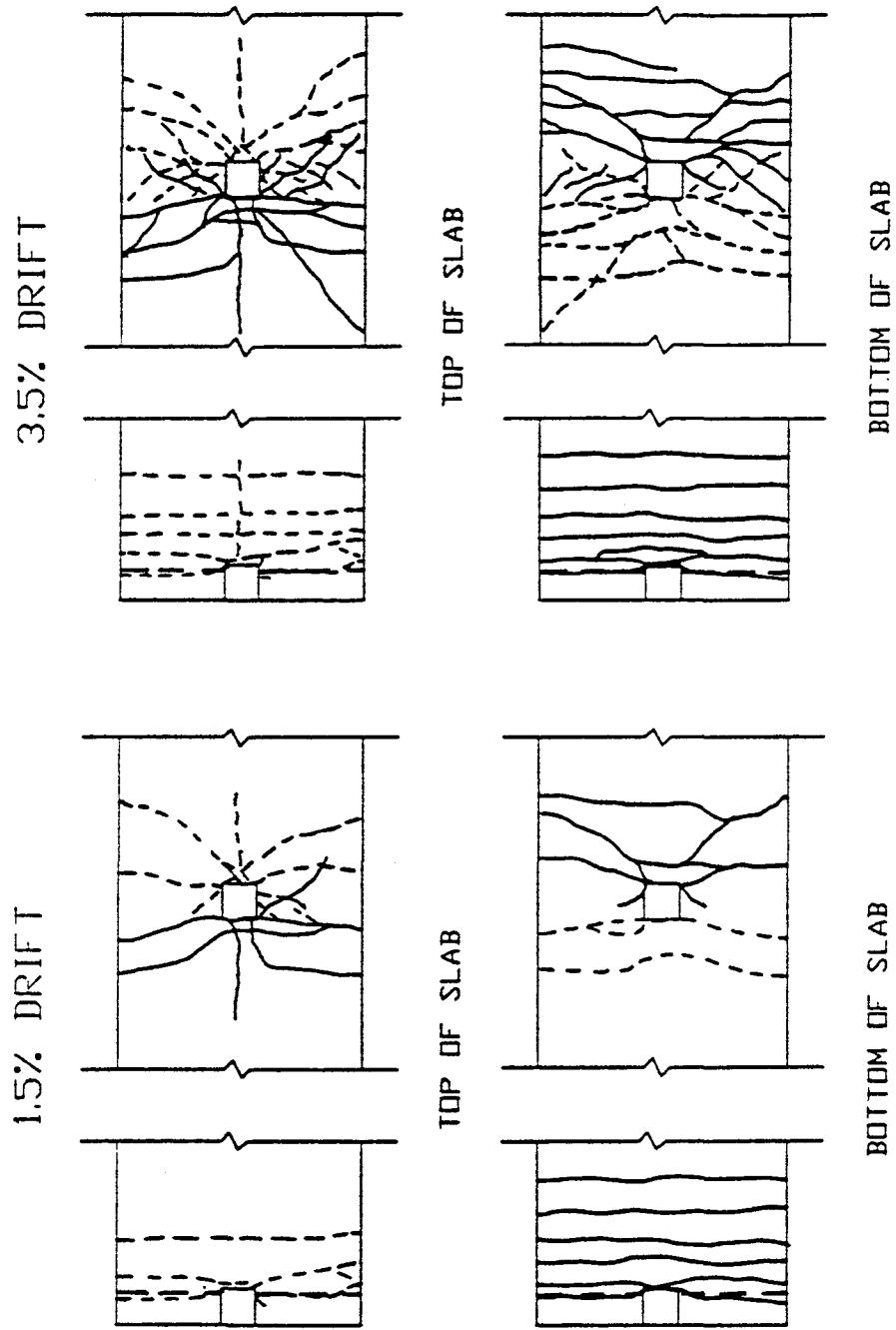
Fig. 3.3   Crack Patterns - Specimen 3SE

181

SPECIMEN 4S

3.5% DRIFT

1.5% DRIFT

TOP OF SLAB

BOTTOM OF SLAB

TOP OF SLAB
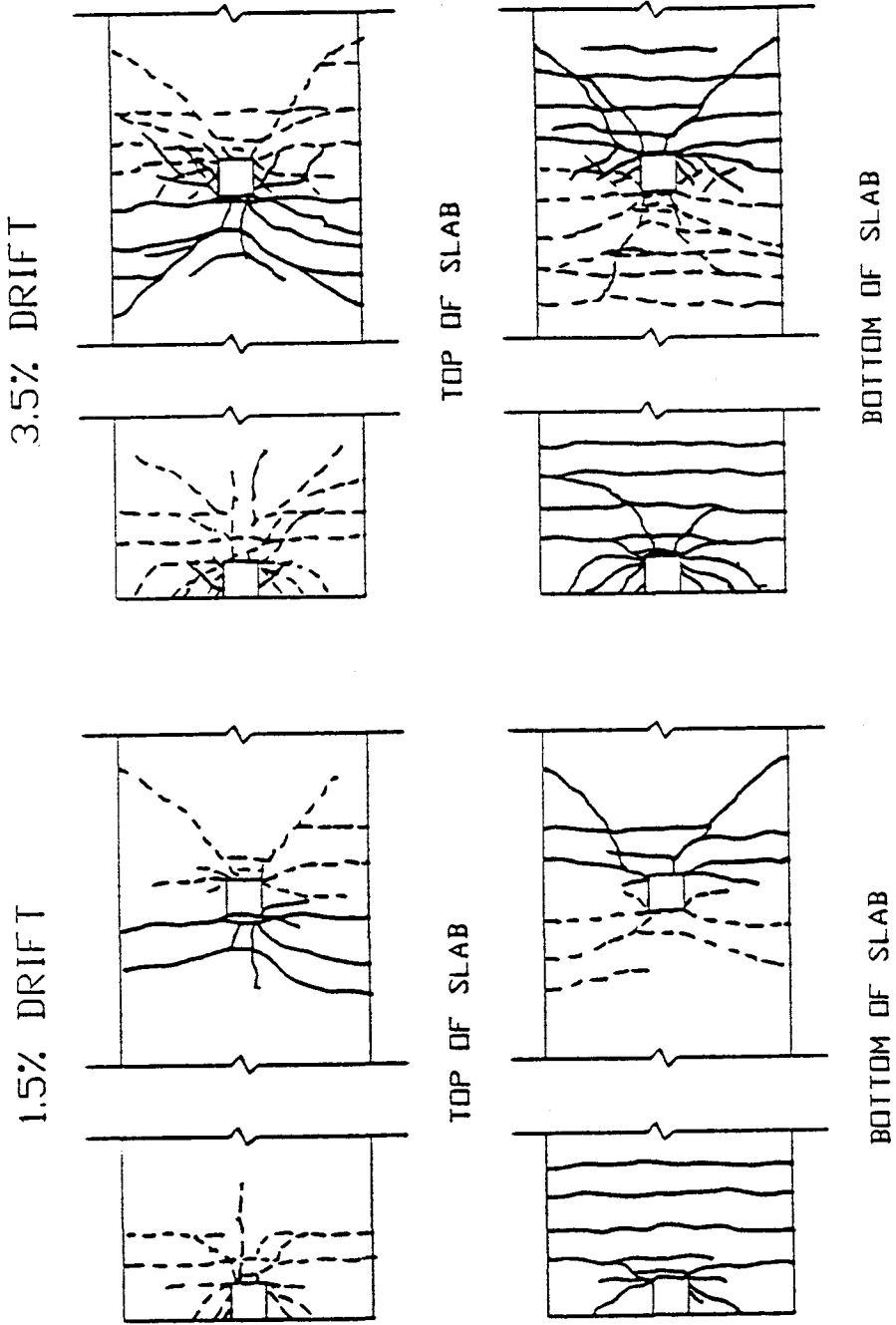
BOTTOM OF SLAB

Fig. 3.4   Crack Patterns - Specimen 4S

182

SPECIMEN 5SO

3.5% DRIFT

TOP OF SLAB

BOTTOM OF SLAB

1.5% DRIFT

TOP OF SLAB
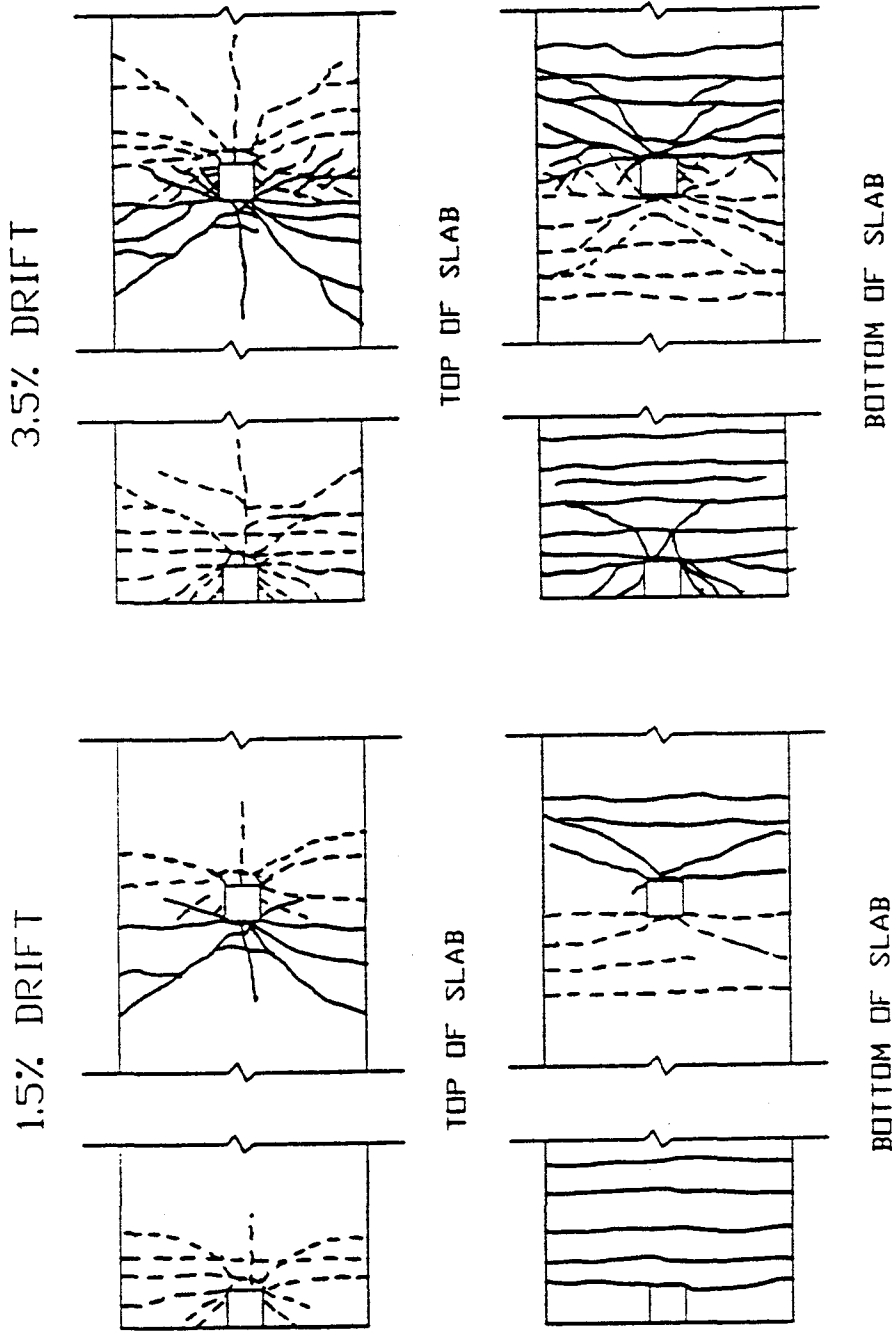
BOTTOM OF SLAB

Fig. 3.5   Crack Patterns - Specimen 5SO
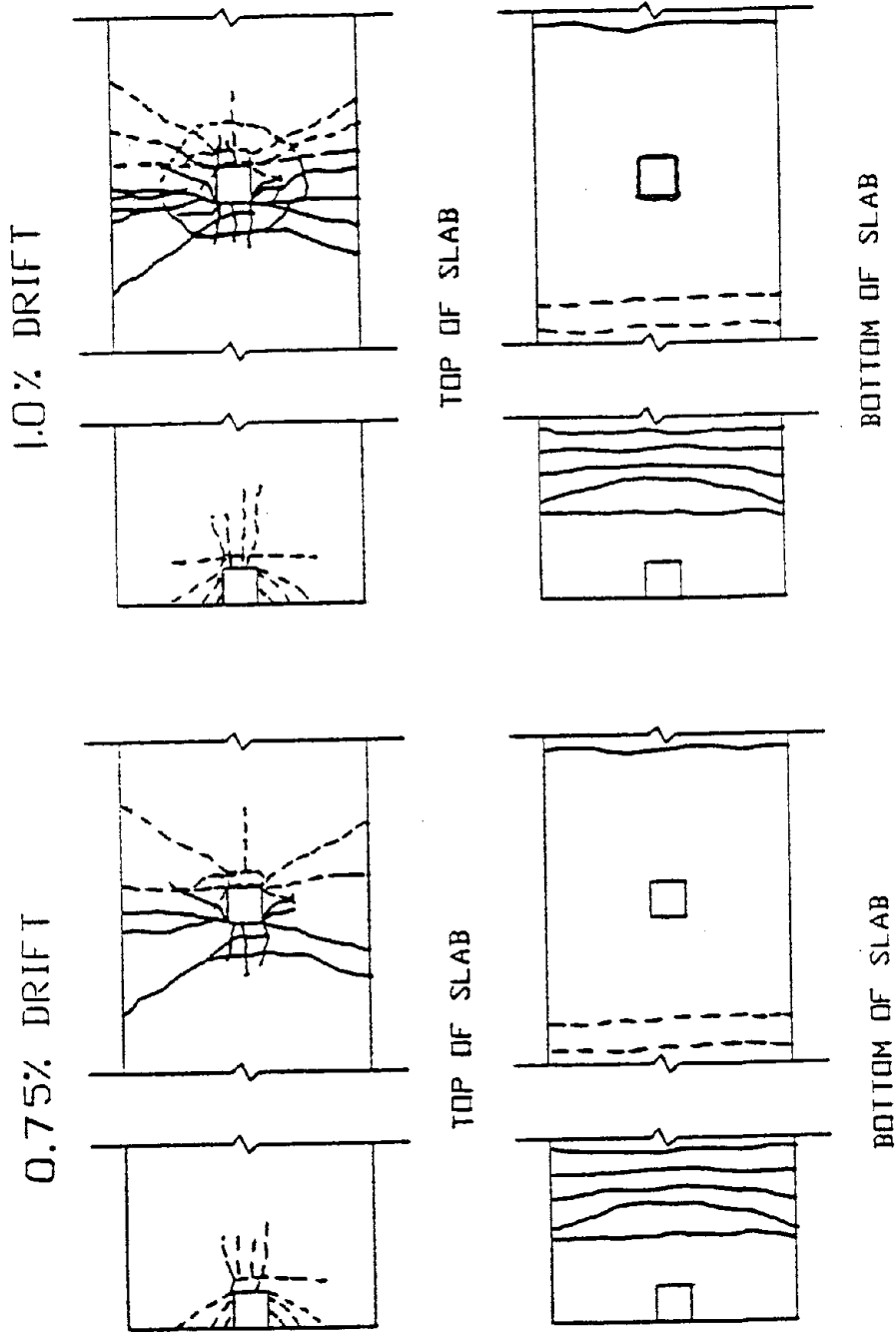
Fig. 3.6   Crack Patterns - Specimen 6LL

184

SPECIMEN 7L

2.0% DRIFT

TOP OF SLAB

BOTTOM OF SLAB

1.5% DRIFT

TOP OF SLAB
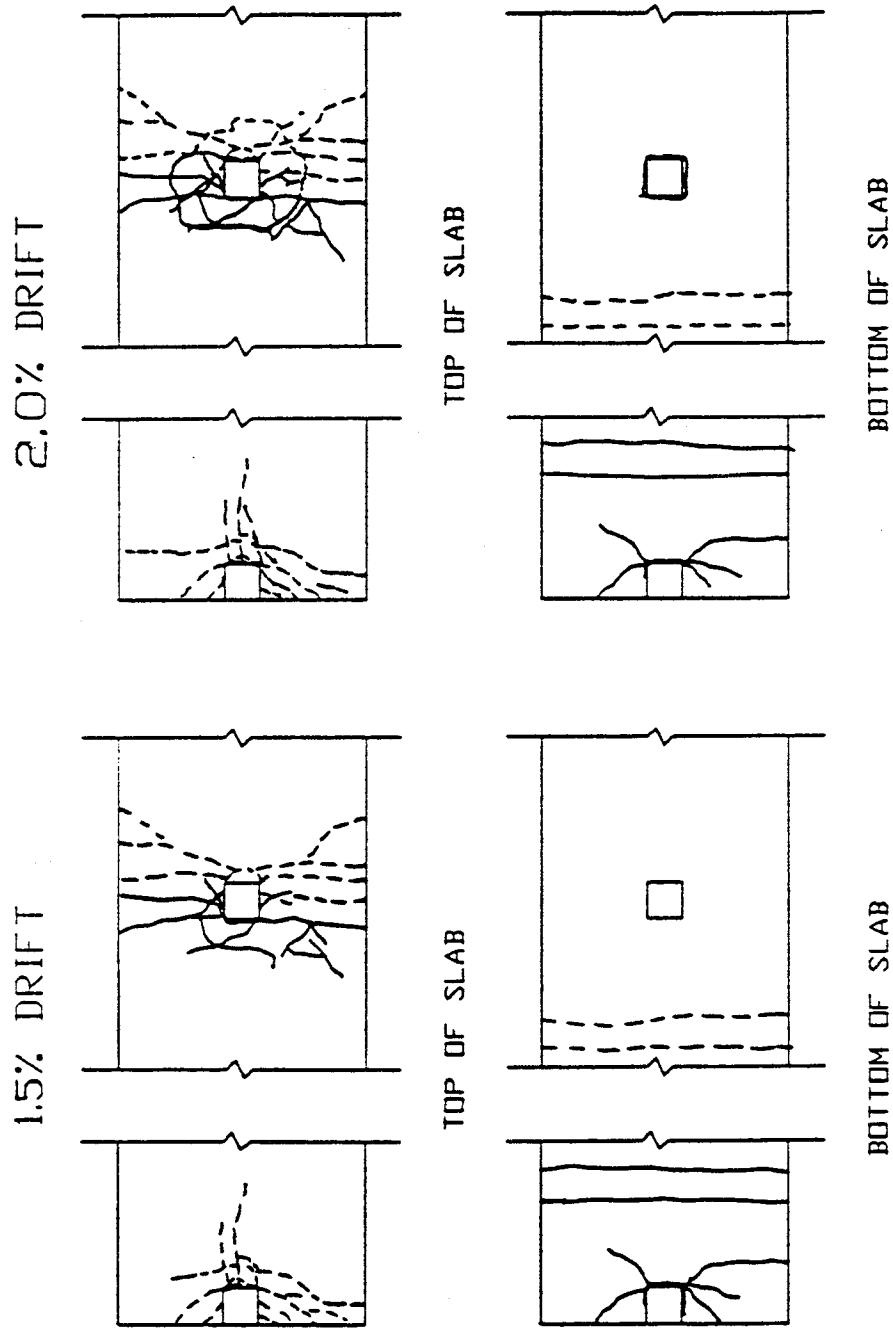
BOTTOM OF SLAB

Fig. 3.7   Crack Patterns - Specimen 7L

SPECIMEN 9E   SPECIMEN 8I

SPECIMEN 9E   SPECIMEN 8I

TOP OF SLAB   TOP OF SLAB

TOP OF SLAB   TOP OF SLAB
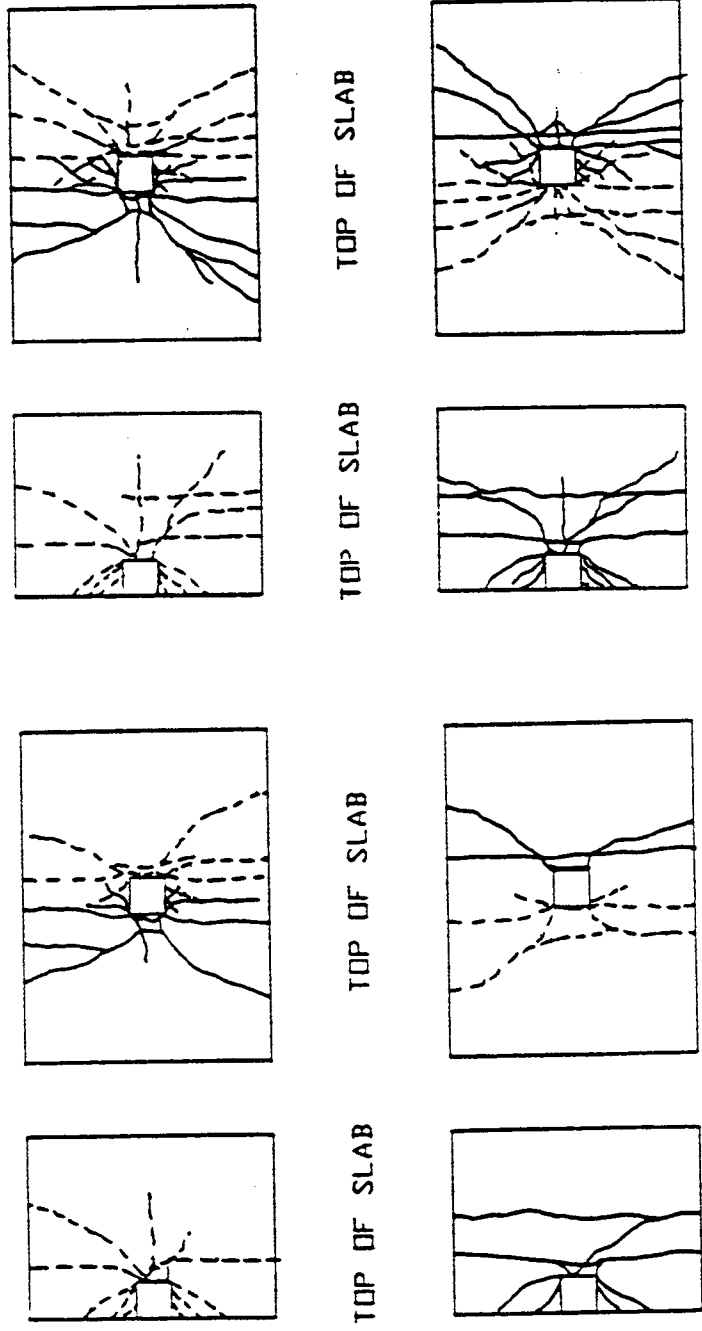
BOTTOM OF SLAB   BOTTOM OF SLAB

BOTTOM OF SLAB   BOTTOM OF SLAB

a)   1.5 percent drift

b)   3.5 percent drift

Fig. 3.8   Crack Patterns - Specimen 8I and 9E

186
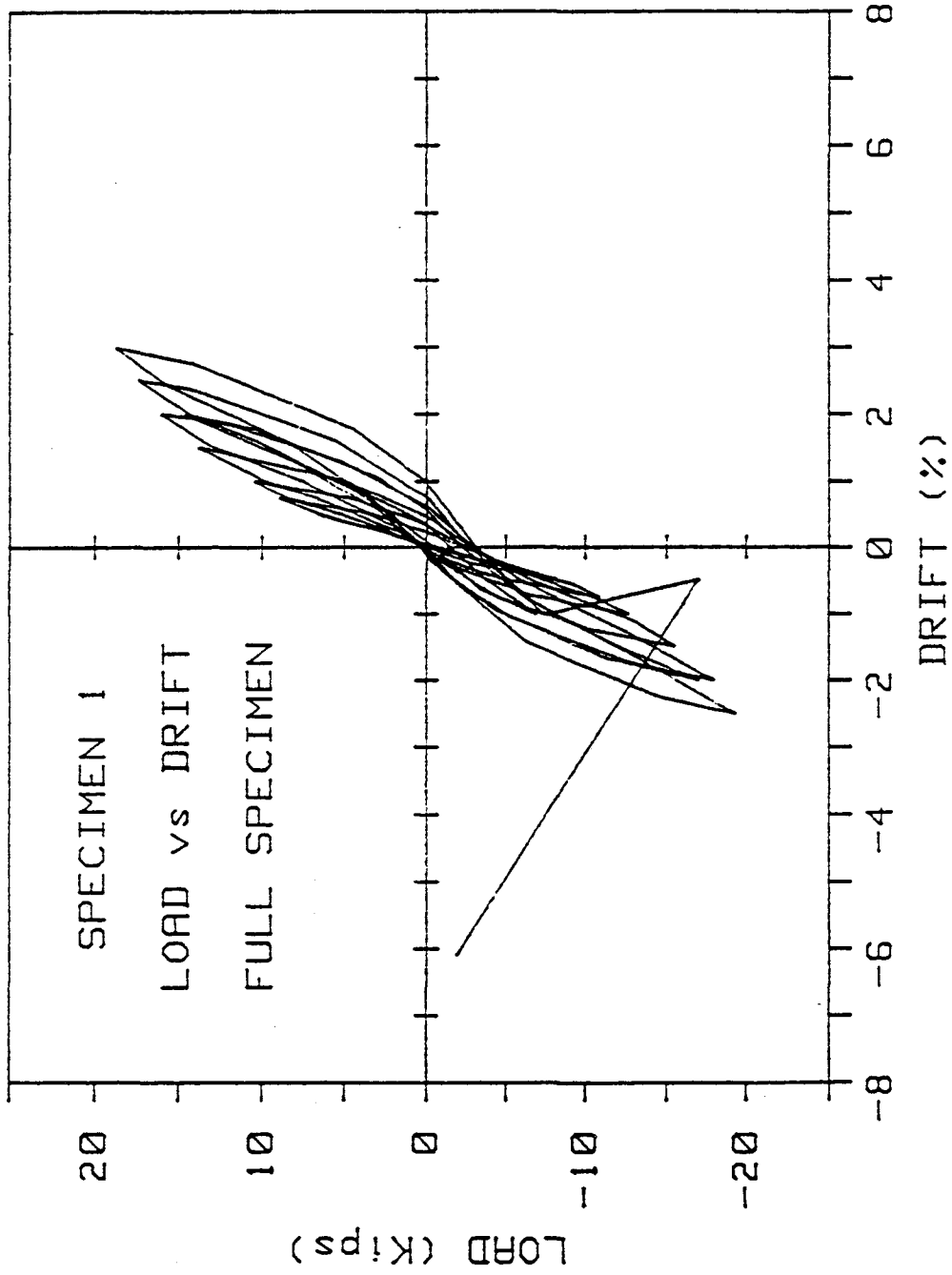
Fig. 3.9   Load vs Drift Relationship - Specimen 1

187

SPECIMEN 2C

LOAD vs DRIFT

FULL SPECIMEN

DRIFT (%)

LOAD (Kips)
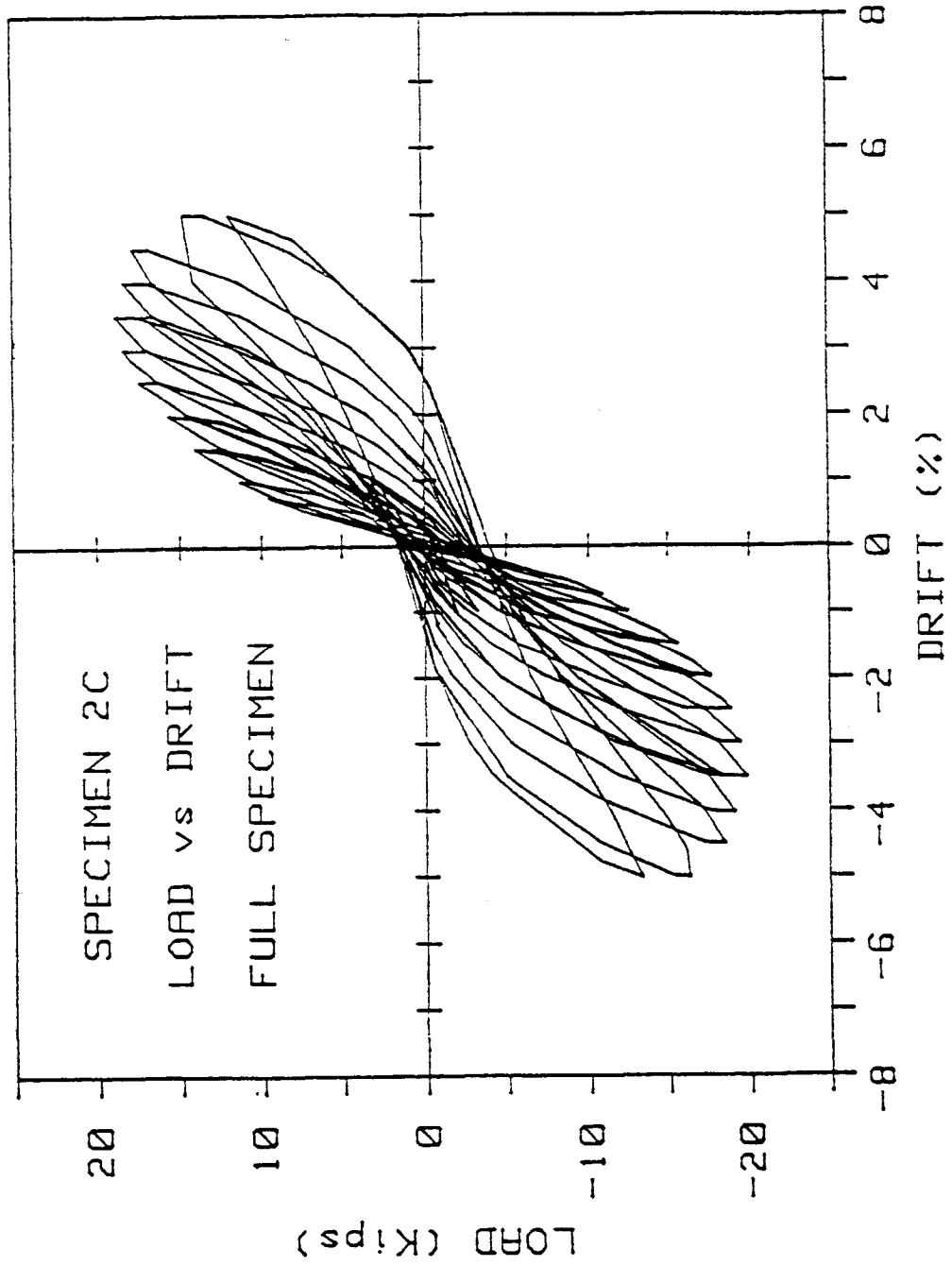
Fig. 3.10   Load vs Drift Relationship - Specimen 2C

188
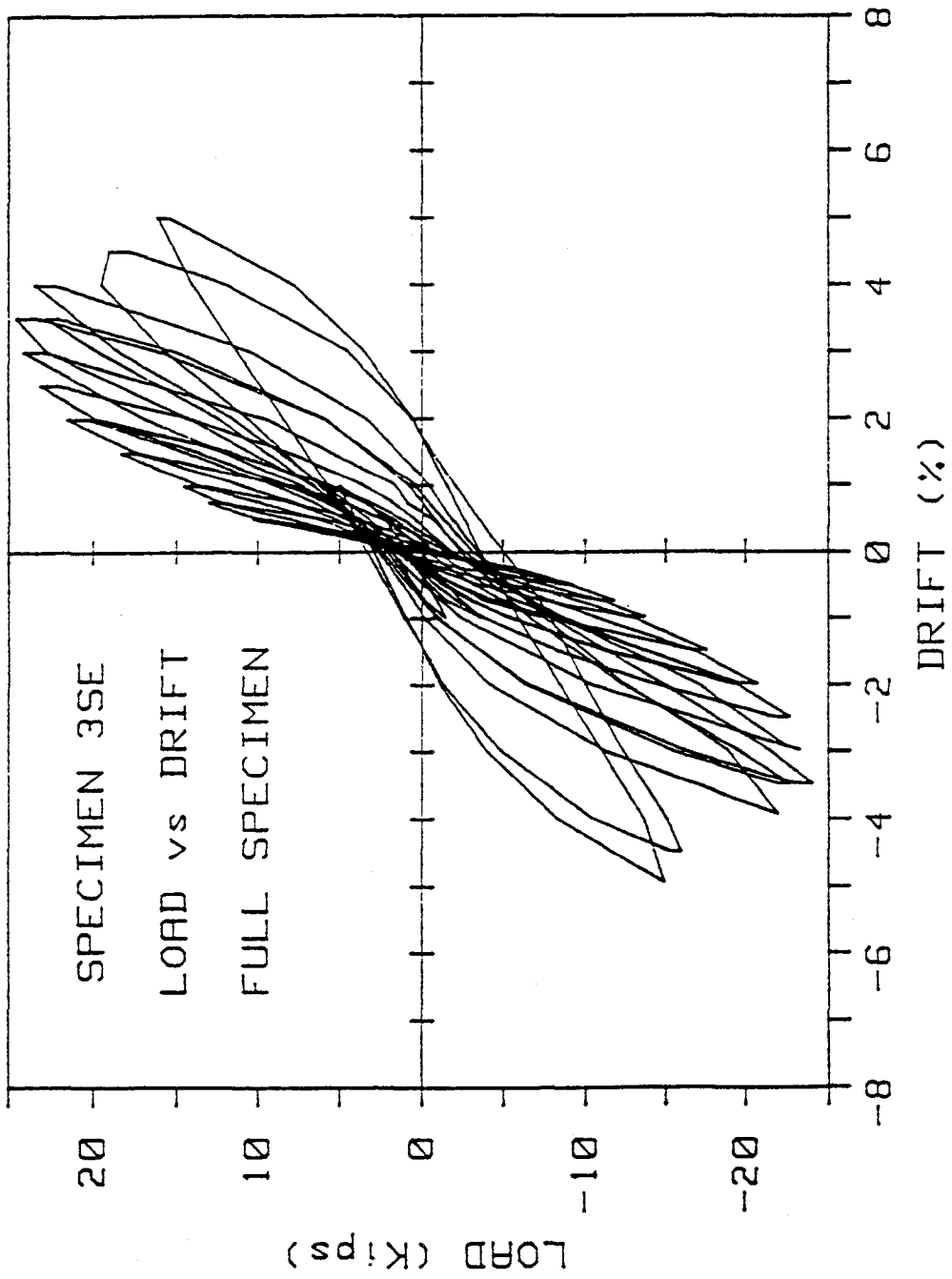
Fig. 3.11 Load vs Drift Relationship - Specimen 3SE
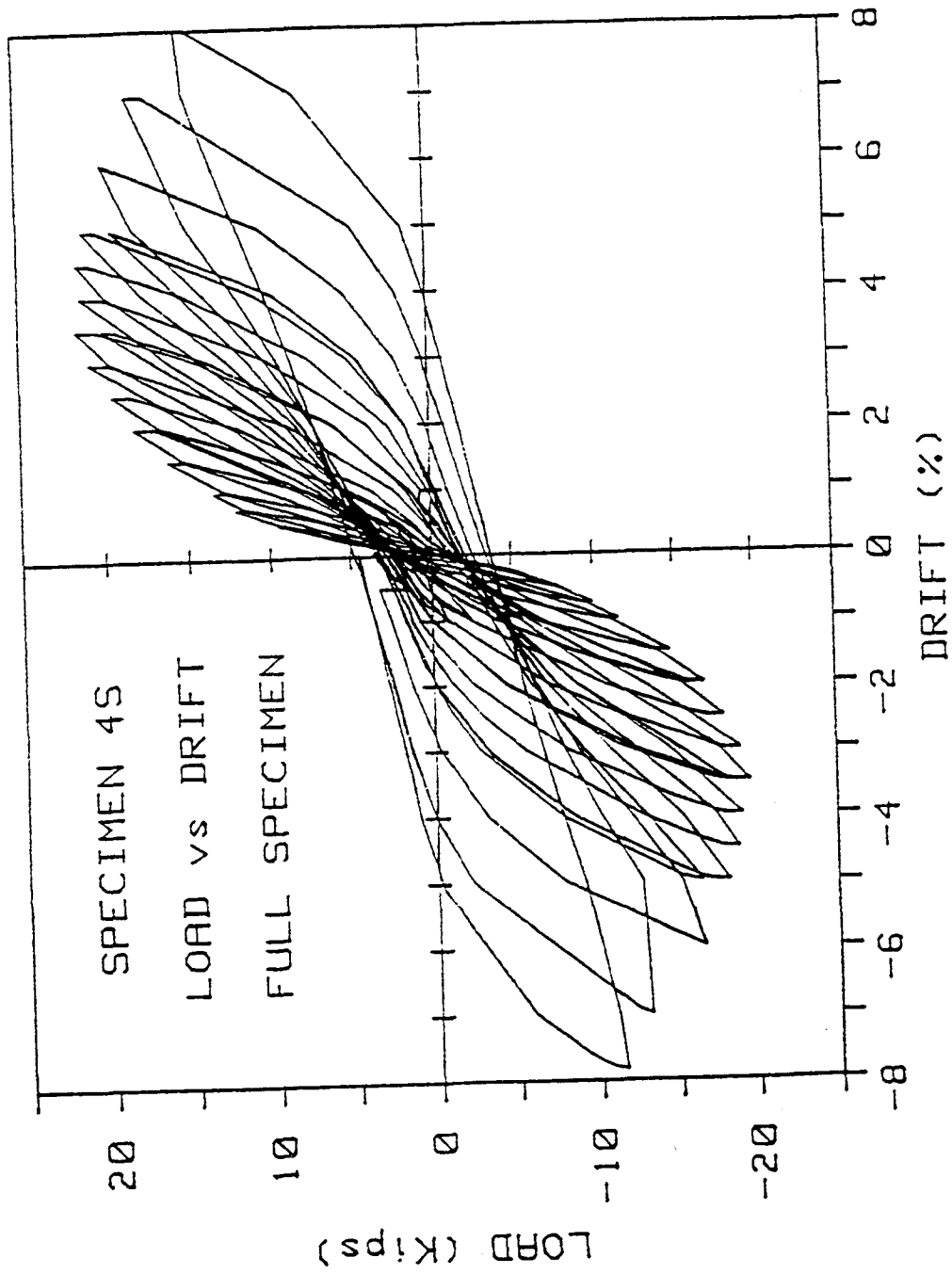
Fig. 3.12 Load vs Drift Relationship - Specimen 4S

190

SPECIMEN 5SO

LOAD vs DRIFT

FULL SPECIMEN
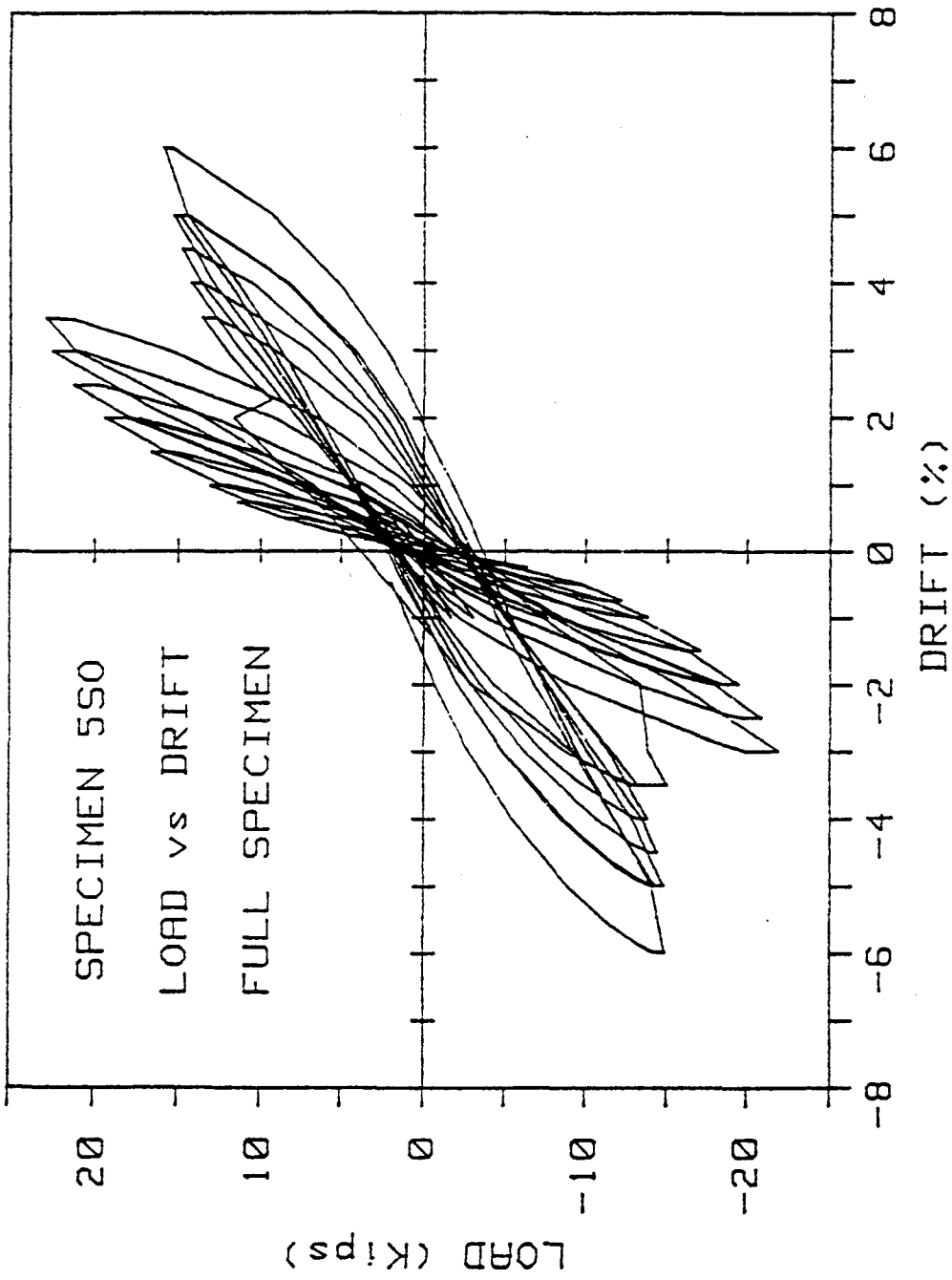
Fig. 3.13   Load vs Drift Relationship - Specimen 5SO

SPECIMEN 6LL

LOAD vs DRIFT

FULL SPECIMEN

LOAD (Kips)
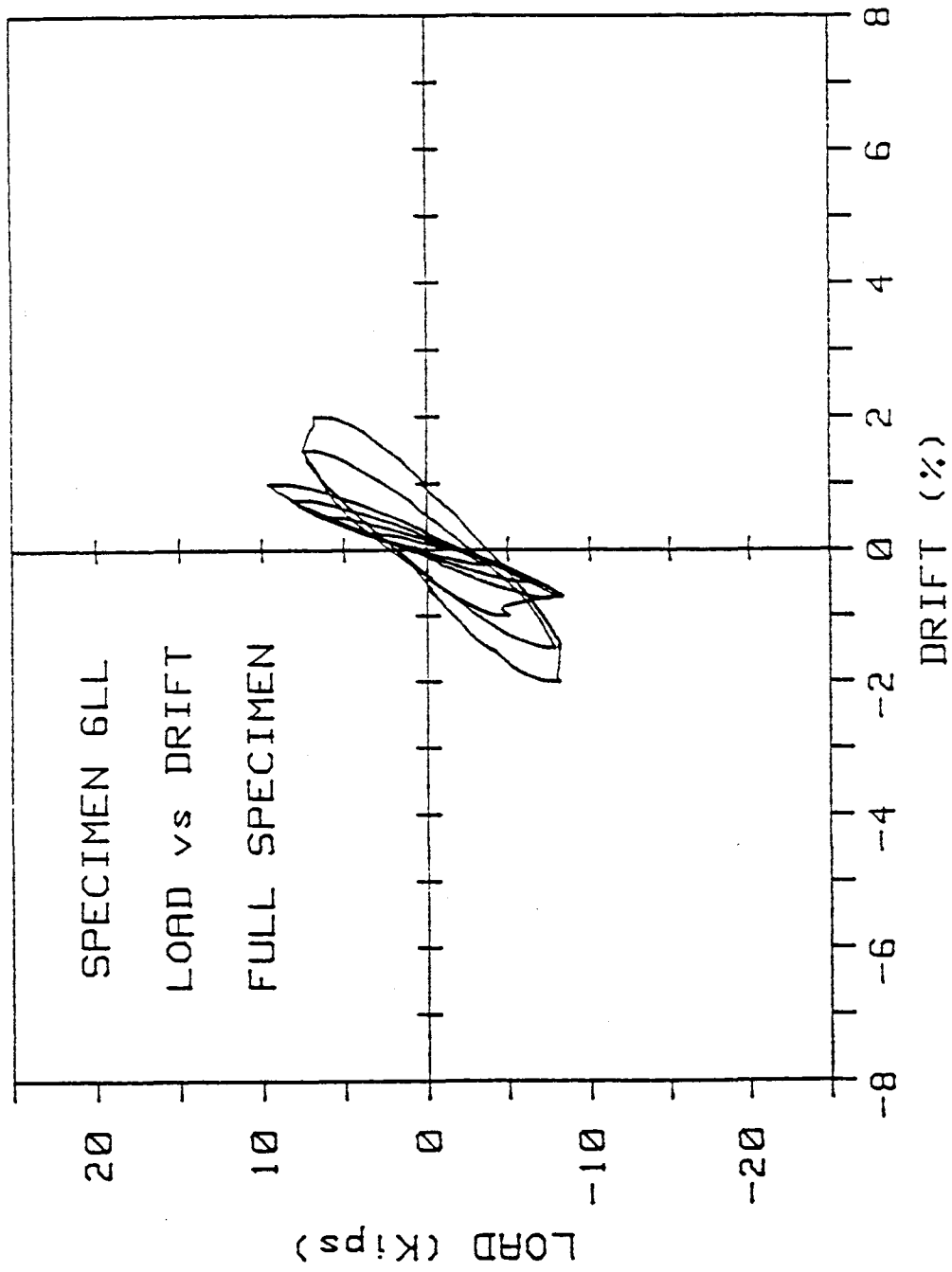
DRIFT (%)

Fig. 3.14   Load vs Drift Relationship - Specimen 6LL

192
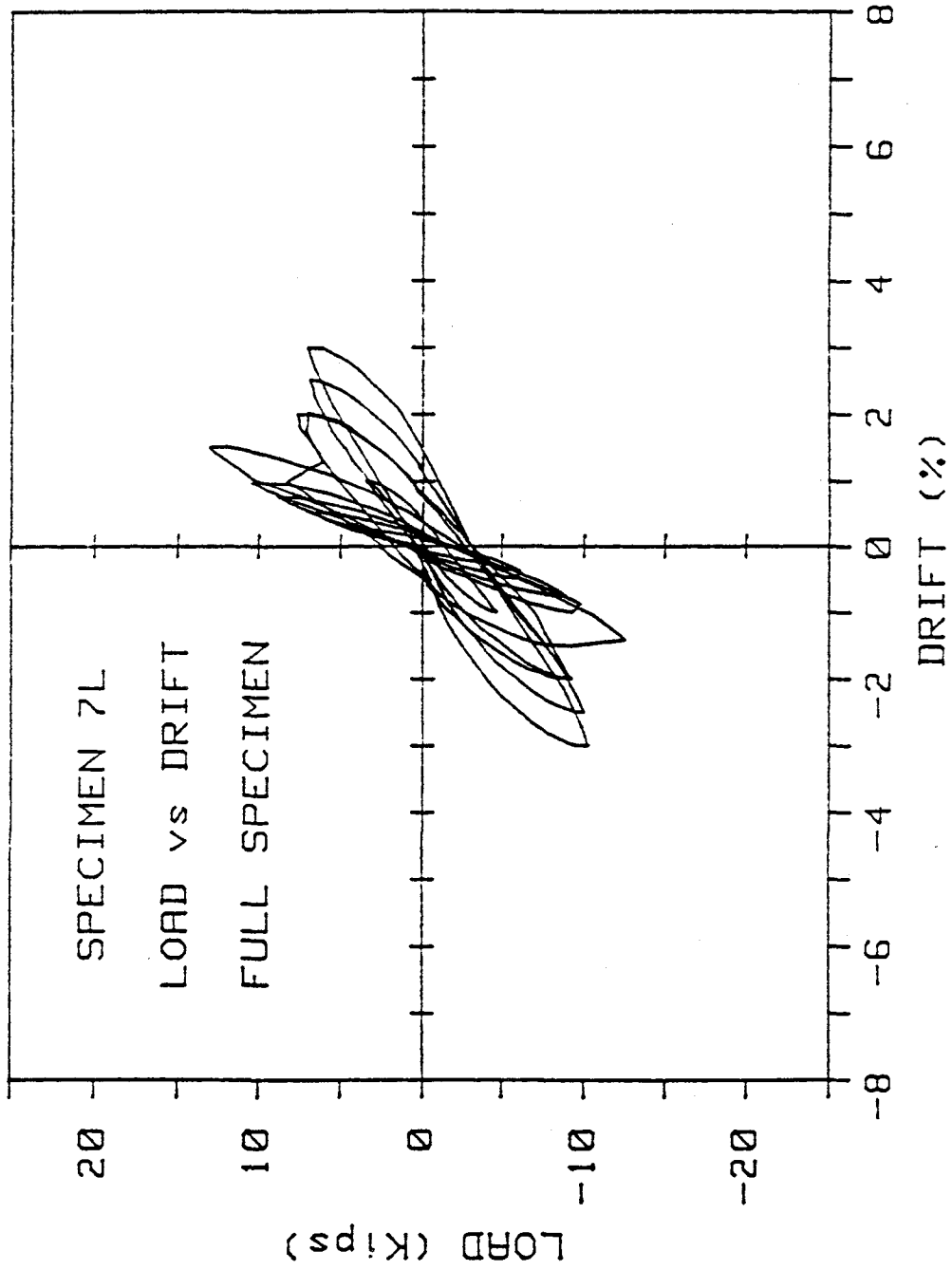
Fig. 3.15 Load vs Drift Relationship - Specimen 7L

193

SPECIMEN 8I

LOAD vs DRIFT

FULL SPECIMEN
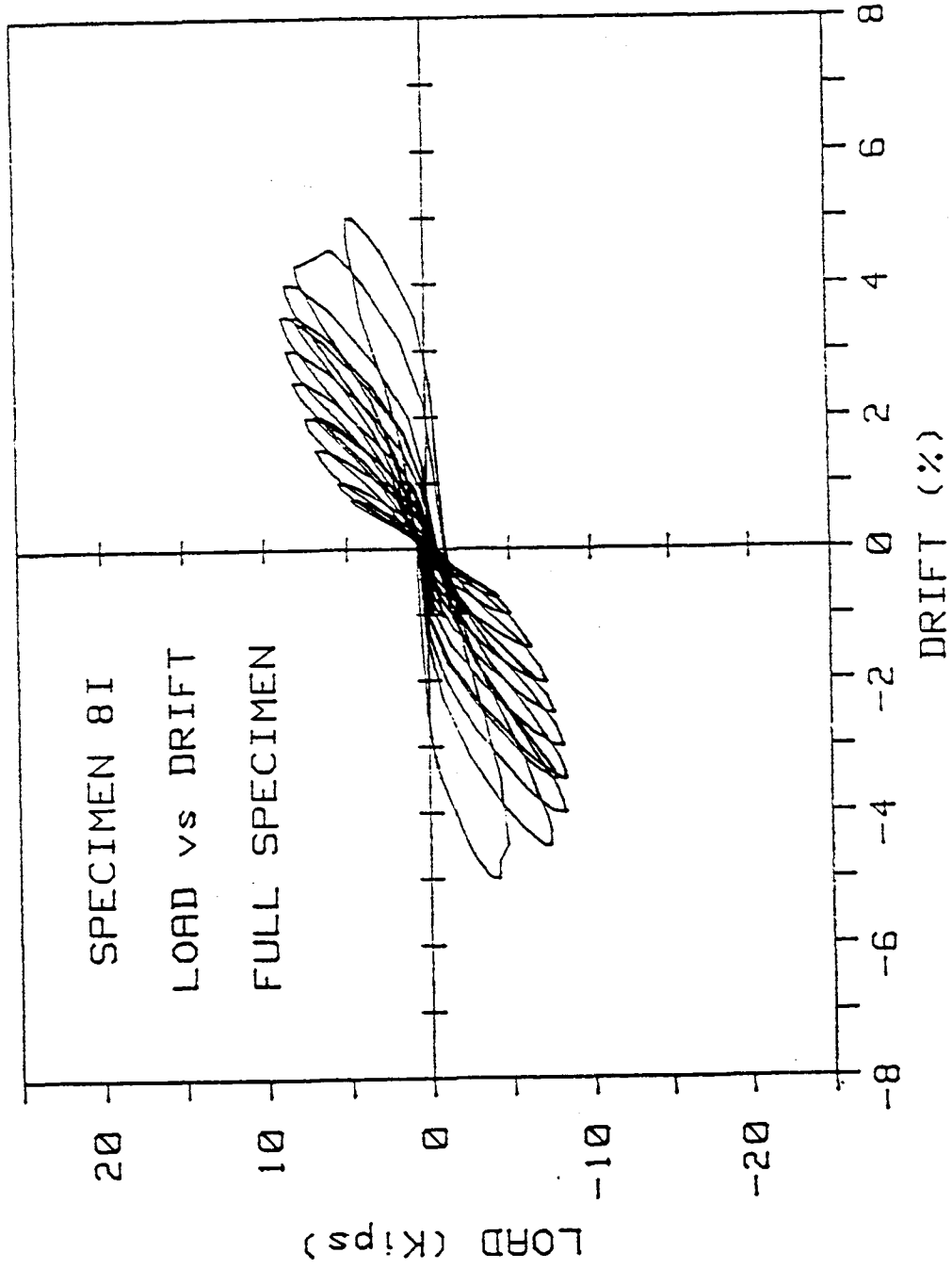
Fig. 3.16 Load vs Drift Relationship - Specimen 8I

194
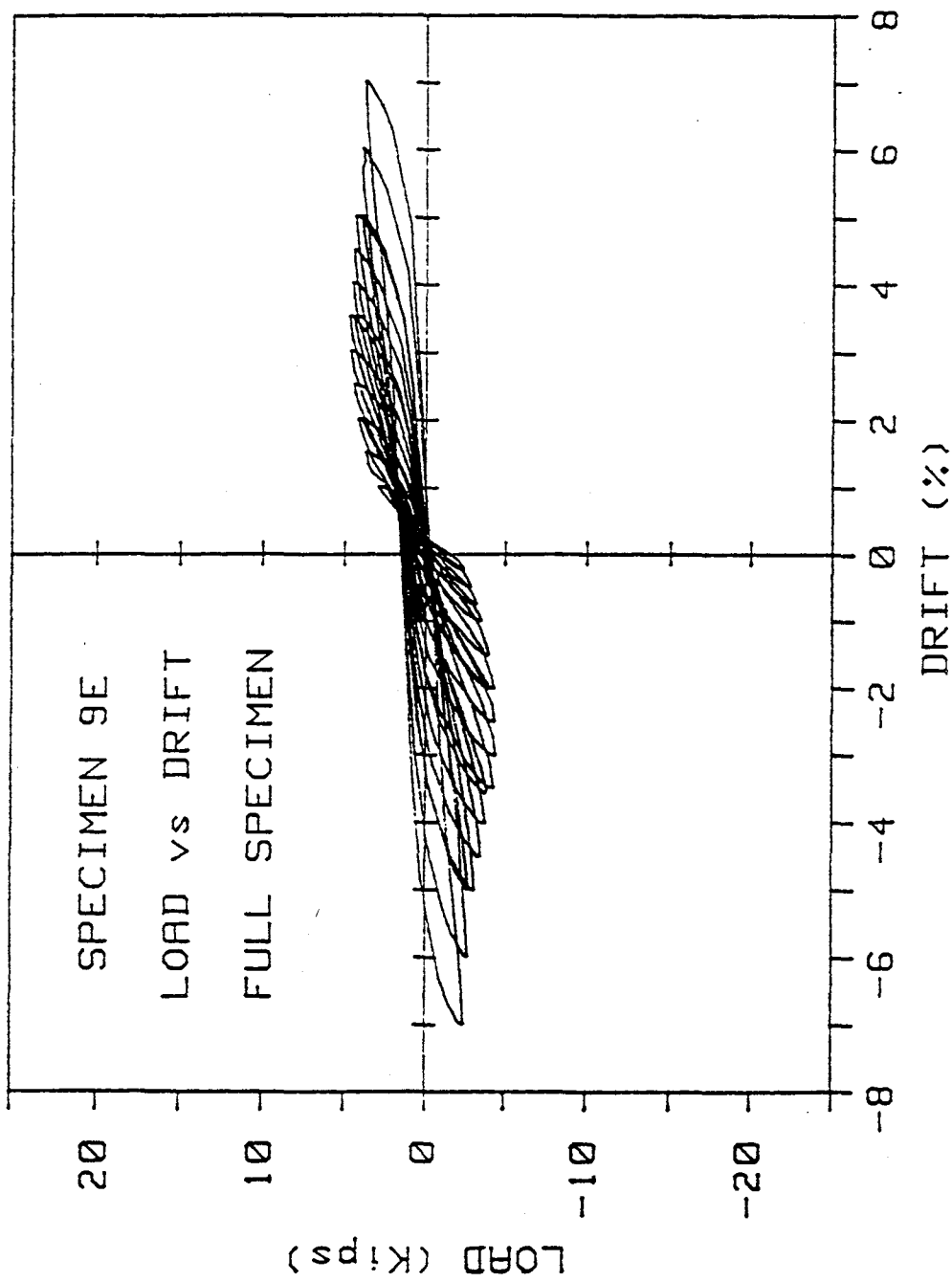
Fig. 3.17 Load vs Drift Relationship - Specimen 9E
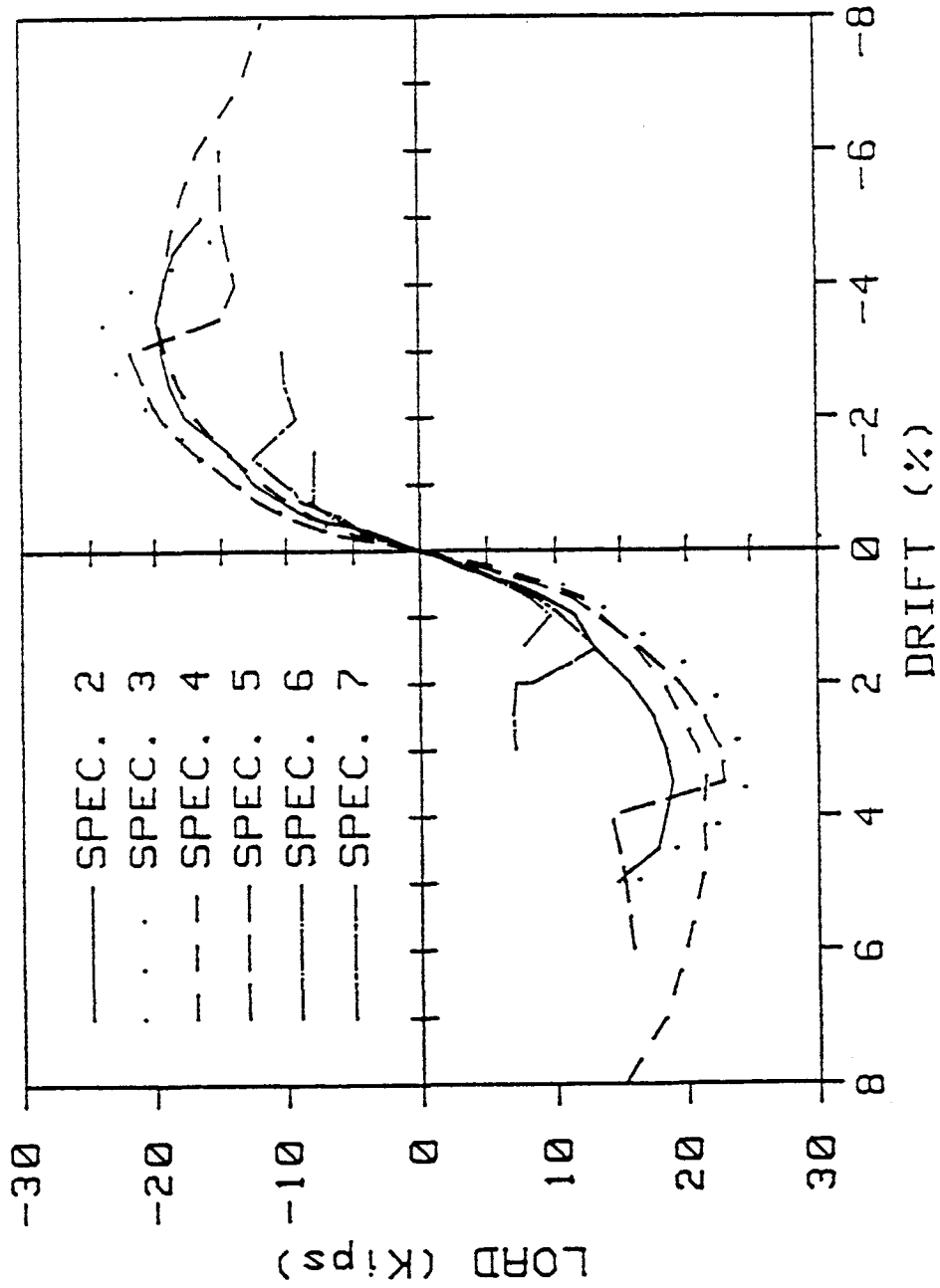
Fig. 3.18   Load vs Drift Envelopes
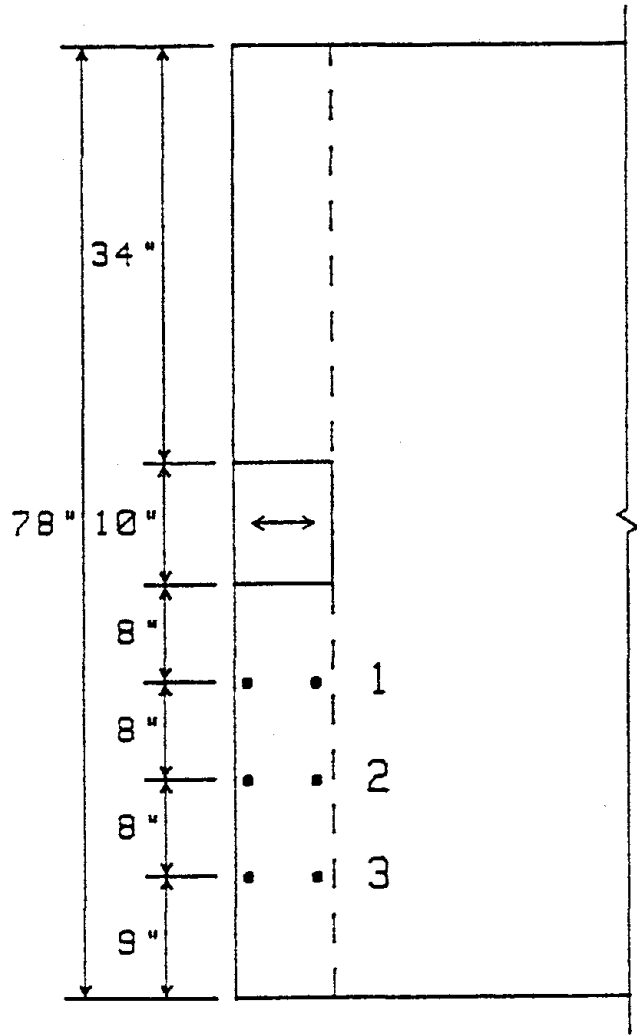
EDGE BEAM ROTATION

Fig. 3.19   Edge Beam Rotation Measurement
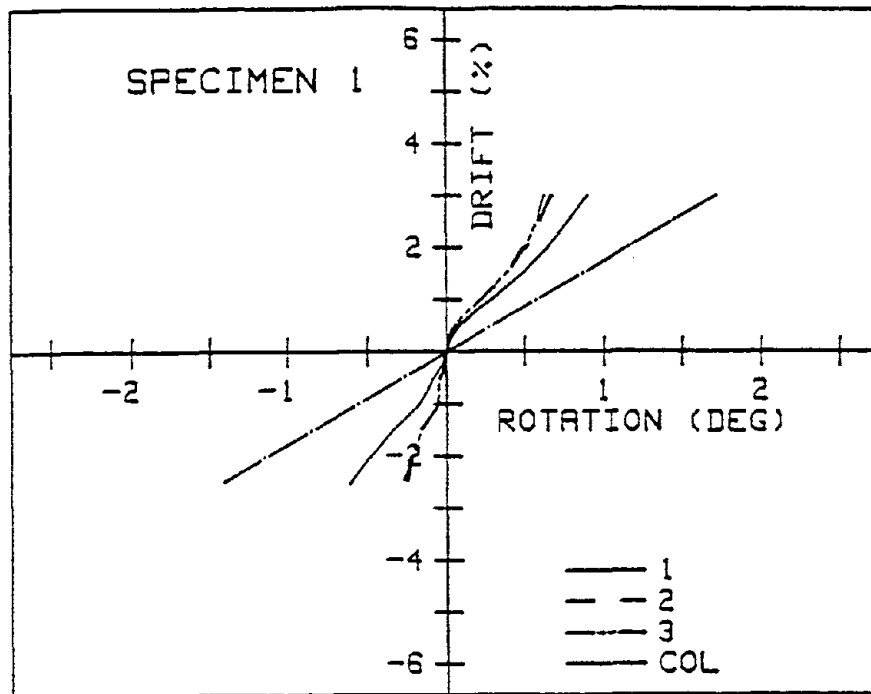
Fig. 3.20   Edge Beam Rotation - Specimen 1
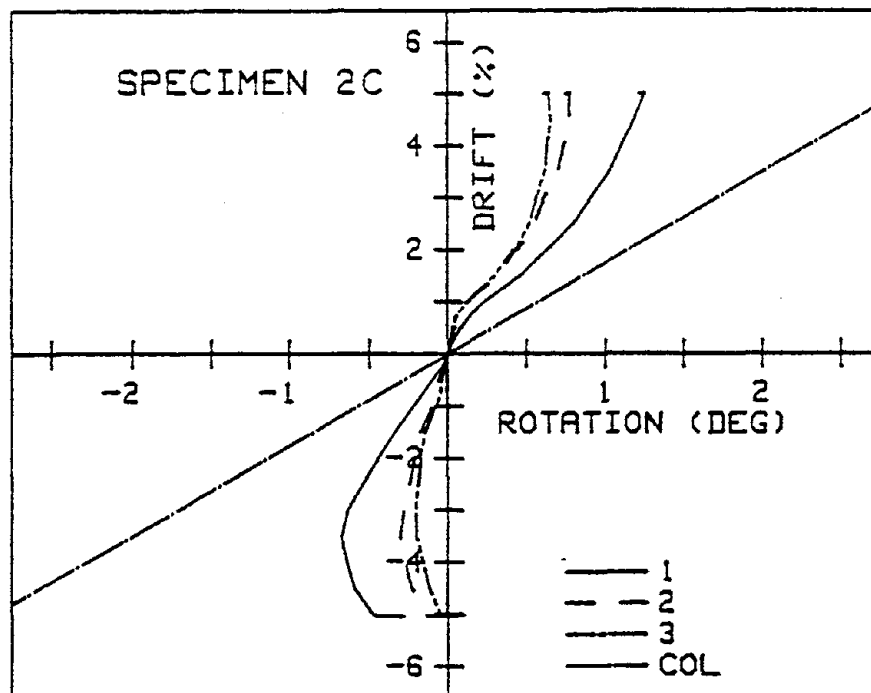
Fig. 3.21   Edge Beam Rotation - Specimen 2C

198
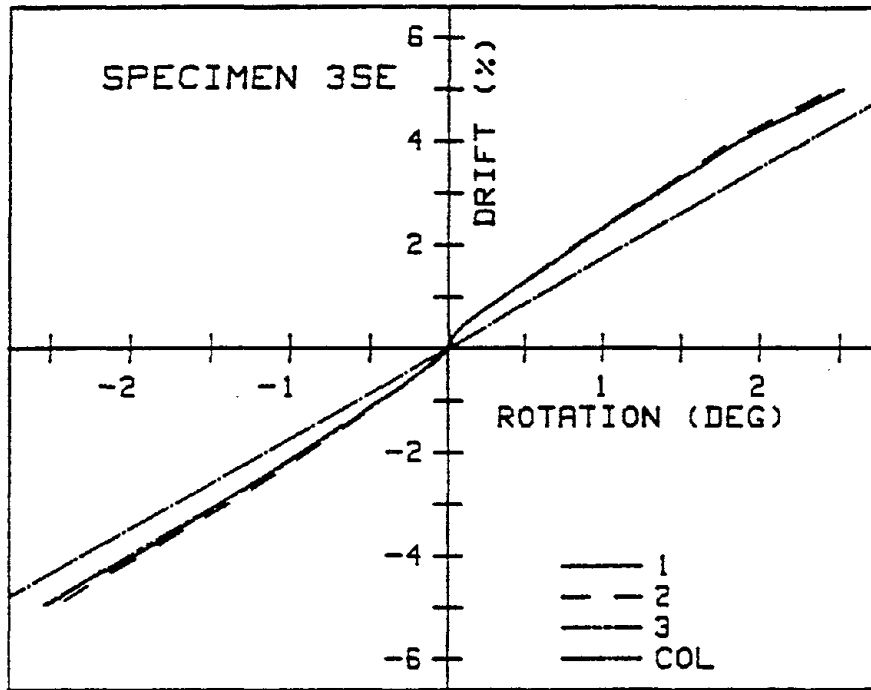
Fig. 3.22   Edge Beam Rotation - Specimen 3SE
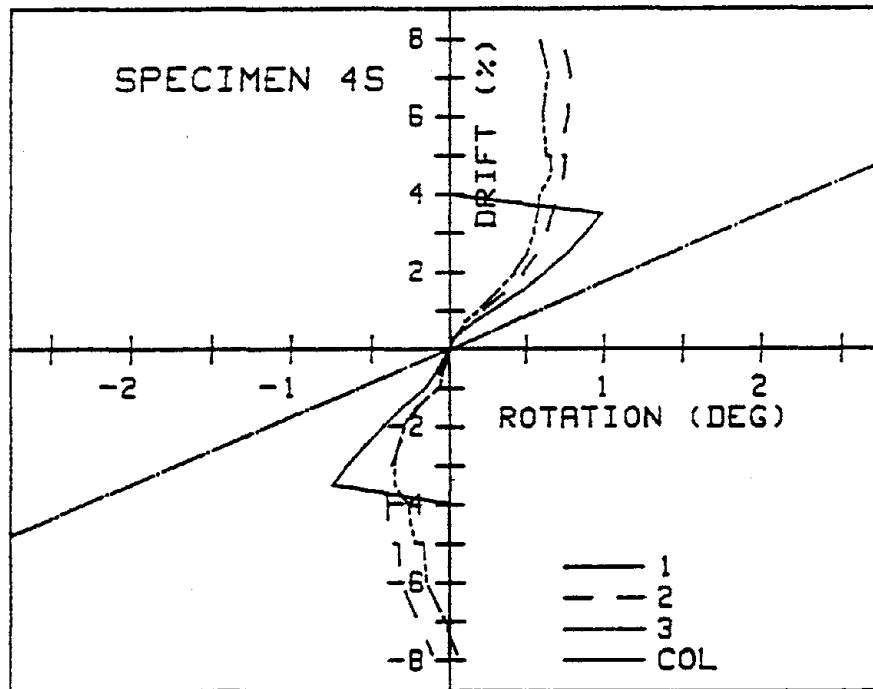
Fig. 3.23   Edge Beam Rotation - Specimen 4S
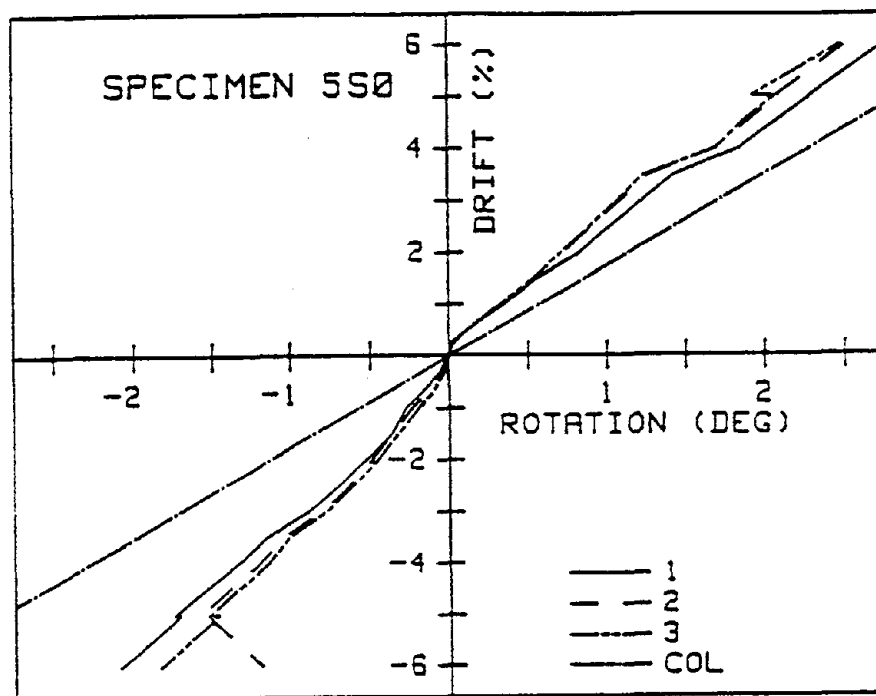
Fig. 3.24   Edge Beam Rotation - Specimen 5SO
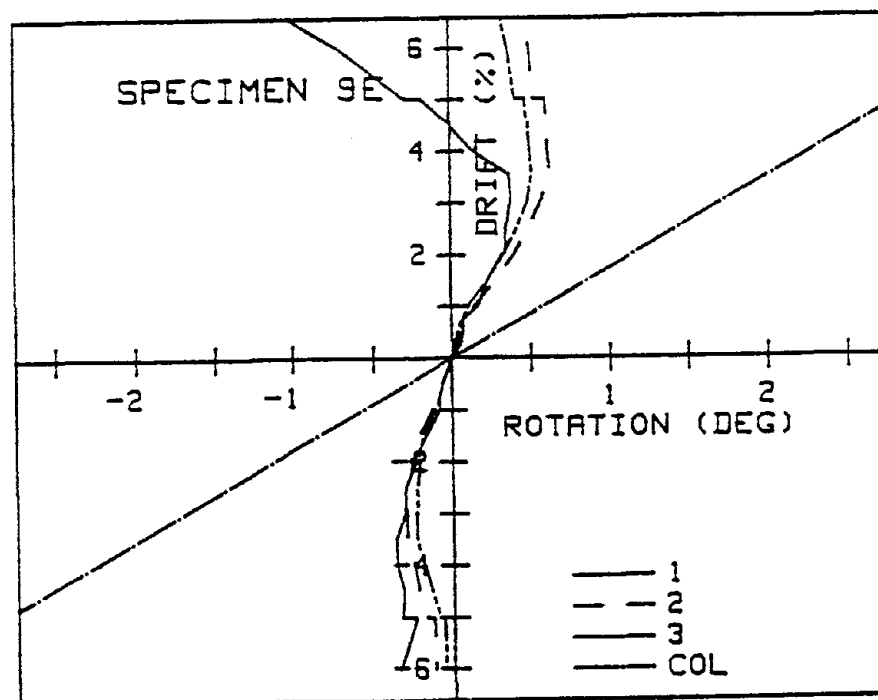
Fig. 3.25   Edge Beam Rotation - Specimen 9E
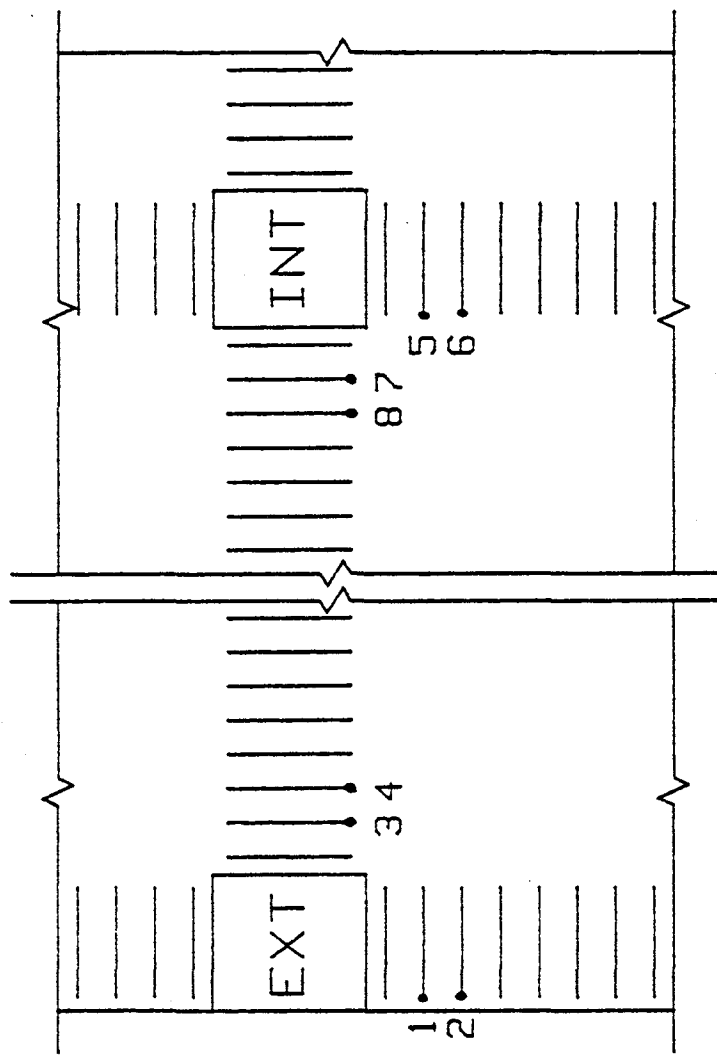
STIRRUP STRAIN GAGES

SPECIMEN 4S

Fig. 3.26   Location of stirrup strain gages
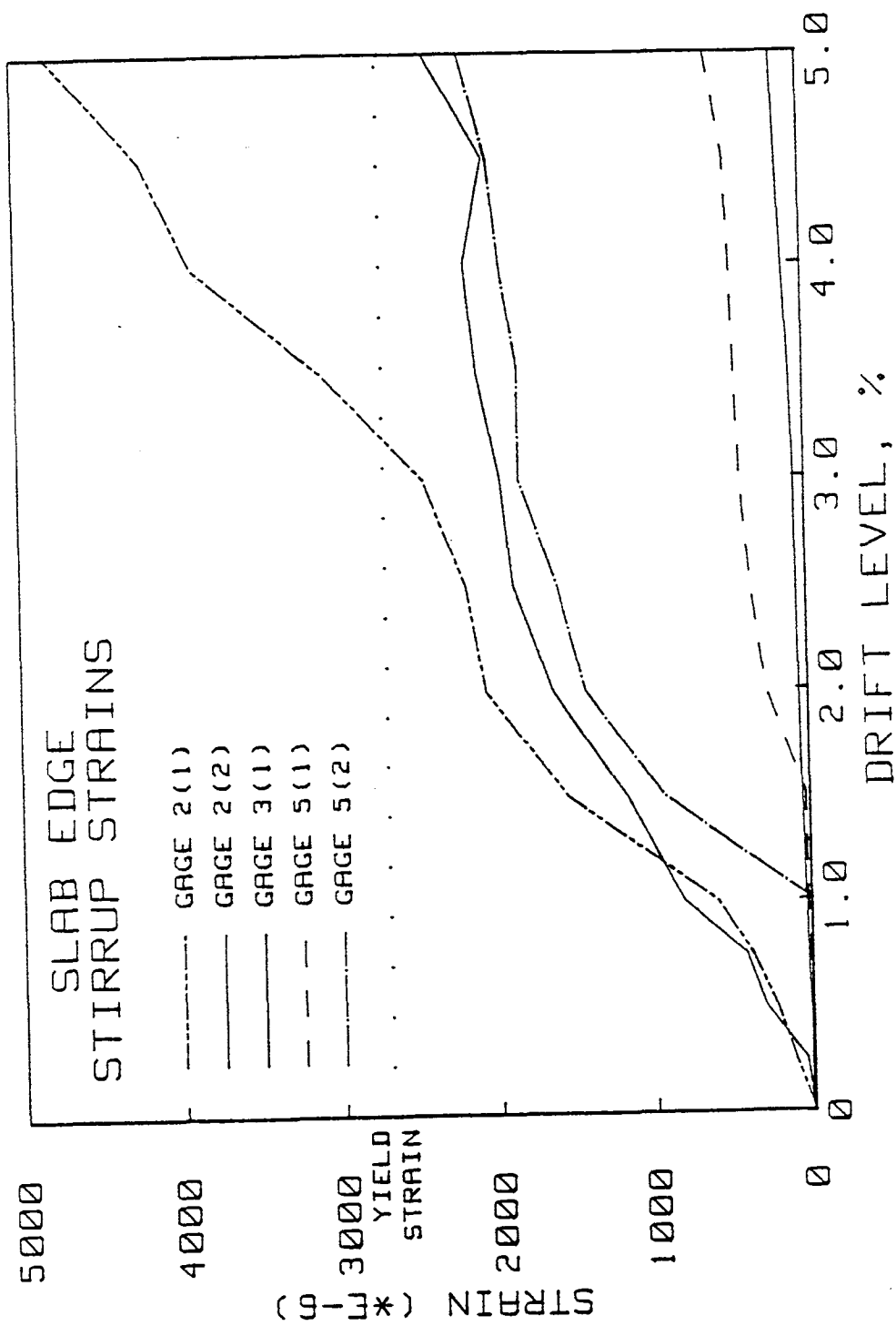
Fig. 3.27   Slab edge stirrup strains
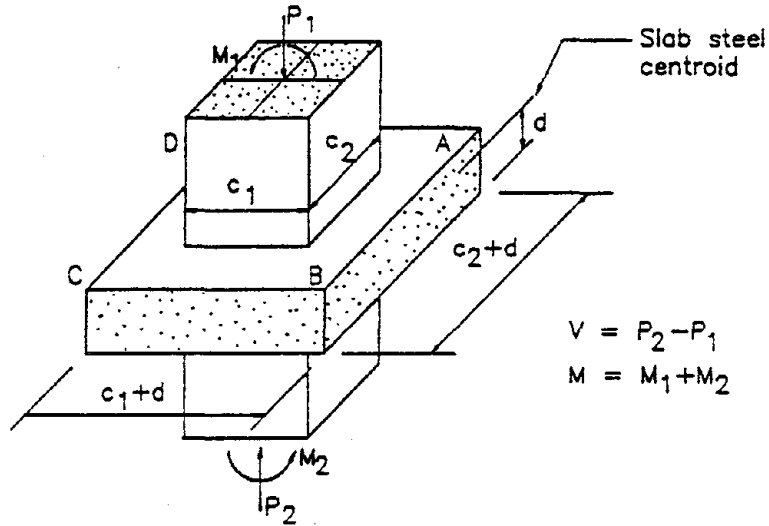
(a) Critical section of slab

$$V = P_2 - P_1$$
$$M = M_1 + M_2$$

$$v_{CD} = \frac{V}{A_c} - \frac{\gamma_v M}{J_c} \frac{(c_1+d)}{2}$$

$$v_{AB} = \frac{V}{A_c} + \frac{\gamma_v M}{J_c} \frac{(c_1+d)}{2}$$
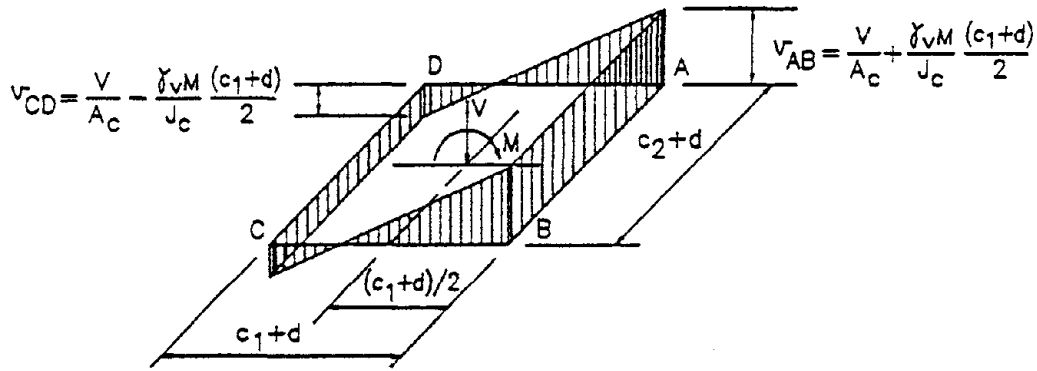
(b) Assumed distribution of shear stress

Shear and Moment Transfer
at Interior Column–Slab Connection

Fig. 3.28   Interior connection critical section

(a) Critical section of slab

$$V = P_2 - P_1$$
$$M = M_1 + M_2$$

$$v_{CD} = \frac{V}{A_c} - \frac{\gamma_v M}{J_c} C_{CD}$$

$$v_{AB} = \frac{V}{A_c} + \frac{\gamma_v M}{J_c} C_{AB}$$

(b) Assumed distribution of shear stress

Shear and Moment Transfer at Exterior Column–Slab Connection
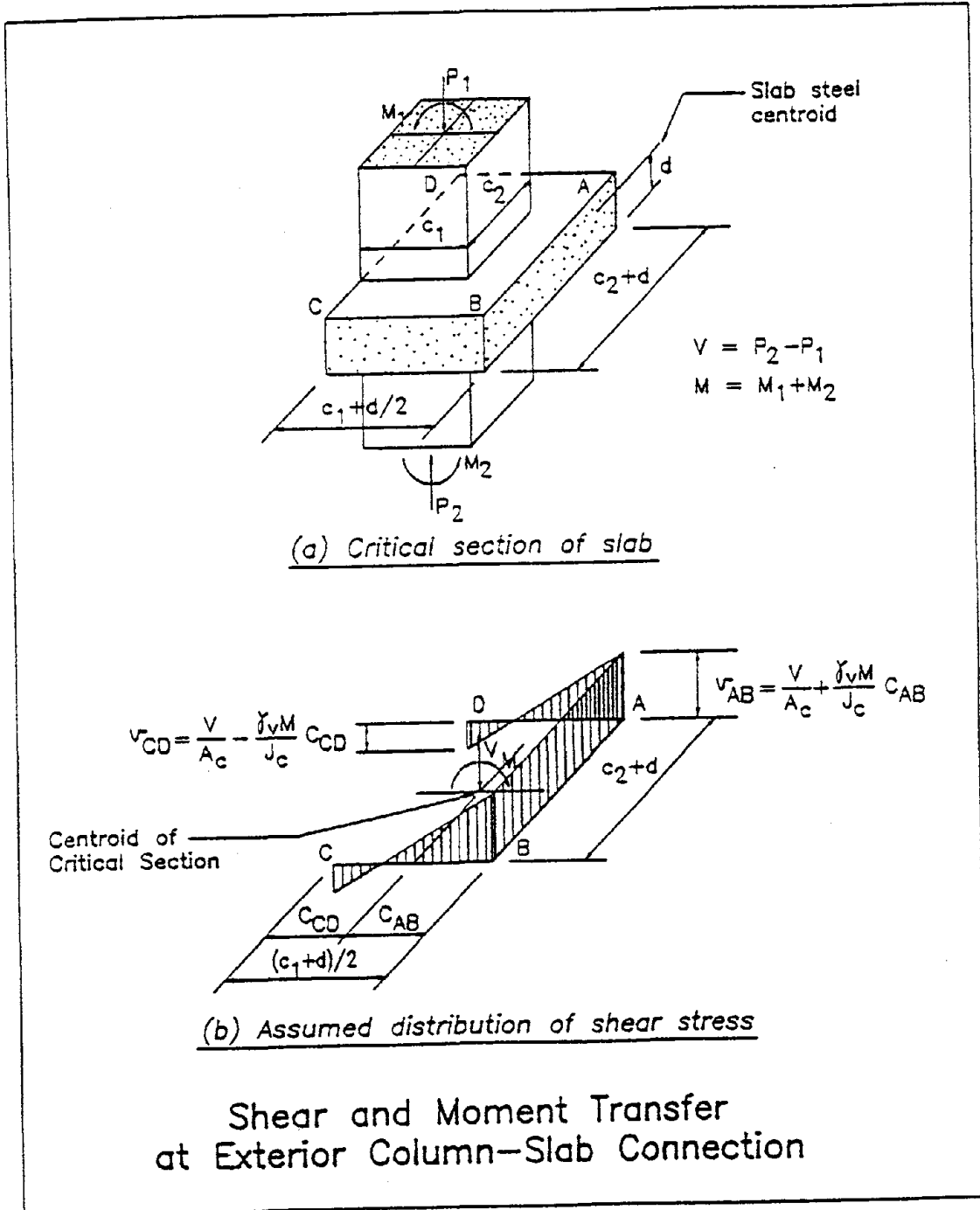
Fig. 3.29 Exterior connection critical section
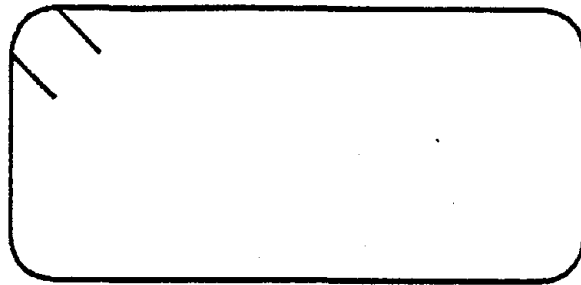
CLOSED HOOP STIRRUPS
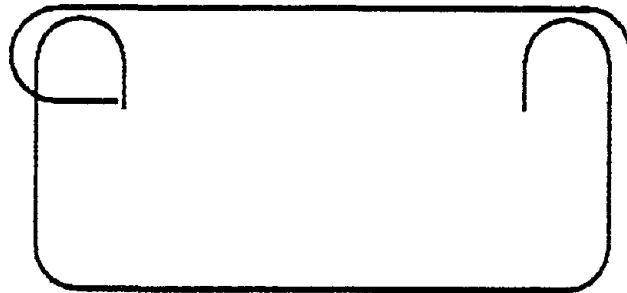
OPEN BEAM STIRRUPS
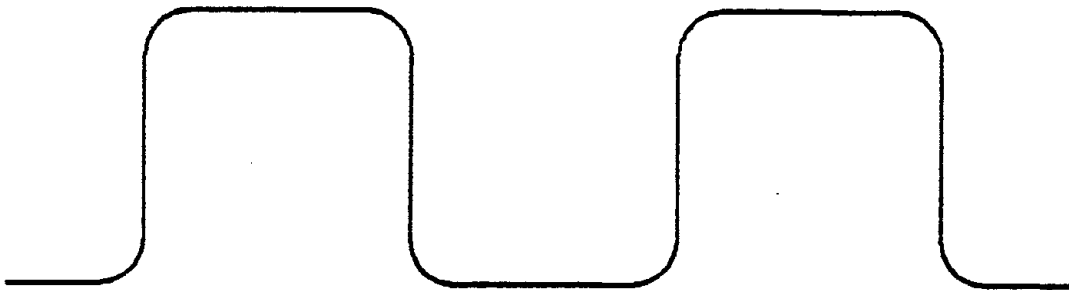
GALLOPING STIRRUPS

Fig. 3.30   Possible shear stirrup configurations
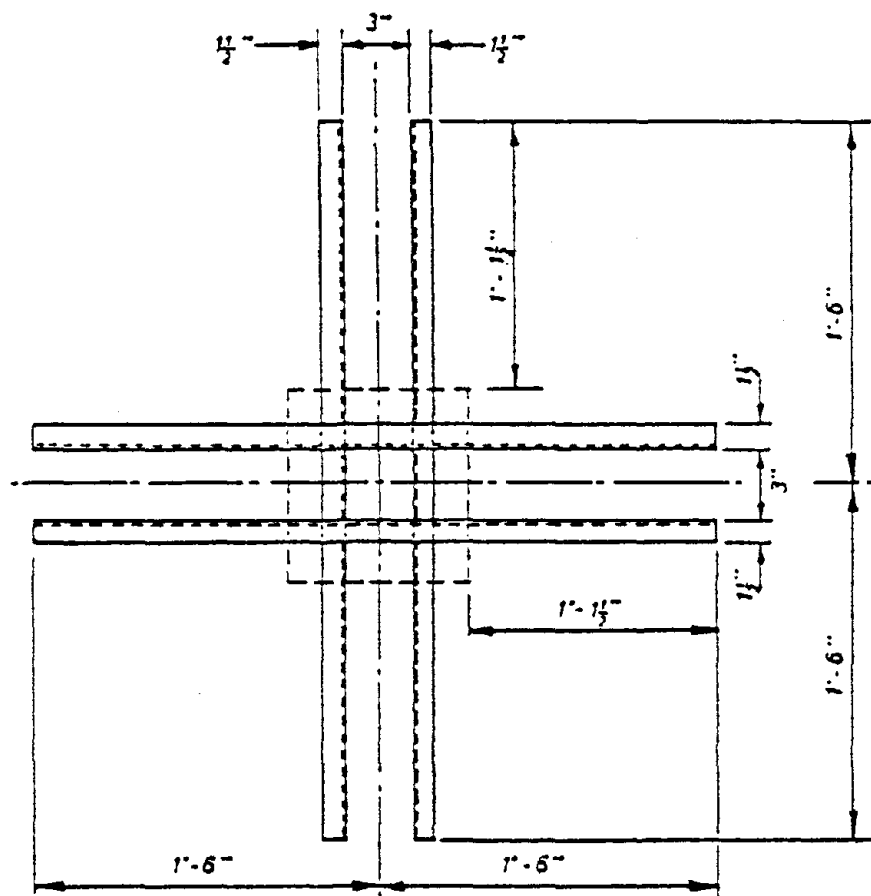
(a) Plan at Column-Slab Junction
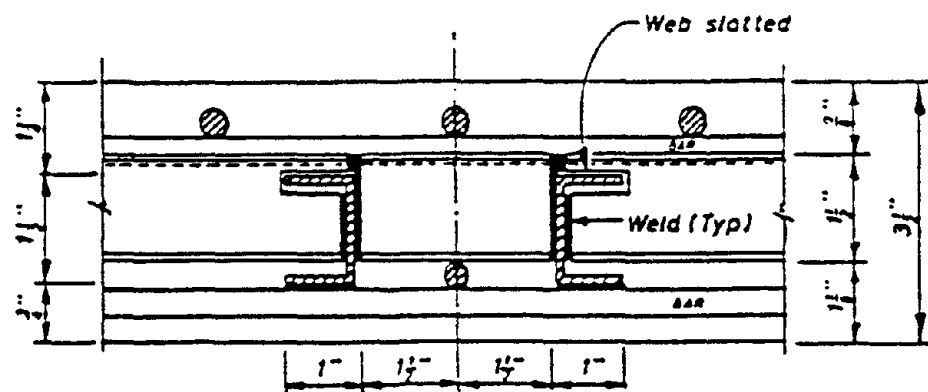
(b) Section Through Slab Showing Intersection of 1½"x 1"x 0.128"thick
Channel Sections

Fig. 3.31   Shearhead at interior slab-column connection
after Islam and Park (Ref. 3.2)

206
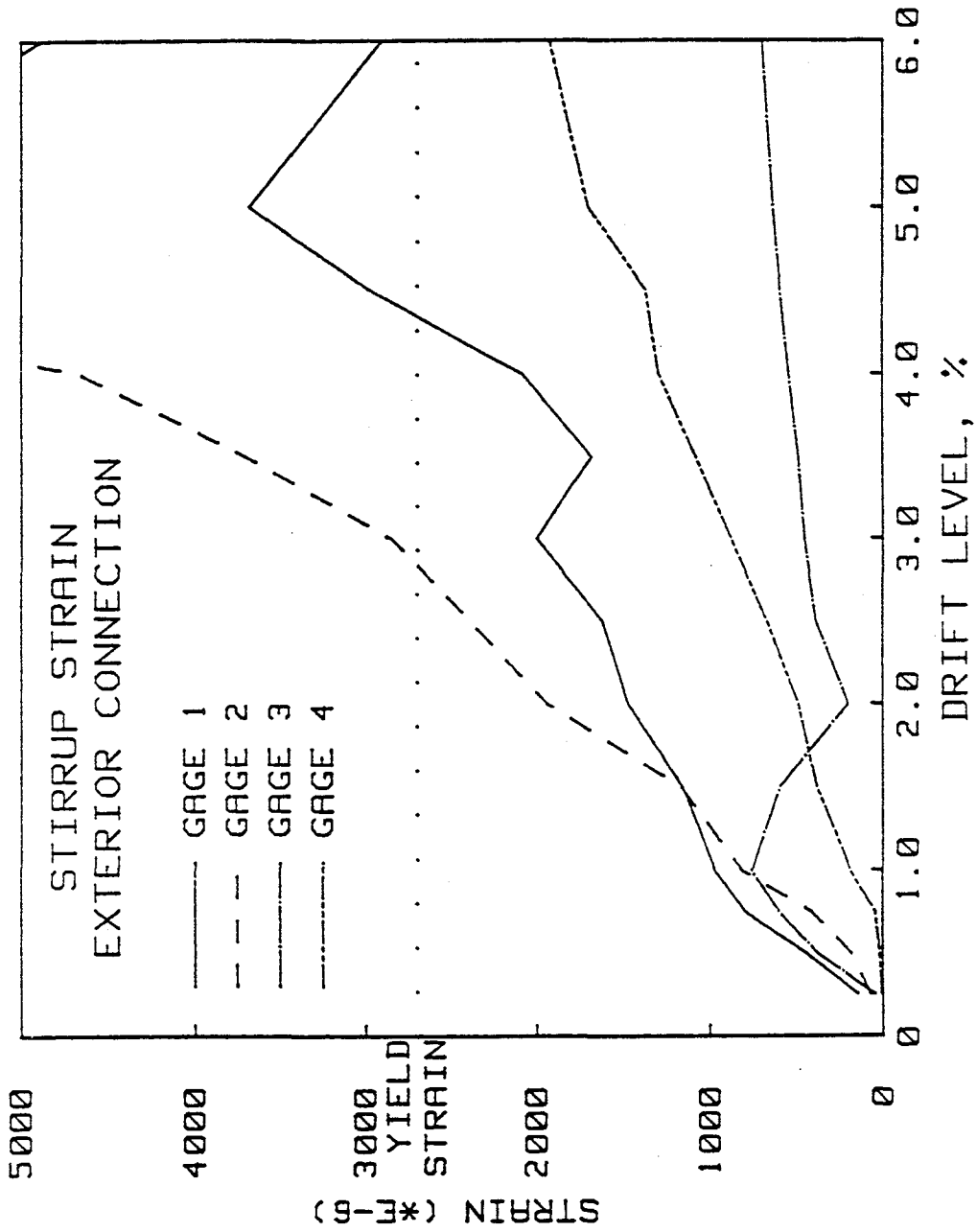
Fig. 3.32 Strain measurements in slab stirrups at exterior
connection of Specimen 4S
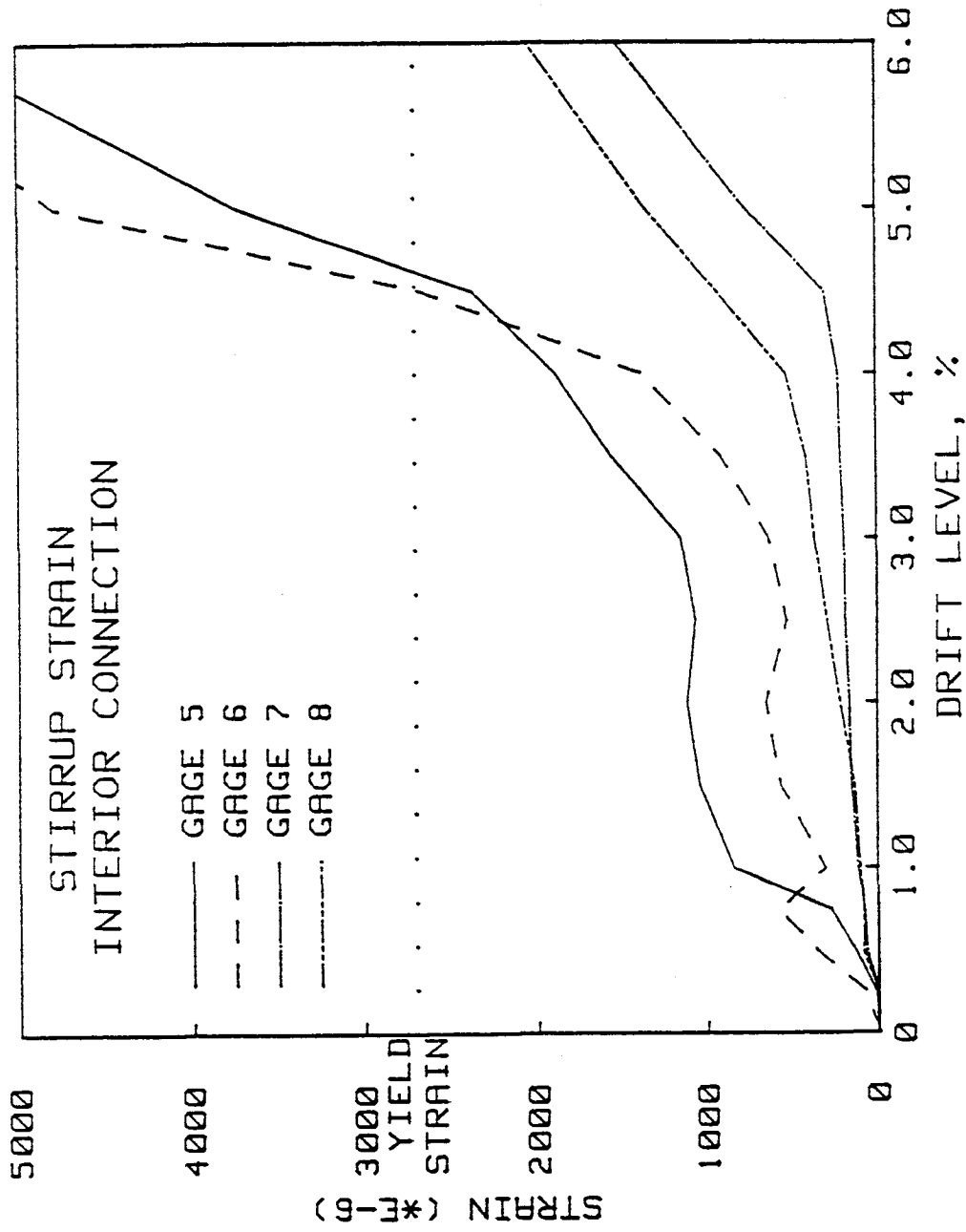
Fig. 3.33 Strain measurements in slab stirrups at interior connection of Specimen 4S

208
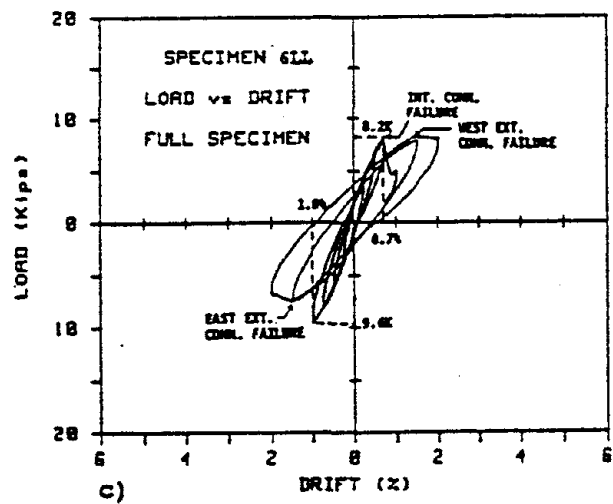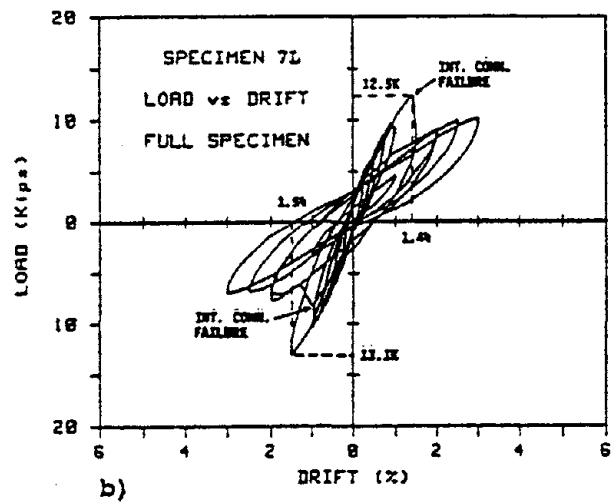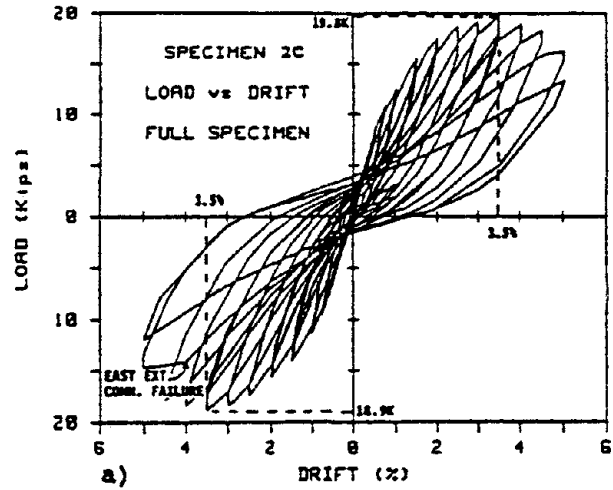
Fig. 4.1   Lateral load vs drift for: a) Specimen 2C,
b) Specimen 7L, c) Specimen 6LL
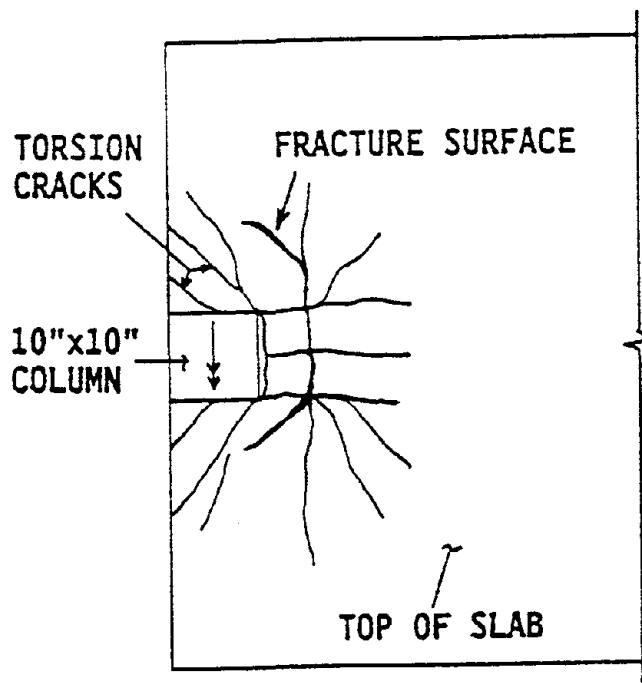
Fig. 4.2   Typical cracking at exterior
connection at failure

210
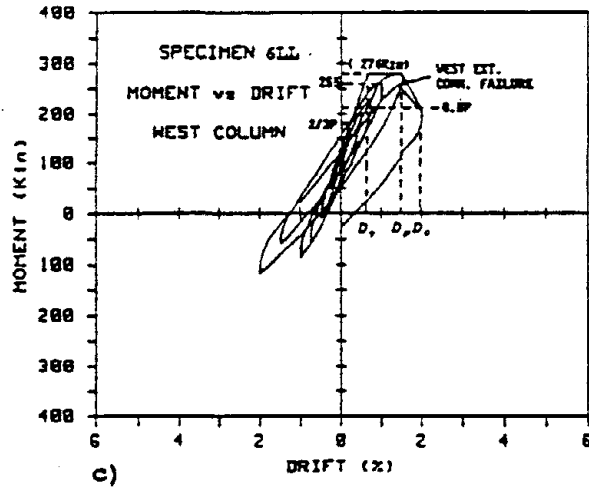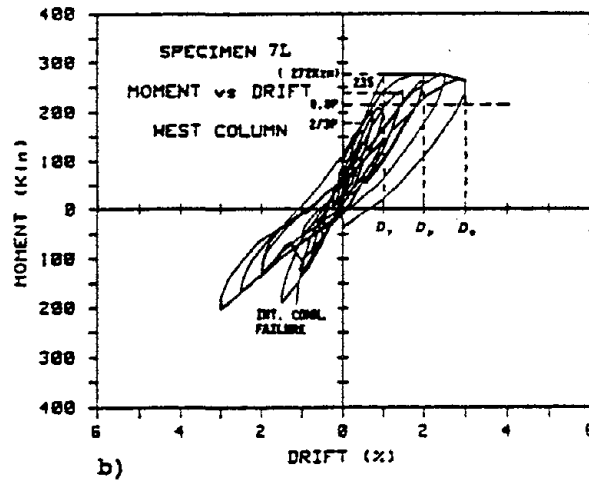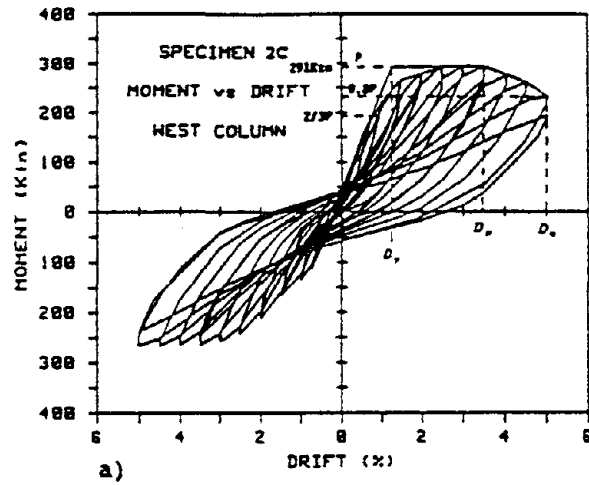
Fig. 4.3   Slab moment at the face of column vs drift for:
a) Specimen 2C, b) Specimen 7L, c) Specimen 6LL

211
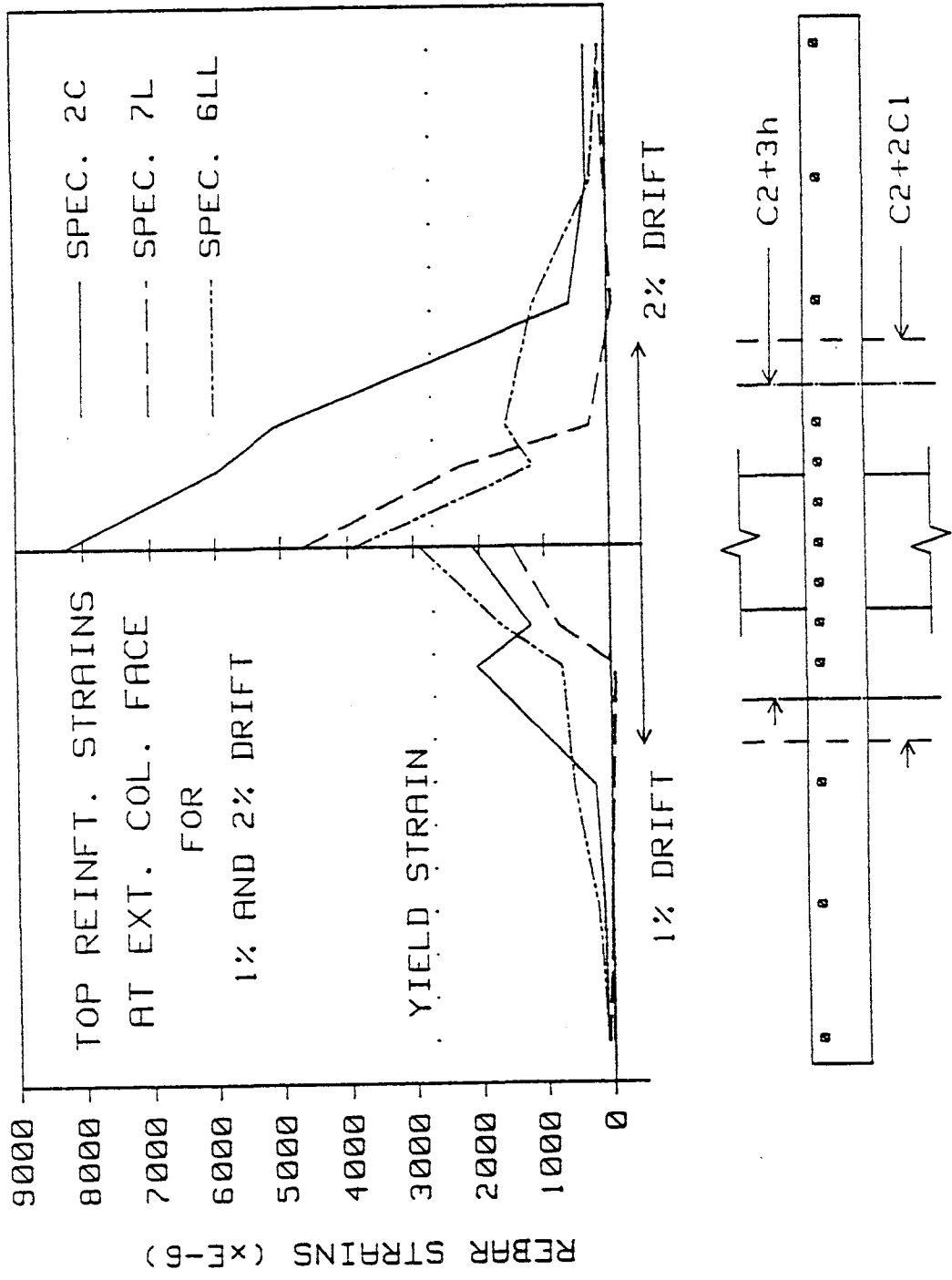
Fig. 4.4   Slab reinforcement strains at exterior connection

The graph shows:

REBAR STRAINS (×E-6)

Y-axis values: 0, 1000, 2000, 3000, 4000, 5000, 6000, 7000, 8000, 9000

TOP REINFT. STRAINS
AT EXT. COL. FACE
FOR
1% AND 2% DRIFT

YIELD STRAIN

—— SPEC. 2C
– – SPEC. 7L
–··– SPEC. 6LL

1% DRIFT   2% DRIFT

C2+3h

C2+2C1

212
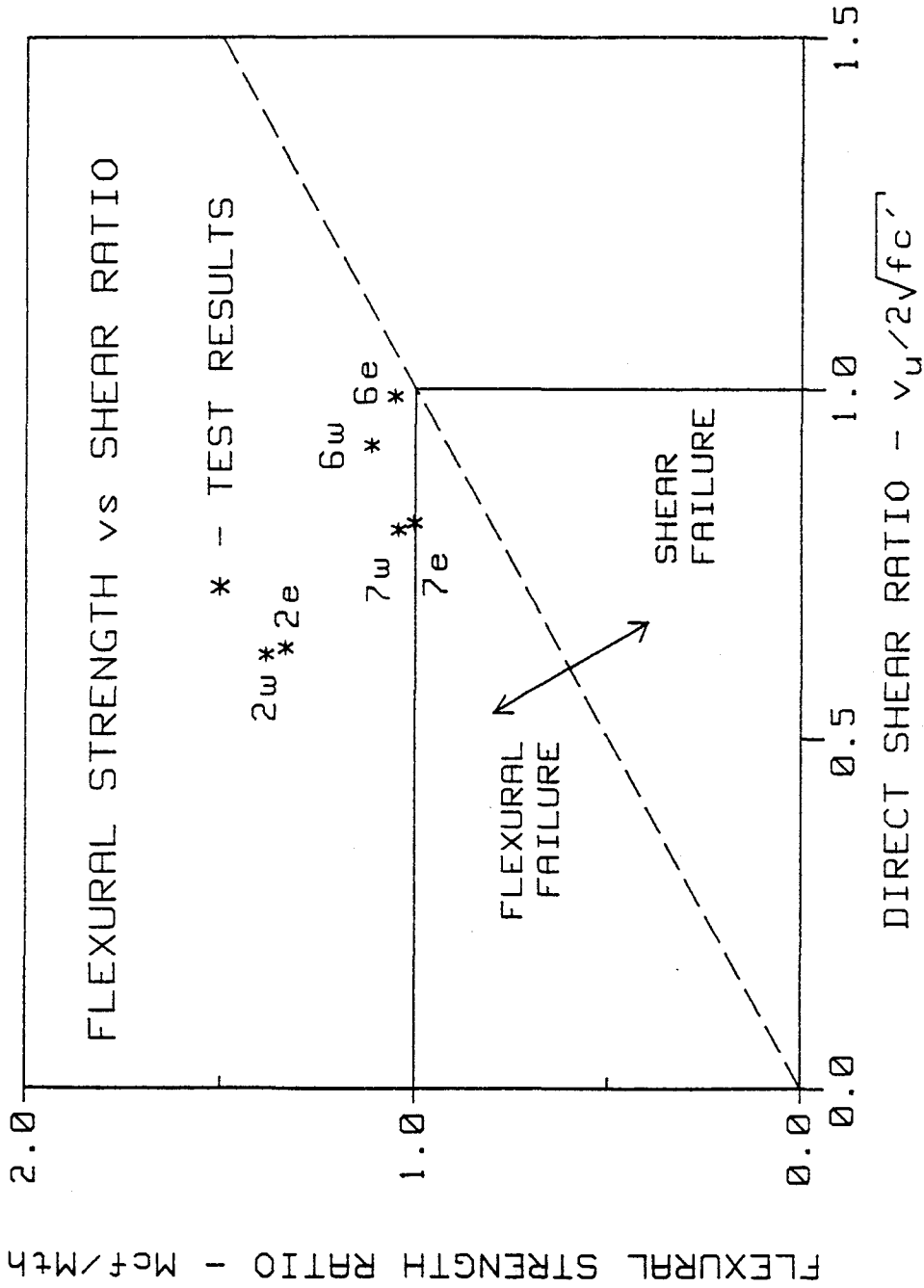
Fig. 4.5   Comparison between measured strength and
strength computed according to the proposed
model

213
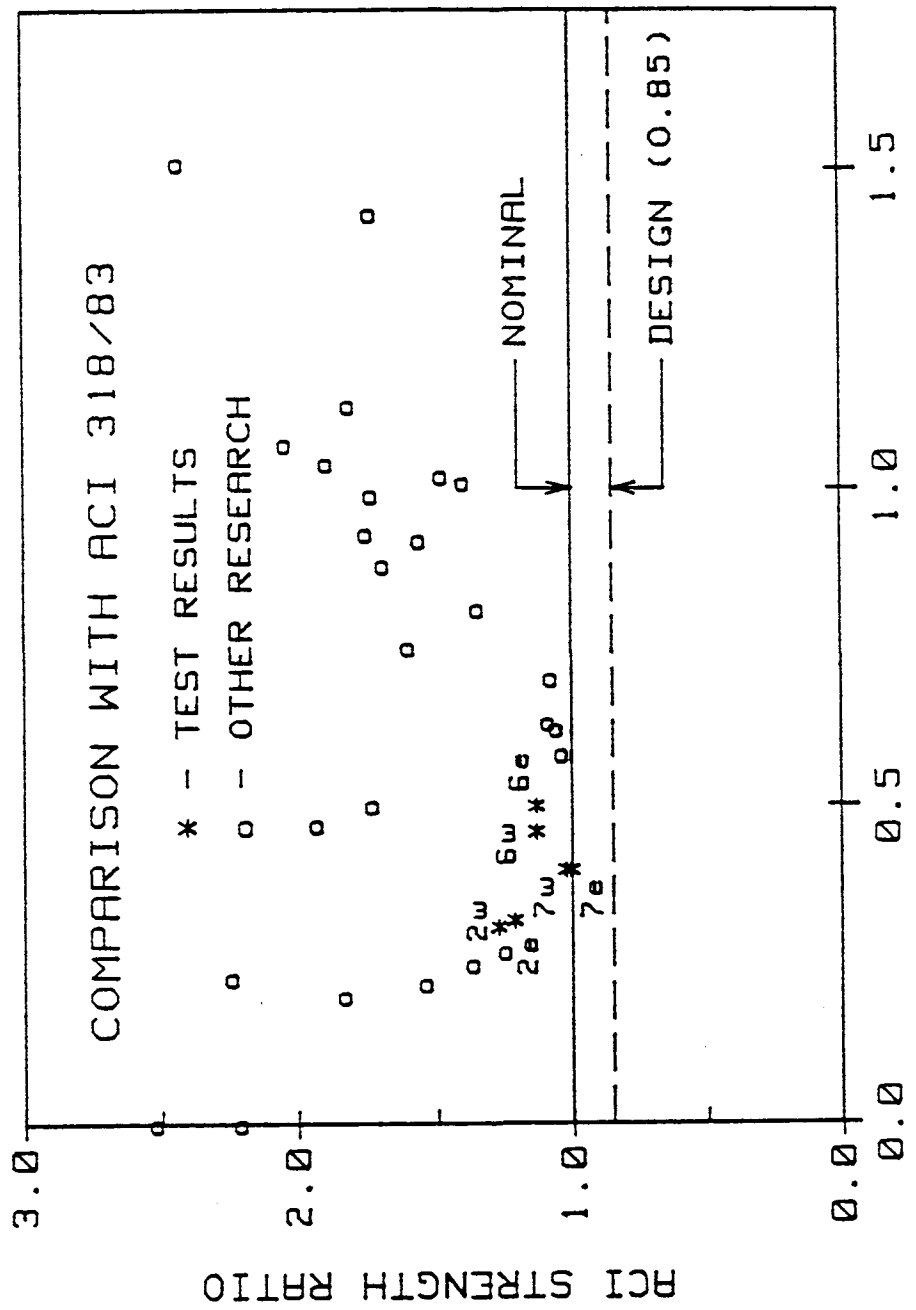
Fig. 4.6   Comparison between measured strength and
strength computed according to the ACI building code
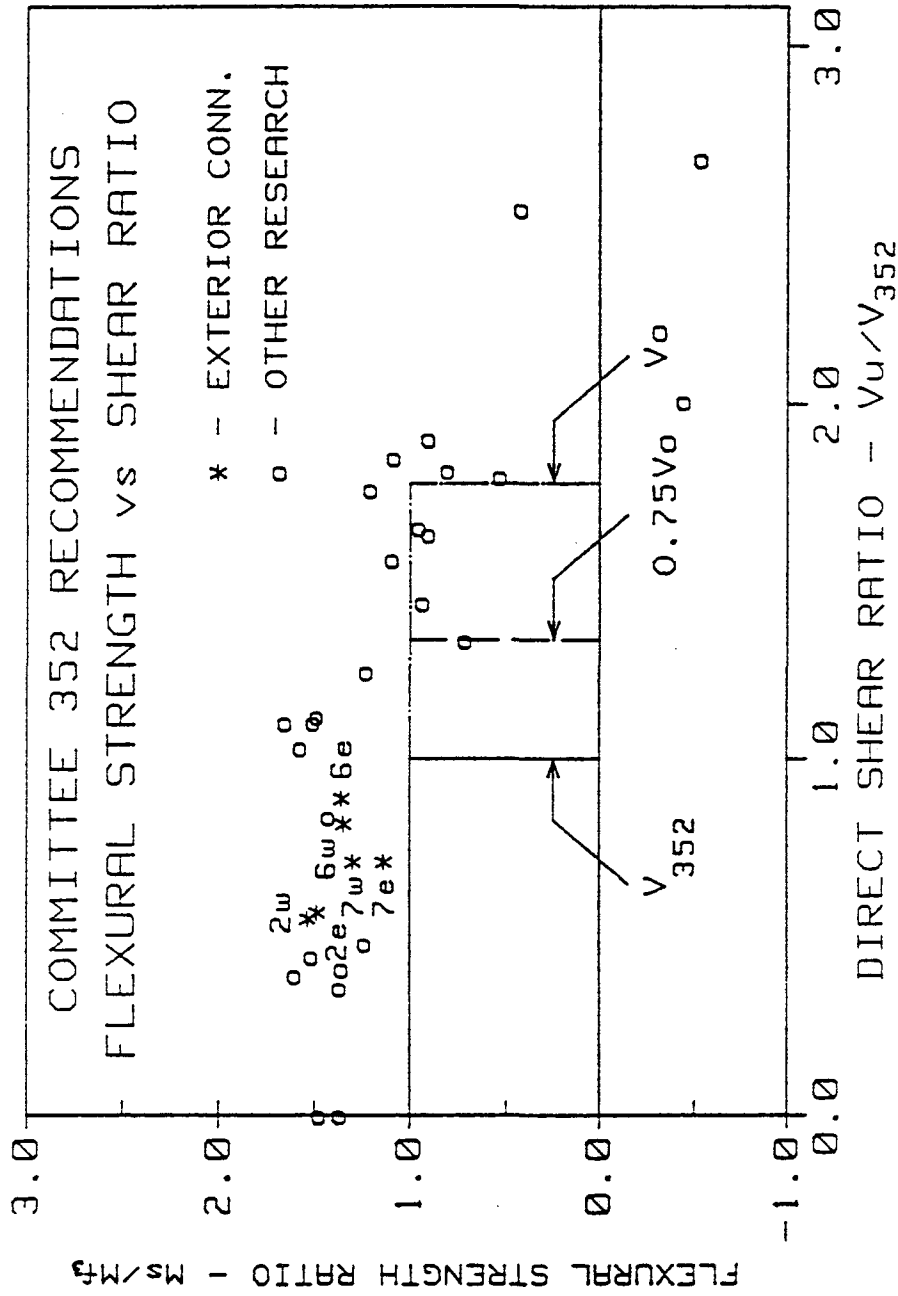
Fig. 4.7 Comparison between measured strength and strength computed according to ACI Committee 352 Recommendations
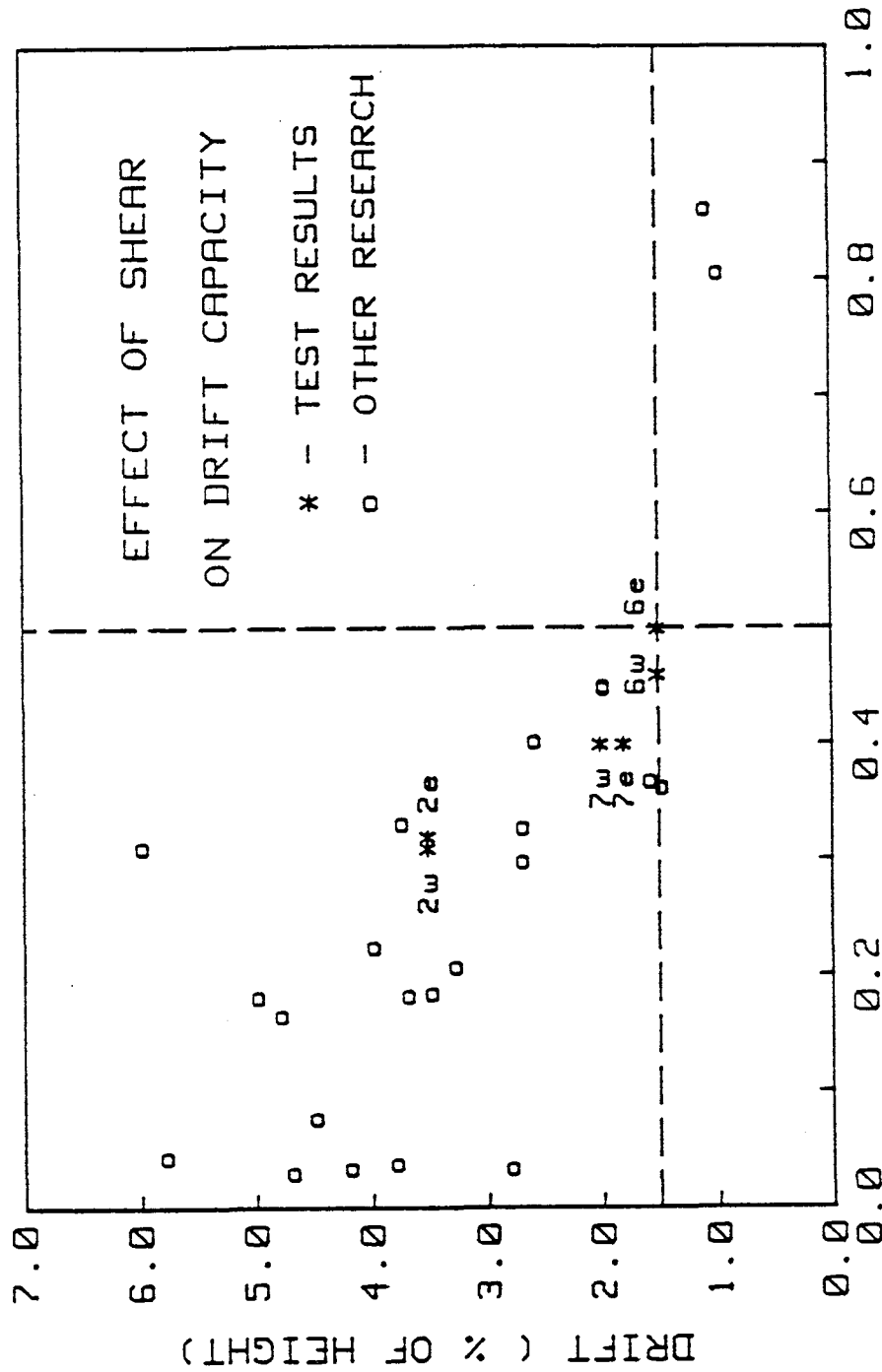
Fig. 4.8   The effect of shear level on drift capacity
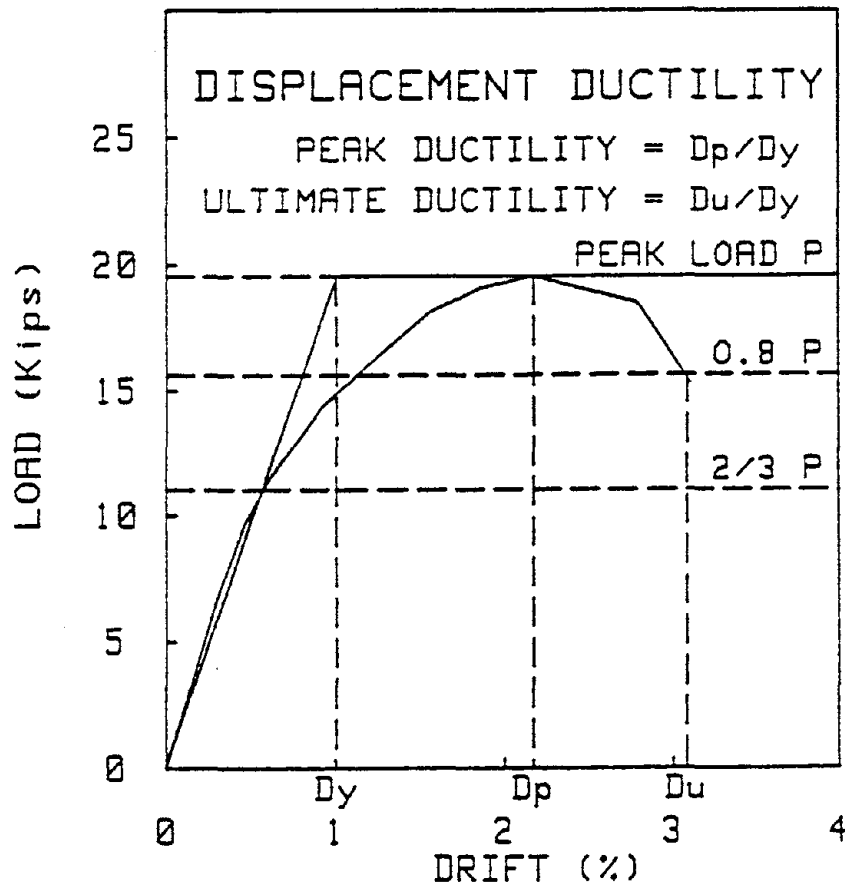
Fig. 4.9   Definition of displacement ductility
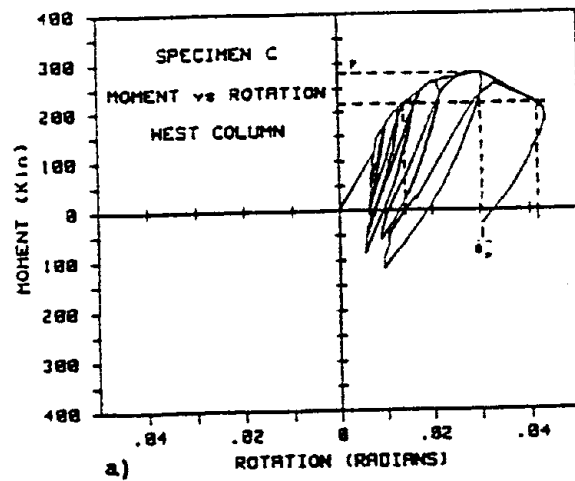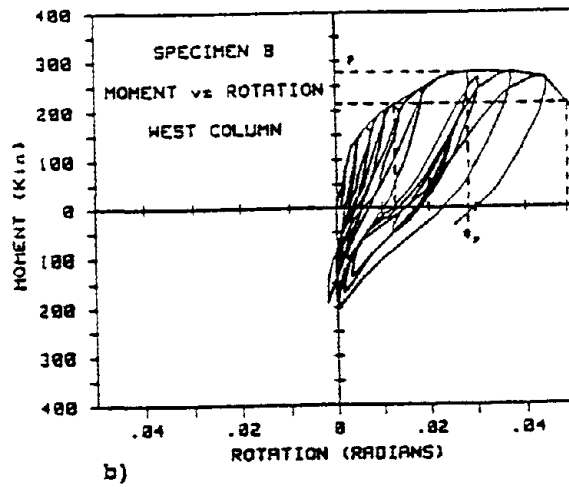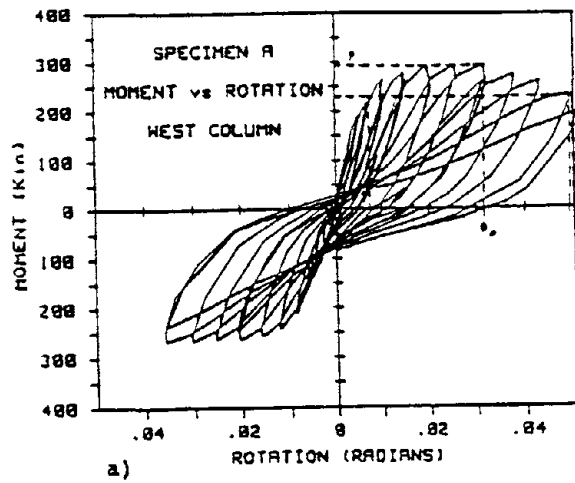
Fig. 4.10   Slab moment at the face of column vs joint
rotation for: a) Specimen 2C,   b) Specimen 7L,
c) Specimen 6LL
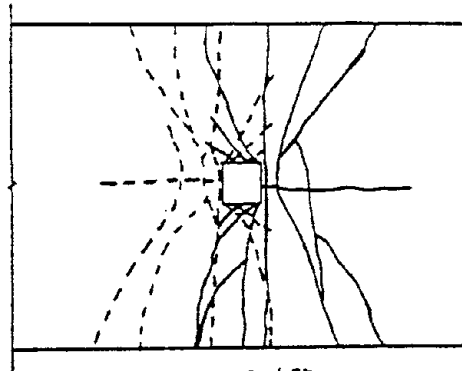
3.5% Drift

SPECIMEN 2C
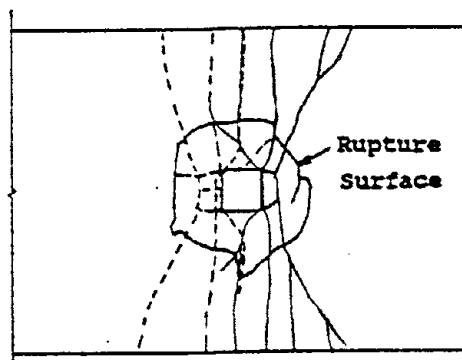
1.5% Drift

SPECIMEN 7L
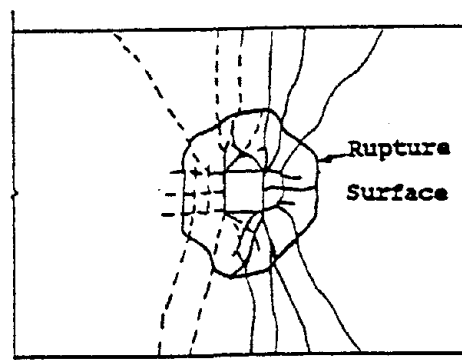
1% Drift

SPECIMEN 6LL

——— Positive Drift Cracks

----- Negative Drift Cracks

Fig. 5.1   Final crack patterns for interior connections
of: a) Specimen 2C,   b) Specimen 7L,
c) Specimen 6LL
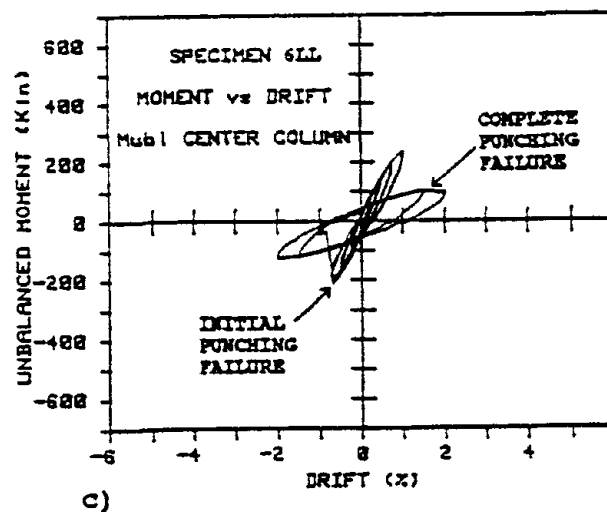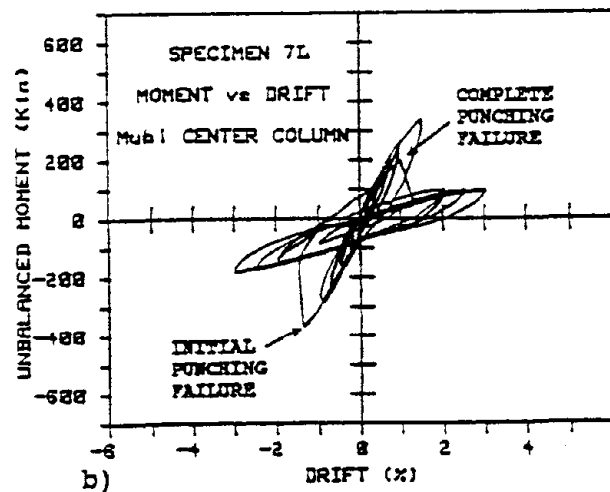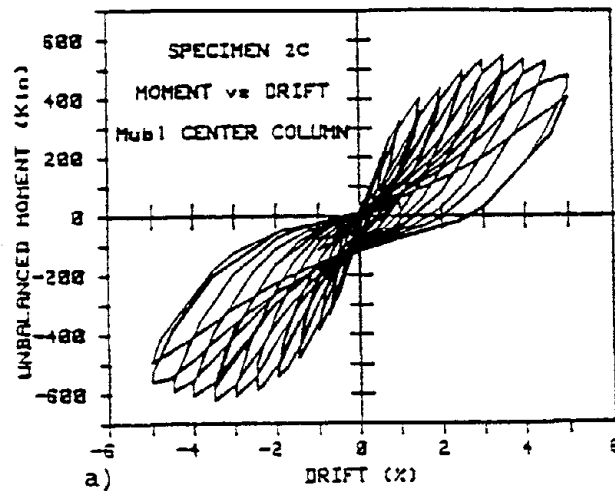
Fig. 5.2   Interior connection unbalanced moment vs Drift
for: a) Specimen 2C, b) Specimen 7L,
c) Specimen 6LL
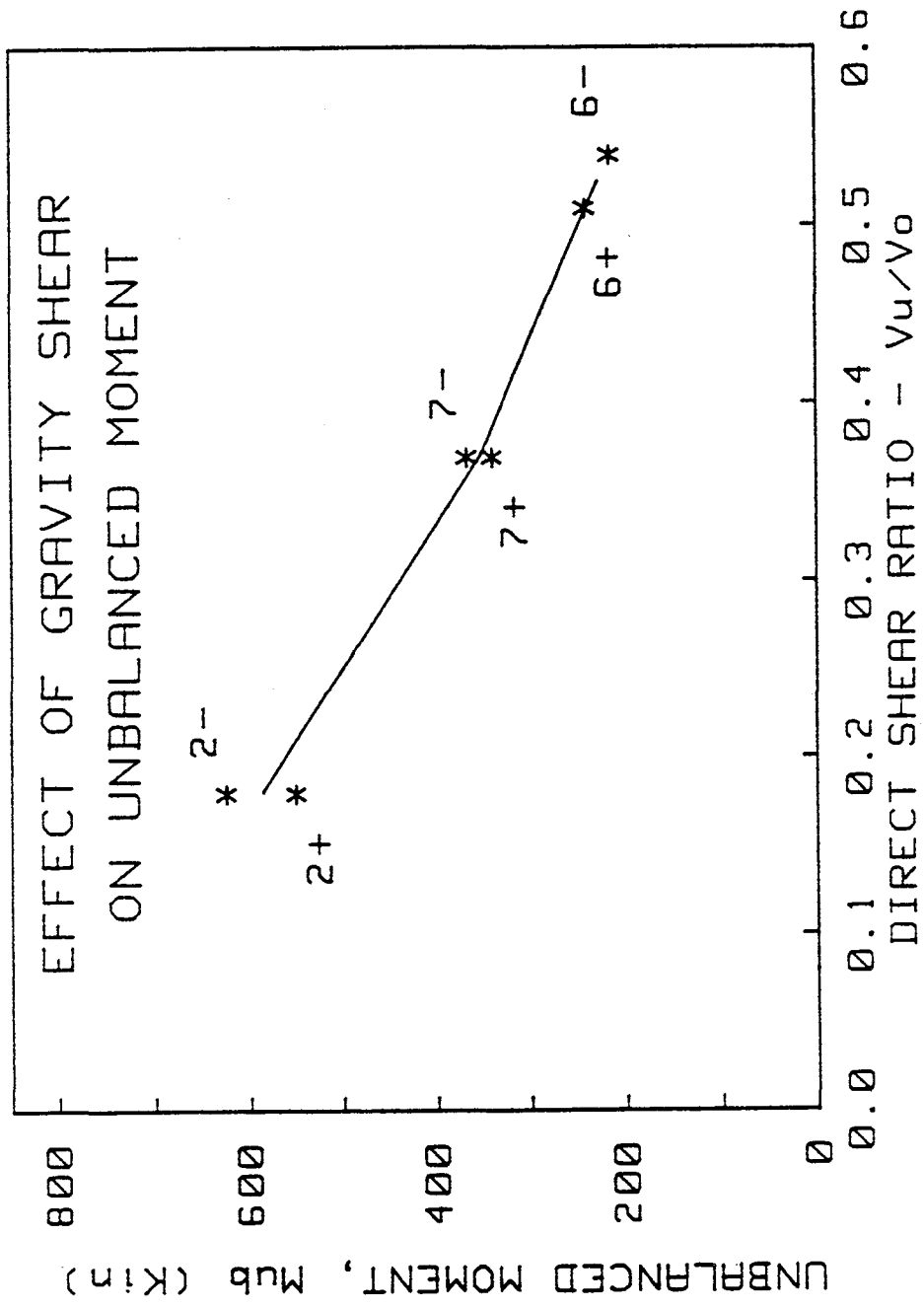
Fig. 5.3   Effect of gravity shear on interior connection
unbalanced moment
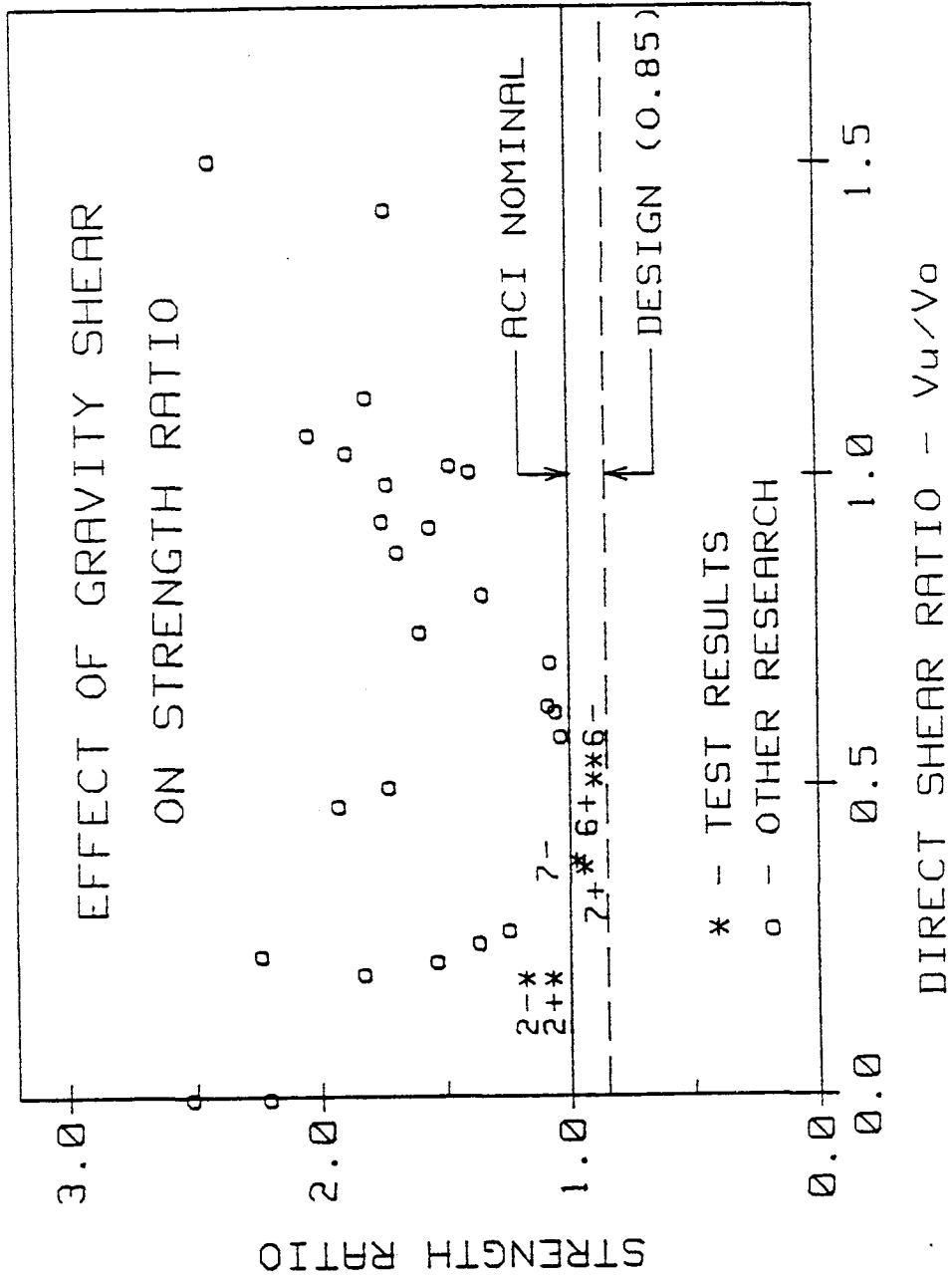
Fig. 5.4 Effect of gravity shear on interior connection strength ratio

222
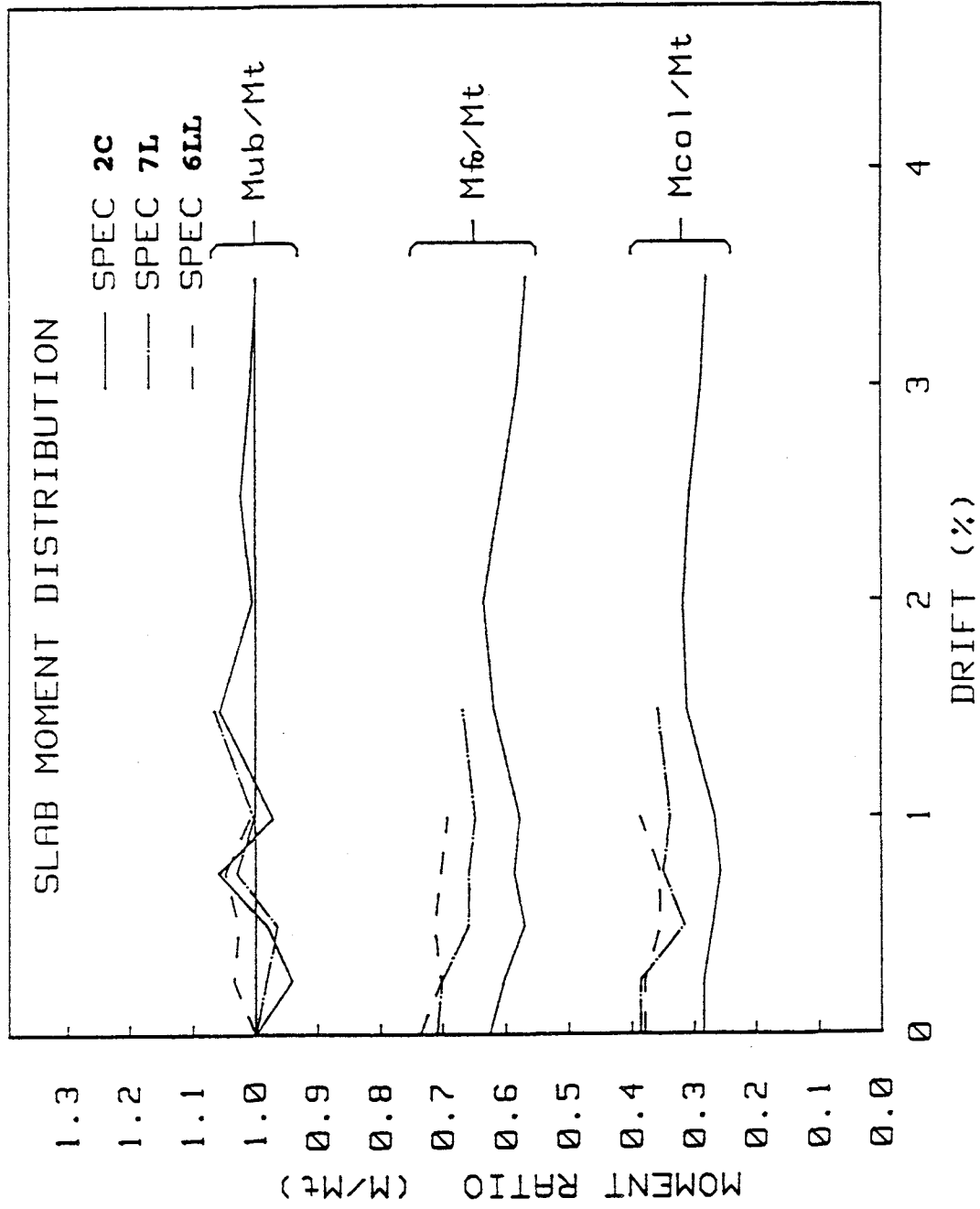
Fig. 5.5 slab moment distribution
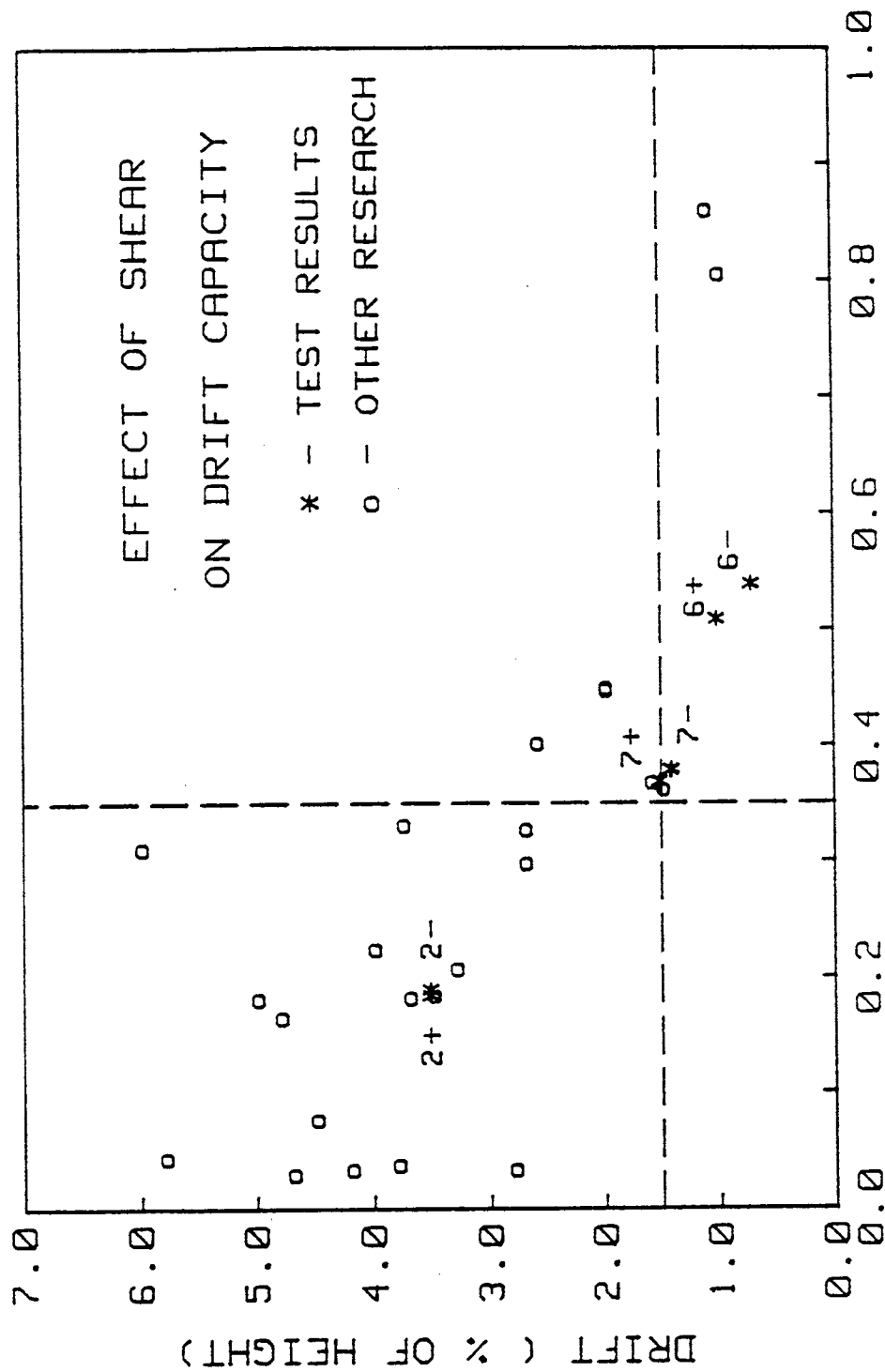
Fig. 5.6   Effect of gravity shear on connection drift
            capacity

224
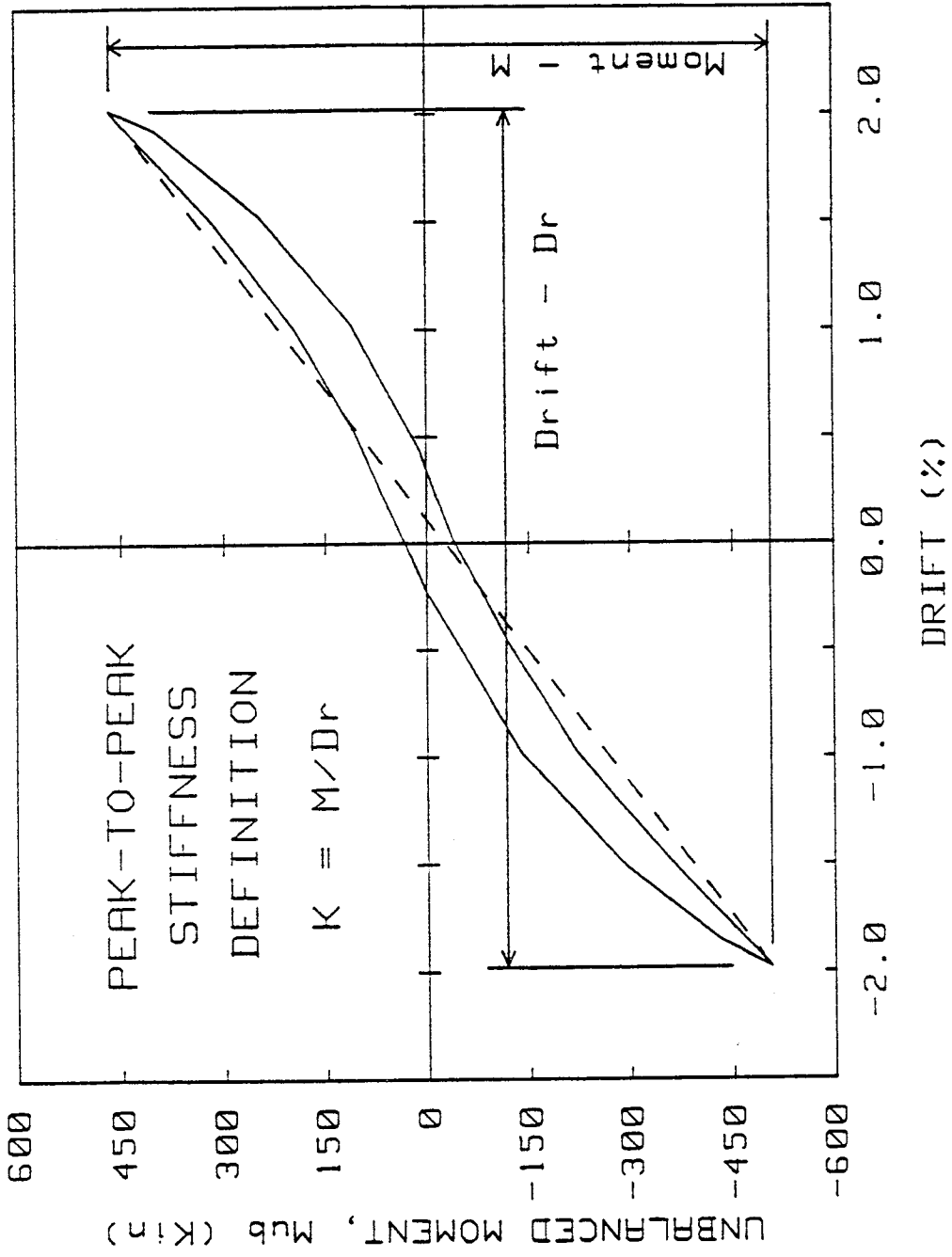
Fig. 5.7   Definition of Peak-to-Peak Stiffness
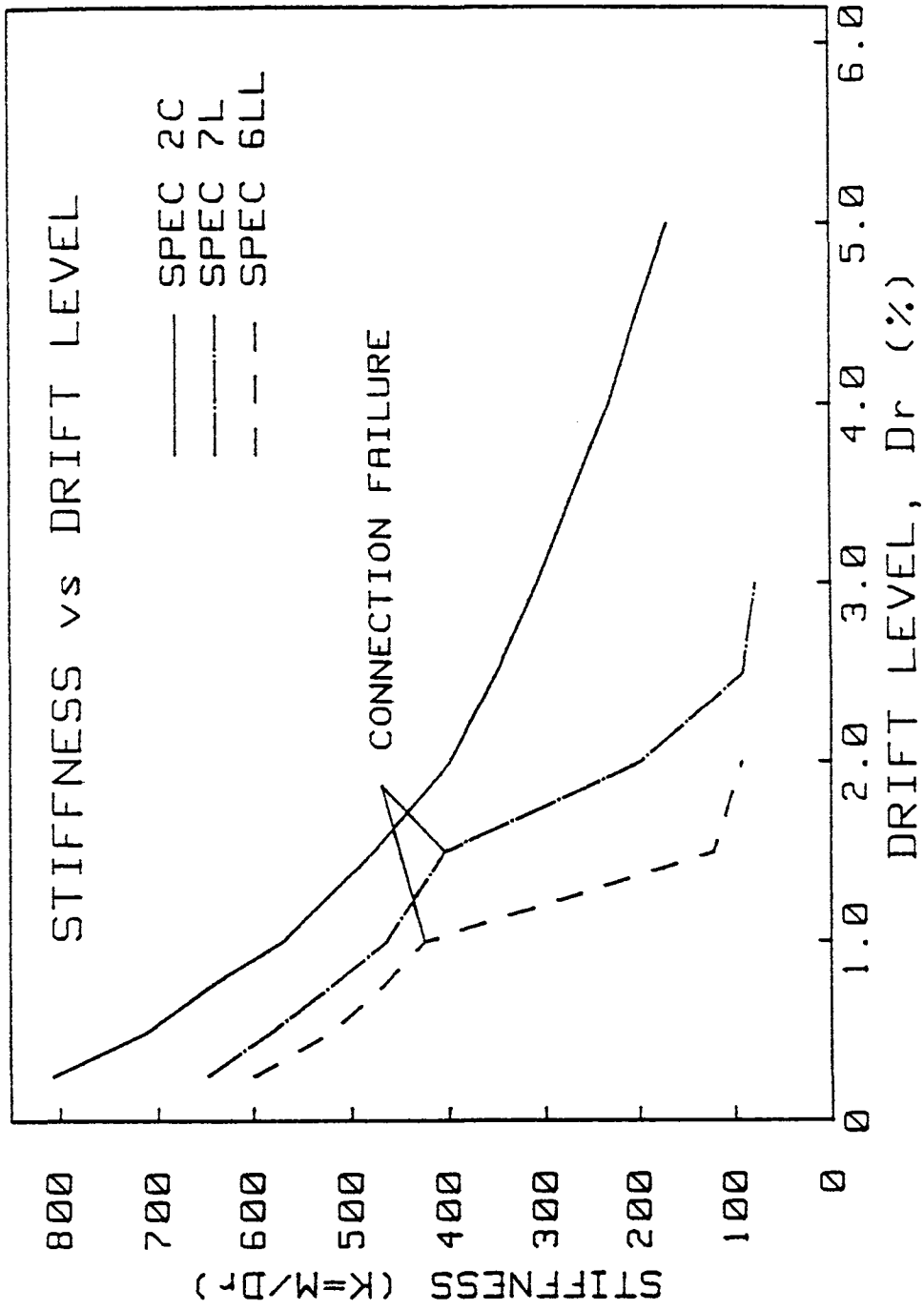
Fig. 5.8   Peak-to-Peak Stiffness vs Drift level

226
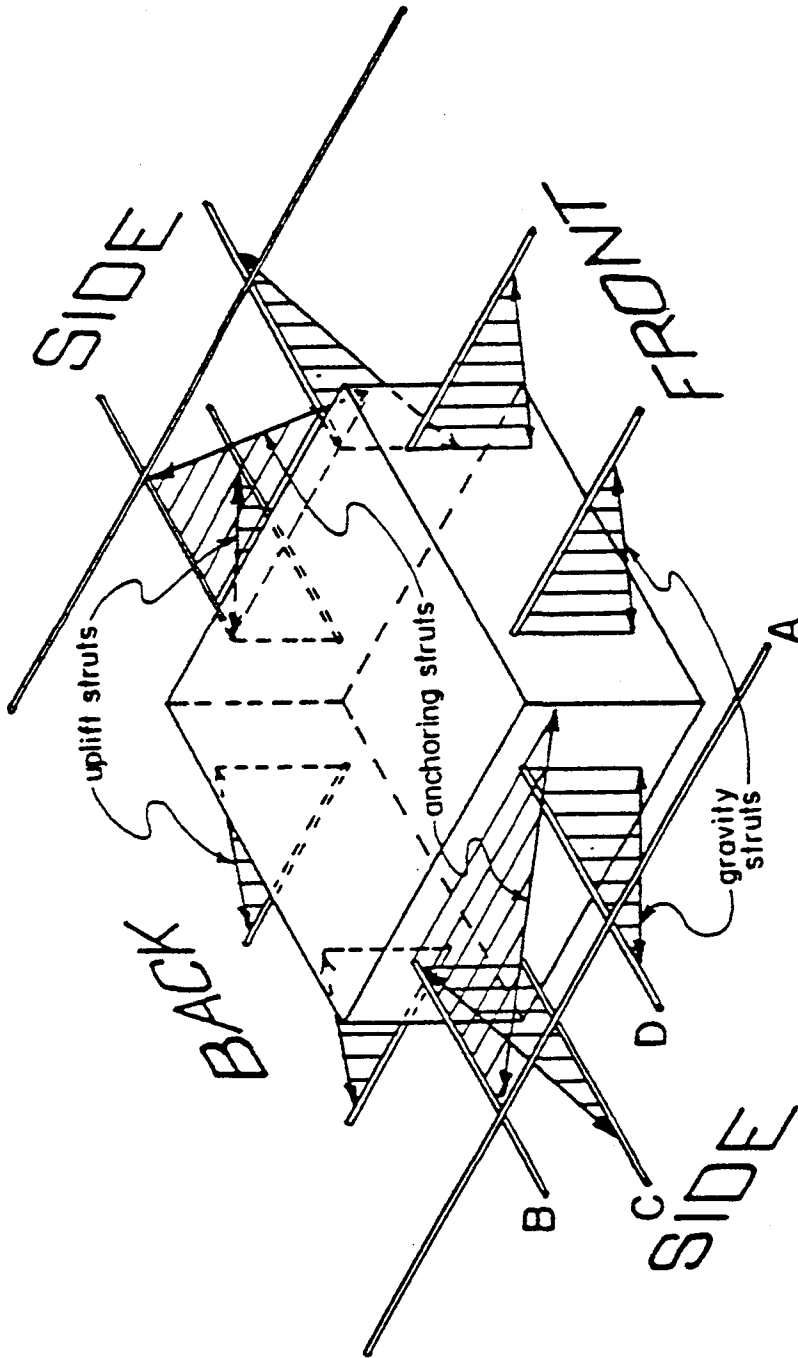
Fig. 6.1   Interior connection model after Simmonds and
Alexander
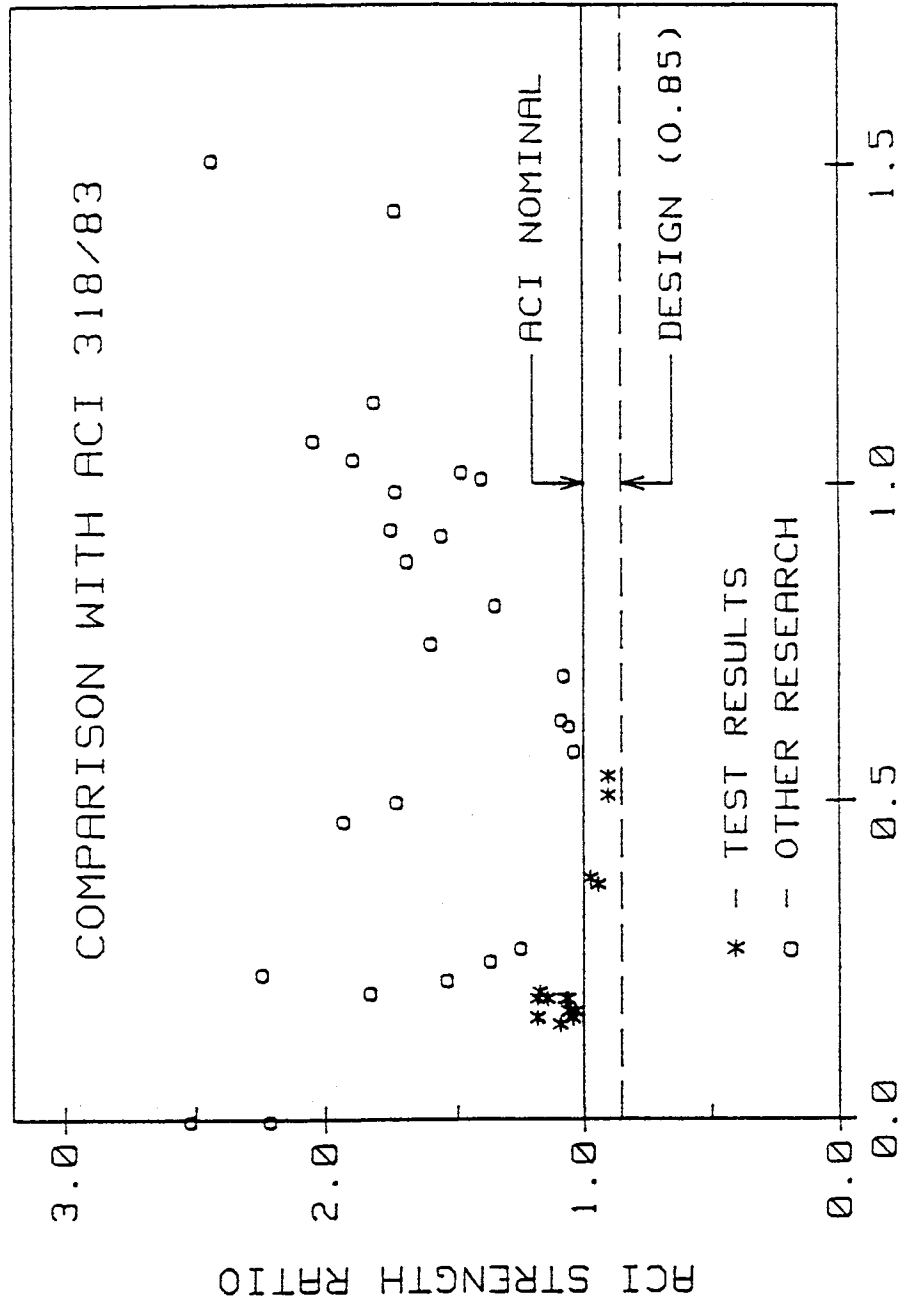
Fig. 6.2   ACI strength ratio for all interior connections
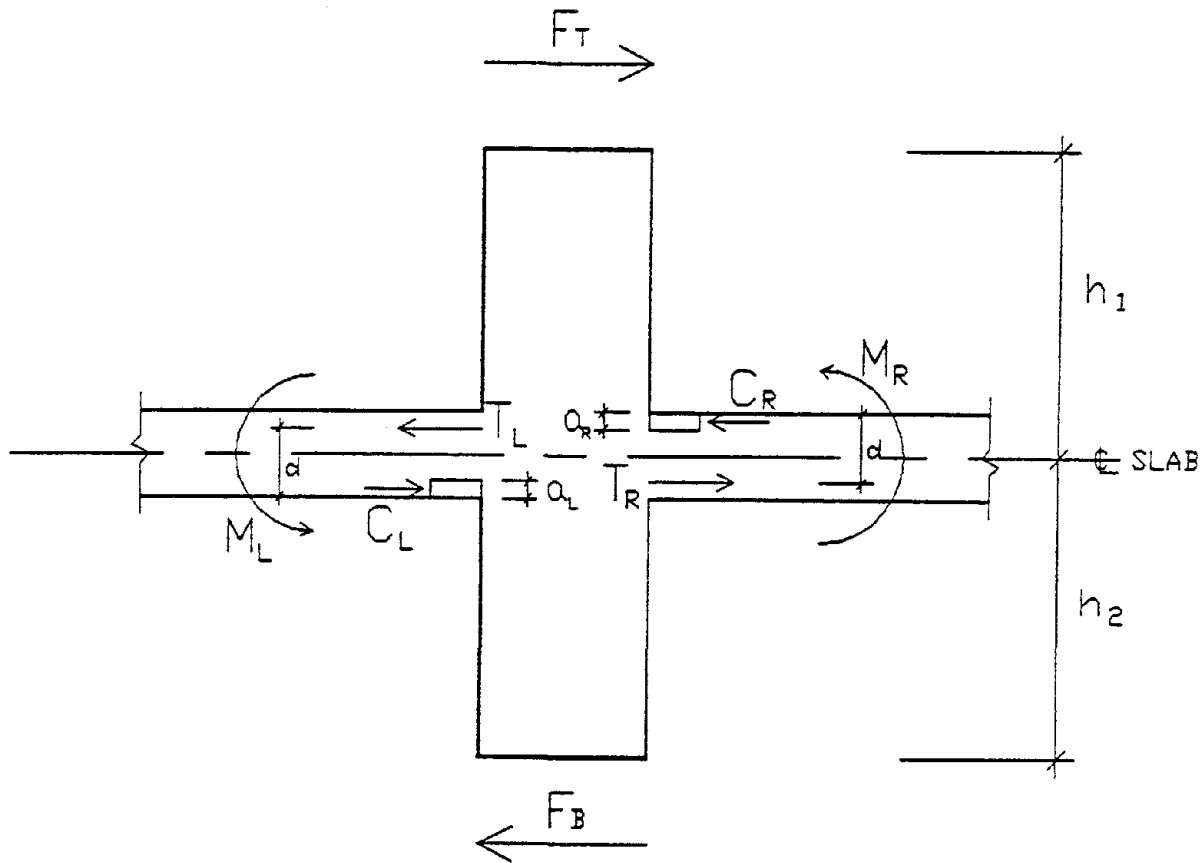
Computation of Connection Unbalanced Moment

1. Based on load cell measurements:

$$M_{ub} = F_T \times h_1 + F_B \times h_2$$

2. Based on strain gage readings:

$$C_L = T_L = \Sigma A_{SL} \times f_{SL} \qquad\qquad C_R = T_R = \Sigma A_{SR} \times f_{SR}$$

$$a_L = \frac{c_L}{0.85 f_c' b} \qquad\qquad\qquad a_R = \frac{c_R}{0.85 f_c' b}$$

$$M_L = T_L \left(d - \frac{a_L}{2} \right) \qquad\qquad M_R = T_R \left(d - \frac{a_R}{2} \right)$$

then: $\qquad M_T = M_L + M_R$

Fig. 6.3   Computation of connection unbalanced moment based on reinforcement strains
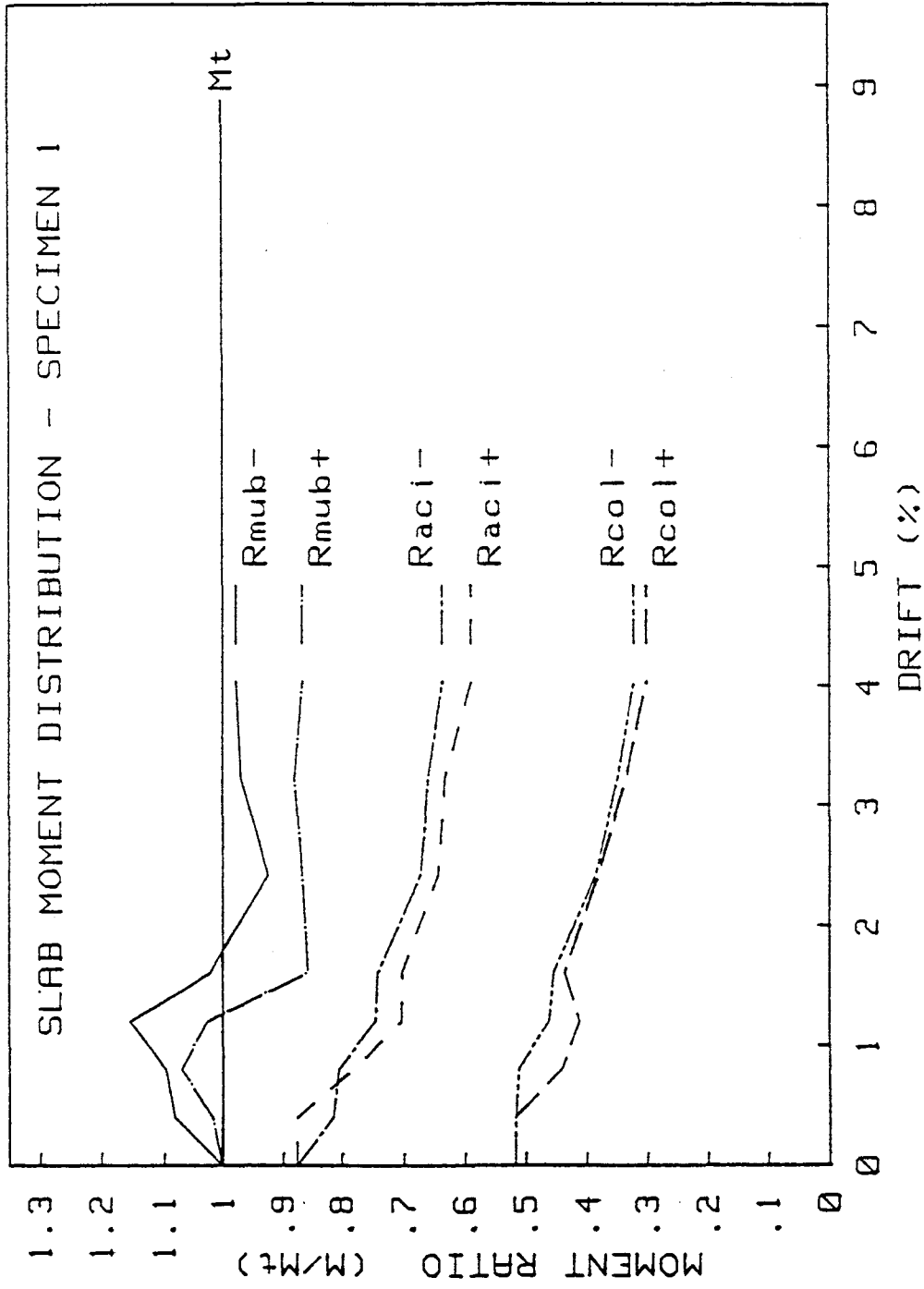
Fig. 6.4 Slab moment distribution at interior connection

of specimen 1
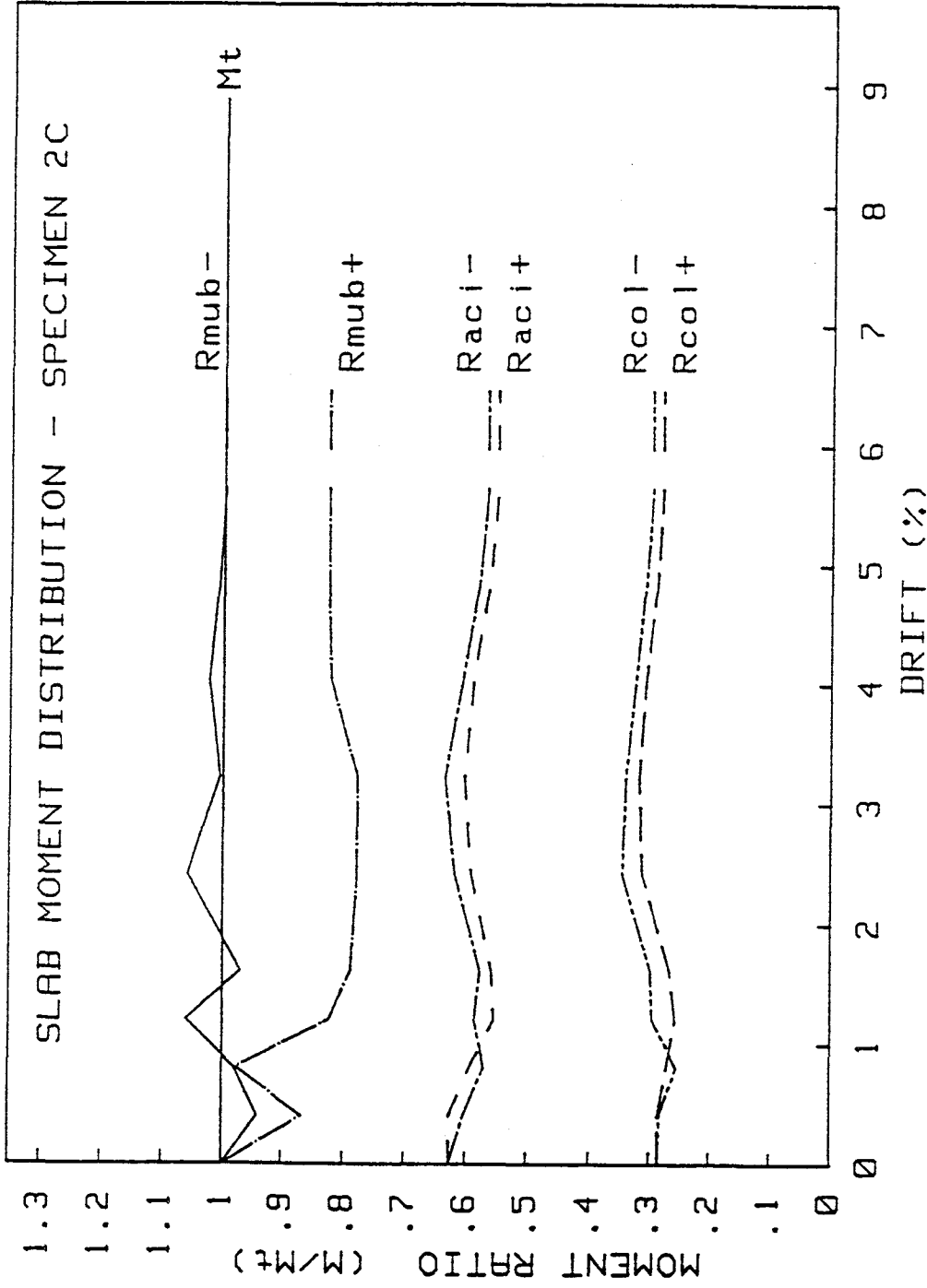
Fig. 6.5   Slab moment distribution at interior connection

of specimen 2C
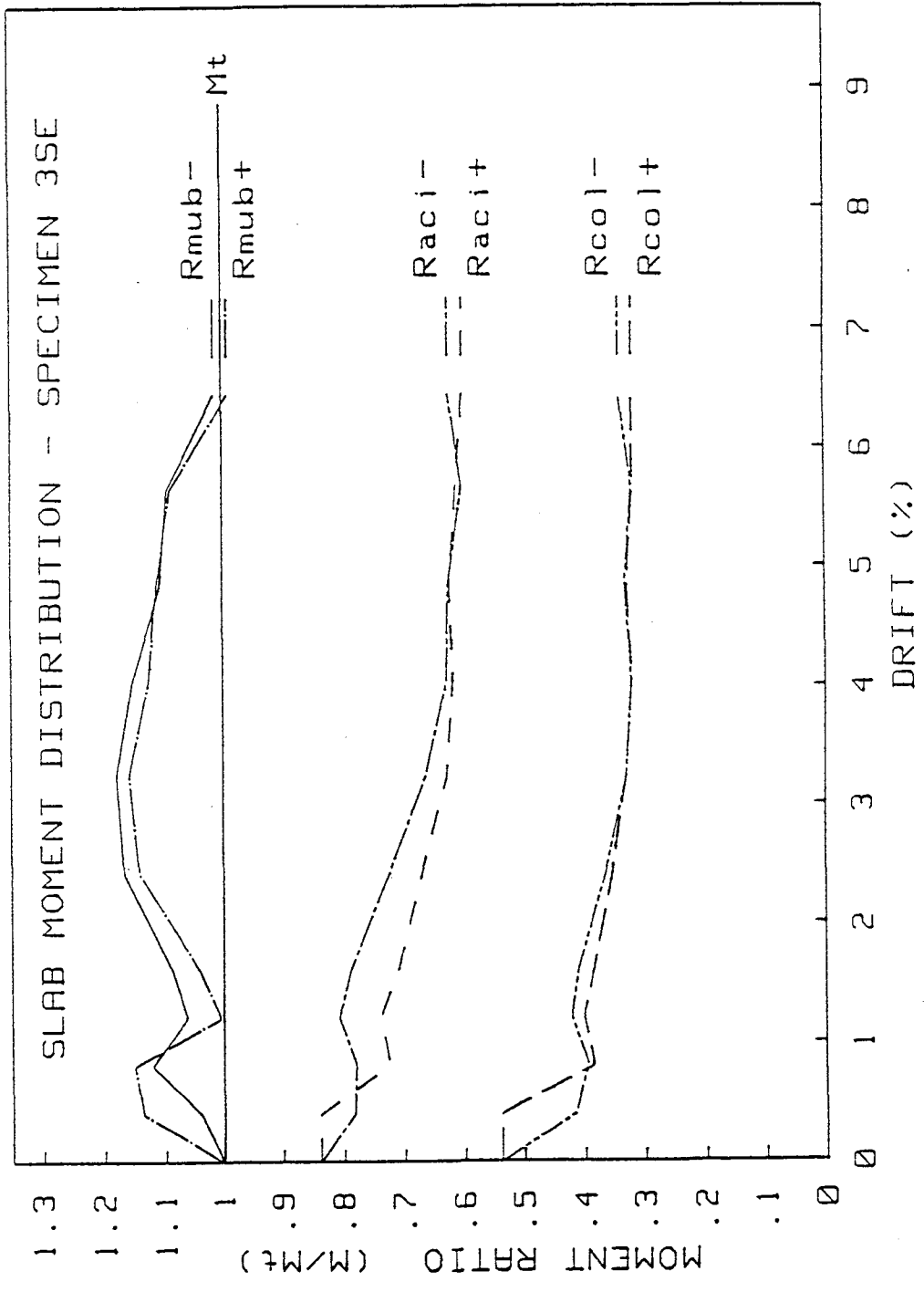
Fig. 6.6   Slab moment distribution at interior connection

of specimen 3SE

232

Fig. 6.7   Slab moment distribution at interior connection
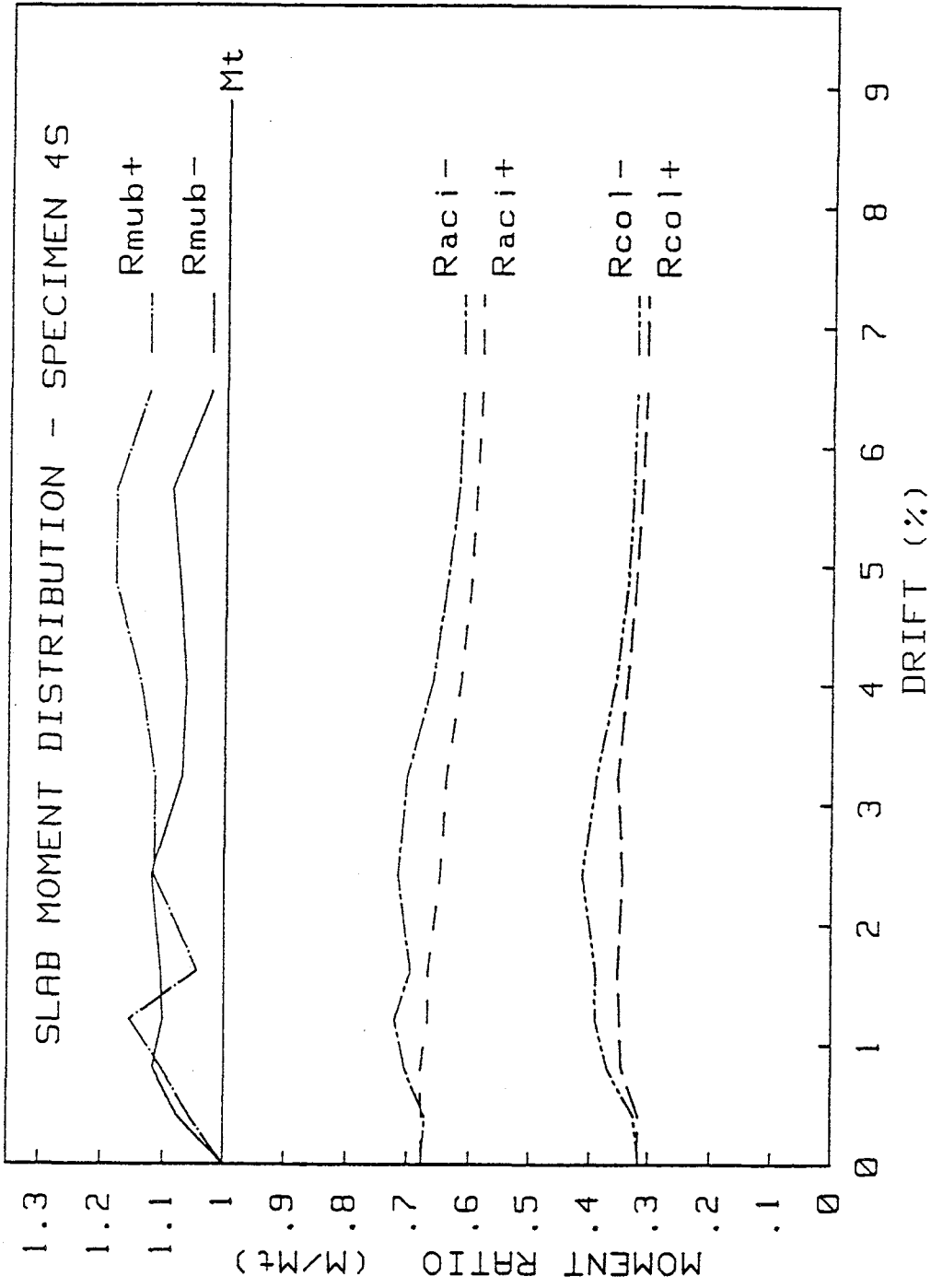
of specimen 4S

SLAB MOMENT DISTRIBUTION – SPECIMEN 5SO
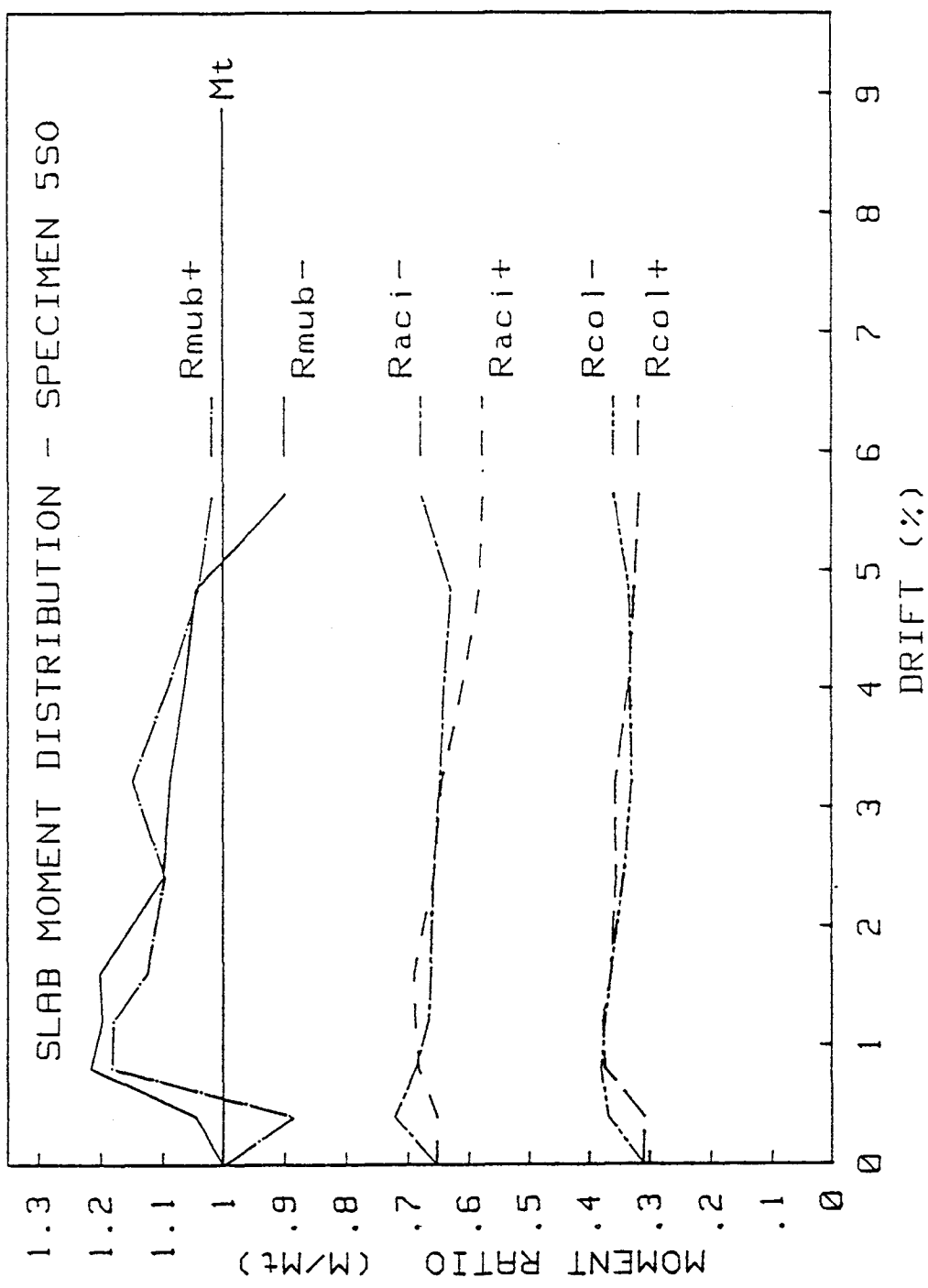
Fig. 6.8   Slab moment distribution at interior connection

of specimen 5SO

234
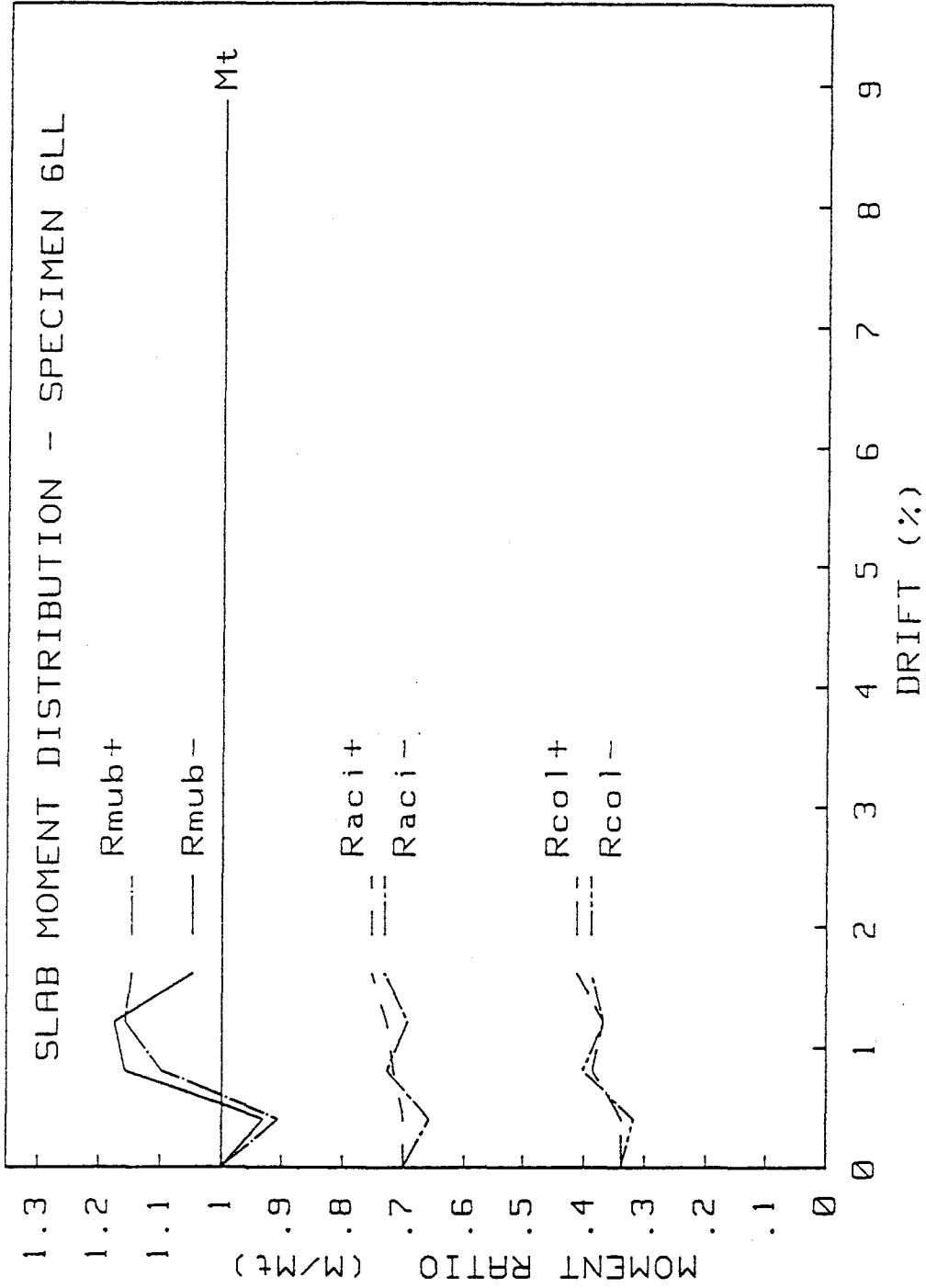
Fig. 6.9   Slab moment distribution at interior connection
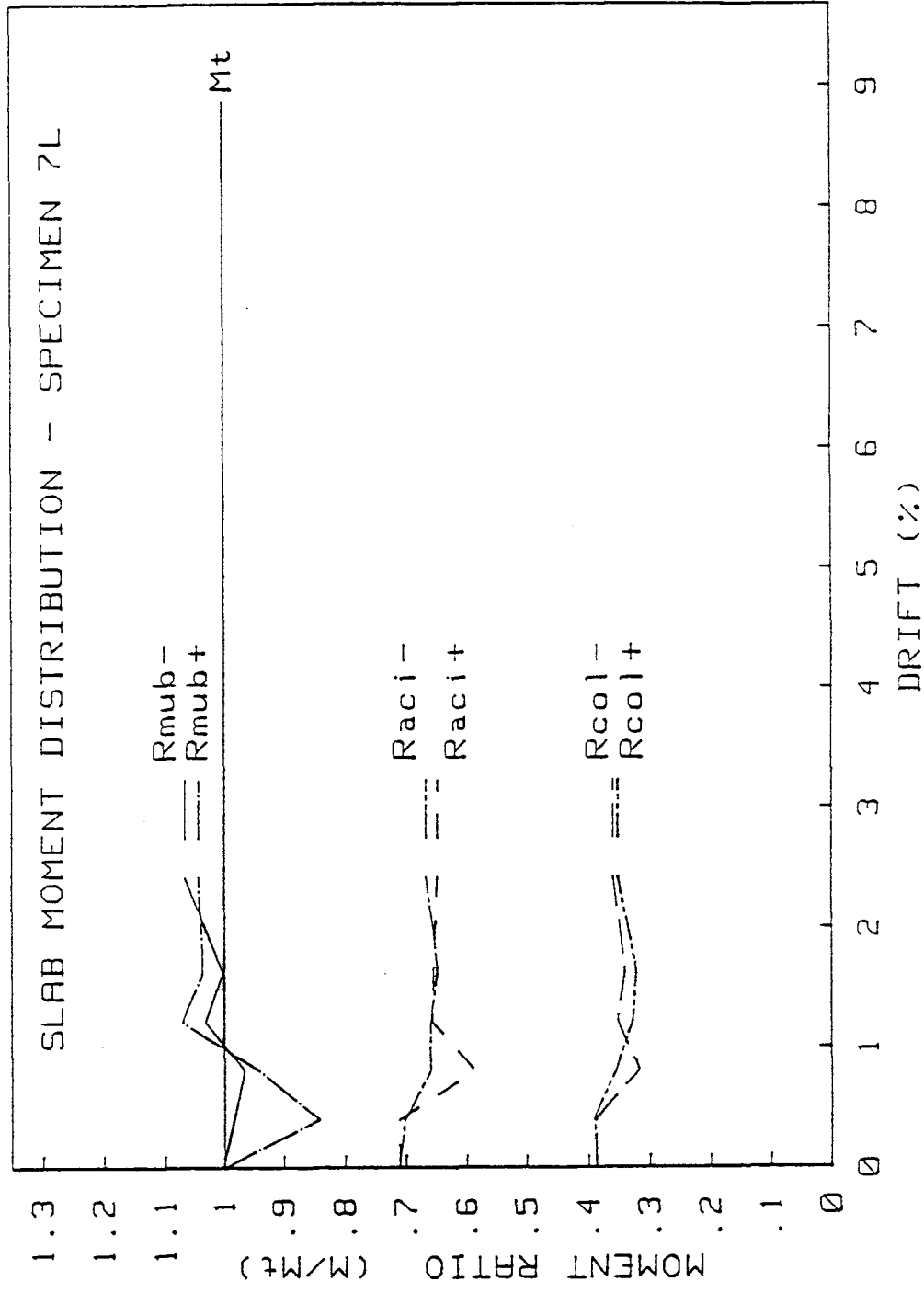
of specimen 6LL

Fig. 6.10 Slab moment distribution at interior connection
of specimen 7L

236
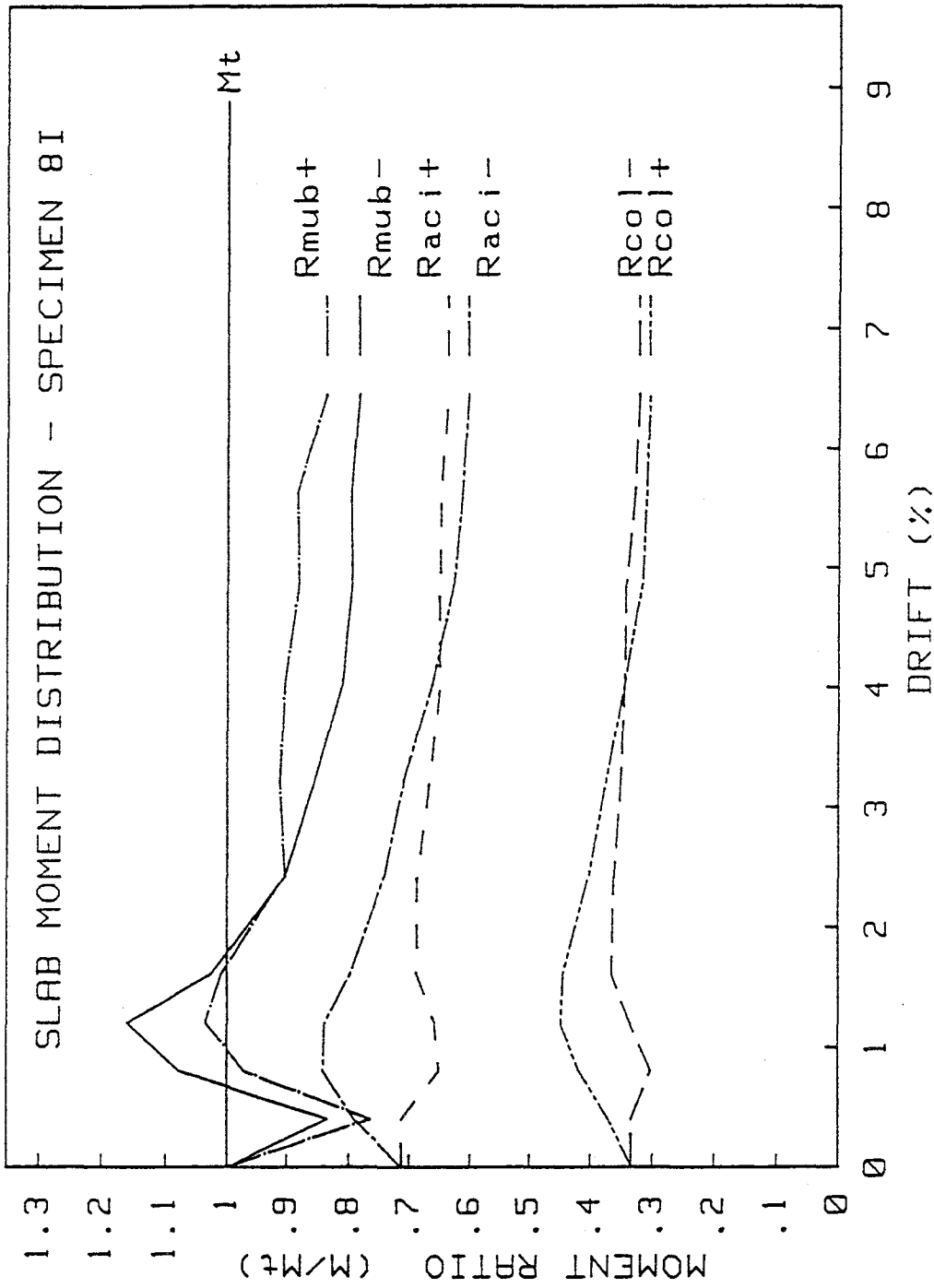
Fig. 6.11 Slab moment distribution at interior connection

of specimen 8I
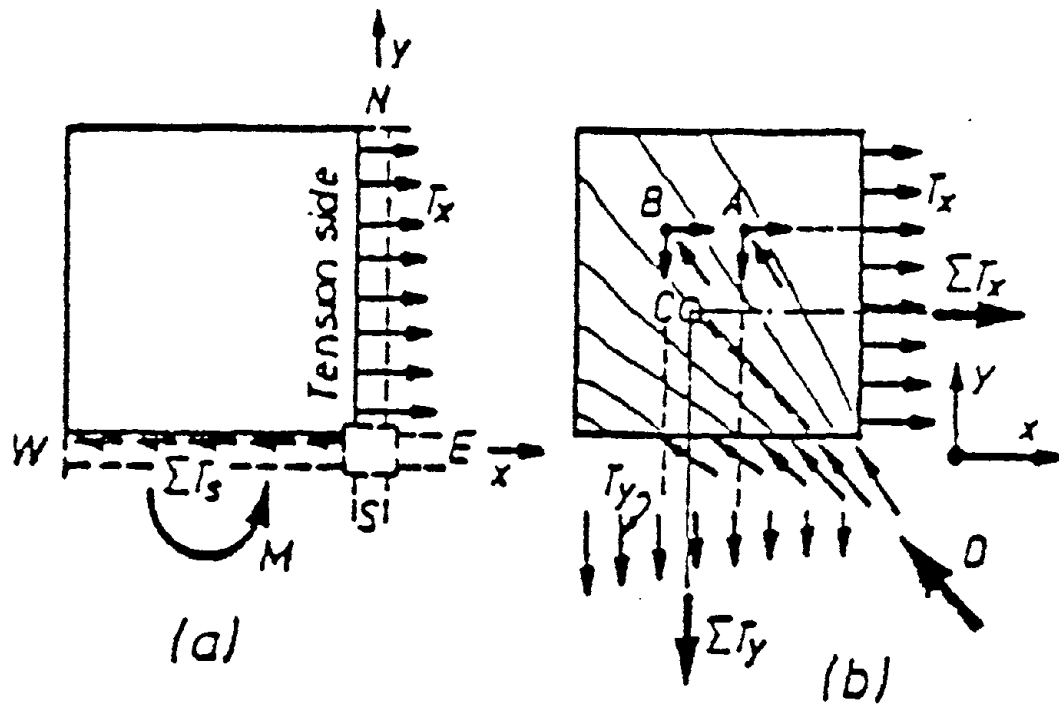
Fig. 6.12   Equilibrium criteria for tension flanges after
Paulay (Ref. 6.5)
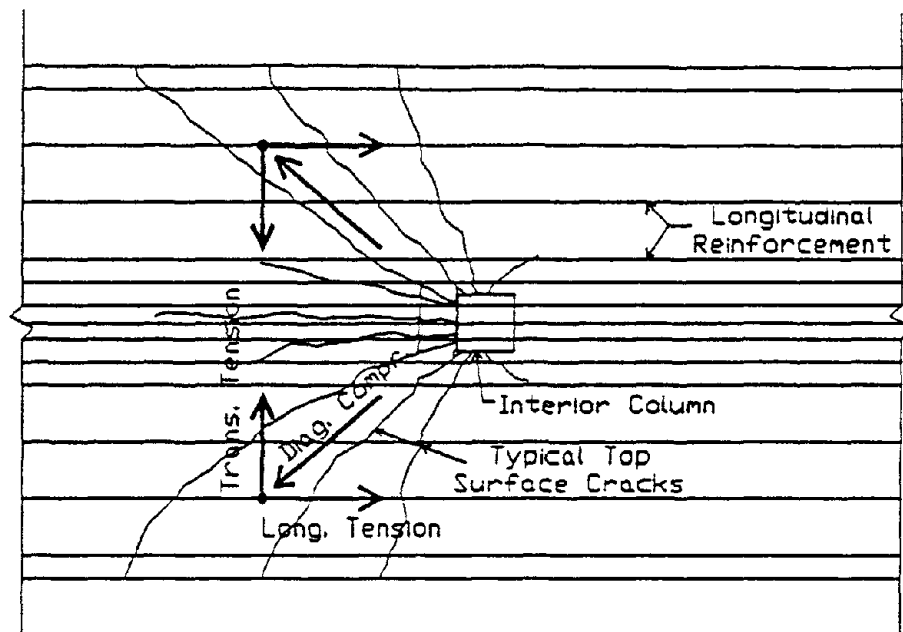
Slab Reinforcement Tension Transfer Mechanism

Fig. 6.13   Load transfer mechanism
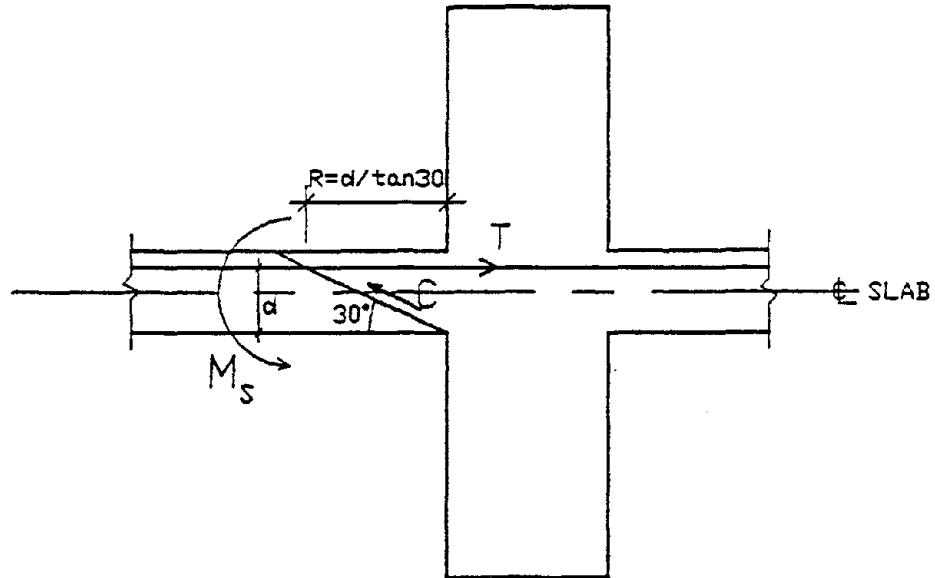
Interior Connection Model

Fig. 6.14   Section through failure plane for punching shear
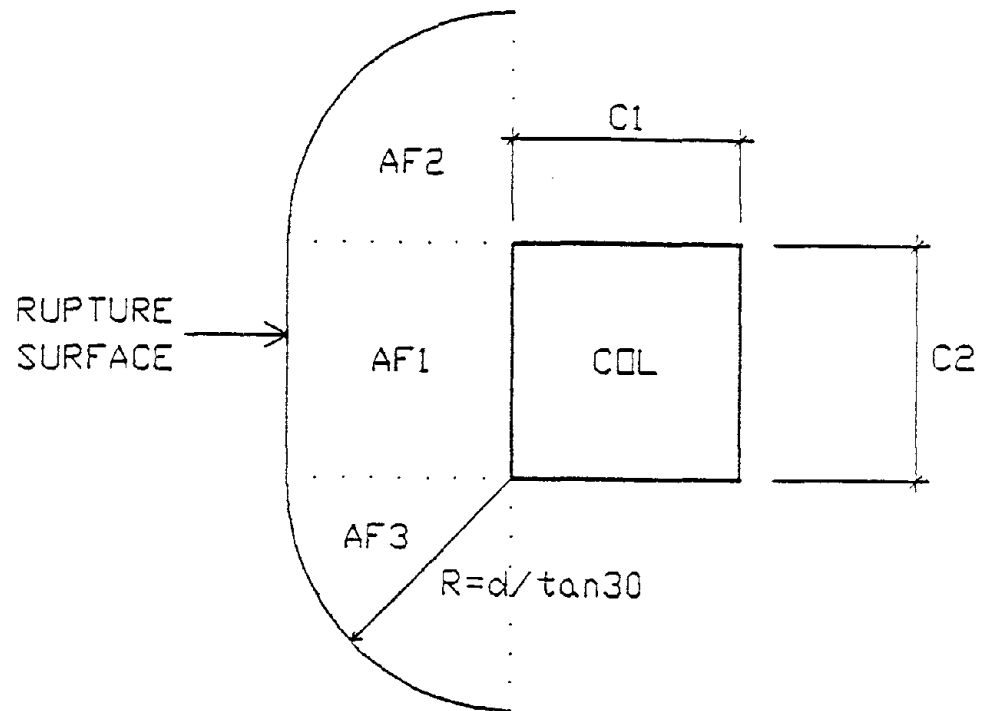
Fig. 6.15   Plan view of failure plane for punching shear
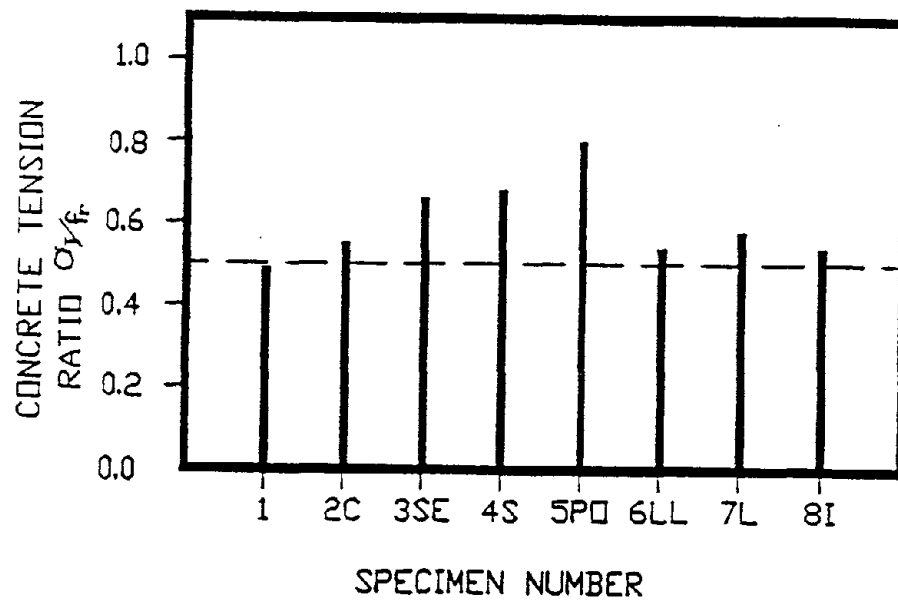
Fig. 6.16   Failure plane tensile stress ratios
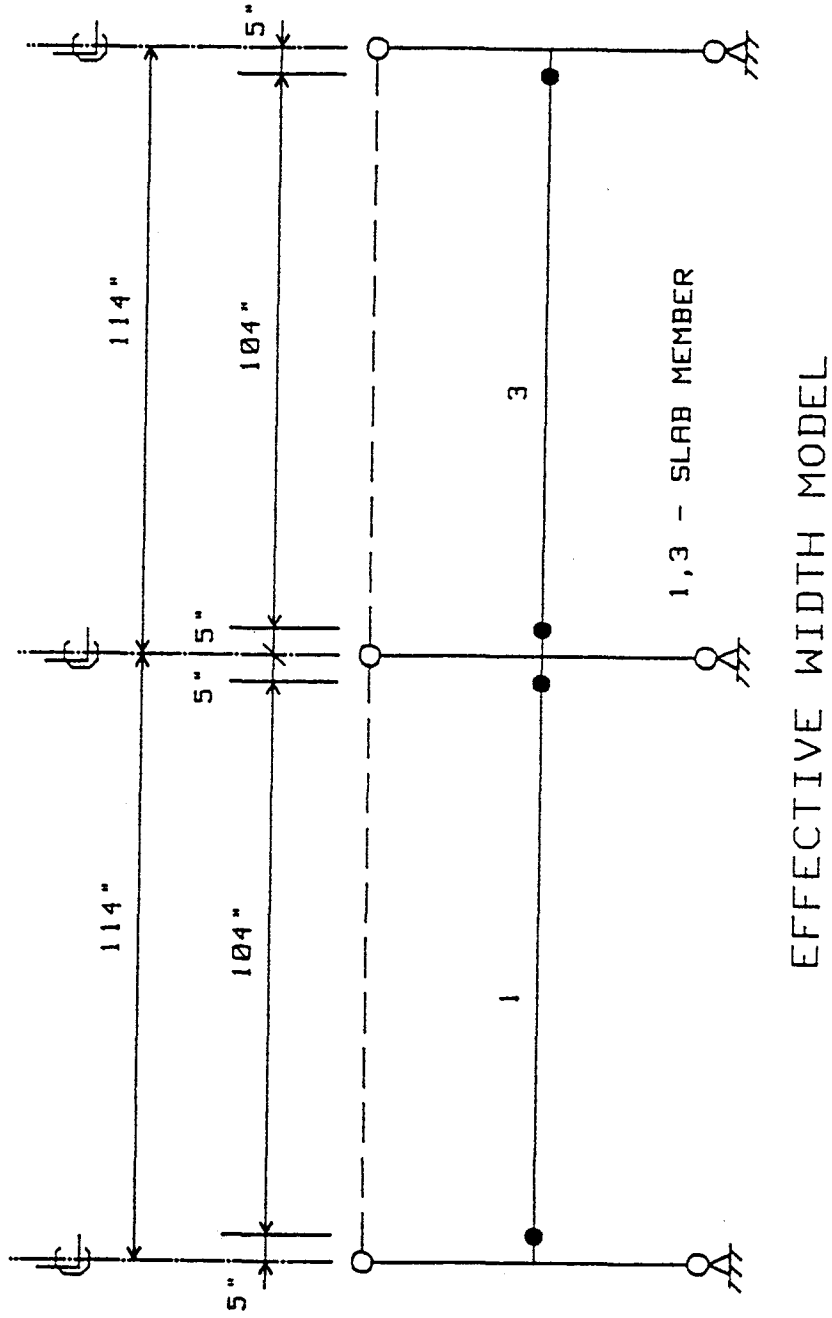
240

EFFECTIVE WIDTH MODEL

1,3 — SLAB MEMBER

114"

104"

5"

5" 5"

114"

104"

5"

3

1

Fig. 7.1   Effective width or equivalent frame model

EXPLICIT TRANSVERSE TORSIONAL MEMBER

Fig. 7.2   Explicit transverse torsional member model

242

MODIFIED EFFECTIVE WIDTH MODEL

1,3 – SAGGING SLAB
2,4 – HOGGING SLAB
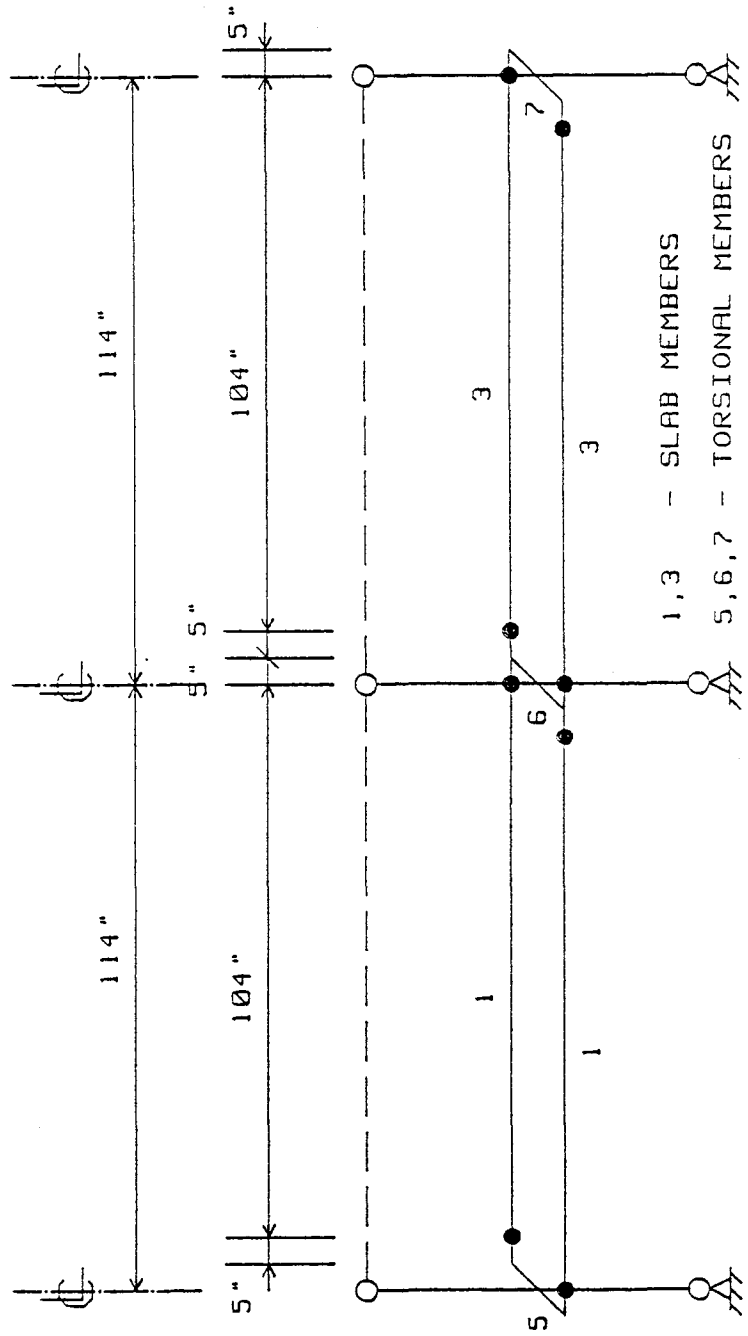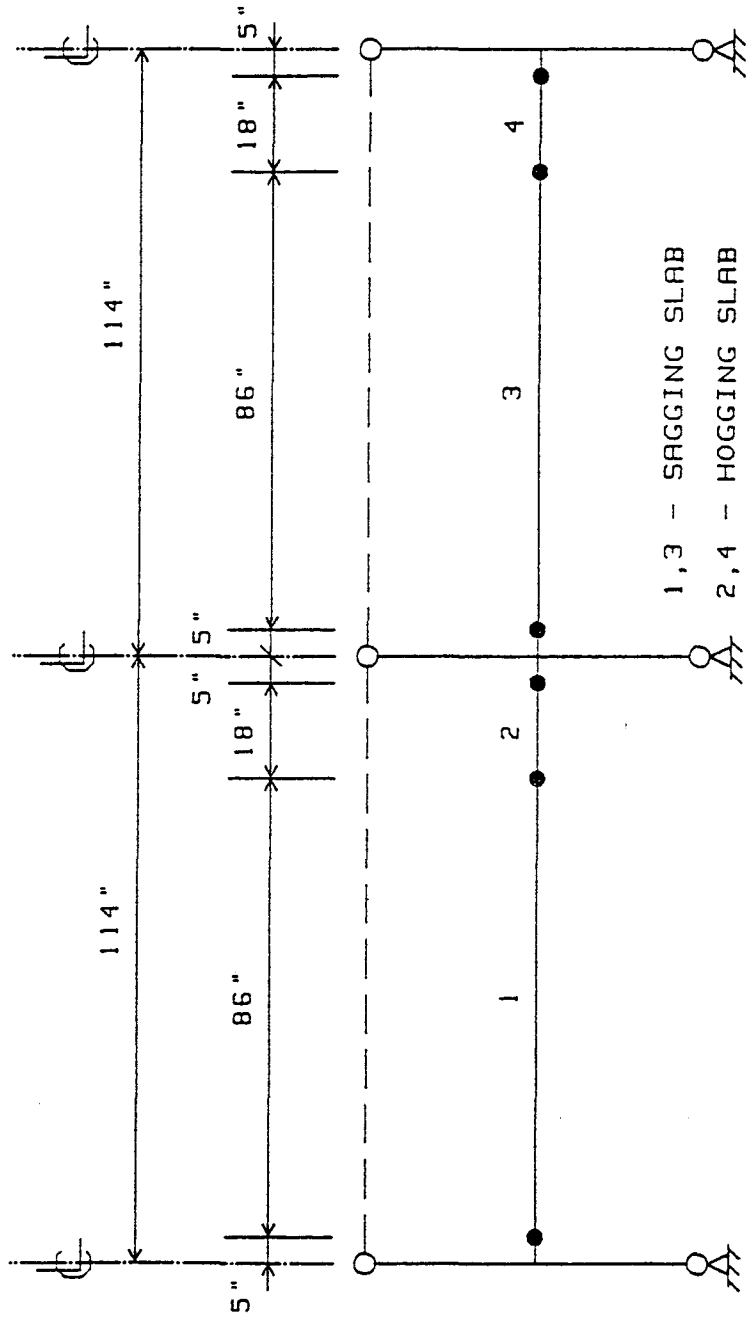
Fig. 7.3   Modified effective width or equivalent frame
model

MODIFIED EXPLICIT TRANSVERSE
TORSIONAL MEMBER

1,3 — SAGGING SLAB
2,4 — HOGGING SLAB
5,6,7 — TORSIONAL MEMBERS
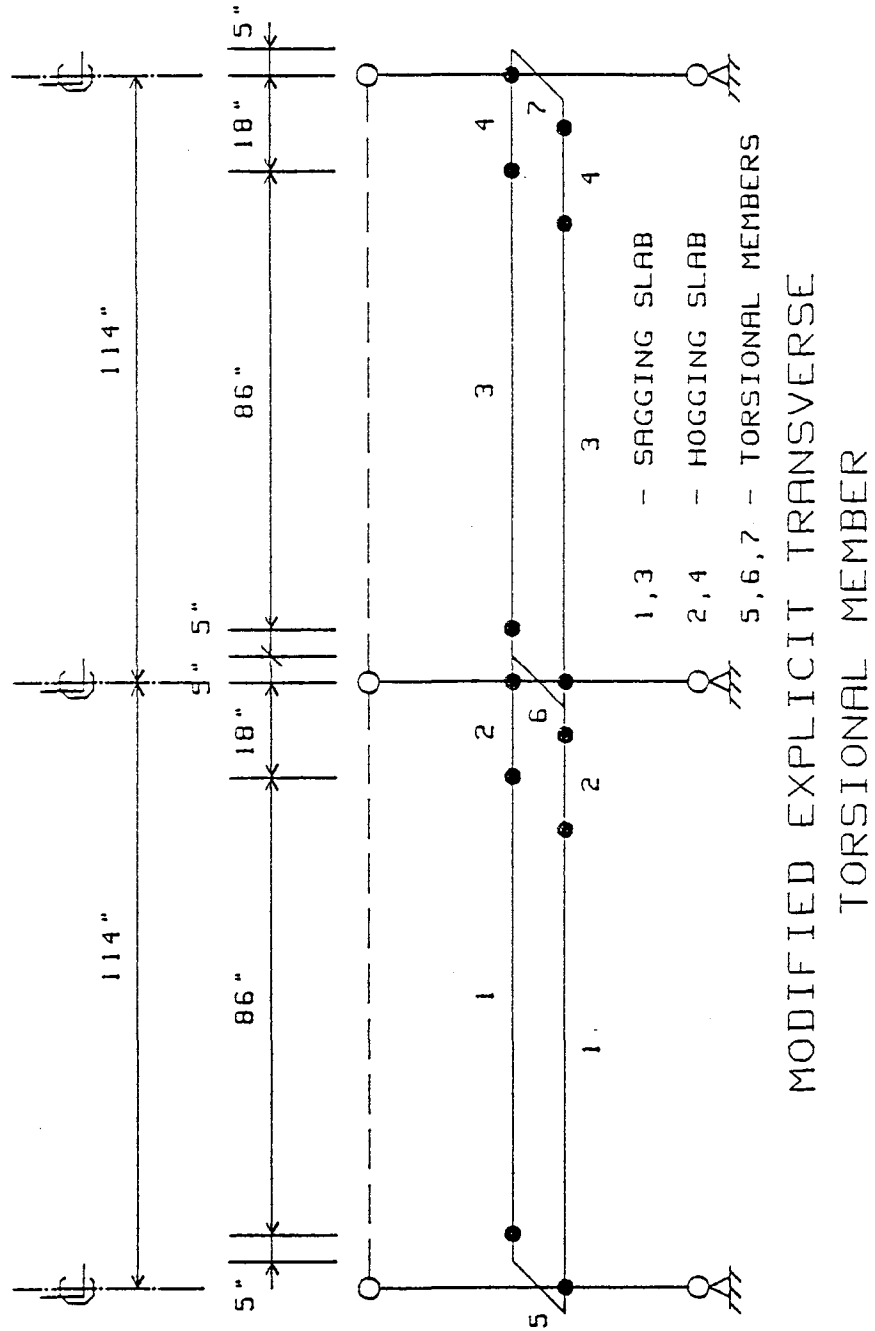
Fig. 7.4   Modified explicit transverse torsional member

model

244
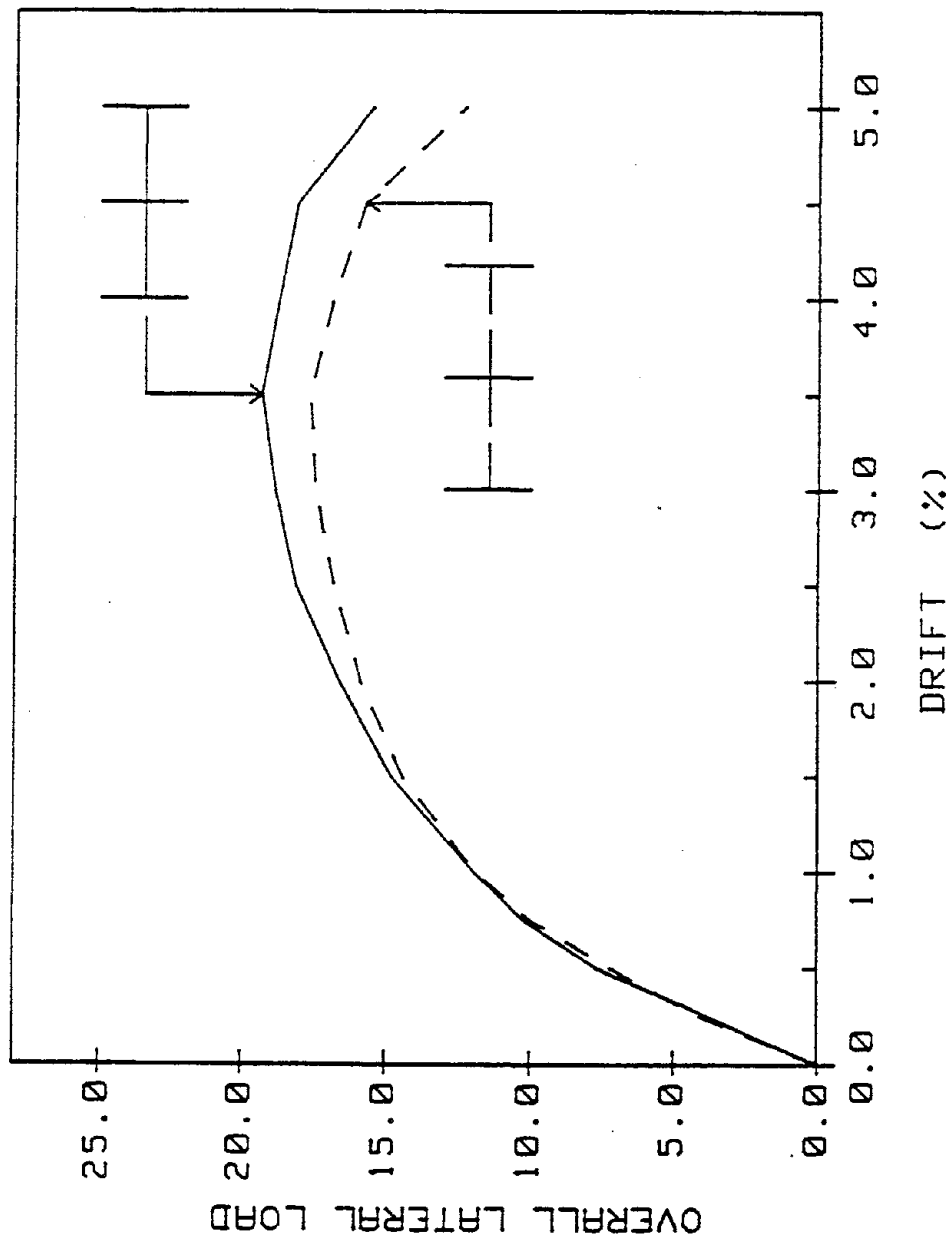
Fig. 8.1   Lateral load vs drift for combined and
            individual specimens
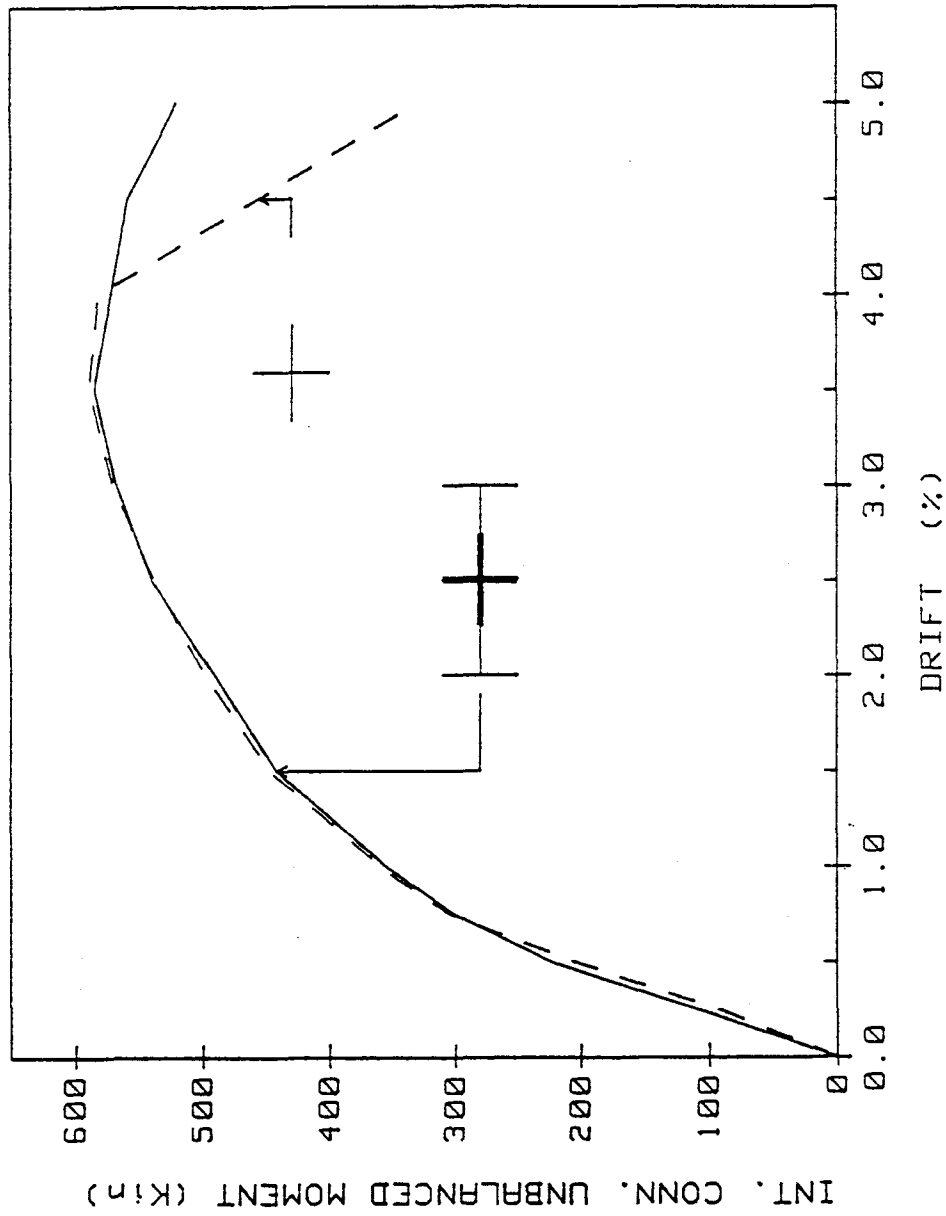
Fig. 8.2   Interior connection unbalanced moment vs drift
for combined and individual specimens

246
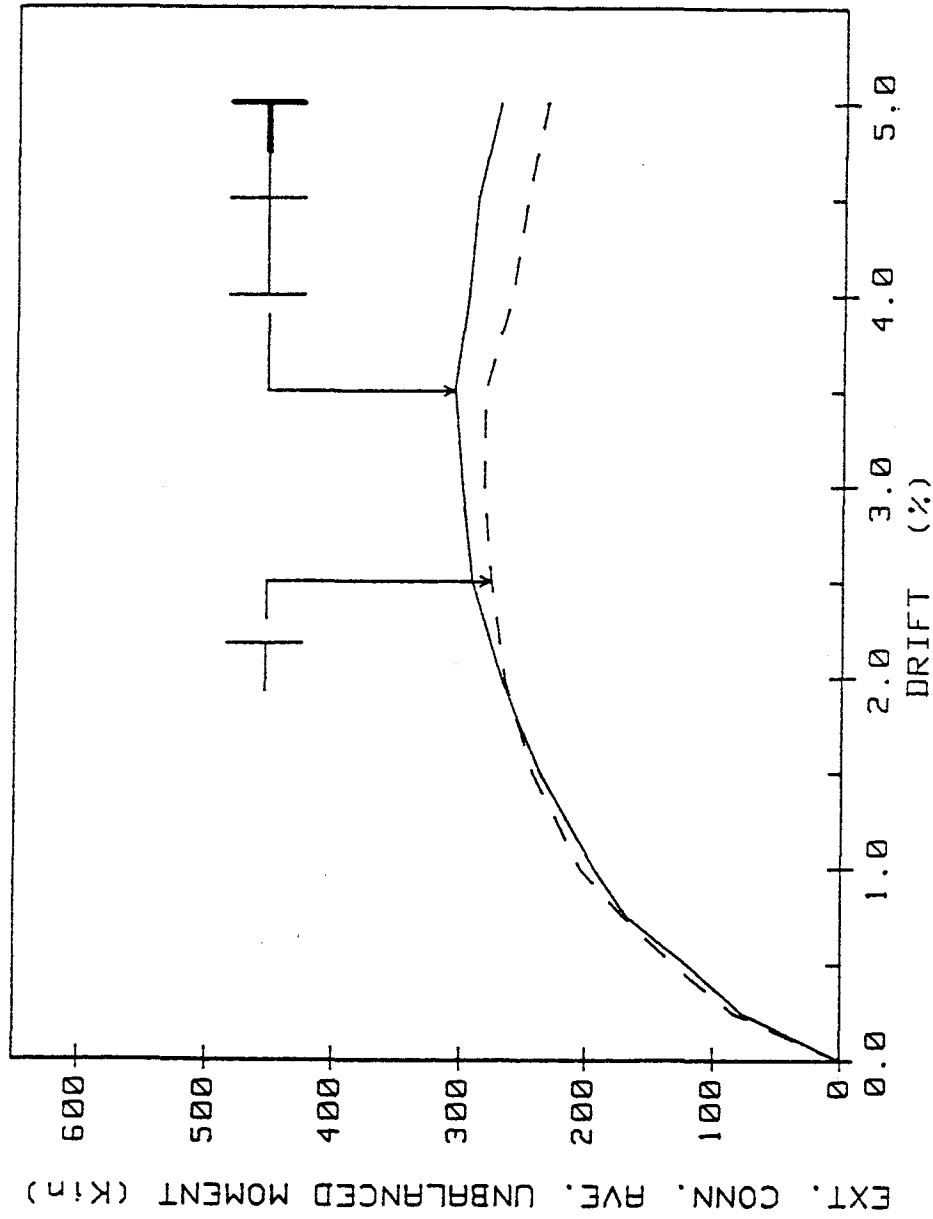
Fig. 8.3   Average exterior connection unbalanced moment vs
drift for combined and individual specimens
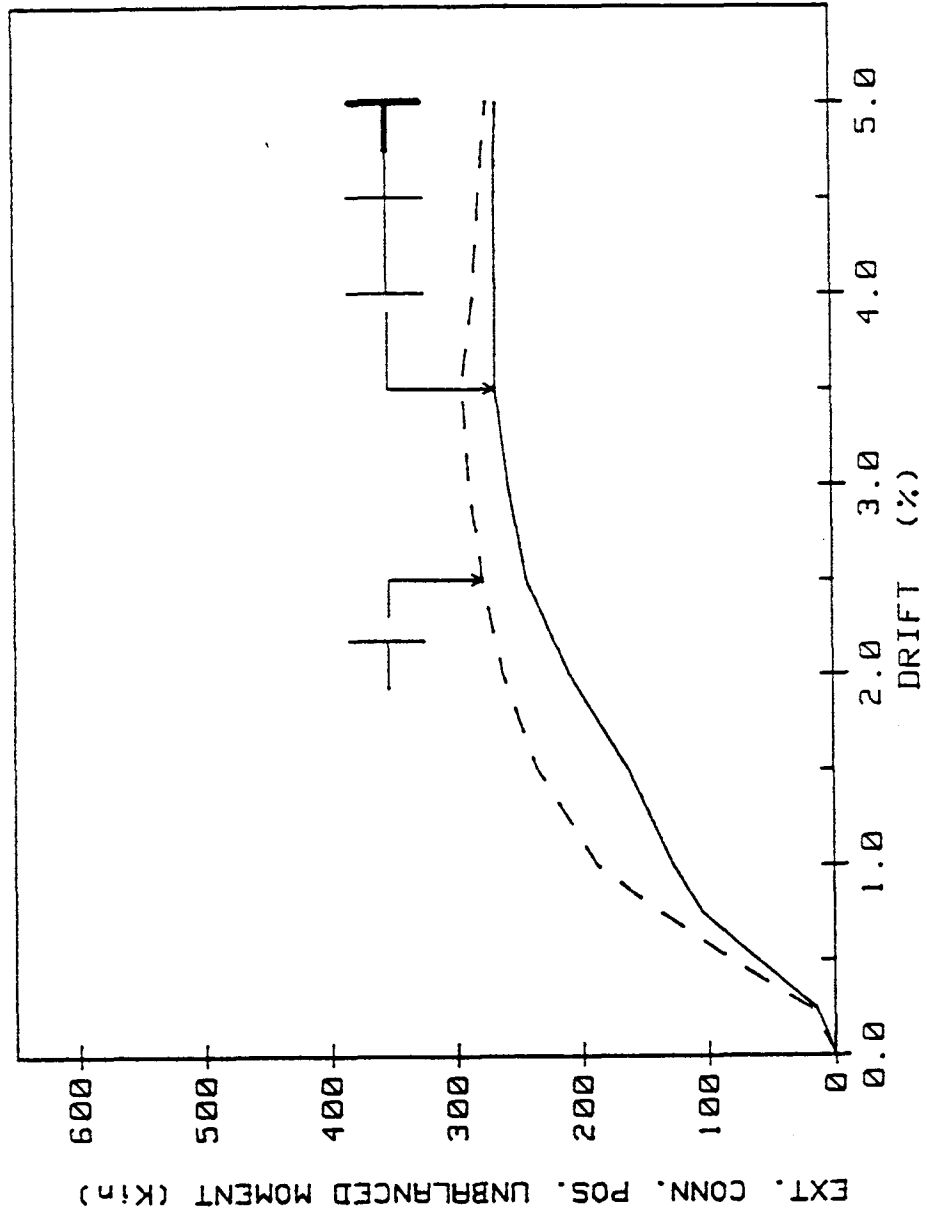
Fig. 8.4   Exterior connection positive unbalanced moment
vs drift for combined and individual specimens
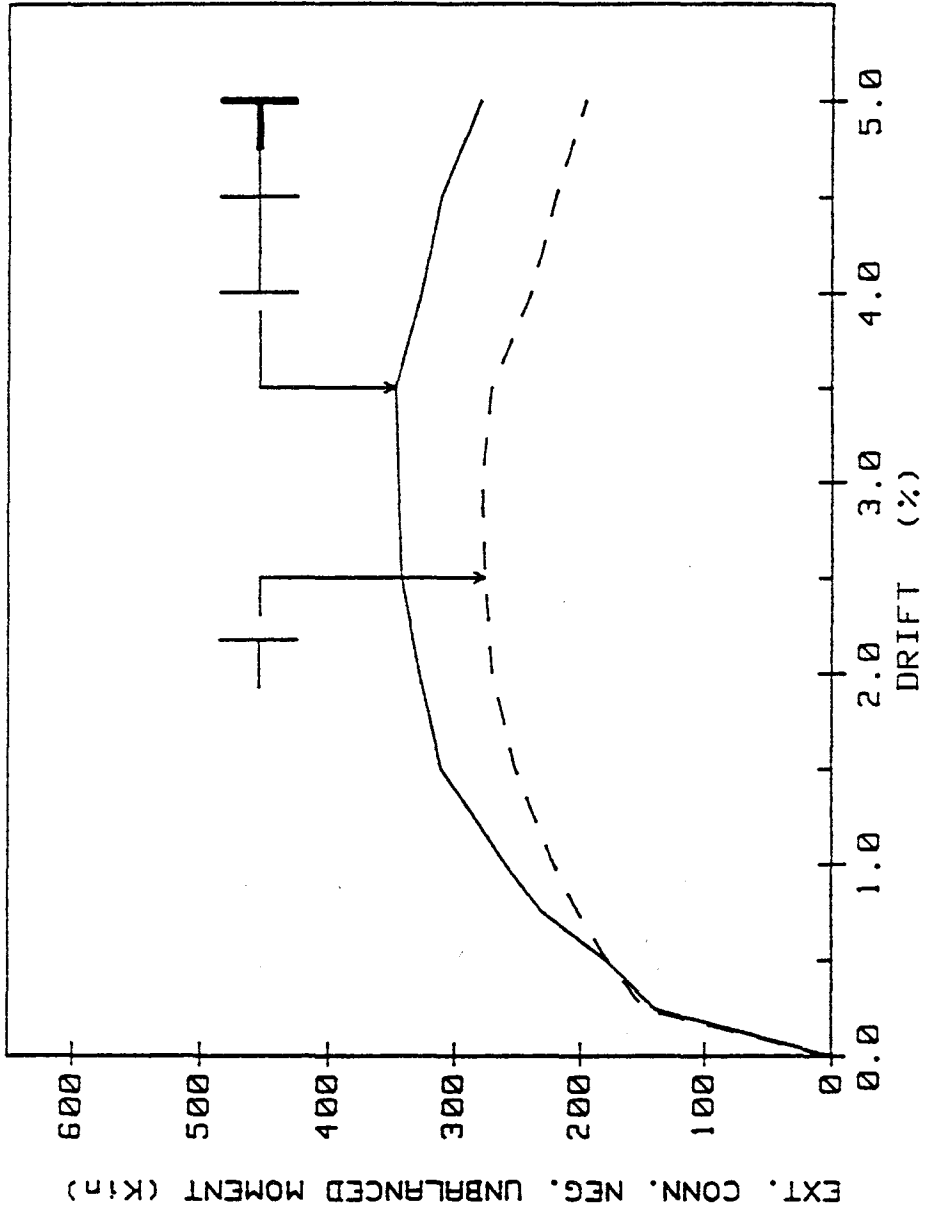
Fig. 8.5   Exterior connection negative unbalanced moment vs drift for combined and individual specimens

a) POSITIVE DRIFT

b) NEGATIVE DRIFT
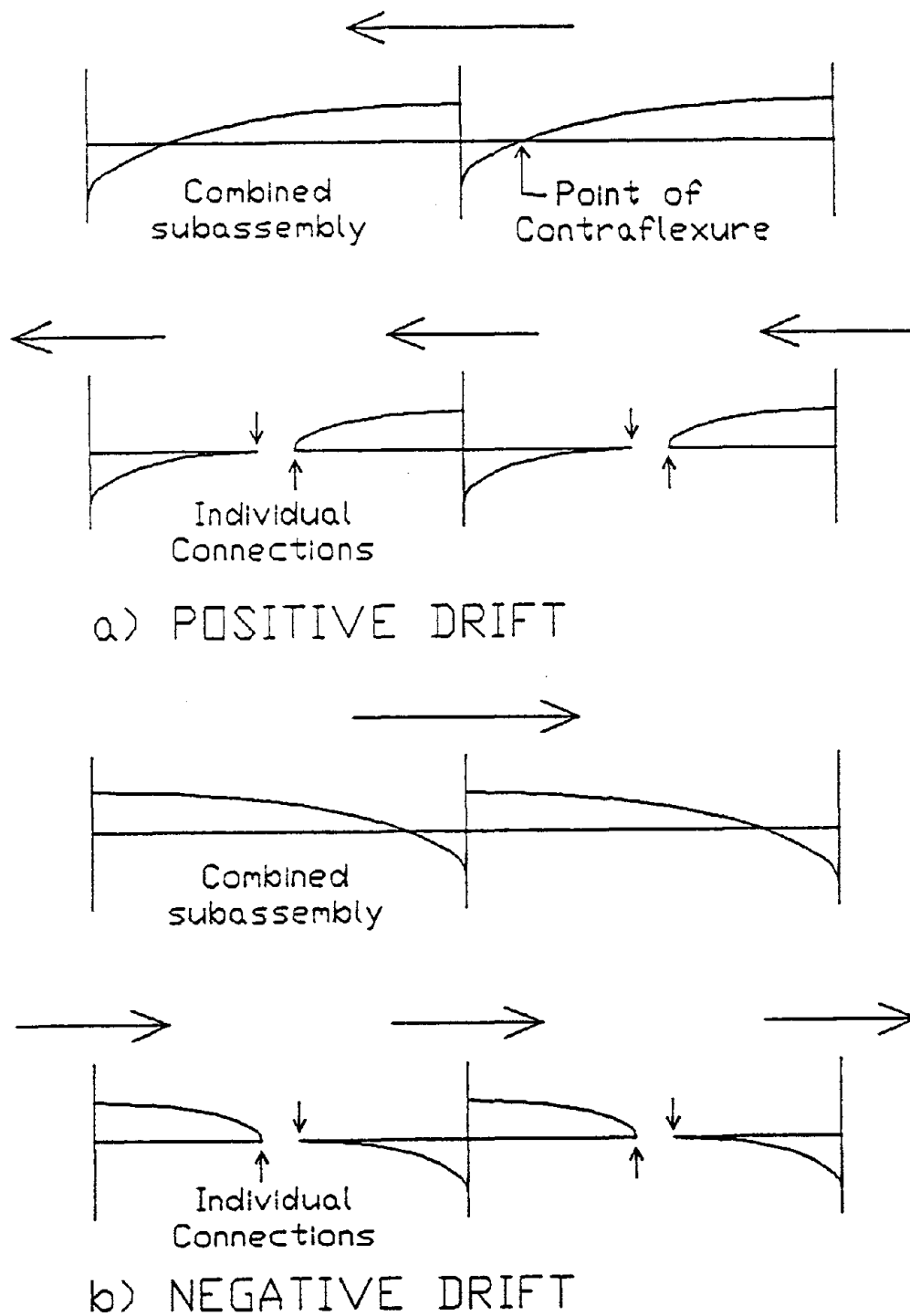
Fig. 8.6   Comparison of bending moment distribution for
combined and individual specimens

250
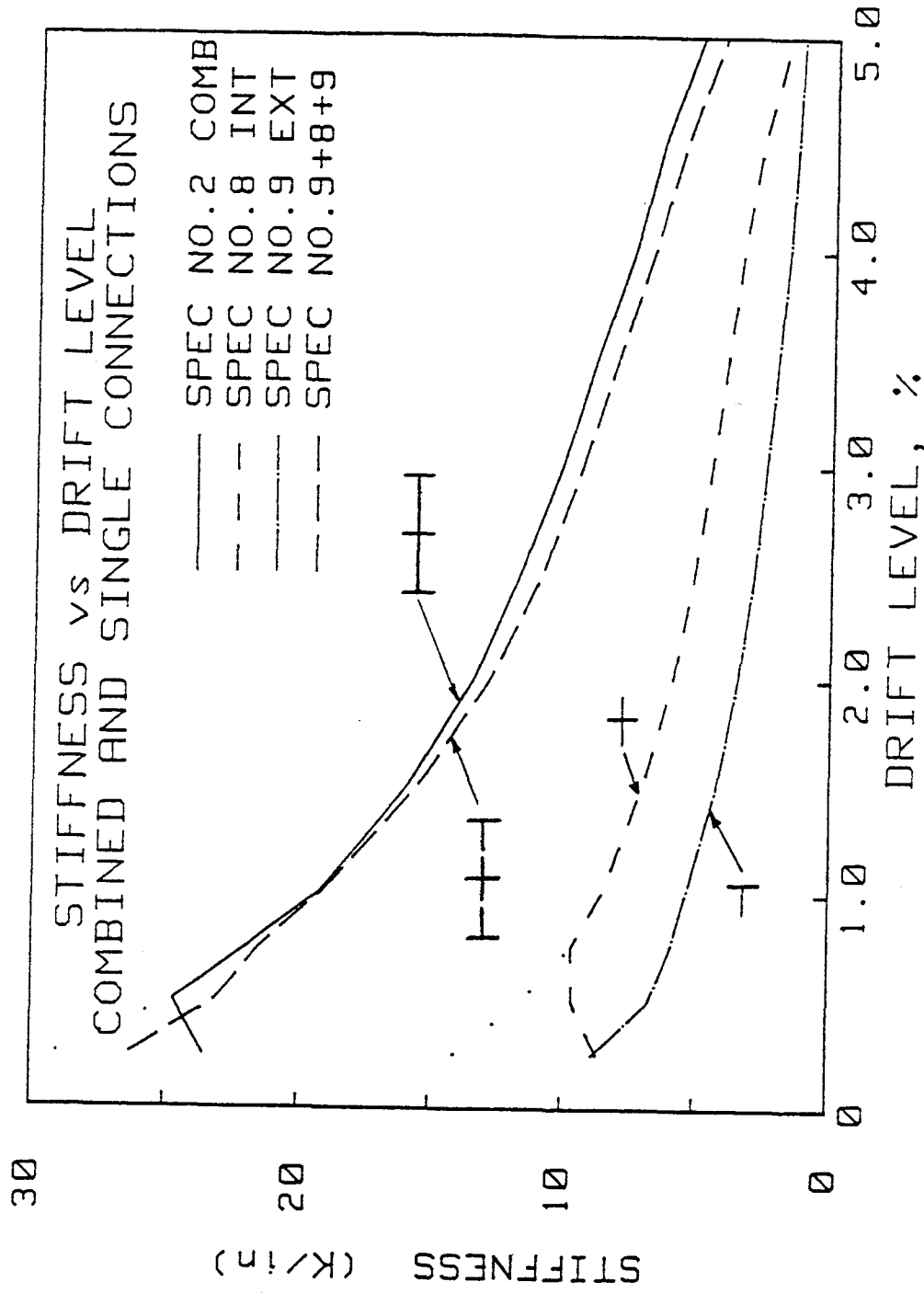
Fig. 8.7 Full specimen peak-to-peak stiffness vs drift
for combined and individual specimens

PHOTOGRAPHS

.
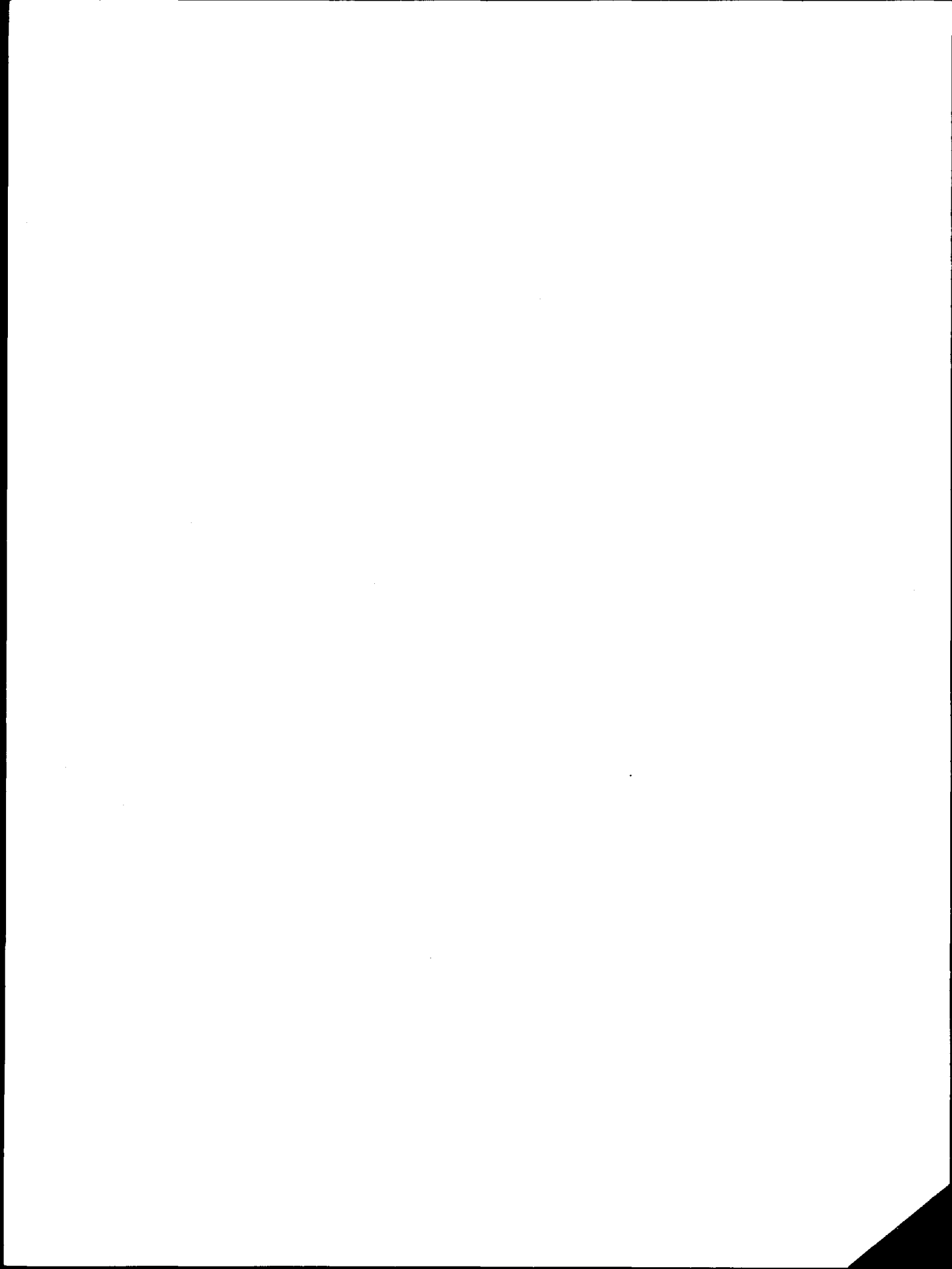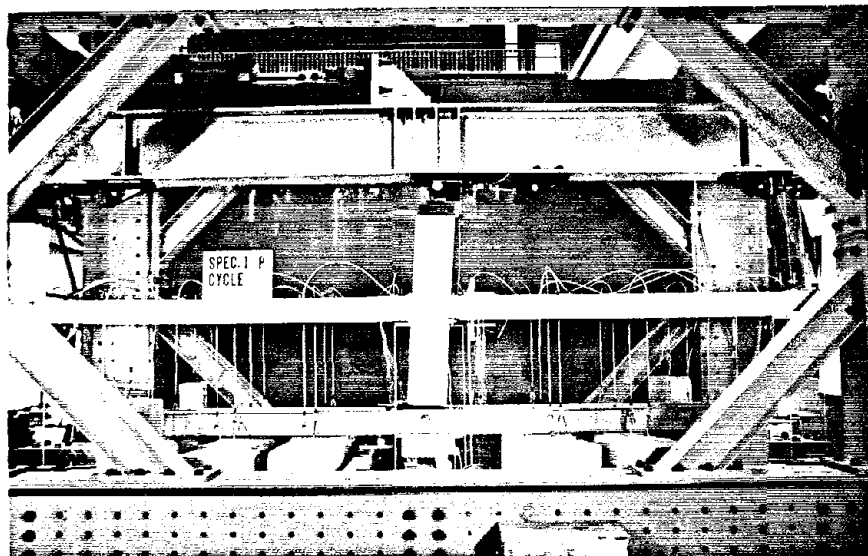
Photo 2.1   Control specimen in the test frame

254
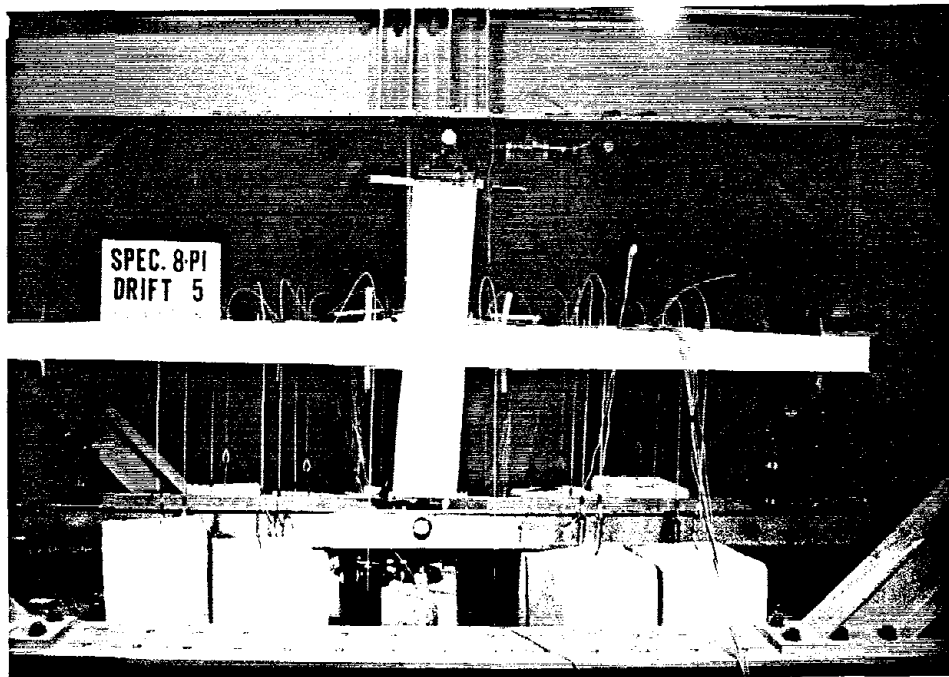
Photo 2.2 Specimen 8I in the test frame
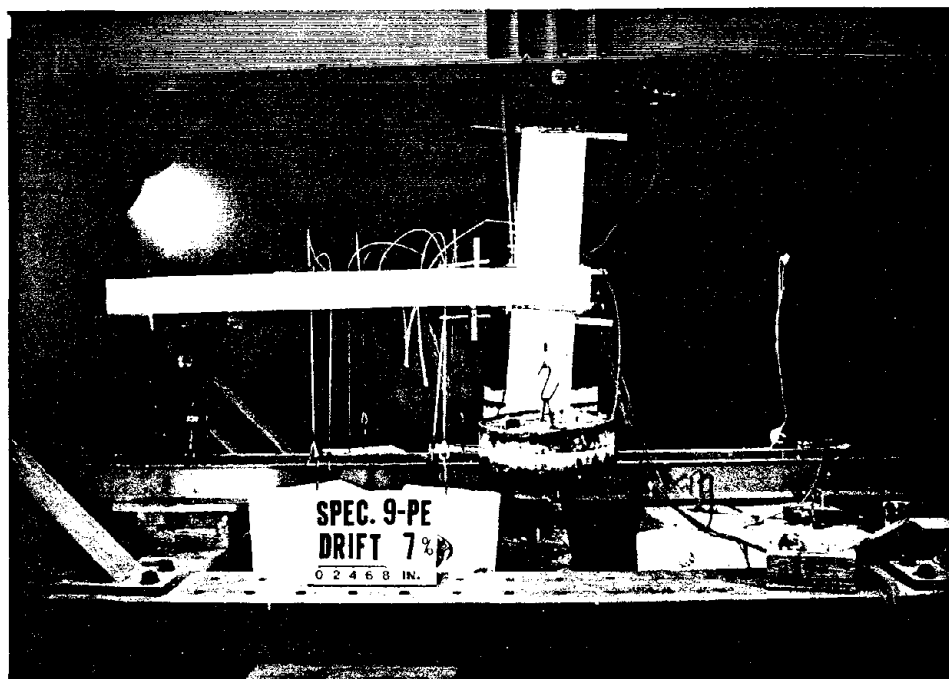
Photo 2.3 Specimen 9E in the test frame
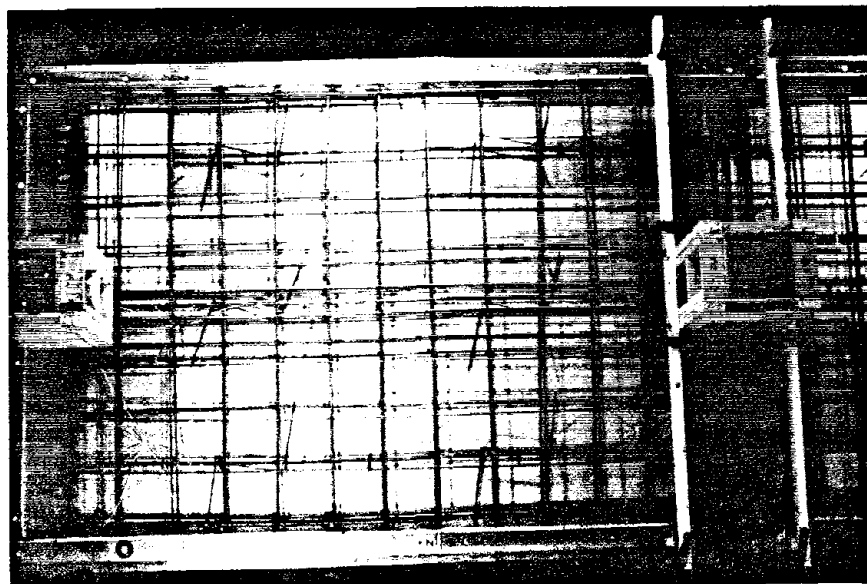
Photo 2.4   Specimen 2C reinforcement
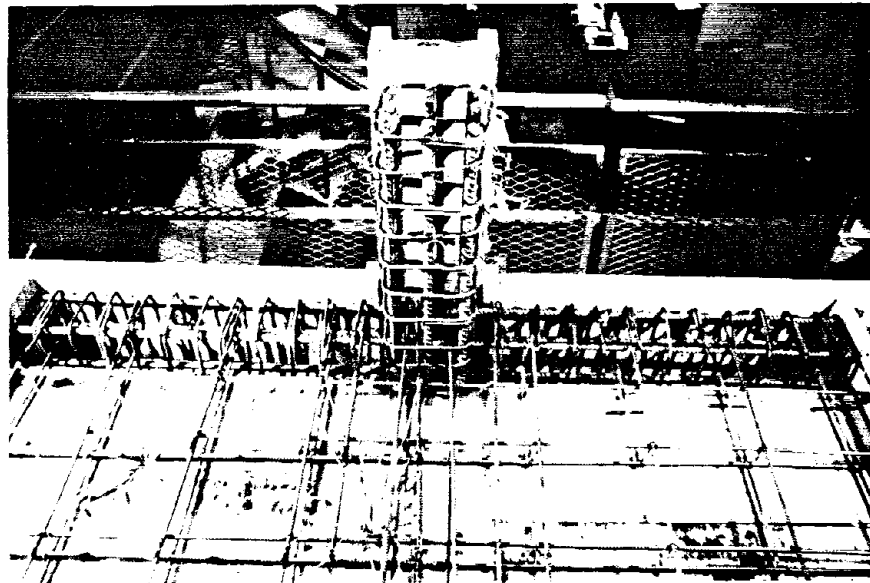
Photo 2.5   Specimen 3SE - Edge beam reinforcement
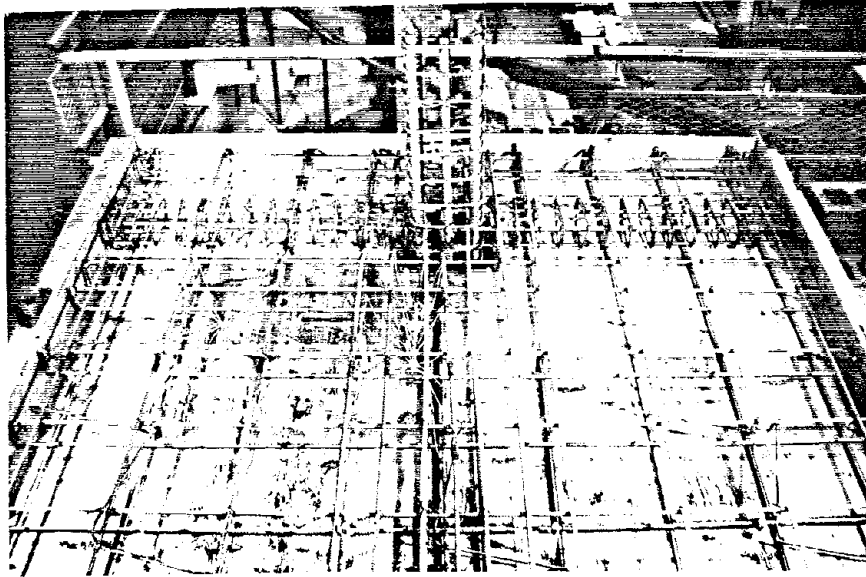
Photo 2.8   Specimen 5SO - Slab overhang reinforcement
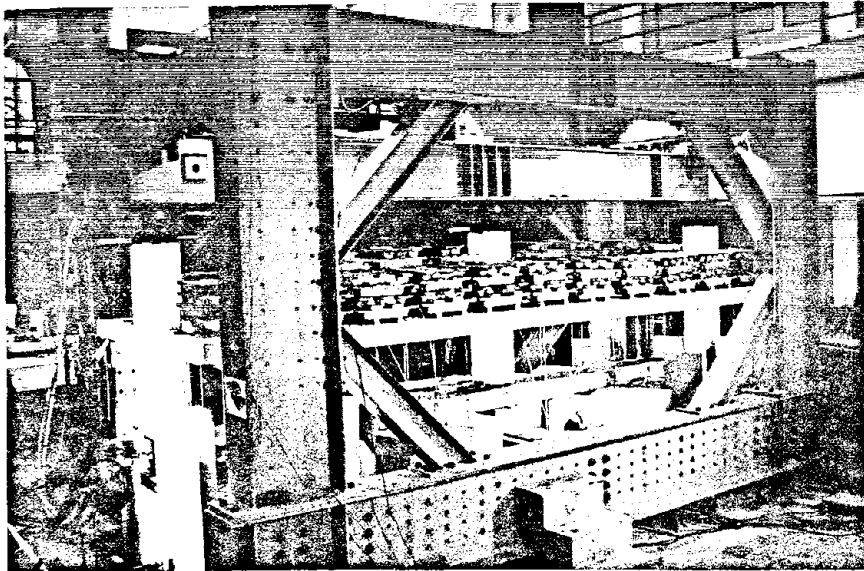
Photo 2.9   Specimen 6LL in the test frame
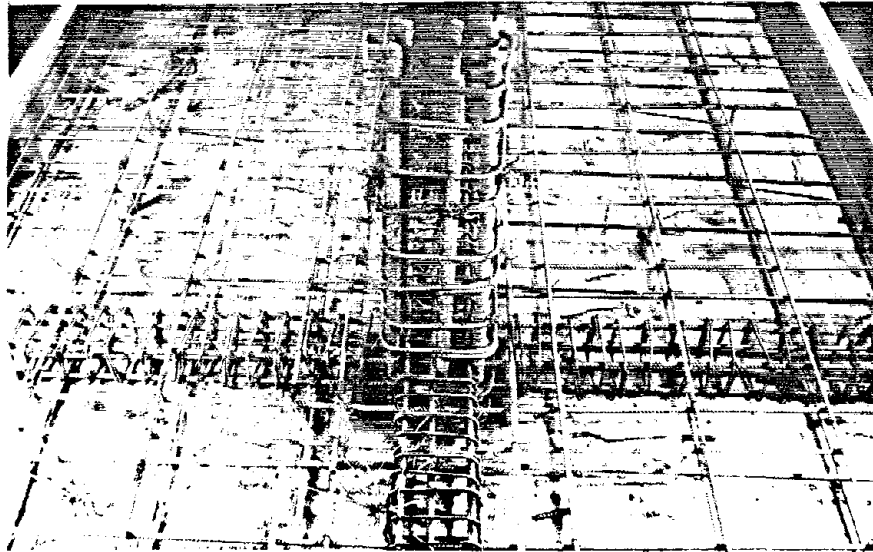
Photo 2.6   Specimen 4S - Interior connection
reinforcement
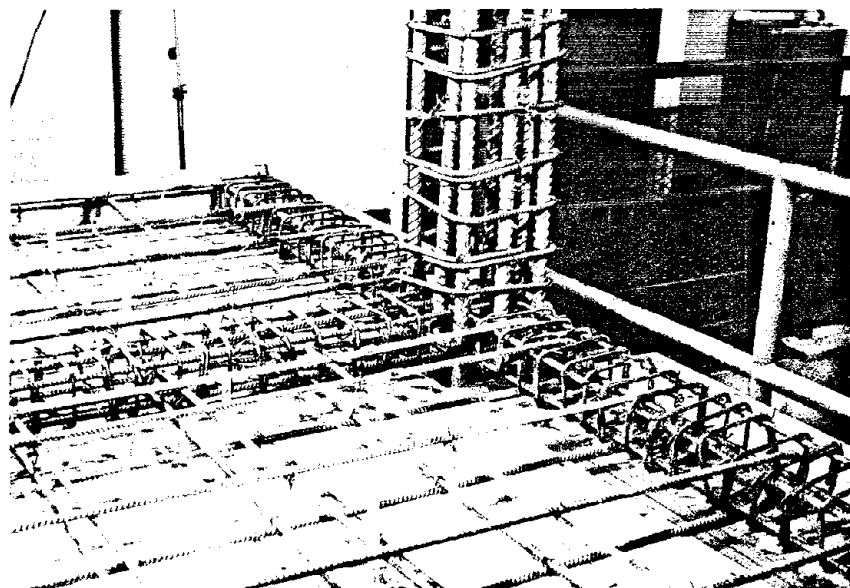
Photo 2.7   Specimen 4S - Exterior connection
reinforcement
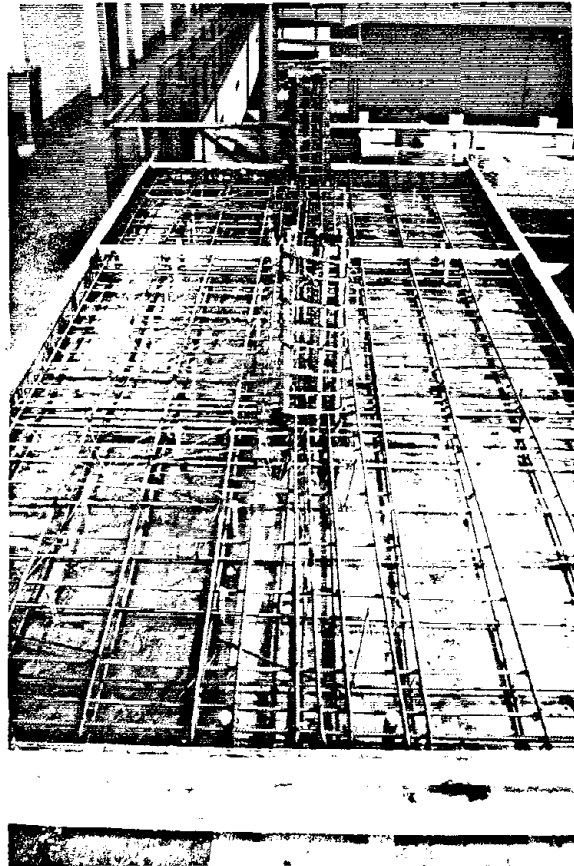
Photo 2.10 Specimen 8I and 9E - slab reinforcement
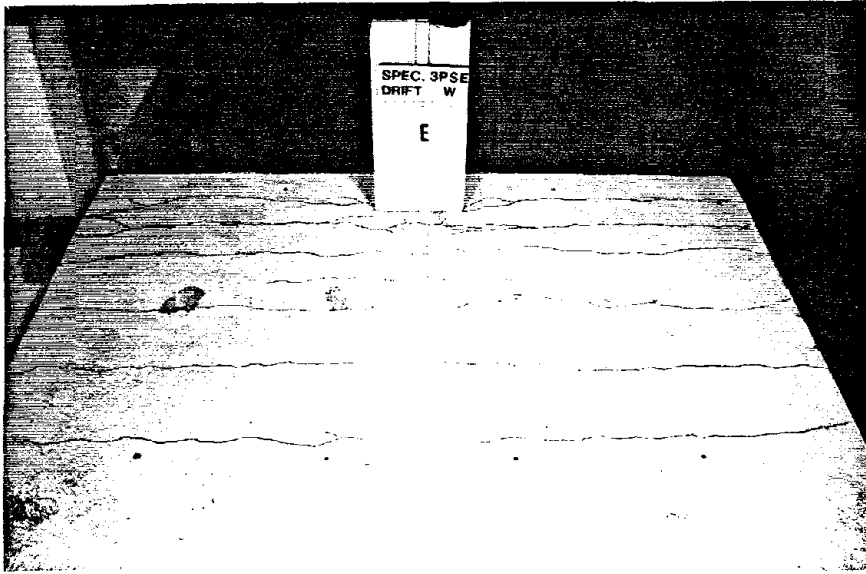
Photo 3.1   Specimen 3SE - Exterior connection crack
            pattern after test
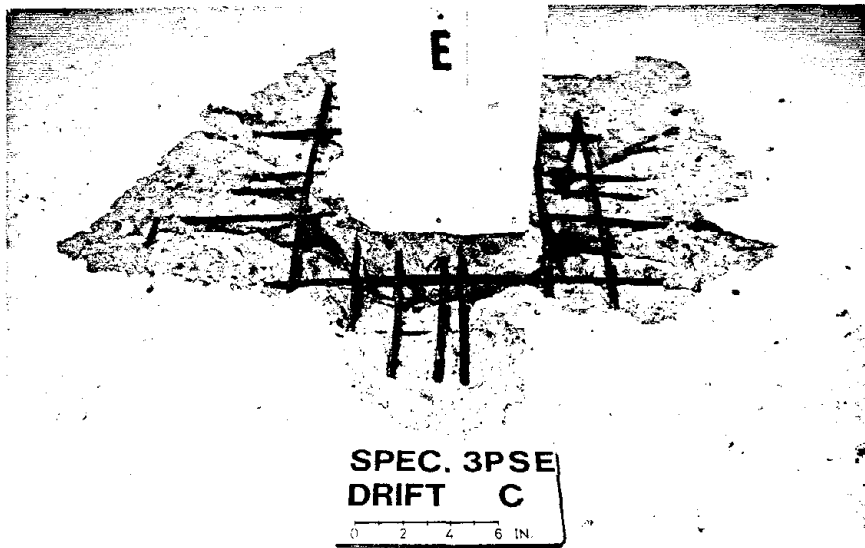
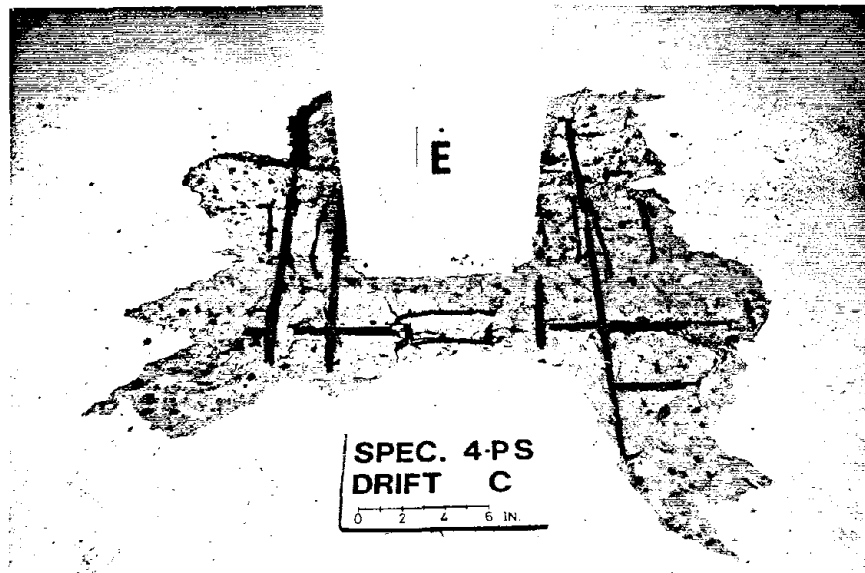Photo 3.2   Specimen 3SE - Interior connection after
            test
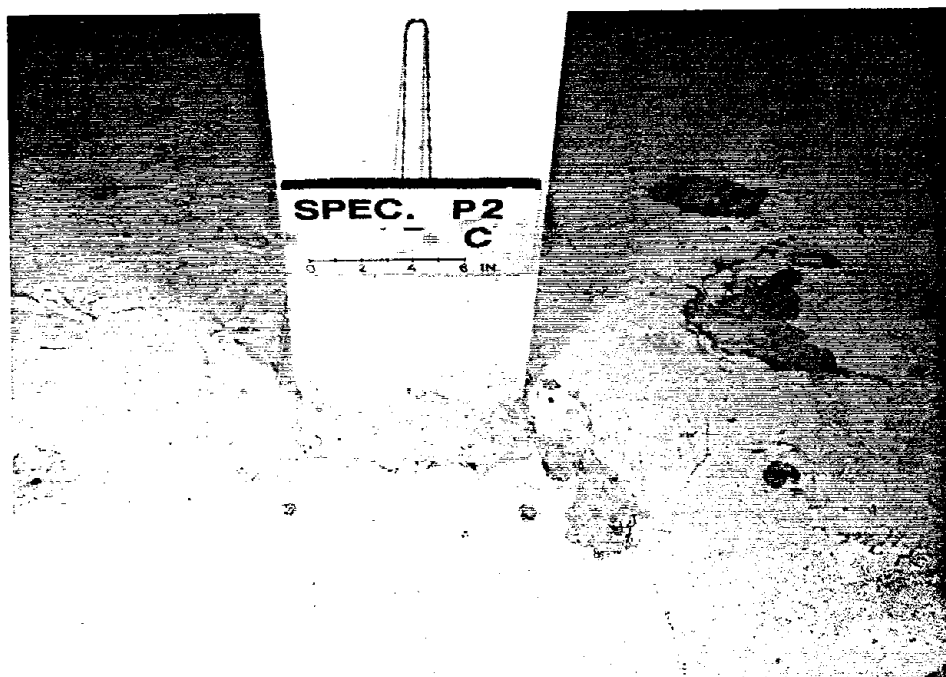
Photo 3.3 Specimen 2C - Interior connection after
           test

Photo 3.4 Specimen 5SO - Interior connection after
           test
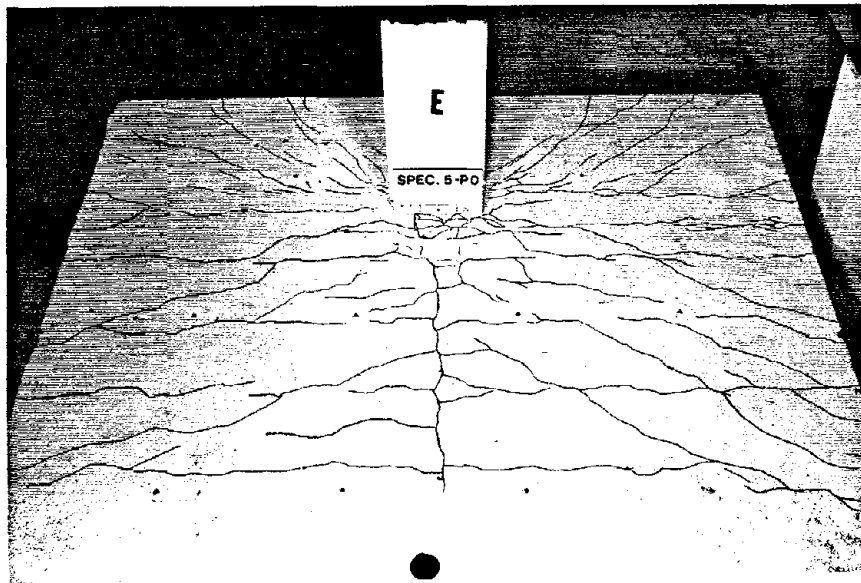
Photo 3.5   Specimen 5SO - Exterior connection crack
             pattern after test
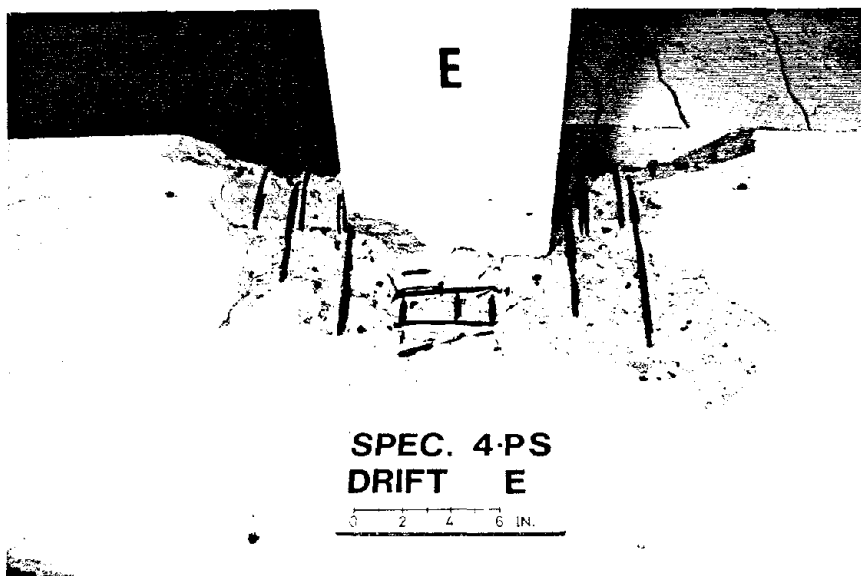
Photo 3.6   Specimen 4S - Exterior connection after 8
             percent drift

Photo 3.7   Specimen 4S - Interior connection after 8
percent drift
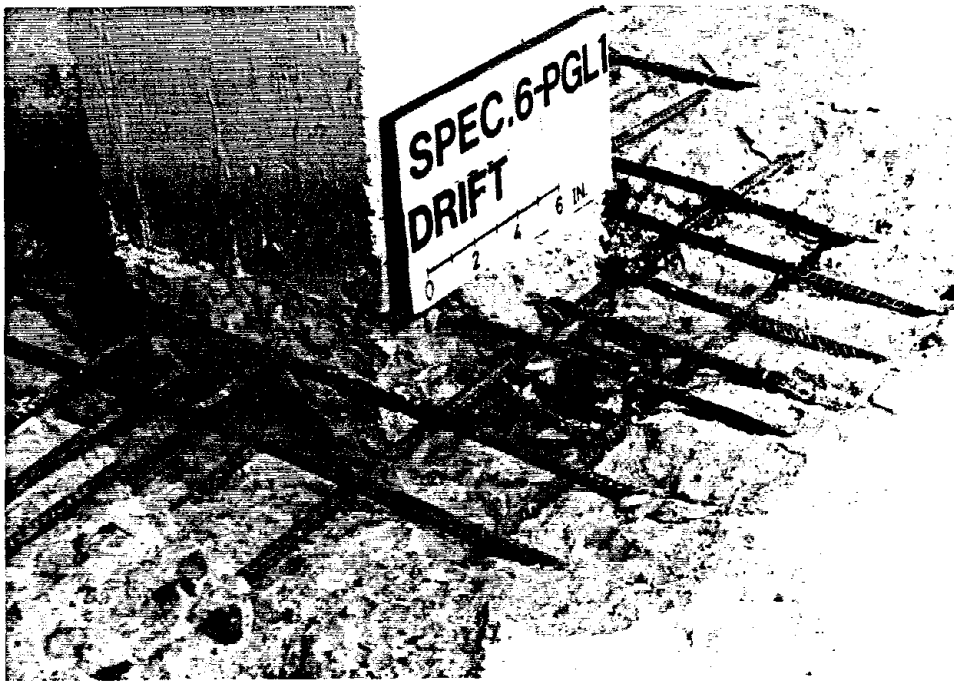
Photo 5.1   Specimen 6LL - Interior connection after
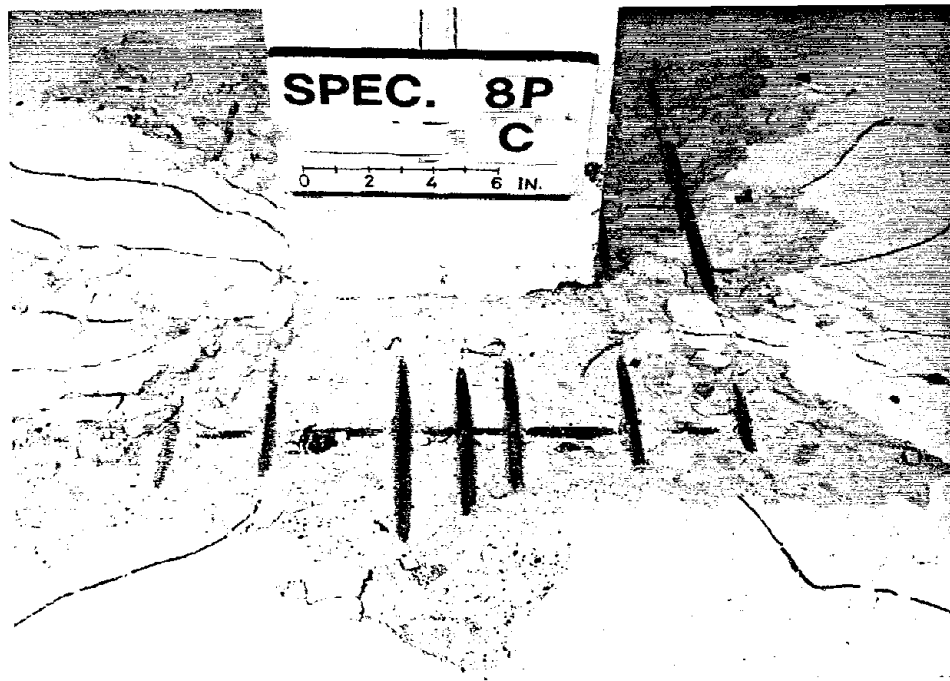   punching shear failure at 1 percent drift
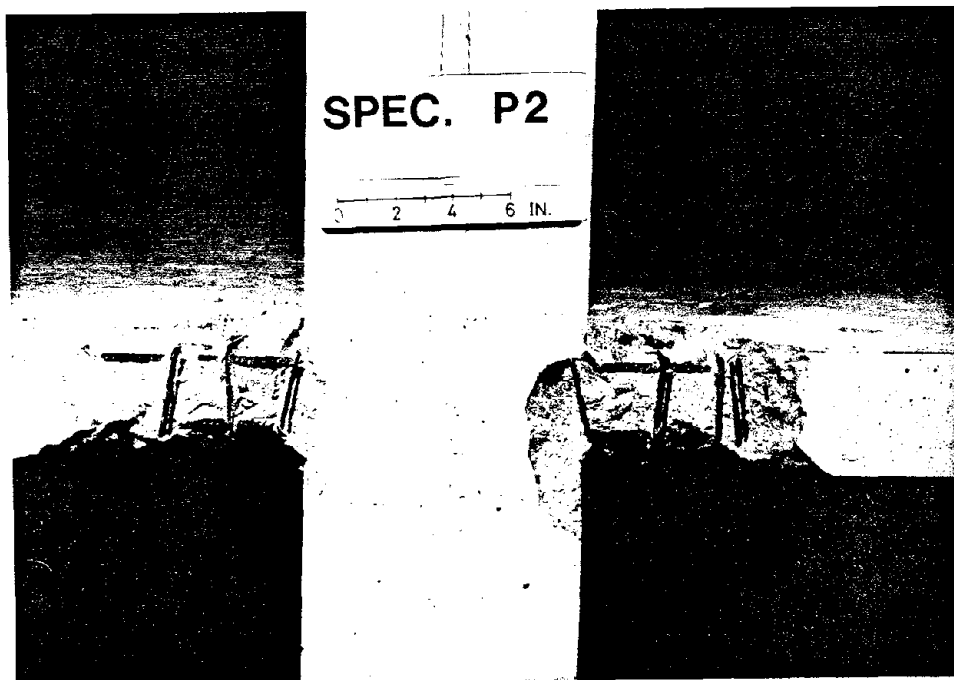
Photo 8.1   Specimen 8I - Interior connection after
test

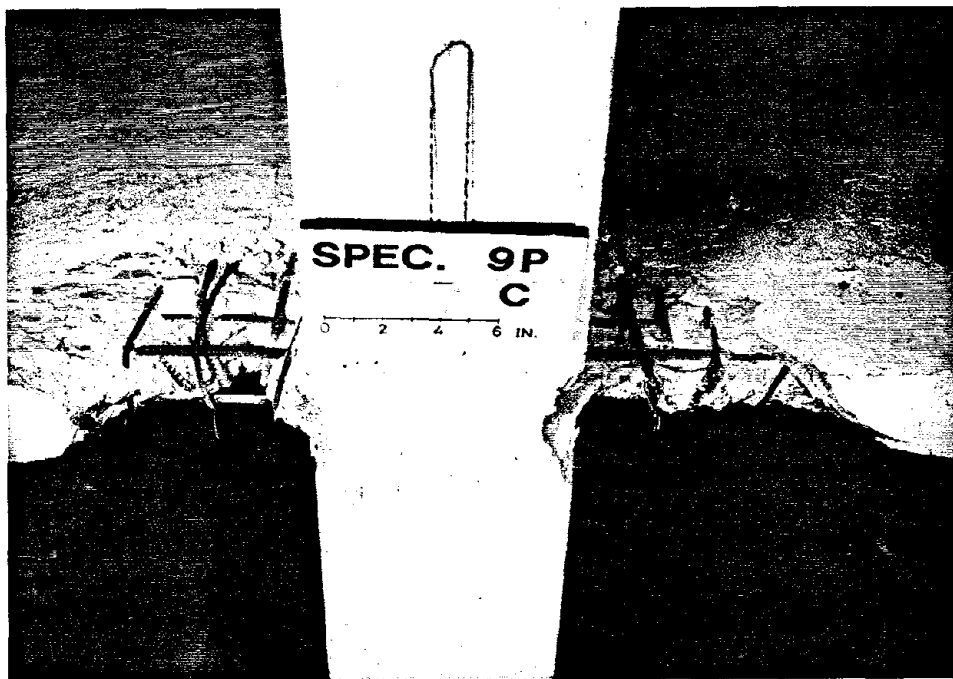Photo 8.2   Specimen 2C - Exterior connection after
test

Photo 3.3   Specimen 9E - Exterior connection after
             test